

Bayesian chronological modelling of the Early Iron Age in Southern Jutland, Denmark

Dissertation
in fulfilment of the requirements for the doctoral degree
at the Faculty of Mathematics and Natural Sciences
at Kiel University

submitted by
Helene Agerskov Rose

Kiel, 2020

First examiner: Priv.-Doz. Dr. Oliver Nakoinz

Second examiner: Prof. Dr. rer. Nat. Rainer Duttmann

Date of the oral examination: 05.06.2020

Approved for printing: 19.02.2021

Contents

<i>List of dissertation publications</i>	5
<i>Acknowledgements</i>	7
INTRODUCTION	9
<i>Research questions</i>	9
<i>Research approach</i>	10
<i>Outline of the dissertation</i>	11
PART A BACKGROUND	13
<i>Introduction to typo-chronology</i>	14
<i>Pre-Roman Iron Age in Denmark</i>	16
The Danish urnfield tradition	17
Cultural affiliations	20
Chronological framework.....	21
Metalwork typology	23
Pottery typology.....	25
<i>Radiocarbon dating in archaeology</i>	28
Dating cremated bone.....	31
Case study: Investigating differences in pretreatment protocols between laboratories	34
Radiocarbon age limit for cremated bone	37
Wood-age offset in cremated bone	38
Applications of radiocarbon dating cremated bone	39
Concluding remarks on dating cremated bone	40
<i>Bayesian chronological modelling</i>	41
Model construction	43
Prior beliefs	44
Trapezoidal phase prior	46
Model evaluation	49
Review of currencies studies applying Bayesian chronological modelling.....	50
Modelling the temporality of change in artefact currencies.....	52
Concluding remarks on Bayesian chronological modelling	54
<i>Part A conclusion</i>	55

PART B	OFFSETS AND OUTLIERS	56
	<i>Modelling offsets and outliers in radiocarbon data</i>	57
	Modelling type-r offsets	59
	Case study: Paleo-dietary reconstruction of five individuals from St Alban's Odense	61
	Evaluating the fit of dietary reconstruction models	64
	Modelling type-t offsets	64
	Case study: Intrinsic age of collagen	66
	Case study: Old wood	68
	Case study: Wood-age offsets in cremated bone	72
	Wood-age offsets in an experimental dataset	75
	Calculating carbon exchange	78
	Wood-age offsets in an archaeological dataset	80
	Proposing a new outlier model	83
	<i>Part B conclusion</i>	89
PART C	MODELLING ARTEFACT CURRENCIES	92
	<i>Bayesian chronological modelling of Early Iron Age urnfield assemblages from Southern Jutland</i>	93
	Dating strategy	93
	Material	95
	Aarupgaard urnfield	96
	Aarre urnfield	100
	Søhale urnfield	103
	Sample selection	105
	Laboratory methods	106
	Results	107
	Artefact frequencies	107
	Radiocarbon data	108
	Exploring the radiocarbon dataset	110
	Chronological modelling	115
	Currency models	115
	Model A - metalwork currencies	117
	Model B - pottery currencies	120
	Site models	123
	Aarupgaard urnfield	123
	Aarre urnfield	125
	Søhale urnfield	126

Discussion	128
Evaluating artefact typologies	128
Temporal processes of change in artefact currencies	130
Residence time of individual artefacts	132
Regionality in material culture	133
Evaluating the chronological framework	135
<i>Part C conclusion</i>	140
ABSTRACT	159
KURZZUSAMMENFASSUNG	161
BIBLIOGRAPHY	163
APPENDICES	179
<i>Appendix 1 Additional case studies</i>	180
Rokaer long grave	181
Sample Selection	182
St Alban's Odense	183
Osteology	185
Sample Selection	186
Experimental material	186
<i>Appendix 2 Metalwork currencies</i>	187
Currency model of pin with type 1 coiled head	188
Currency model of pin with type 2 coiled head	189
Currency model of pin with circular head	190
Currency model of combined belt equipment	191
<i>Appendix 3 Pottery currencies</i>	192
Currency model of pottery type 12B	192
Currency model of pottery type 15B	193
Currency model of pottery type 15C	194
Currency model of pottery type 18C	195
Chronological model of pottery types modelled in unbounded phases	196
<i>Appendix 4 Paper 1</i>	197
Rokaer – an early Neolithic long barrow from East Jutland	197

<i>Appendix 5</i>	<i>Paper 2</i>	203
	High-Resolution Dating of a Medieval Multiple Grave.....	203
<i>Appendix 6</i>	<i>Paper 3</i>	217
	Radiocarbon Dating Cremated Bone: A Case Study Comparing Laboratory Methods.....	217
<i>Appendix 7</i>	<i>Paper 4</i>	229
	Bayesian modeling of wood-age offsets in cremated bone	229

List of dissertation publications

PAPER 1

Kristiansen, A.M., Eriksen, B.V. & **Rose, H.A.** (forthcoming). Rokaer – a Neolithic long barrow.

PAPER 2

Rose, H. A., Meadows, J., & Bjerregaard, M. (2018). High-Resolution Dating of a Medieval Multiple Grave. *Radiocarbon*, 60(5): 1547-1559. doi:10.1017/RDC.2018.43

PAPER 3

Rose, H. A., Meadows, J., Palstra, S., Hamann, C., Boudin, M., & Hüls, C. M. (2019). Radiocarbon dating cremated bone: a case study comparing laboratory methods. *Radiocarbon*, 61(5): 1581-1591. doi:10.1017/RDC.2019.70

PAPER 4

Rose, H. A., Meadows, J., & Henriksen, M. B. (2020). Bayesian modeling of wood-age offsets in cremated bone. *Radiocarbon*. *Radiocarbon*, 62(2): 379-401. doi:10.1017/RDC.2020.3

Acknowledgements

The research presented here is part of subproject G1 'Timescales of Change – Chronology of cultural and environmental transformation' of the Collaborative Research Centre 'Scales of Transformation: Human-environmental Interaction in Prehistoric and Archaic Societies' that is funded by the German Research Foundation (CRC 1266). Analyses were funded through the CRC 1266 and the Center for Baltic and Scandinavian Archaeology (ZBSA)'s Man and Environment research theme.

I am grateful for all the support and guidance I have received from present and former colleagues at the ZBSA. You kindly pushed me to do better while feeding me chocolate. Special thanks goes to Berit Valentin Eriksen for always having my back, and to Sonja Grimm for housing me and explaining German concepts, whenever I ran into cultural peculiarities. Oliver Nakoinz from Kiel University was my supervisor, and I am grateful for his clear head and knowledge of the German academic system. I have had the great pleasure of having John Meadows as PI in the project and no matter how busy he was, he always made time for me.

I would like to thank the following people and institutions for providing me access to material and granting me permission to conduct destructive sampling: Lillian Matthes at Museum Southern Jutland, Tine Lorange at ARKVEST – Arkæologi Vestjylland, Mette Søvsø at Museum of Southwest Jutland, Michael Manøe Bjerregaard and Mogens Bo Henriksen at Odense City Museums, and Marie Louise Jørkov and Niels Lynnerup at the Unit of Forensic Anthropology, Copenhagen University. Claus Kjeld Jensen from Varde Museerne and Kamilla Terkildsen from Viborg Museum have both worked intensively with Aarupgaard urnfield and I was permitted to use their results in this project, for this I am very grateful. I thank Niels Algreen Møller from Museum Thy for providing access to CT-scans of material from Søhale urnfield cemetery, and for discussions on urnfield cemeteries as a wider phenomenon.

I would like to thank my family and friends for their patience and understanding these past years. My dear two boys were never great fans of me working away, but they were proud of their 'mummy writing a book'. Most importantly I would like to express my deepest gratitude towards my husband Simon Rose, without his loving support through everything none of this would have been possible.

INTRODUCTION

The question of *when* change occurred in the past is a fundamental aspect of archaeological research and has traditionally been approached by analysing material culture and creating chronological frameworks that divide the past into cultural epochs, such as *the Iron Age* (Gräslund 1974). Chronologies provide the basic framework for analysis although change in the material culture is often modelled as though it occurred simultaneously over large areas, and allow. Refining the chronological resolutions of the processes of change can help establish a more refined sense of regional difference and diversity and allow us to understand the timing and nature of change in the human past (Denaire et al. 2017).

This dissertation approaches the question of *when* by investigating temporal processes of change in material culture in a case study of Early Iron Age urnfield assemblages from Southern Jutland. Investigating small-scale transformations such as change in material culture is relevant because they can be regarded as an indicator of social and cultural transformations. The Pre-Roman Iron Age (c.500 BC) is the initial Iron Age period in Southern Scandinavia and the chronological framework has traditionally been based on artefacts of metalwork from urnfields, whereas pottery has only played a secondary role (Becker 1961; Jensen 2005). Metalwork is however practically absent from contemporary settlements, making it difficult to compare settlement and funerary evidence without a detailed typo-chronology that incorporates both metalwork and pottery. The dissertation thesis seeks to resolve this by applying a research approach that combines the prior archaeological information with radiocarbon data in a Bayesian framework and provides new independent insight into the temporal processes of change in metalwork and pottery artefact types (currencies). This approach will not only improve the current understanding of scales of transformation in material culture, but also enables a critical evaluation of the chronological framework of the period.

Research questions

This dissertation aims to investigate temporal processes of change in archaeological material culture and to improve the current understanding of scales of transformations. The Pre-Roman Iron Age in Southern Jutland, Denmark, is selected as case study, but because it coincides with a major plateau in the radiocarbon calibration curve (c.800-400 cal BC) there are precious few dates available. A major dissertation objective is therefore to produce a large radiocarbon dataset relevant for answering the following research questions:

- Can temporal processes of change in artefact currencies be modelled dynamically?
- Do metalwork and pottery types have divergent chronological sensitivities?
- Can metalwork and pottery typologies be correlated?
- Is the chronological framework of Pre-Roman Iron Age in Southern Scandinavia supported by the radiocarbon data?

Dating cremated bone is a relatively new method and because radiocarbon apply different pretreatment protocols on cremated bone it is a dissertation objective to test if these differences might affect the radiocarbon results.

The majority of datable material from the urnfields is cremated bone, which is susceptible to wood-age offsets. This causes calendar date offsets between the real cremation events and the radiocarbon dates, which can significantly affect the modelling outcome. It is a research objective, and prerequisite for answering the research questions, that a statistical method for formally handling wood-age offsets in cremated bone is developed.

Research approach

Before the archaeological dataset can be modelled the research objectives need to be addressed. The effect of pretreatment protocols on radiocarbon results on cremated bone measured at three radiocarbon laboratories is tested through a comparison dating program (Paper 3: Rose et al. 2019). The program compares replicate measurements in order to compare differences in pretreatment protocols and specific step of the conversion and measuring process. The other research objective of proposing a statistical model for handling the unknown wood-age offsets in cremated bone necessitates the inclusion of additional datasets that provide important insight into the different types of offsets that might affect radiocarbon dates and how these might be modelled statistically. An experimental case study is included in order to investigate the scale and scatter of empirical wood-age offsets in cremated bone with a known-age. Additionally, a Neolithic case study is included (Paper 1: Kristiansen et al. forthcoming), because it allow modelling of wood-age offsets in charcoal with varying intrinsic ages. Together with a medieval case study (Paper 2: Rose et al. 2018), that allow modelling of dietary offsets and of individual offsets tailored to specific material. Based on the additional datasets a new statistical model is proposed and applied to all radiocarbon dates on cremated bone within this dissertation project.

With the research objectives in place the corrected radiocarbon data can be combined in a Bayesian framework with prior information on artefact typology and site formation processes, i.e. how the urnfields developed spatially over time or how the graves relate to each other stratigraphically (Fig. 1). This allows the temporality of transformations in the urnfield assemblages to be modelled dynamically and the comparison of processes of change. The chronological framework of Pre-Roman Iron Age in Southern Scandinavia is critically evaluated using probabilistic chronologies.

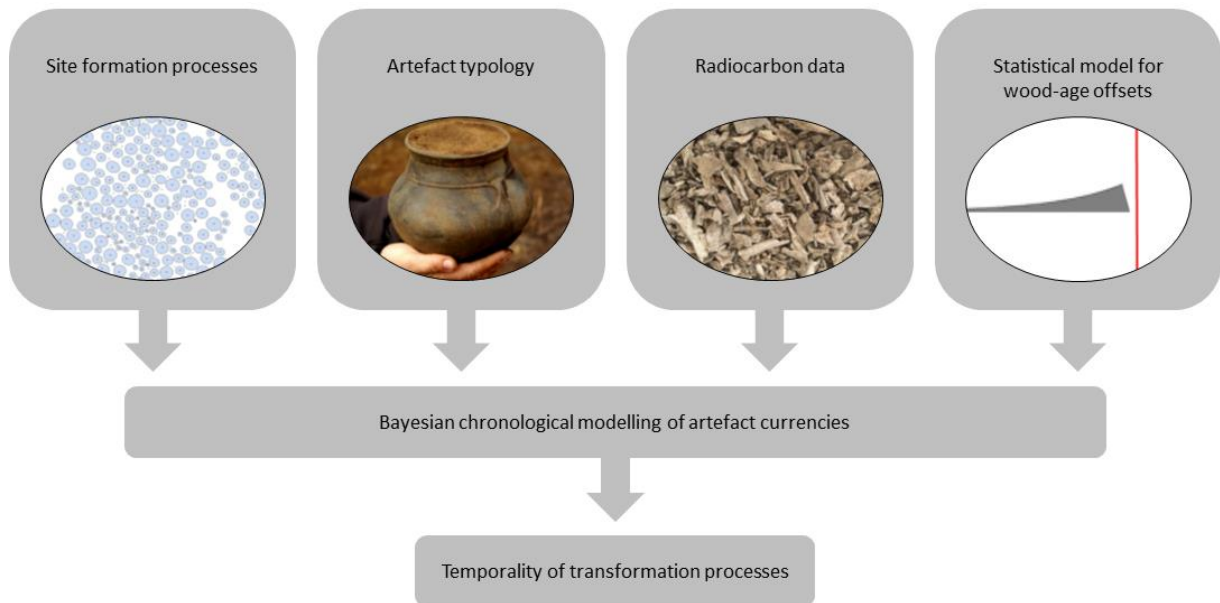


Figure 1: Schematic illustration of the dissertation research approach.

Outline of the dissertation

The cumulative dissertation thesis is largely based on results presented in Paper 1-4 (Rose et al. 2018; Rose et al. 2019; Rose et al. 2020; Kristiansen et al. forthcoming). The main body of the thesis is divided into three parts: Part A providing the archaeological background and main methodological tools; Part B introducing statistical outlier modelling of radiocarbon data; and Part C presenting a large study of artefact currencies from the Early Iron Age in Southern Jutland, Denmark.

Part A introduces the use of typo-chronology as an archaeological method for ordering material culture and interpreting change in the prehistoric record. The Pre-Roman Iron Age in Denmark and a chronological framework are presented, along with the urnfield burial tradition and cultural connections that has come to mark the onset of the Iron Age. Radiocarbon dating in archaeology is introduced with particular attention to the relatively recent method of dating cremated bone. For this

reason it is necessary to investigate methodological aspects relating to laboratory techniques and a laboratory intercomparison is carried out in collaboration with researchers from Kiel, Groningen and Brussels (Paper 3: Rose et al. 2019). Finally the basic principles of Bayesian chronological modelling are introduced along with a review of published studies modelling artefact currencies and theories on the life of an artefact type.

Part B presents different types of outliers and offsets that might affect radiocarbon data and through a series of case studies, involving the urnfield material but also additional case studies, the statistical modelling of such outlier dates is explored. One case study includes the paleo-dietary reconstruction of a medieval multiple grave at St Albans Odense based on stable isotope analysis and tailoring individual offsets to match the difference between intrinsic ages of collagen and ages-at-death (Paper 2: Rose et al. 2018). Another case study includes estimation and modelling of varying intrinsic ages of the charcoal from the Neolithic Rokaer long grave (Paper 1: Kristiansen et al. forthcoming). Part B is mainly concerned with wood-age offsets in cremated bone and an investigation into the empirical distributions of these offsets in an experimental dataset is carried out in collaboration with Mogens Bo Henriksen from Odense City Museums. Offsets are further tested and refined using combinations of short-lived archaeobotanical remains and cremated bone from Aarre urnfield, and based on these results a new statistical model is proposed for modelling wood-age offsets in cremated bone dates (Paper 4: Rose et al. 2020).

Part C presents a case study of artefact currency modelling of three Early Iron Age urnfield assemblages from Southern Jutland. A large number of graves from Aarupgaard, Aarre and Søhale urnfields are ¹⁴C dated in collaboration with Museum of Southwest Jutland, ARKVEST, and Museum of South Jutland. Temporal aspects of change is documented for 24 artefact types of metalwork and pottery and chronological models are provided for 14 of these. The currency models provide independent evidence of different temporal patterns of production increase and decrease and periods with higher and lower rates of change in material culture are identified. The significance of residence offsets is discussed and the regional differences in rates of change is tentatively explored. Site models are presented for the three urnfields and finally the chronological framework of the period is critically evaluated.

PART A BACKGROUND

Introduction to typo-chronology

Prehistory can be described in terms of long-term transformations, i.e. from stone to metal technology, but any transformation entails a multitude of smaller-scale transformations, such as change in material culture. Sequential ordering of archaeological material is a fundamental part of interpreting such change (Brainerd 1951; Plog and Hantman 1990), and it can help us understand how change in one domain of a society, such as change in the material culture or the introduction of a new burial practise, might be linked to broader transformations in the society and its environment. Typo-chronologies are good at showing long-term and geographically broad patterns of change in the archaeological record, but because every system is based upon different choices with regard to data selection, analysis and interpretation, every system will present a different version of the past.

Artefact typologies describe and create entities according to a set of formal morphological characteristics (e.g. weight, height, colour), followed by a seriation. It is a heuristic tool, aiming to describe a specific artefact as opposed to similar objects that preceded it and followed it (Fowler 2017), creating schemes of relatedness of types (Stig Sørensen 2015). It relies on the idea that every artefact is a copy of an 'ideal' (Normark 2010), but Fowler has suggested ideals do not exist but to rather perceive artefact types as arising from similar iterative processes in the past (Fowler 2017). Several different types might be contemporaneous, as their 'relatedness' does not imply a linear chronological sequence (Stig Sørensen 2015). Typology has an inherent risk of forcing artefacts into too rigid schemes, obscuring or even erasing their differences (Boozer 2015), but typology it is nonetheless indispensable for understanding change and continuity (Fowler 2017).

Seriation of artefact typologies relies on three basic principles: all artefacts from a 'closed find' are contemporaneous; layers are deposited in stratigraphic succession with the oldest at the bottom and the youngest at the top; change in material culture occurs gradually and artefacts close in time are more likely to look similar than chronologically distant artefacts (Gräslund 1974; Trachsel 2004). Sorting large numbers of attributes or variables into matrices are computational demanding and have since the 1980s often been carried out using correspondence analysis (Jensen and Høilund Nielsen 1997; Bayliss et al. 2013a; Kneisel 2013). Established seriations can then be grouped into relative chronological units of periods, phases or horizons, and archaeologists have since the 19th century strived to construct increasingly detailed chronologies on the assumption that change in material culture is gradual and continuous (Parzinger 1989; Trachsel 2004; Roberts et al. 2013). The frequent

use of type fossils¹ is problematic in this regard (Jensen 2005), and it is debatable whether the chronological divisions carry real cultural meaning (Malmer 1984). The construction of chronological blocks cause the systems to treat transitions between periods as abrupt events, disregarding the temporality of transformation processes within and between individual phases. This inevitably obscures the small-scaled transformation processes in the material culture, e.g. did the introduction of a certain type occur slowly or rapidly? Typo-chronological systems however remain essential for interpreting the archaeological record.

Burials have traditionally provided closed context material for typo-chronological analyses (e.g. (Becker 1961), but because mortuary practices are often conservative in nature (O'Shea 1984; Pearson 1999), the temporal scale of grave good chronologies might not equal the temporal scale otherwise observable at contemporaneous settlement sites (Zavodny et al. 2019). It has been suggested that pottery from graves are not representative of the style otherwise in use at the time of death, but rather a style produced or selected specifically for funerary purposes (Strien 2019). Also the possibility of objects being passed down generations as heirloom objects pose a threat to chronological analyses of burial assemblages (Trachsel 2004), leading to a need of evaluating the existing typo-chronologies and solving such possible temporal discrepancies using radiocarbon dating.

¹ A type fossil is a specific type of artefact with a wide geographical distribution, but a restricted distribution in time. Its presence in a context is used as an indicator of a specific period or culture, and it might be used to cross-date across larger regions and correlate typo-chronological frameworks.

Pre-Roman Iron Age in Denmark

In the early years of archaeology, the Iron Age was thought to have been brought to Scandinavia by Roman influences (Thomsen 1836; Worsaae 1859; Gräslund 1974), but with a growing mass of material from most importantly Hallstatt in Austria (Sacken 1868) and La Tène in Switzerland (Keller 1858; Desor 1865), it was realised that the Iron Age started centuries before Roman artefacts appear in Scandinavia (Vedel 1872; Undset 1881). In 1886 Professor J. Mestorf presented urnfield material from Schleswig-Holstein belonging to this Pre-Roman Iron Age period (Mestorf 1886), whereas the Danish urnfield assemblages have been investigated since the early 1890s, when antiquarians from the Danish National Museum travelled the country parish by parish and registered places of archaeological interest (Neergaard 1892; Madsen and Neergaard 1894). With the large find material from the newly excavated urnfield graves, C. Neergaard was able to establish the presence of the Pre-Roman Iron Age in Jutland, and describe the Danish urnfield phenomenon in detail (Neergaard 1892; Madsen and Neergaard 1894). He later transferred results from Schleswig-Holstein (Knorr 1910) and divided the material from Jutland into three periods (Neergaard 1916). More urnfields were excavated in the next decades with the aim to obtain datable material for typo-chronological studies (Neergaard 1916; Neergaard 1931; Neumann 1947). Professor C. J. Becker conducted a large excavation of Aarre urnfield in 1954-54, which he later published in a large monograph presenting Pre-Roman Iron Age material from Southern and Central Jutland, along with a discussion on the Danish urnfield phenomenon (Becker 1961). He retained the three chronological periods corresponding to Central European La Tène I-III, but divided period I into phases I.a and I.b, and period III into phases III.a and III.b.

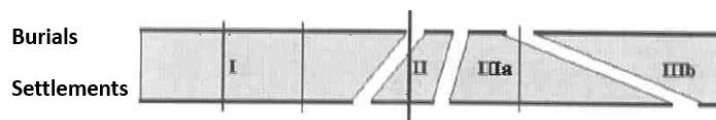


Figure 2: Correlation of Pre-Roman Iron Age chronologies used on material from burials and settlements in Jutland (from Jensen 1996: 200).

Becker's chronology remains highly influential in Danish archaeology, although C.K. Jensen has demonstrated it to produce an uneven distribution of material over the Pre-Roman period, when applied to pottery and metalwork respectively (Fig. 2) (Jensen 1992; Jensen 1996). He has also shown it to be difficult to harmonize the materials, possibly because of divergent chronological sensitivities (Jensen 1996). Metalwork typology has been assumed to be chronologically sensitive with more rapidly changing typological traits, whereas pottery types are considered to be more 'conservative' and longer-lasting (Hingst 1959). Mixed find assemblages of metalwork and pottery artefacts are almost exclusively found in urnfield burials, and without a detailed chronology for pottery, it is impossible to

compare settlement and funerary evidence, i.e. to understand how changes in funerary practice are connected to broader transformations in society.

Conventionally the transition from Late Bronze Age to Early Pre-Roman Iron Age in Denmark is set to occur around 500 BC (Vandkilde et al. 1996; Jensen 2005), but it is difficult to test this because of a lack of directly datable objects from specifically Late Bronze Age. Additionally, there is a lack of artefacts with a wider European distribution, inhibiting cross-referencing of dates. Even though dress pins is a European-wide tradition starting in the Early Bronze Age (Stockhammer et al. 2015), most types are restricted to Northern Germany (Hingst 1980) or even to Southern Scandinavia (Becker 1961; Jensen 2005). Olsen et al. (2011) have published a chronological model suggesting the final Bronze Age period VI to end 762-411 BC (*95.4% probability*). Jensen (1997) has suggested the transition to occur already 530-20 BC, coinciding with the HaD1-D2 transition, and in a recent study of Søhale urnfield by Møller et al. (2020) the transition is estimated to occur in the second half of the 6th century BC. The same study estimates the transition period I.1 – I.2 to occur around 400 BC. The transition from Early to Late Pre-Roman Iron Age (period I – II) is traditionally set to around 200 BC, by cross-referencing fibulas to La Tène D in Central European (Jensen 2005). Martens (1996) have suggested the transition to occur slightly earlier around 250 BC, which is supported by Møller et al. (2020) who estimate it to occur in the early or middle of the third century BC.

The Danish urnfield tradition

Cremation has been practiced occasionally throughout prehistory, and it was the dominant burial practice in Denmark in the Late Bronze Age and Early Iron Age. In the Late Bronze Age cremation graves were interred in existing burial mounds, but with the beginning of the Iron Age (c.500 BC) large collective burial grounds were established. The Danish urnfield phenomenon was first described by A. P. Madsen and C. Neergaard, at a time when the mounds were still visible in the heathland landscape (Neergaard 1892; Madsen and Neergaard 1894). They excavated the central part of close to 500 mounds in order to retrieve material for typo-chronological studies. Even though they largely ignored the rest of the monument, C. Neergaard nonetheless soon concluded that the character of the urnfield graves were so homogenous, that future excavations were not likely to alter this picture (Madsen and Neergaard 1894).

The new funerary practices appear to have been swiftly integrated in the Danish area, yet adjusted to incorporate local traditions (Jensen 2006). It lasted c.300 years, largely corresponding with the Early

Pre-Roman Iron Age (Becker 1961; Jensen 2005; Møller et al. 2020). To date, 66 certain and another 22 possible urnfields have been recorded. They are primarily situated in south and southwest Jutland, but also occur in eastern Jutland and even on Lolland (Møller et al. 2020). They vary in size from a few graves as at Tuesbøl (Dollar and Grundvad 2015), Jernvedlund (Møller 2013), and Grøntoft (Rindel 2015), over a few hundred graves as at Veldbæk and Søhale (Møller et al. 2020), to more than 1000 graves at Aarre (Becker 1961; Lorange 2015b), and Aarupgaard (Jørgensen 1975; Terkildsen 2015). The urnfields are an integrate part of the Pre-Roman cultural landscape, continuing the Bronze Age tradition of demarcating major routes of transport by lines of burial mounds, but at the same time separate from contemporary settlements. The cemeteries are often constructed in the vicinity of Neolithic or Bronze Age barrows, showing a continuity across millennia in the cultural landscape (Møller 2013). It has been suggested to interpret the cemeteries as sites for large communal gatherings of an otherwise geographically dispersed population (Lorange 2015b). It would appear that they express the solidarity of a group and consolidate their territorial structure, as is also expressed by use of Celtic fields systems (Fokkens 1997).

Following the Danish urnfield tradition the deceased were cremated, and the cremated bone and possible dress accessories were subsequently deposited in ceramic vessels (a traditional 'urn grave'). At some cemeteries a small part of the pyre debris (i.e. charcoal and other charred archaeobotanical remains) were also transferred to the urn. All urn graves are classified as secondary deposits, and so far no cremation pyres have been located in the vicinity of the burial grounds (Møller et al. 2020). A few urns have a flat stone as lid (Becker 1961), but lids of organic material cannot be ruled out (Jørgensen 1975). The urns were buried individually by placing them either on the ground or in a small pit, which were sometimes lined with stones. The grave could be covered by a stone paving as at Uldal urnfield (Ethelberg et al. 2003), but the majority was covered by small barrows or hillocks. Also other graves types occur, such as 'bone-layer graves' (German: *Brandgrubengräber*) without a (discernible) container and without substantial amounts of pyre debris, 'urn-bone layer graves' as a hybrid burial form containing cremated bone and pottery shards and possible cenotaph graves (Harvig et al. 2014b). Some graves contain more than one vessel, either deposited within the barrow or in the circular ditch (Jørgensen 1975; Terkildsen 2015). Approximately a third of the urn graves contain burial goods, representing a limited range of dress accessories and other related adornments, allowing the sites to be relatively dated to the Pre-Roman Iron Age (c.500-200 BC) using typo-chronology.

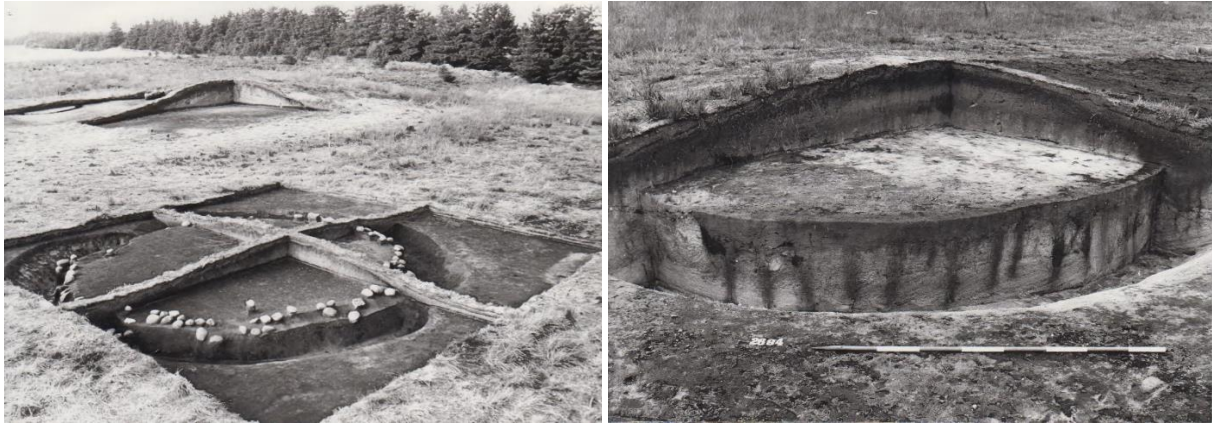


Figure 3: Excavation at Aarupgaard urnfield. To the left, the circular ditch has been emptied out and the curb stones are visible. To the right, dark marks after wooden posts placed inside the circular ditch (pictures by Museum of South Jutland).

C. Neergaard was the first to register circular ditches enclosing the largest mounds (Neergaard 1892; Madsen and Neergaard 1894), but at Aarre urnfield C.J. Becker observed circular ditches around almost all mounds. He also observed interruptions in the ditches, forming bridges or pathways into the central barrow (Becker 1961). The mounds are created by using the soil from the circular ditch, and have diameters from a few meters and up to 14.5m (Frandsen and Jørgensen 2013). Occasionally, additional soil would have been needed to give the mounds the estimated original height of 1-2 m. At Aarupgaard urnfield E. Jørgensen observed that some mounds were demarcated with kerbstones (Fig. 3), or wooden posts inside of the circular ditch, but similar features have not been observed at other cemeteries. By cross sectioning the urnfield mounds, he was able to refute earlier theories that the urn had been inserted into the mound through a central shaft, and instead interpreted the stratigraphy as soil settling, following the collapse of an organic urn lid (Jørgensen 1975).

Small and large mounds are closely spaced, but do in general not inter-cut one another (Jørgensen 1975), possibly because the ditches were left open and clearly demarcating the monument (Møller et al. 2020). It is difficult to determine any direct stratigraphic relationship between graves, but early on, C.J. Becker (1961) pointed out how graves are often arranged in lines, creating a form of horizontal stratigraphy. This phenomenon has later been confirmed (Jørgensen 1975; Jensen 1996; Martens 1996).

Cultural affiliations

The Danish Pre-Roman Iron Age appears to be a hybrid cultural group, whose urnfield funerary practises resemble urnfields from the Jastorf core area in Holstein and Mecklenburg, and the Lower Rhine area (Mestorf 1886; Schwantes 1911; Hingst 1959; Hingst 1980; Hingst 1986; Fokkens 1997; De Mulder et al. 2009; Møller et al. 2020). The German scholar Gustav Schwantes (1911) included Jutland into the area of the Jastorf culture with its core area found in Holstein and East Hannover, based on common traits in burial custom and dress accessories. This was disputed by C. Neergaard, who instead emphasized a close relationship between material from Southern Jutland and Northern Jutland (Neergaard 1916). The disagreement of cultural affiliation of the Early Iron Age in Denmark was probably rooted in the contemporary political situation regarding the Danish-German border in Schleswig (Martens 2014; Møller et al. 2020). Even today, Danish scholars discuss the Pre-Roman Iron Age as a cultural period in Southern Scandinavia, but without mentioning cultural groups (although see Martens 2014).

The Danish urnfield tradition is a late part of a wider European tradition, although in Continental Europe its onset marks the beginning of the Late Bronze Age (Fokkens 1997), rather than the onset of Early Iron Age as in Denmark. Regardless of timing, the urnfield tradition marks a fundamental break with the earlier burial practices, which has, along with a number of other archaeological phenomena, been explained as being caused by migration from Central Europe (Childe 1950). This 'migration paradigm' was rejected in the 1970s, where 'social change' was instead emphasized as causing transformations (Renfrew and Bahn 2001). New Archaeology interpret economic processes or crises as transformation triggers, but Fokkens (1997) has pointed out how this fails to explain changes in a culture's ideology, i.e. changes in funerary rites. Specifically, "*an economic crisis does not explain why in the Late Bronze Age almost every individual was allowed to become visible as an ancestor, whereas in the Middle Bronze Age only a small selection of the population was entitled to this privilege*" (Fokkens 1997: 369). He instead proposes that a social and ideological transformation of the prehistoric communities acted as a transformation trigger, which was first visible in the urnfield burial practice. In opposition to the previous period, it is assumed that the urnfields represent the entire population, allowing practically everyone to be transformed to ancestors. There are still differences in the treatment of the dead, although these are less obvious, i.e. inclusion of burial goods and size of barrows. For the Dutch area, Fokkens' view these changes in ideology and social organization in relation to exchange, coinciding with a period of an increased production and deposition of bronzes (Fokkens 1997). This is not immediately transferrable to the Danish area, but the introduction of iron

technology and new exchange networks along with a change in social organization (Hedeager 1990; Jensen 2006) could be argued to serve as a comparable transformation trigger.

Recent years has seen a return to the 'migration paradigm' or population replacement, but hopefully interpreted in a more nuanced context (Ion 2017). A paleo-mobility study of burials from the central Netherlands using strontium isotope analysis, shows an increasing heterogeneity of the population in terms of provenance in the 6th century BC, coinciding with a change in burial rite from only cremation graves to a mixture of inhumation graves and cremation graves (Kootker et al. 2018). Whether this was introduced or catalysed by the presence of foreign individuals and/or cultures remains debatable as only inhumation graves were studied. Additional research including cremations graves are needed in order to validate the authors' conclusion that the presence of foreign cultures may have introduced a shift in the Iron Age burial practice. Another paleo-mobility study on Iron Age (500 BC – AD 400) inhumations graves from the Swedish island of Öland also identified a substantial part of the population as being non-locals (Wilhelmson et al. 2015; Wilhelmson and Price 2017). The introduction of the urnfield burial tradition in the Danish area might possibly also be seen in relation to mobility, but this questions remains unanswered as analytical results are lacking at this point.

Chronological framework

It is the chronological framework of C.K. Jensen (2005) that is applied and tested in the present dissertation. Jensen initially analysed material from Aarupgaard urnfield using correspondence analysis (1996), but later expanded to include material from both burials and settlements from Southern Scandinavia in a revision of the chronological basis for Pre-Roman Iron Age (Jensen 2005). His aim was to seriate all available find combinations within closed finds, weighing metalwork and pottery equally. Based on clusters in his correspondence analyses, he divided the material into 10 burial phases and five settlement phases, correlated by the pottery. Burials are dated by their 'mean', and not by the youngest artefact, as C.K. Jensen specifically avoids the use of type fossils. He observed a break in between Early Pre-Roman Iron Age (burial phases 1-6 and settlement phases 1-3) and Late Pre-Roman Iron Age (burial phases 8-10 and settlement phases 4-5), with burial phase 7 as an intermediate phase. He observed a gradual transition from Bronze Age to Iron Age, but a clear break from Early to Late Pre-Roman Iron Age.

Based on these results, C.K. Jensen divided the Pre-Roman Iron Age into two main chronological periods, which are then further divided into sub-periods and phases specific to the geographical area.

The correlations between Becker’s and Jensen’s Pre-Roman Iron Age chronologies are depicted in Figure 4 (Jensen 2005). He correlated his regional chronologies from Holstein, Jutland, Funen, Bornholm and Gotland and created a master typo-chronology of the Pre-Roman Iron Age in Southern Scandinavia (Fig. 5). The Danish urnfields were mainly in use in period I.1-2, although Aarupgaard was probably in use up until period II.1. No artefact types relatively dated to period II.2 are however included in this investigation.

Becker	Jensen	
Ia	I.1	I.1a
		I.1b
		I.1c
Ib	I.2	I.2a
		I.2b
		I.2c
II	II.1	II.1a
		II.1b
IIIa	II.2	II.2a
IIIb		II.2b

Figure 4: Correlations of Pre-Roman Iron Age chronologies by Becker (1961) and Jensen (2005) (from Jensen 2005, vol.1: 98).

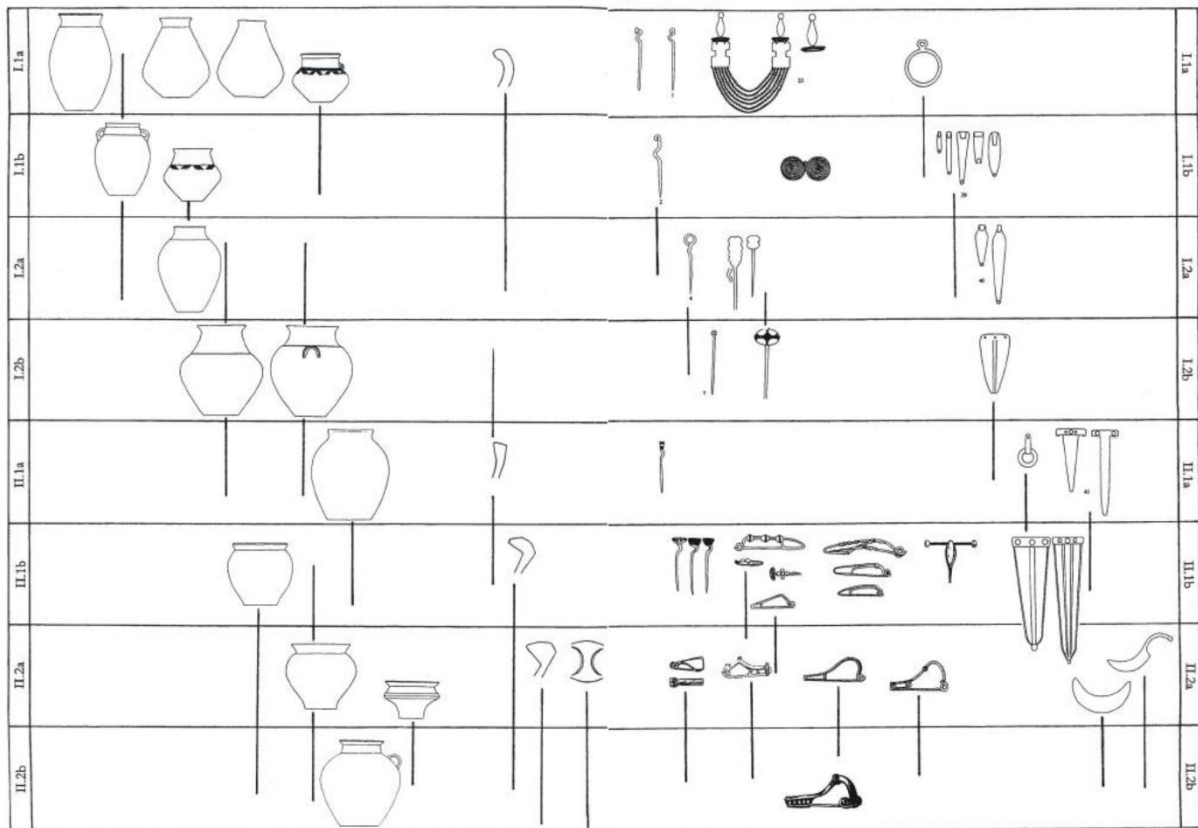


Figure 5: Master typo-chronology of the Pre-Roman Iron Age in Southern Scandinavia. The most prevalent artefact types are placed in the phases where they have the highest frequencies (from Jensen 2005, vol.1: 164-65).

Metalwork typology

There are no weapon graves from the period and all metalwork artefacts are related to the personal dress attire. Dress pins from the Bronze Age are made in bronze, but with the onset of Early Iron Age the pins are now primarily made of iron. Certain pin types along with neck rings do however continue to be made of bronze. More types of pins and belt equipment are also known from Holstein in Northern Germany (Hingst 1959; Hingst 1980; Hingst 1986), whereas pins with coiled heads appears to be restricted to Southern Scandinavia. The repertoire of pins in the Danish area are restricted compared to Holstein.

The earliest pin type has a coiled head and a bend in the upper part of the pin, just beneath the head (Fig. 6a) (Becker 1961). In period I.1b-I.2a the bend moves down the needle, creating a neck beneath the head (Fig. 6b) (Becker 1961). In period I.2 pins with a circular head are introduced (Fig. 6c) (Jensen 2005), along with pin types with *bomb-shaped head* (Fig. 6d) or *spade-shaped heads* (Hingst 1959). The

youngest pin type are *Holstein pins* (Fig. 6e) (Hingst 1986) dating to period II.1. Contemporaneously with the pins are different types of belt related equipment. The earliest type occurring in period I.1 are *iron ring with eyelet* (Fig. 6f) (Hingst 1986). In period I.1b belt buckles with protruding clasps are introduced, initially they are *tongue-shaped* in outline (Fig. 6g), then *triangular* (Fig. 6h) and by period II.1 they are *narrow* in outline (Fig. 6i) (Hingst 1980). Also occurring in period II.1 are *iron rings with shank* (Fig. 6j) (Hingst 1980).

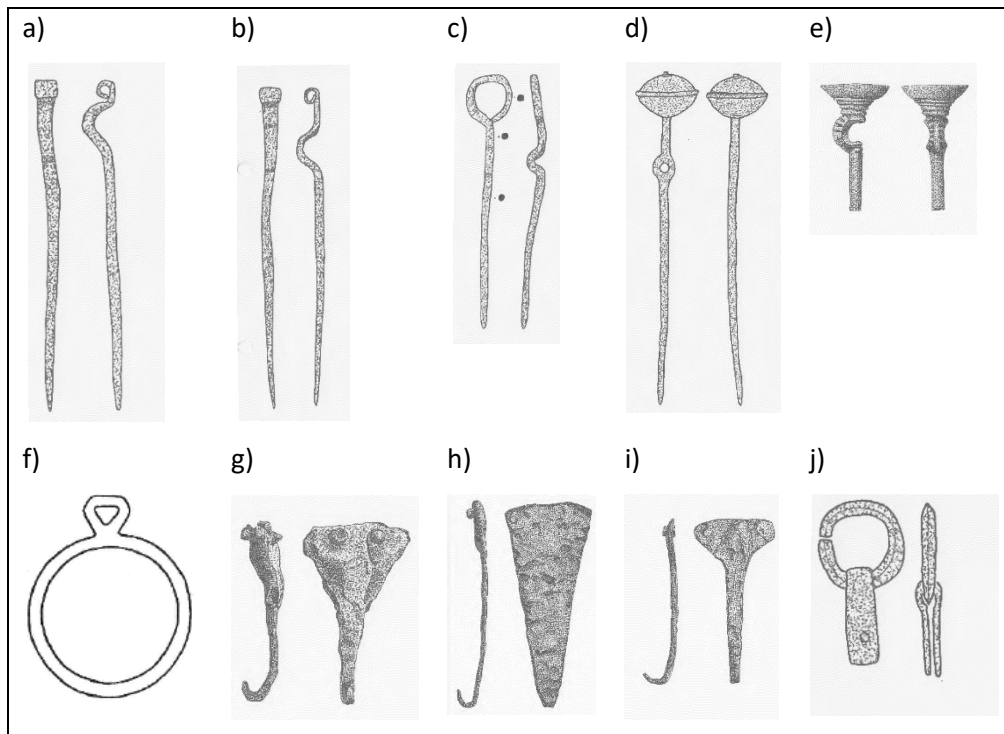


Figure 6: Types of dress pins and belt related equipment. a) pin with type 1 coiled head, b) pin with type 2 coiled head, c) pin with circular head, d) pin with bomb-shaped head, e) Holstein pin, f) iron ring with eyelet, g) tongue-shaped belt clasp, h) triangular belt clasp, i) narrow belt clasp, j) iron ring with shank. Drawings of artefacts are from Aarupgaard urnfield (Museum of South Jutland), except illustration (f) from Jensen (2005, vol.2: 25)).

Jensen (2005) differentiates between pins with small and large circular head. Small heads are defined as having a head diameter less than 2 x the pin width, and large heads as having a diameter larger than this. Figure 7 plots the pin size index (diameter of inner head / pin width) of 22 pins with circular heads from 11 graves at Aarupgaard urnfield, showing a large variety in sizes from the smallest to the largest. Only two pins can be defined as having a 'small circular head' (head size index > 2). The size index is continuously distributed showing no clear typological categories. Based on this, it can be suggested that pins with circular head belong to one typological group, although with varying sizes of the head.

This analysis only incorporate material from Aarupgaard, and it is therefore possible that it is a site specific trait, but within this dissertation pins with circular head will be treated as a single type.

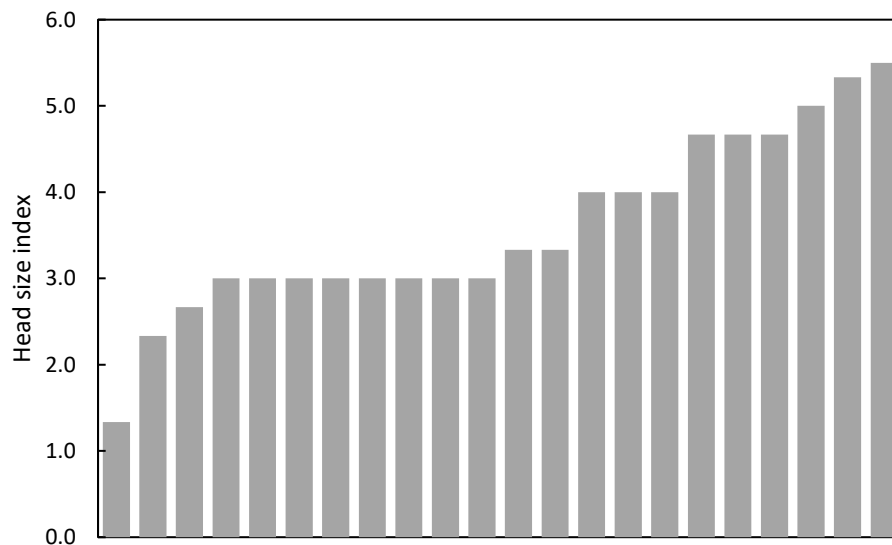


Figure 7: Distribution of head size index (inner head diameter divided by pin width) of pins with circular head from Aarupgaard urnfield.

Pottery typology

The full pottery repertoire found at settlement sites includes storage vessels in different sizes, small bowls, cooking vessels, open dishes and cups. Only a subset of these occurs at burial sites, where mainly small to medium sized storage vessels are used as funerary urns, and small bowls and cups as accompanying vessels (Jensen 1996; Jensen 1997; Jensen 2005). Ornamentation is rare but do occur (Jensen 2005; Martens 2017).

Jensen has divided the vessels into groups based on proportions (height and width). Individual type names have a number referring to the shape of the vessel body (Table 1), and a capital letter referring to the shape of the vessel neck (Table 2). A number of types are in use for most of the Early Pre-Roman Iron Age and then disappear at the transition to Late Pre-Roman Iron Age, when a number of new types are introduced. Vessels with shape 11, 12 and 13 with cylindrical or concave neck are most prevalent in Early Pre-Roman Iron Age, as are vessels with shape 16, 17 and 20 with no neck in Late Pre-Roman Iron Age. It is possible to further subdivide the Early Pre-Roman Iron Age into early types 13A, 13C, 11A, 12A and 11D, and late types 13B, 13D, 18C, 15B and 15C.

Table 1: Descriptions of vessel body shapes (Jensen 2005).

Code	Shape of vessel body
11	Double conical shape, widest point in the lower part of the vessel
12	Double conical shape, widest point in the central part of the vessel
13	Evenly curved vessel
14	Domed, widest point in the central part of the vessel
15	Domed, widest point in the upper part of the vessel
16	Domed lower body, straight upper body, widest point in the upper part of the vessel
17	Domed lower body, conical upper body, widest point in the upper part of the vessel
18	Domed lower body, widest point in the absolute upper part of the vessel
19	Slightly domed – lenticular shape
20	Domed, widest point in the central part of the body – almost round corpus shape

Table 2: Descriptions of vessel neck shapes (Jensen 2005).

Code	Shape of vessel neck
A	Cylindrical
B	Conical
C	Concave
D	Rim, but no neck
E	Conical rim, but no neck

Radiocarbon dating in archaeology

Radiocarbon dating is a standard method in archaeology for determining the age of ancient material and it has had a significant influence on our perception of the past (Bayliss 2009). Arnold & Libby proposed the dating method in 1949 after observing that decay of ^{14}C could be used to assess the elapsed time since a material stopped sequestering carbon. They assumed the amount of ^{14}C in the atmosphere to be stable and assessed a half-life of 5720 ± 47 years (Arnold and Libby 1949), which was later corrected to 5568 ± 30 years (Libby 1952), also known as 'The Libby half-life'. Conventional radiocarbon ages are for historical reasons still calculated using the Libby half-life (Stuiver and Polach 1977), even though the first half-life was closer to the correct half-life 5730 ± 40 years (Godwin 1962). Libby was awarded the Nobel Prize for Chemistry in 1960 for developing the method (Taylor 2016).

Carbon is a chemical element with three naturally occurring isotopes: most abundant of these is ^{12}C with six neutrons (98.89% of the carbon atoms on Earth), followed by ^{13}C with seven neutrons (1.11%) and ^{14}C with eight neutrons that only occurs in trace amounts (c. one in every trillion (10^{12}) C atoms). The ^{14}C isotope is radiogenic, meaning it will spontaneously emit a β particle (electron) (Trumbore et al. 2016). ^{14}C is produced in the upper atmosphere where thermal neutrons react with the nitrogen atoms in air, but the production rate varies due to changes in cosmic rays and variations in the Earth's magnetic field. ^{14}C reacts with the free radical OH and initially forms ^{14}CO , followed by $^{14}\text{CO}_2$. The $^{14}\text{CO}_2$ is mixed through the tropopause into the troposphere with a mixing time in the order of weeks (Bronk Ramsey 2008b). The movement of carbon in the Earth's biosphere, hydrosphere, atmosphere, and geosphere is described as a 'carbon cycle' (Schoor et al. 2016). The oceans provide a large carbon reservoir with a much slower mixing time (or even residence time), increasingly so in the deep oceans. The ocean surface is on average c. 5% depleted in ^{14}C , which corresponds to about 400 ^{14}C yr. Atmospheric CO_2 is sequestered as organic carbon in living organisms through photosynthesis, but will start decaying after the organisms die (Bronk Ramsey 2008b). Atmospheric nuclear bomb testing has since the mid-1950s caused a massive influx of radiocarbon, almost doubling the concentration in the atmosphere in the mid-1960s (Hua et al. 2013). Also the rising use of fossil fuels on a global scale is contributing fossil carbon into the atmosphere at an unprecedented rate. Post-bomb ^{14}C data is indicative of ^{14}C activity of the atmosphere rather than radioactive decay, which has proven useful in forensic, biology, and geosciences (Reimer et al. 2004). It has only found limited use in archaeological research, but it was important for analysing the modern experimental dataset used in this dissertation (Part B).

The mass difference between ^{14}C and ^{13}C is twice that between ^{13}C and ^{12}C , which can be used to predict mass-dependent fractionation in the ^{14}C content of organic matter (Trumbore et al. 2016). Radiocarbon laboratories use accelerator mass spectrometers (AMS) to measure $^{14}\text{C}/^{12}\text{C}$ and $^{13}\text{C}/^{12}\text{C}$ isotope ratios, in order to correct the reported ^{14}C -content for fractionation. This process also includes background corrections by measuring blanks and internationally agreed standards, e.g. the carbonate fossil *Bellemnitella americana* from the Pee Dee formation in South Carolina (PDB) and the NIST OX-II standard (Wood 2015). Backgrounds and standards are also used to test that samples have been adequately pretreated. It was Libby who few years after the dating method was introduced realized that archaeological samples needed to be 'laundered' (1952), i.e. pretreated to remove exogenous sources of carbon. Radiocarbon laboratories are continuously developing and improving protocols of physical and chemical steps to remove the most likely contaminants (Wood 2015). The corrected ^{14}C -content is reported in pMC (percent Modern Carbon) or $F^{14}\text{C}$ (fraction modern) related to a hypothetical atmospheric value of 1950, and used to calculate radiocarbon ages according to Stuiver and Polach (1977). Calibrated radiocarbon ages are reported as cal BP (before 1950), as opposed to conventional BP (before present).

A radiocarbon age is normally distributed, but using the basic intercept method to calibrate it will produce a date range or set of ranges corresponding with the earliest and latest points that the radiocarbon age and its error term intercept with the calibration curve (Stuiver and Reimer 1986). Calibrated dates have a tendency to spread across centuries because of the non-linear nature of the calibration curve, but at some point within this range, the radiocarbon 'event' occurred. The calibration program OxCal (Bronk Ramsey 1995) calibrates radiocarbon ages using the probability method (Stuiver and Reimer 1993), which is essentially Bayesian and produces probability distributions for the radiocarbon event on the calendar scale (Bronk Ramsey 2009a). Depending on the error terms of the radiocarbon age, the shape of the calibration curve can significantly influence the length of the calibrated probability distributions (e.g. simulated distributions marked in red in Fig. 8), such as the so-called Hallstatt plateau in the middle of the first millennium cal BC (c.800-400 BC), or the radiocarbon inversion around 350-250 BC (red circles in Fig. 8). Dates falling on these parts of the calibrations curve are heavily affected and it has been largely detrimental to Iron Age research (Hamilton et al. 2015), and specifically to research into the Danish urnfield phenomenon (c.500-200 BC, grey area in Fig. 8). Hopefully single-year dating will in the future reveal more structure of the calibration curve in this period.

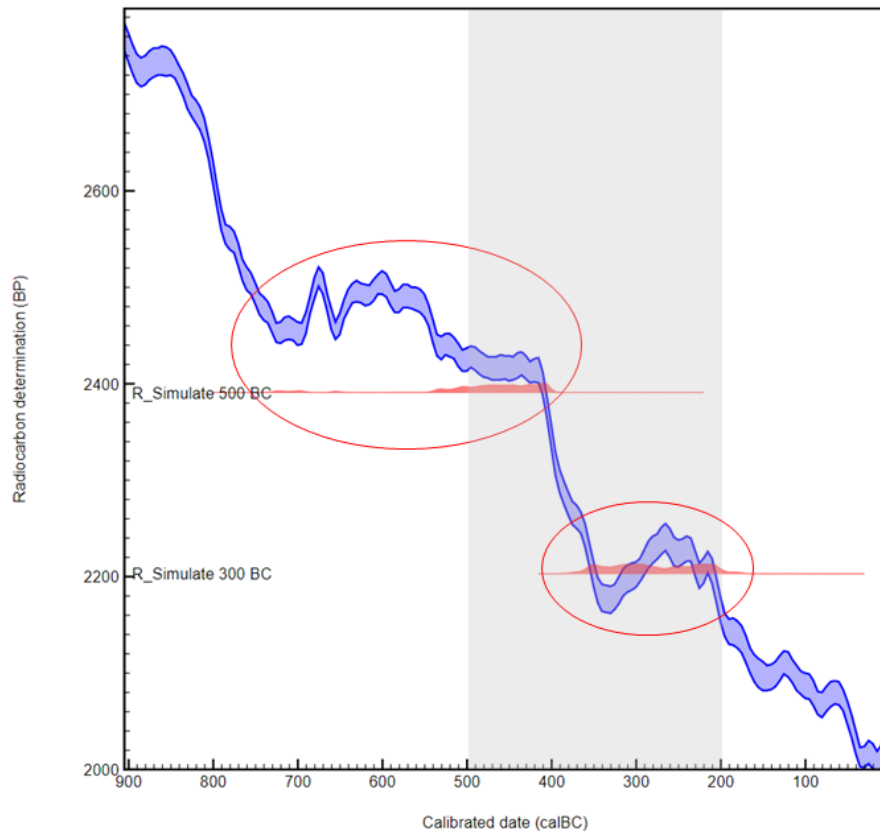


Figure 8: Simulated radiocarbon dates with true calendar dates 500 BC and 300 BC have been calibrated and plotted in red against the IntCal13 calibration curve (Reimer et al. 2013). The Hallstatt plateau c.800-400 BC and the radiocarbon inversion around 350-250 BC are circled in red. The Danish urnfield phenomenon c.500-200 BC is marked in grey.

Where Libby had assumed the amount of radiocarbon in the atmosphere to be stable through time (Arnold and Libby 1949; Libby 1952), De Vries (1958) recognized wiggles in atmospheric radiocarbon amounts by directly dating known-age tree rings. If the advent of the dating method was the first ‘radiocarbon revolution’, then the realisation that radiocarbon dates need to be calibrated was the second. The long-lived Bristlecone pine trees were used to establish the first non-linear calibration record (Suess 1967), followed by other calibration datasets correcting for the uneven distribution of radiocarbon throughout the carbon cycle (e.g. Pearson and Stuiver 1986; Stuiver et al. 1986). Today the IntCal working group oversees the construction and update of internationally agreed calibration curves related to specific carbon reservoirs, i.e. the mid-latitude Northern and Southern Hemisphere atmospheric reservoirs, and a global marine reservoir (Reimer et al. 2013), along with a post-bomb curve (Hua et al. 2013). The IntCal13 uses a Markov Chain Monte Carlo (MCMC) approach, including the random walk method to constrain the inevitable scatter of data points and to incorporate the uncertainty in the calendar ages of the calibration data (Niu et al. 2013). The Holocene calibration sets are quite robust as they are primarily derived from decadal measurements of long, dendrodated tree

ring chronologies (0-13,500 cal BP), but the resolutions are currently being improved through single-year measurements of radiocarbon in tree rings (e.g. Jacobsson et al. 2018; Kudsk et al. 2020). Single year dating has revealed short-term events in form of short global spikes in radiocarbon production, such as in AD 774-75 (Miyake et al. 2012) and AD 993-94 (Miyake et al. 2013), which in some circumstances can help date archaeological events to a single calendar year.

Dating cremated bone

Radiocarbon dating organic bone-collagen is not straightforward, but it is today considered to be one of the most reliable materials for dating (Higham et al. 2011). Whereas the carbon content in inorganic bone-apatite was rejected as a suitable dating material up until 20 years ago (Mook and Streurman 1983). Partly because the carbon content in apatite is low, but mainly because the apatite structure is porous and susceptible to post-depositional changes. The first issue was solved with the advent of AMS, which needed radically smaller sample sizes than the previous radiometric beta-decay counters, and the turning point for the second issue was the realisation that the re-crystallization occurring when bone calcines, makes it less susceptible to contamination and thus suitable for radiocarbon dating (Lanting et al. 2001).

Bone consists of water, organic matter (fat and collagen) and inorganic bio-apatite. When heated the crystalline structure of the bone will change, causing it to shrink in size, develop cracks, deform and fragment, and change in colour from black over to white as a function of temperature (McKinley 1994; Holden et al. 1995). Water will evaporate at temperatures below 225 °C, followed by organic matter at temperatures below 500 °C. Skin, fat and flesh will burn away before collagen. At temperatures above 600 °C the structure of the inorganic bio-apatite rapidly changes: the hydroxyl bonds in the apatite crystals break down, resulting in structural carbonate being released as CO₂, and a reduction in crystal size. The now cremated bone is fragile, but it regains strength and solidity by reabsorbing water, and the apatite will re-crystallize forming larger crystals (Holden et al. 1995; Stiner et al. 1995). White calcined bone is referred to as cremated bone, as opposed to burned or charred bone (Olsen et al. 2008). Experimental studies have shown isotopic values of cremated bone to be highly influenced, although to variable degrees, by fuel source, cremation temperature and duration (Van Strydonck et al. 2005; Olsen et al. 2008; Van Strydonck et al. 2009; Zazzo et al. 2009; Hüls et al. 2010; Van Strydonck et al. 2010; Zazzo et al. 2012; Olsen et al. 2013; Snoeck et al. 2014; Snoeck et al. 2016a). This causes cremated bone to be an unreliable material for paleo-dietary reconstructions (Zazzo et al. 2009; Van Strydonck et al. 2010; Zazzo et al. 2012; Snoeck et al. 2016a). Studies have however shown it to be

possible to investigate paleo-mobility using strontium isotope analysis of cremated petrous bone (*Pars petrosa*) (Harvig et al. 2014a; Snoeck et al. 2015; Snoeck et al. 2016b; Snoeck et al. 2018).

In a pioneer study from 2011 Lanting et al. presented a new method for radiocarbon dating cremated bone. They demonstrated that it was possible to obtain comparable radiocarbon dates on the bioapatite of fully calcined bone and context-associated charcoal, something that was later confirmed in an intercomparison study (Naysmith et al. 2007). Here six radiocarbon laboratories produced uniform results within measurement errors, although they had different perception of what sources of contaminants might still be present in the cremated bone and different opinions on what pretreatment protocol that was most suitable (Van Strydonck et al. 2005, 2009; Olsen et al. 2008). In the comparison study one laboratory (Kiel) pretreated the material using either an acetic acid treatment (Lanting et al. 2001; Olsen et al. 2008) or a leaching treatment (De Mulder et al. 2007), whereas the other laboratories used only variations on the first treatment.

Within this dissertation project cremated bone samples were submitted for radiocarbon dating to the Laboratory for Radiocarbon Dating (RICH) in Brussels, the Leibniz Laboratory (KIA) in Kiel, and the Center for Isotope Research (CIO) in Groningen. Pretreatment protocols vary significantly between these, with Groningen using the traditional acetic acid treatment (Lanting et al. 2001), and Brussels (Van Strydonck et al. 2009) and Kiel (Hüls et al. 2010) using variations of an acid-leaching treatment (Fig. 9). The laboratories all have a long history of dating cremated bone and were among the six laboratories which participated in the before mentioned intercomparison study (Naysmith et al. 2007). They all use acetic acid to dissolve calcite, but add it at different points in the process and at different concentrations, temperatures and reaction times. After an initial sodium hypochlorite treatment, Groningen treats the solid bone with acetic acid for 24 hours, thus targeting the surface of the sample along with the surface in the voids of the cremated bone. Kiel starts the pretreatment with acetic acid, but only washes the crushed bone for 5 x 30 min. Brussels on the other hand uses acetic acid for 24 hours, but only after leaching and grinding the sample. These differences in method result in varying weight losses: Kiel removed less than 0.5% of the starting weights, Groningen removed c. 3% and Brussels removed c. 15%. The comparatively high removal percentage by Brussels, even though Groningen uses a higher concentration of acetic acid, suggests that the increased surface area due to grinding is a decisive factor. These differences also suggest that much of the material dissolved during the 24 hour acetic acid treatments at Groningen and Brussels was apatite, not calcite. Kiel and Brussels assume the apatite might be diagenetically altered with carbon substitution being greater near the surface of a bone, and they consequently etch the outer 30-50% of the sample. Groningen on the other

hand assumes apatite to be resistant to contamination and uses the least aggressive pretreatment method, removing only calcite, absorbed carbonates and the less crystalline fractions of apatite (Van Strydonck et al. 2005; Olsen et al. 2008; Van Strydonck et al. 2009). On average, Groningen removed only 3% of the sample mass during pretreatment, whereas Brussels removed 36.5%, and Kiel removed 41.2%.

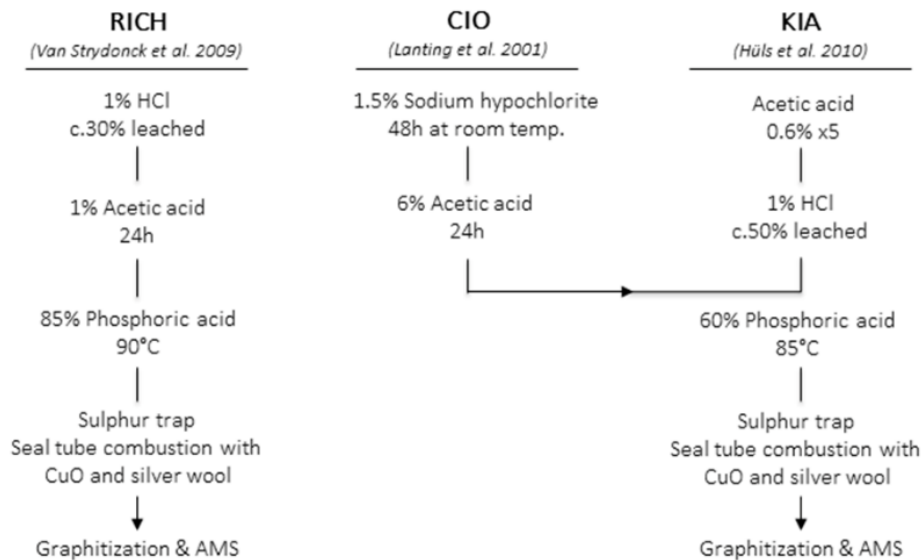


Figure 9: Pretreatment protocols for cremated bone. Laboratory for Radiocarbon Dating (RICH) in Brussels, the Leibniz Laboratory (KIA) in Kiel and the Centre for Isotope Research (CIO) in Groningen (from Rose et al. 2019: 1583).

There are no agreed indicators to assess sample quality when radiocarbon dating cremated bone, but it is useful to visually inspect whether the cremated bone is fully calcined (Fig. 10). To confirm complete calcification it is recommended to analyse its degree of re-crystallization (Olsen et al. 2008). The crystallinity index (CI) is measured as the splitting factor between the two absorption bands at c. 603 and c. 565 cm^{-1} ($\text{CI} = (A_{603} + A_{565})/A_{\text{valley}}$). It is a function of temperature, where high CI values indicate high burning temperatures and thus a high degree of re-crystallization (Person et al. 1995; Olsen et al. 2008). CI values >5 are agreed to be acceptable for samples of cremated bone. Comparing infrared spectroscopy (FTIR) and x-ray diffractometry (XRD) spectra at different stages in pretreatment, and giving more weight to results from samples whose spectra do not change much between pretreatment steps might also prove useful, but it needs further investigation. Inter-laboratory replication may be a useful approach for detecting contamination problems, particularly when there are significant differences in laboratory protocols. In Paper 3 (Rose et al. 2019) it is suggested to report type of burial environment along with any other risk of contamination (e.g. chalk manuring).



Figure 10: To the left is a piece of unburned bone, in the middle a piece of burnt bone and to the right two pieces of cremated bone.

Case study: Investigating differences in pretreatment protocols between laboratories²

As illustrated in Figure 9 the radiocarbon laboratories used for this dissertation apply different pretreatment protocols on cremated bone. It is a specific dissertation objective to test if these observed differences had a measurable influence on the obtained radiocarbon results and an intercomparison study was carried out as an extension of a contamination investigation. In Paper 3 (Rose et al. 2019) six sets of replicate dates were presented in order to compare laboratory pretreatment protocols, along with a further 16 sets of inter-laboratory replicate measurements to compare specific steps of the conversion to CO₂ and AMS measuring of cremated bone. Different types of replicates were considered in the analysis of inter-laboratory differences in pretreatment protocols. Type 1 replicates provide an estimate of the inter-laboratory reproducibility, by comparing independent dating by two laboratories of the same cremated bone fragment ('true replicates') or of different cremated bone fragments from the same burial context, whose radiocarbon ages are expected to be congruent. Whereas type 2 replicates provide insight into specific steps of the conversion and measuring process, by comparing conversion and measurement at two laboratories of material pretreated by one of them.

Cremated bone were sampled from 20 graves from Aarre urnfield (c. 8 °dH) and Aarupgaard urnfield (c. 10 °dH), both situated on sandy soil with low carbonate levels (material presented in Part C). All samples had acceptable CI values (> 5), and were sent to Brussels, Kiel and Groningen for AMS dating, with a few samples replicated between laboratories. A total of 43 radiocarbon results on 20 samples are reported. Results from Groningen have a slight tendency towards lower $\delta^{13}\text{C}$ values compared to results from Kiel, which could indicate incomplete conversion, but here probably reflects use of

² Adapted from Paper 3: Rose et al. 2019.

different AMS system. Results from Groningen have lower %C values (mean = 0.09%) than from Kiel (mean = 0.23%), whereas results from Brussels fall in between (mean = 0.16%, n = 2). Differences in %C do however not appear to be correlated with ^{14}C ages.

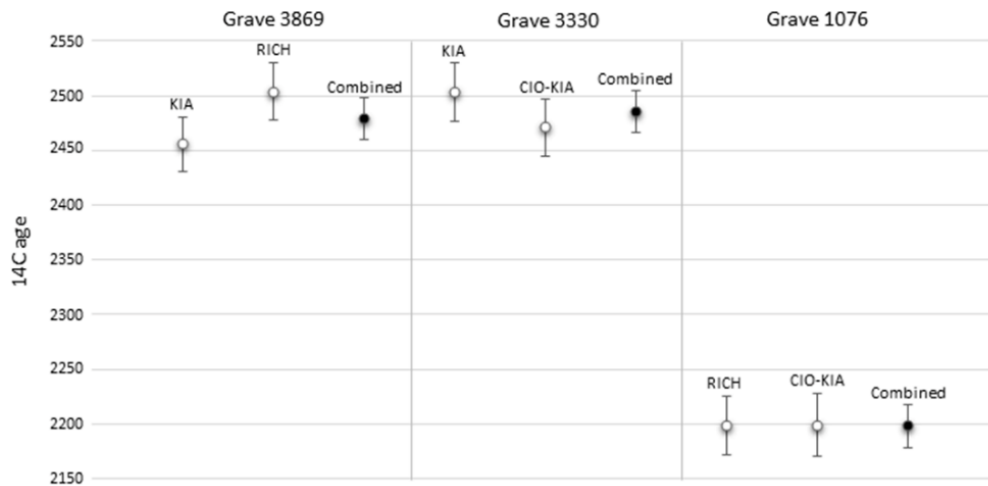


Figure 11: Radiocarbon results ($\pm 1\sigma$) on type 1 replicate dates from Aarupgaard urnfield (from Rose et al. 2019: 1585).

Type 1 replicate results were overall consistent, with four out of six pairs of results passing a χ^2 test, i.e. are statistically consistent at the 5% significance level (Fig. 11) (Ward and Wilson 1978). Results from Groningen are on average slightly older than results from Brussels and Kiel, as are results from Brussels compared to results from Kiel. Results from grave 1076 narrowly fail the χ^2 test ($T = 4.0$, $T'(5\%) = 3.8$, $\nu = 1$), but would be regarded as consistent based on the traditional formula whereby their difference is less than 2σ (twice the uncertainty in the difference). A slight discrepancy like this might possibly reflect an inhomogeneity of ^{14}C ages in the two dated cremated bone fragments, caused by an uneven influence of 'old-wood' from the pyre-fuel (Olsen et al. 2013). Results from grave 3869 narrowly fail the χ^2 test ($T = 6.9$, $T'(5\%) = 6.0$, $\nu = 2$), whereas if the test is limited to results from either Kiel and Brussels ($T = 1.8$, $T'(5\%) = 3.8$, $\nu = 1$) or Brussels and Groningen ($T = 1.8$, $T'(5\%) = 3.8$, $\nu = 1$) it is acceptable. The overall consistent results from the three laboratories demonstrate the inter-laboratory reproducibility to be satisfactory, which indicates that the least aggressive pretreatment method (bleaching and acetic acid) applied in Groningen was probably sufficient in most cases. The results do not show whether the weaker acetic acid wash in Kiel would also be adequate in this case. Also, the opposite order of the acetic acid and the hydrochloric acid steps between Kiel and Brussels appears to have no influence on the results. If the samples were only contaminated by secondary

calcite, without diagenetic alteration of apatite (or if diagenetically altered apatite was soluble in 6% acetic acid), this would however also be the expected outcome.

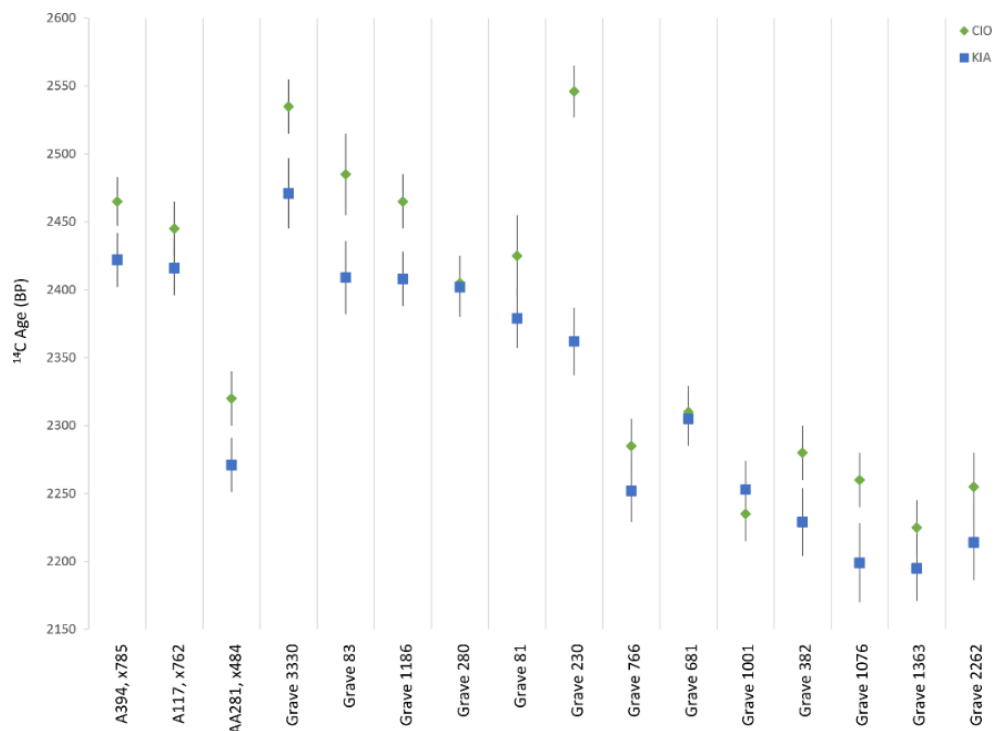


Figure 12: Radiocarbon results ($\pm 1\sigma$) on type 2 replicate dates from Aarre and Aarupgaard urnfields (from Rose et al. 2019: 1587).

Type 2 replicate results were also overall consistent, with 15 out of 16 pairs of results passing a X^2 test (Fig. 12) (Ward and Wilson 1978). One or both dates on grave 230 must however be an outlier ($T = 34.1$, $T'(5\%) = 3.8$, $\nu = 1$, difference = 5.9σ), which cannot be explained by differences in wood-age offset, as the sample was homogenized by crushing before being split between laboratories. The Kiel date fits the expected age range, whereas the Groningen date is well back in the Late Bronze Age and can thus be rejected, based on the archaeological information. There is no technical explanation for this difference, with $\delta^{13}C$ and $\%C$ values from both laboratories within the normal ranges. The overall consistent results show that the differences in conversion and measuring processes between the Groningen and Kiel laboratories did not significantly affect the radiocarbon results. Results from Groningen are on average slightly older than results from Kiel, but differences in blank correction would account for most of this pattern; the results from Kiel are calculated using the Kiel blank correction, but as these samples were pretreated in Groningen, the Groningen blank correction is perhaps more appropriate.

Fortunately, the radiocarbon results showed dates to be reproducible between the laboratories and consistent with the expected archaeological chronology. It was concluded that differences in pretreatment, conversion to CO₂ and AMS measurement have no measurable influence on the majority of obtained results, suggesting that any possible diagenesis was probably restricted to the most soluble $\leq 5\%$ of each sample, as this proportion of the sample mass was removed under all laboratory protocols.

Radiocarbon age limit for cremated bone

It is possible that cremated bone has a lower effective radiocarbon age limit compared to other material types, because secondary calcite will make the dates younger and even by etching part of the sample, there is no guarantee it has been completely removed. Results from a few studies do, however, indicate that it is possible to reach similar ages as with collagen beyond the Late Holocene. Cooper et al. (2017) have successfully dated 23 samples of cremated mammal bone from a middle Mesolithic site at Asfordby in Leicestershire. They used the pretreatment protocol described in Lanting et al. (2001) and besides from five samples that failed to produce sufficient carbon, the dates fall into a coherent group concentrated on the first half of the 8th millennium cal BC, which is acceptable by the expected archaeological chronology (Cooper et al. 2017). Veil et al. (2012) have dated two samples of cremated bone fragments from a Federmesser occupation site in Northern Germany, again using the Lanting et al. pretreatment protocol (2001). The combined dates provide a calibrated date range *11,801-11,537 cal BC (95.4% probability)*, which is contemporaneous with the early Allerød period and in agreement with the archaeological dating. Zazzo et al. (2013) have tested whether it is possible to date even older material from Aurignacian and Gravettian layers at the Upper Palaeolithic site of Abri Pataud in south-west France. The chronology of the site had previously been investigated using ultrafiltrated bone collagen results, showing occupation activity between the millennium prior to 40 kyr cal BP and 26 kyr cal BP (Higham et al. 2011). Zazzo et al. selected 24 cremated bone samples for radiocarbon dating, which were cleaned in demineralized water and surfaces and cracks were drilled to remove secondary sediments. The cleaned samples were finely crushed and treated in 1N acetic acid under vacuum for 24 hours, before being reacted in 100% orthophosphoric acid at 70 °C for 20 min. CO₂ from most of the samples were reacted with Sulfix to remove SO₂ that can otherwise interfere with graphitisation, but almost all of these samples returned ages that were systematically too young. This suggests that Sulfix can contaminate samples with modern carbon, and Zazzo et al. recommend avoiding the use of Sulfix altogether. This is in line with findings presented in Paper 3 (Rose et al. 2019) and in Part B. The study of Zazzo et al. (2013) also demonstrates that calcined bone can behave

as a closed system for more than 38,000 years and therefore provide suitable material for radiocarbon dating, at least if samples are not treated with Sulfix.

Wood-age offset in cremated bone³

The only source of carbon in bio-apatite is carbonate ions formed through energy production in cells, which can substitute with hydroxyl (OH, A-type carbonates) or phosphate (PO₄, B-type carbonates) in the bone-matrix (Lee-Thorp 2008; Hüls et al. 2010). This results in an intrinsic age of the bio-apatite equal to the turn-over rate of the bone-matrix, probably comparable to turn-over rates in bone-collagen (Hedges et al. 2007). Intrinsic ages may vary between individuals (depending on e.g. their age at death) and between bones of the same individual (due to differences in bio-apatite remodelling rates), but given expected mortality patterns in prehistoric populations it probably seldom exceeds 1-2 decades. Experimental studies have demonstrated the apatite carbon signature changes when a bone is cremated. Hüls et al. (2010) cremated modern bone in a sealed furnace filled with ¹⁴C-free CO₂ obtained from fossil fuel, and by dating the cremated bone found that 53-86% of carbon in re-crystallized bio-apatite was derived from the cremation atmosphere. This was confirmed by open-air experiments under natural conditions, where Zazzo et al. (2012) using archaeological bone and recent wood measured a percent carbon exchange of 48-91%, while Snoeck et al. (2014), using modern bone and old wood of known-age, measured a % carbon exchange of 39-95%. Carbon exchange between the bone and the combustion atmosphere will cause a calendar date offset between the calibrated radiocarbon measurement and the main event of interest (the date of cremation), hereafter referred to as a 'wood-age offset'. Unless a body is cremated with recent, short-lived fuel, the wood-age offset will always make the cremated bone date older than original unburned bio-apatite. This is illustrated in Figure 13 where the mixed carbon signal of the cremated bone has an unknown calendar offset to the true cremation event, i.e. the cremated bone dates earlier than the true cremation event. The size of the wood-age offset is decided by the intrinsic age of the pyre wood, where material with a negligible intrinsic age, such as small branches or cereal grains, will cause no calendar offset, material with medium intrinsic age, such as short-lived wood species, will cause a medium sized calendar offset, and finally material with high intrinsic age, such as heart wood from short-lived species of wood or even trunk wood from long-lived species, will cause large calendar offsets. Unfortunately it is not possible to assess the size of these calendar offsets because of a general lack of information about pyre wood from cremation pyres, predominately caused by preservation circumstances. Instead it is necessary to approach the wood-age offsets statistically, which is the aim on Part B.

³ Adapted from Paper 4: Rose et al. 2020.

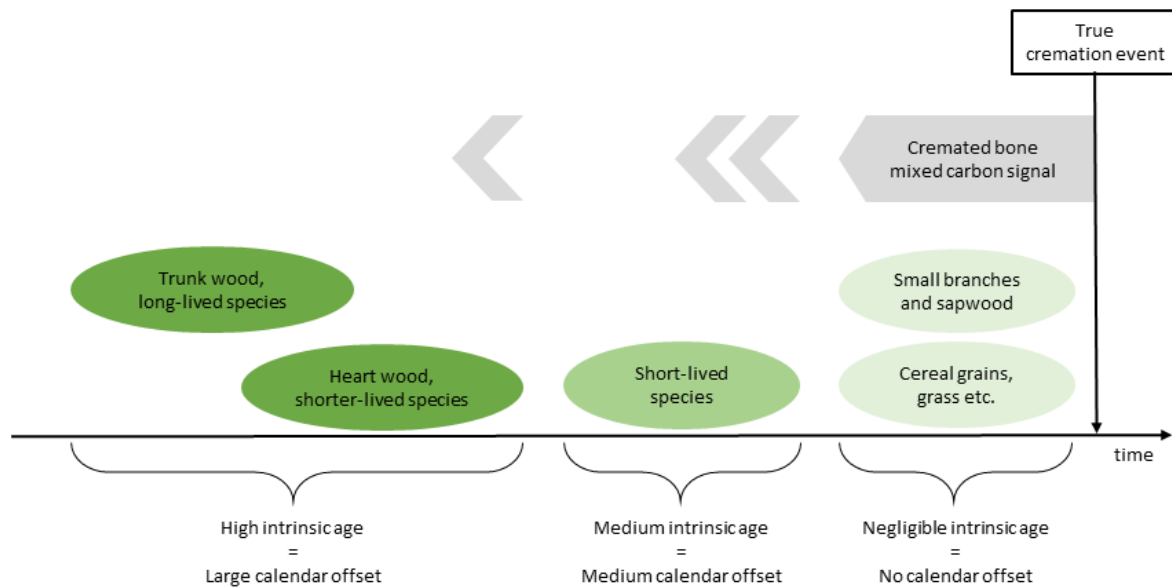


Figure 13: Schematic illustration of wood-age offsets in cremated bone on a calendar scale.

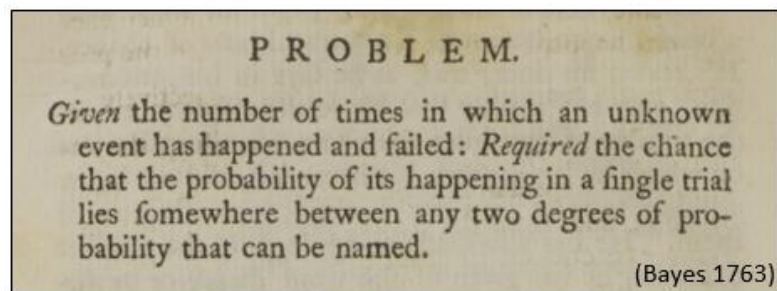
Applications of radiocarbon dating cremated bone

Radiocarbon samples of cremated bone has become a standard procedure and applications of the method are frequently published in high-ranking journals (Willis et al. 2016; Fitzpatrick et al. 2017; Minami et al. 2019). It is now possible to date archaeological phenomena that could previously only be datable indirectly, e.g. the urnfields from the Netherlands and Belgium that have received particular keen interest. This has served to demonstrate that the internal chronology and development of urnfields are more complicated than previously anticipated (De Mulder et al. 2009; De Reu et al. 2012), and that the urnfields have been in use longer than otherwise expected based on typo-chronology (De Reu et al. 2012; De Mulder et al. 2017). It has also been demonstrated that the typological sequences of pottery and grave types as well as the chronological framework of the period need reworking (De Mulder and Van Strydonck 2004; De Mulder et al. 2007; De Mulder et al. 2009; De Mulder et al. 2013; De Mulder et al. 2014). Olsen et al. have contributed with important insights into wood-age offset in cremated bone (Olsen et al. 2008; Olsen et al. 2013), as well as reviewing the relative chronology of the Danish Bronze Age using Bayesian modelling (Olsen et al. 2011; Hornstrup et al. 2012). Møller et al. (2020) have published the first Bayesian model with cremated bone dates from a Danish urnfield and thus initiating the investigation into the Danish urnfield tradition that is carried forth in the present dissertation.

Concluding remarks on dating cremated bone

In this chapter the use of radiocarbon as a dating method in archaeology was introduced with special attention to dating cremated bone as that is the main material analysed in this dissertation. The cremated bone pretreatment methods applied at the radiocarbon laboratories in Brussels, Groningen and Kiel was introduced and the differences in pretreatment protocols and specific step of the conversion and measuring process were compared using replicate measurements. The intercomparison study served to answer the dissertation objective if these differences might affect the radiocarbon results, and fortunately it demonstrated results to be reproducible between laboratories and consistent with the expected archaeological chronology. It was concluded that any possible diagenesis was restricted to the most soluble $\leq 5\%$ of the samples, which was removed under all laboratory protocols. Published literature was reviewed in search of a possible age limit to dating cremated bone, but it was found that if Sulfix is avoided in the pretreatment process reliable dates can be produced even on Palaeolithic samples. Finally intrinsic age of the bio-apatite and wood-age were introduced as offsets that both affect cremated bone. Particularly the wood-age offsets in cremated bone is important for the dissertation and it will be investigated in detail in Part B.

Bayesian chronological modelling



Thomas Bayes (1701-61) was an English statistician and Presbyterian minister, who in the 18th century formulated the above fundamental theorem for determining conditional probability, i.e. the probability of an event given that another event occurred. The paper 'An essay towards solving a problem in the doctrine of chances' was published posthumous (Bayes 1763). The theorem was since developed by other authors, but it was not until the 1950s that the term *Bayesian* was used to describe the method.

Bayes' theorem can be described using the equation:

$$P(A|B) = \frac{P(B|A)P(A)}{P(B)}, \quad (1)$$

where $P(A|B)$ is the probability of event A occurring given event B, also called the posterior and what we are trying to estimate. $P(B|A)$ is the probability of event B occurring given event A, called the likelihood. $P(A)$ is the probability of event A occurring and is called the prior. $P(B)$ is the probability of event B occurring, called the marginal likelihood. Bayesian statistical methods incorporate prior probability distributions in order to generate posterior distributions, where the prior probability is defined as our current knowledge of the probability of an event, and the posterior probability is our revised knowledge of this probability, taking into account our new information. The theorem can, in other words, be used to update existing probabilities of an event, after incorporating new data (Gelman 2004; Blasco 2017).

Bayesian modelling has gained a widespread use within the last 40 years, in e.g. finance for risk evaluation and in medicine to determine the accuracy of medical test results (Gelman 2004; Blasco 2017). It has since the early 1990s been used for formal chronology building in archaeology (Naylor and Smith 1988; Buck et al. 1991; Buck and Litton 1991; Litton and Leese 1991; Buck et al. 1992; Buck

et al. 1994a; Buck et al. 1994b; Christen 1994; Buck et al. 1996; Buck and Christen 1998). Applying Bayesian statistics to archaeological chronology means that new data ('the standardized likelihoods') is being evaluated in the context of existing experience and knowledge about a problem (our 'prior beliefs'). By incorporating both our previously existing knowledge and our new data (our 'posterior belief'), this enables us to arrive at a new understanding of the problem at hand. The application of Bayes' theorem to archaeological chronologies has been described as:

$$\text{Posterior Belief} = \text{Standardized Likelihood} \times \text{Prior Beliefs} \quad (2)$$

Where standardized likelihood equals calendar date information (most often radiocarbon dates), prior beliefs equal the existing archaeological information (relative date information inferred from e.g. stratigraphy and typology), and posterior beliefs equal the now updated beliefs (Buck et al. 1991; Bronk Ramsey 2009a; Bayliss et al. 2016). This process might be run in a loop, using the posterior beliefs to update the prior beliefs (Gelman 2004; Bayliss et al. 2013a).

Bayesian chronological modelling offers a coherent framework for modelling calendar information in view of the prior beliefs. It calculates posterior probabilities in form of density distributions of all the dated samples, which provide more precise and realistic probability distributions for the dates of individual samples (Bayliss 2007; Bayliss et al. 2013b). From this posterior probability distributions can be calculated for other events related to the model, but that are not immediately possible to sample (Meadows 2012). This might be the earliest burial at a cemetery, when an artefact type came into use of when a settlement site was abandoned. Similarly, also the duration of activity can be calculated, such as how long a cemetery was in use for, or how much time elapsed from between two separate events of activity. The sensitivity of the posterior probabilities to the prior beliefs can be tested, ensuring that the model arrive at realistic and consistent chronologies for the archaeological phenomena being investigated.

Bayesian chronological modelling has had a large impact on archaeology, so profound that it has been described it as the third 'Bayesian revolution' (Bayliss 2009), and as "*the dominant paradigm in archaeological chronology construction*" (Buck and Meson 2015: 567). It has been critiqued for not being scientifically objective (Lekson 2015), but criticism are probably mostly voiced in smaller forums and remains unpublished (although see Strien 2017; 2019).

Bayesian chronological modelling is essentially the integration over a large number of inter-related and often complex probability distributions and this cannot be done analytically (Buck and Meson 2015). The method was not applied until computing power increased significantly in the 1980s, and gained widespread use with the introduction of Bayesian calibration tools, such as BCal (Buck et al. 1999), DateLab (Jones and Nicholls 2002) and Chronomodel (Lanos and Philippe 2015; Lanos and Philippe 2017; Lanos and Philippe 2018; Lanos and Dufresne 2019). Recently, also the free and open-source platform R is being used to perform Bayesian chronological modelling (Philippe and Vibet 2018; McLaughlin 2019). This is a powerful platform with a wide range of additional statistical ‘packages’, but it also demands a high degree of statistical understanding from the user. The most often applied software is OxCal that was first introduced in the mid-1990s (Bronk Ramsey 1995; Bronk Ramsey 1998), and its methods and applications have since been continuously updated (Bronk Ramsey 2008a; Bronk Ramsey 2009b; Bronk Ramsey 2009a; Bronk Ramsey and Lee 2013; Bronk Ramsey 2017). OxCal v4.1 uses the Metropolis-Hastings algorithm to perform Markov Chain Monte Carlo (MCMC) analysis, to generate random draws from a target distribution and produce a range of posterior probabilities. Each iteration of the MCMC analysis provides a possible solution set of all of the parameters of the model and the number of iterations is increased until it finds ‘convergence’, i.e. consistent posterior density estimates for the dates and parameters of interest.

Buck and Meson (2015) has raised concerns that the introduction of plug-and-play calibration tools also introduced the risk of reducing the Bayesian process to a black box. They emphasize that being ‘a good Bayesian’ requires *“mindfulness when selecting the initial model, defining prior information, checking the reliability and sensitivity of the software runs and interpreting the results obtained”* (Buck and Meson 2015: 567).

Model construction

The following is not intended as a how-to guide to Bayesian chronological modelling, but rather as an introduction to key aspects relevant for this dissertation. OxCal v4.3 (Bronk Ramsey 2009a) is used to conduct Bayesian chronological modelling and OxCal terms and notations are written with Courier font (Chronological Query Language, CQL: (Bronk Ramsey 1998; Bronk Ramsey 2009a). There are a number of instructive and informative papers published on the topic (Bayliss and Bronk Ramsey 2004;

Bayliss 2007; Bayliss 2009; Bayliss et al. 2013b; Bayliss 2015; Buck and Juarez 2017; Hamilton and Krus 2018).⁴

At the heart of any Bayesian model of archaeological material, is the connection between sample, its context, and the event under consideration (Dean 1978; Bayliss 2009). It is important to differentiate between the ‘radiocarbon event’, i.e. when atmospheric CO₂ is sequestered as organic carbon in a living organism, and the time over which this occurs (from formation to death, also known as intrinsic age), and the ‘archaeological event’ we are actually interested in dating. A precise radiocarbon measurement is only helpful if the chronological relationship between these two events is understood. Here it is fundamental to consider the taphonomy of the dated samples and the process from deposition to recovery. Charcoal from a hearth might for example have a high intrinsic age, making the chronological relationship between the charcoal and the hearth from which it is recovered difficult to interpret (Bayliss 1999). Wood has an inhomogeneous ¹⁴C signal relating to its period of growth, and a radiocarbon date on the charcoal will in this scenario provide a mean date of the tree rings in the specific charcoal fragment. Most importantly, it does not date the hearth context in which it is deposited. Offsets between the ‘radiocarbon event’ and the ‘archaeological event’ can be modelled using outlier modelling (see Part B) (Bronk Ramsey 2009b).

Prior beliefs

The prior beliefs can be divided into informative priors and uninformative priors, which are translated into information on the distribution of values of specific model parameters. The model is informed of the relative, temporal relationships between individual events, or most often between groups of events, based on the prior understanding of the archaeology. Archaeological priors are (in principle) ordered according to basic laws of stratigraphy, as defined in a Harris matrix (Harris 1989), but it still requires subjective judgement about the associations between the samples and the archaeological phenomena of interest (Meadows 2012).⁵ Constraints on the order of events are in OxCal defined using `Sequence (ordered)` and `Phase (unordered)`. These can be delineated by a start `Boundary` defining the time that the dated activity starts, and an end `Boundary` defining the time that the dated

⁴ For a basic instruction in how to construct Bayesian chronological models readers are referred to the online how-to boklet by McNutt (2013), the OxCal google discussion group (Google Groups 2017), and the OxCal online manual (Bronk Ramsey 2017b).

⁵ See also Dye and Buck (2015) for a discussion of how to construct chronological directed graphs from stratigraphic graphs, and Holst (2004) and Nakoinz (2012) for alternative approaches to fuzzy stratigraphy.

activity ends. Boundaries are themselves modelled as events (Bronk Ramsey 2009a). In its simplest form a chronological model encompasses a single phase of dated events within a set of boundaries, often called a 'bounded phase model', but the `Sequence`, `Phase` and `Boundary` commands are flexible building blocks that can be combined to define more advanced multiple-phase models. OxCal offers default phase models with contiguous phases (the temporal order is defined and each phase follow the next phase without overlap or hiatus), sequential phases (defining a temporal order of phases, but allowing hiatuses between them), overlapping phases (assuming no temporal order of phases, allowing them to overlap), and trapezium phases (define boundaries as transitions with a duration) (Bronk Ramsey 2009a). The prior probability density function of individual model parameter can be specified using different distributions, such as the normal distribution or the uniform distributions. This approach can also be extended to other OxCal commands, such as `Boundary`, `Difference`, `First`, `Last` and `Span` (Bronk Ramsey 2009a; Bronk Ramsey and Lee 2013).

It is necessary to define a prior distribution for the dated events, because calibrating radiocarbon dates is a probabilistic process (Stuiver and Reimer 1993), resulting in measurement scatter around the real date of the radiocarbon event. Visual inspection of a group of unmodelled, calibrated dates will overestimate their activity duration and it is necessary to impose a statistical distribution on the dates in order to counteract this inevitable statistical scatter (Bayliss 2009; Bronk Ramsey 2009a).⁶ Prior distributions are defined according to our *a priori* information relating to the rate of deposition of datable material within an archaeological period or phase. From the onset of Bayesian chronological modelling this was achieved by using a uniform prior distribution, which structures the data as a continuous period of activity, i.e. assuming that our data is randomly sampled from a continuous process bounded by a start event and an end event (Buck et al. 1991; Buck et al. 1992). It does not favour either long or short phases and it still today remains the most used prior distribution (Bronk Ramsey 2009a). A uniform distribution can provide accurate date estimates, even though the underlying distribution of sampled dates are not strictly uniformly distributed. Simulation studies have demonstrated that the 'uninformative' prior beliefs have to be grossly incorrect before the outputs of the model are importantly wrong (Bayliss et al. 2007; Bayliss et al. 2013a).

⁶ This effectively equals applying a null prior, which is very highly weighted to higher values when the number of dates is large. For further discussions see Bronk Ramsey 2000; Steier and Rom 2000; Bronk Ramsey 2009b.

Given the prior beliefs, the actual underlying distribution of the data might be suspected to be non-uniformly distributed. In OxCal the distribution of events within a group are modelled using boundary commands, and the prior distribution can be altered by applying different types of boundaries (Fig. 14). A simple `Boundary` at the start and end defines a uniform phase with an abrupt transition between adjacent phases. A `Zero_Boundary` defines a group of events with a ramped distribution (increasing or decreasing). A `Tau_Boundary` defines a group of events with an exponential distribution with a long tail (increasing or decreasing). Modelling both start and end with a `Sigma_Boundary` defines a group of events with a normal distribution, with a gradual onset and tailing off (Bronk Ramsey 2009a).

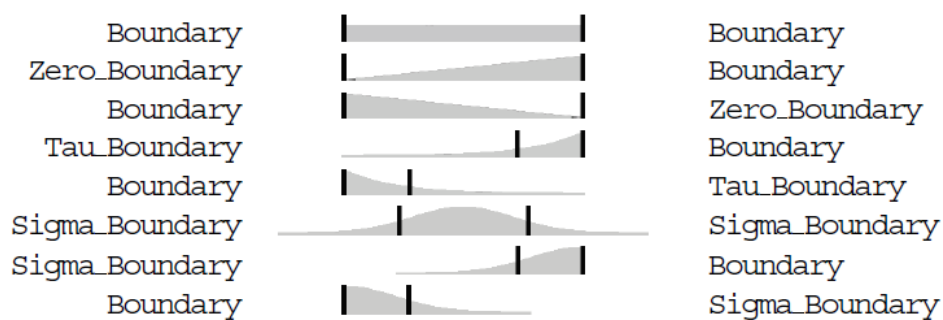


Figure 14: The range of `Boundary` commands applied in OxCal v.4.0 to define the distribution of events within a group (from Bronk Ramsey 2009a: 346).

`Tau_Boundary` has been used to model the exponential distribution of samples susceptible to intrinsic age. Such samples have been proposed to approximate an exponential probability density function, i.e. most samples will date close to the event in question, but a diminishing number of dates will be increasingly older (Nicholls and Jones 2001), which is implemented in OxCal as the `Charcoal Outlier_Model` (Bronk Ramsey 2009b; Dee and Bronk Ramsey 2014). `Sigma_Boundary` can be used to model a smooth transition between groups of events, but it is not commonly applied in the published literature (although see Kneisel 2013).

Trapezoidal phase prior

The boundary commands can be combined to define more complicated distributions, as in the trapezium model that allows for the possibility of gradual transitions taking a period of time (Karlsberg 2006). Brainerd stated that "Each type originates at a given time in a given place, is made gradually in increasing numbers as time goes on, then decreases in popularity until it becomes forgotten, never to reoccur in an identical form" (Brainerd 1951: 305). This translate into a unimodal distribution, which

has been demonstrated using known-age datasets (Deetz and Dethlefsen 1965; Lyman and Harpole 2002). Karlsberg (2006) developed a trapezium-shaped prior distribution separated into three parts, first allowing for a gradual increase (introductory period); then a period with a constant rate of activity (blooming period); and finally a gradual demise (period of decline) (definitions by Lee and Bronk Ramsey 2012). She tested it against a uniform prior on a case study of Roman and Coptic textiles (Van Strydonck et al. 2004), and on a case study of the human reoccupation of NW Europe after the last Ice Age (Housley et al. 1997). She found that assuming different *a priori* information about the rate of deposition significantly influences the posterior density estimates, and hence the archaeological interpretations (Karlsberg 2006). Lee and Bronk Ramsey further developed the model and tested it on a number of archaeological case studies. In their 2012 paper (Lee and Bronk Ramsey 2012) they modelled the Irish Bronze Age Bowl tradition (Brindley 2007), and found that even though boundary parameters of the uniform-phase model give more precise estimates, they preferred the trapezoid phase model because they found it to better reflect the prior archaeological information. In the same paper they modelled a second case study on British Bronze Age metalwork (Needham et al. 1997), and found that the trapezium model parameter provided information about the duration of transitions between adjacent phases. Their trapezium model estimated comparable boundaries as those of a uniform model, backing up the validity of the results (Lee and Bronk Ramsey 2012). Lee et al. (2013) tested the trapezium model on a case study on Iron Age chronology in Israel, using a compilation of more than 400 legacy radiocarbon dates from 26 sites in order to model the transition between Iron Age phases I-II B. They argued that cultural changes can be characterized as a non-instantaneous process and that different cultural phases can be overlapping, indicating transitional periods. They assumed the Iron Age phases to be contiguous to each other, and allowed transition between adjacent phases to have a duration, with the decline of the former phase overlapping with the increase of the later phase. They found that the trapezium model provided an alternative and more suitable approach to modelling transitional processes (Lee et al. 2013).

The trapezium prior model was introduced in OxCal v.4.2 (Lee and Bronk Ramsey 2012; Bronk Ramsey and Lee 2013). The model requires four parameters: boundary parameters t_1 and t_2 (thick vertical lines in Fig. 15), and transition parameters d_1 and d_2 (dotted horizontal lines in Fig. 15). The boundaries are comparable to those of the uniform prior, and if the transition period approaches zero, the trapezium model effectively becomes a uniform model (Lee and Bronk Ramsey 2012). Modelling a contiguous multi-phase model with a trapezium prior model requires the adjacent phases to share a transitional

boundary parameter (t_2-t_4 in Fig. 16), each with a transition parameter (d_2-d_4 in Fig. 16), so that the duration of transition can be calculated (grey areas in Fig. 16).

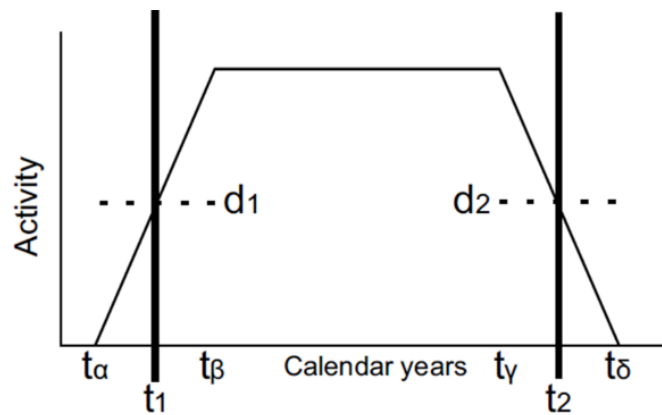


Figure 15: Schematic representation of the trapezoid prior model, where activity here refers to the currency of an artefact type. The thick horizontal lines are boundary parameters t_1 and t_2 , and the dotted horizontal lines are transition parameters d_1 and d_2 . Remaining parameters t_α , t_β , t_γ , and t_δ are Karlsberg's (2006) parameters for the model (from Lee & Bronk Ramsey 2012: 110).

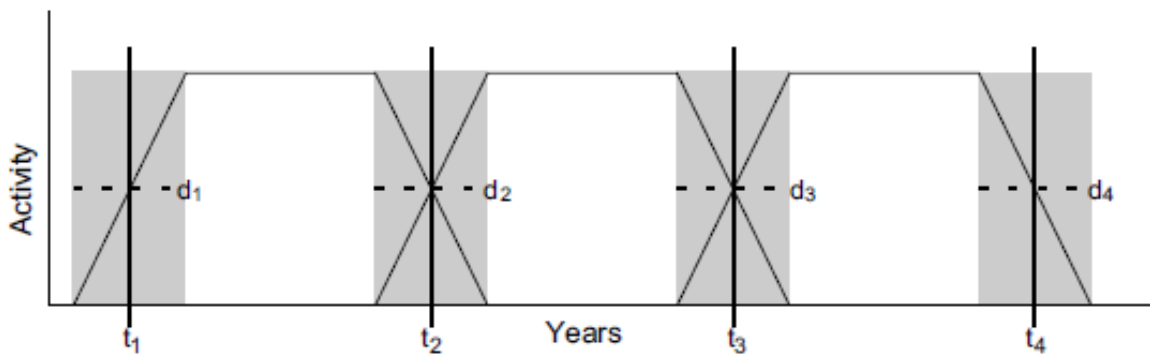


Figure 16: Schematic representation of the trapezoid prior used in a contiguous multi-phase model. The thick horizontal lines are boundary parameters, the dotted horizontal lines are transition parameters, and the grey areas are the duration of transitions (from Lee & Bronk Ramsey 2012: 111).

To implement a trapezium model in OxCal a `Transition` command is nested within the `Boundary`, along with `Start` and `End` queries to recover the start and end of the transition period. The `Start Boundary` will return the midpoint of the transition, the `Transition Period of Start` will return the duration of the transition, and the `Start` and `End` commands will return the start and end of the transition, respectively. A prior distribution can be defined for each of these commands, e.g. constraining the transition to take place within 100yr (Lee and Bronk Ramsey 2012). The trapezium prior model allows the timescales of change in material culture to be approached, and it might be the

most appropriate model in archaeological situations with a slow start and end to a phase. It is data and computationally demanding, which is probably why it is not commonly applied in the published literature. The model has however been used to model pottery phases where it is believed to better reflect the more gradual changes seen in typological sequences (Hanna et al. 2016), and to investigate contiguous overlapping phases of dietary shifts (Meadows et al. 2018). It has been used to model start and end of cremation cemeteries with no *a priori* information indications of abrupt changes (Willis et al. 2016; Fitzpatrick et al. 2017), and to model successive and possibly overlapping sites (Manning et al. 2018b).

Model evaluation

The fit of a model can be evaluated using the OxCal index of agreement. The overlap integral between the likelihood distribution and the posterior distribution is calculated to give a measure of agreement between the model and the data. The agreement index is calculated for individual dates (A) and for the model (A_{overall} and A_{model}), and is approximately scaled 0-100%. Values below 60% indicate a high likelihood that the model is inconsistent with the data and are unlikely to pass a chi-square test at the 5% confidence interval (Bronk Ramsey 1995; Bronk Ramsey 2009a). The agreement index cannot be used to choose between competing models (Bronk Ramsey 1995; Bronk Ramsey 2000). In order to achieve coherent and rigid results it is important to conduct sensitivity testing of the impact of the prior information on the posterior estimates. Some elements in a model might be wrong, but if they do not affect the posterior date estimates, the model is not importantly wrong (Bayliss et al. 2007). It can be difficult to choose between alternative and competing models, which might reflect different but equally possible archaeological interpretations of the data. If the posterior results of the questions being investigated are comparable this poses no great problem, but if they are not, it is advisable to re-examine the interpretations of the taphonomy of the dated samples and possibly redesign the model construction (Bayliss and Bronk Ramsey 2004).

Sensitivity testing can also be conducted using simulated datasets (Griffiths 2014). A powerful tool in OxCal is the possibility to simulate radiocarbon dates (R_{simulate}) and calendar dates (C_{simulate}) from known calendrical dates (Bronk Ramsey 1998; Bronk Ramsey 2009a). When the initial chronological questions are identified, it is an inexpensive way to test whether it is possible to investigate those questions on a particular part of the calibration curve using the available archaeological material. It can also be used to estimate the most appropriate sample size for answering the defined questions (Christen and Buck 1998; Bayliss and Bronk Ramsey 2004; Bayliss et al. 2013a).

Review of currencies studies applying Bayesian chronological modelling

The majority of Bayesian models on archaeological material are aimed at establishing chronologies at the local or regional level and typological sequences are often used as prior information (Olsen et al. 2011; Makarowicz et al. 2018; Asscher and Boaretto 2019). Artefact currencies are rarely the intended focus of investigation, although a number of studies do stand out in this respect and they will be presented below.

In a pioneer study from 1997, Needham et al. critically evaluate the existing Bronze Age chronologies for metalwork using a large number of radiocarbon dates and Bayesian modelling. They model the duration of individual phases and possible temporal overlap between phases, by using independent phases and sequential phases, both with uniform distributions. They re-align the metalwork and settlement sequences and propose a new chronology, independent of cross-linking to other regions (Needham et al. 1997). About a decade later Garrow et al. (2009) follow the same approach, exploring the chronology of Celtic art of Iron Age and Early Roman metalwork in Britain using a large dating program and Bayesian modelling. They construct models using continuous phases, but testing for the presence of a possible hiatus between two of these. They conclude that some of the styles of decorative metalwork were not strictly successive and find an apparent hiatus of about a century between successive stages. They provide posterior estimated durations of the modelled stages, but not currency distributions of individual artefact types (Garrow et al. 2009).

Bayliss et al. (2013a) have in the Anglo-Saxon project conducted a large chronological study of graves and grave goods from the 6th-7th centuries AD, using artefact typology, correspondence analysis (CA) and Bayesian chronological modelling of radiocarbon dates of bone-collagen. They found only a small degree of overlap in chronologically significant artefact types between male and female graves, and had to model the currency and development of artefact types in male and female graves separately. Additionally, the female graves have a non-uniform distribution, which they investigated extensively with simulated datasets. Bayliss et al. recognise a trapezoidal prior distribution to probably be the most appropriate for modelling artefact currencies, but as this was not yet implemented in OxCal at the time of modelling, they instead applied a uniform prior distribution. More grave assemblages and artefact types are continuously implemented in the CA and Bayesian model, a process the authors describe as a 'hermeneutic cycle'. Non-overlapping and sequential artefact types are identified from the CA plots and new models are constructed, not building on the earlier models of grave assemblages (Bayliss et al. 2013a). At the time it was not yet possible to cross reference an event more than twice in OxCal

(Bronk Ramsey 2009a), which was a challenge when 58% of female graves contain beads of more types. Female burials were instead modelled in a single burial phase, and the first and last dates associated with each bead type were calculated. Bayliss et al. points out that this is in disagreement with the strong bimodality of the female graves (2013a), but this was probably the best solution at the time. The authors mention that some artefact types might not be very chronologically sensitive and that others might be too poorly defined to be useful, but unfortunately this aspect is not followed up in their discussion, as is neither the duration of currencies.

In 2015 Stockhammer et al. published a large dating project of Early Bronze Age metalwork from burials in southern and eastern Germany. The artefacts were indirectly dated by dating human skeletal remains (bone collagen) from the same graves as the artefacts. A single Bayesian model is constructed (two phases within an overall phase) to investigate if there is an overlap between chronological phases, but besides that no modelling is applied. Instead dates on artefacts of the same type are either combined or treated as summed calibrations. Without posterior estimated boundaries, the 2-sigma range of the earliest and the latest date of a specific type is used to estimate start and end of the type. In contrast to earlier research (Reinecke 1924) that assumed a restricted use life of individual pin type and that similarity of types indicates contemporaneity, Stockhammer et al. find the pin sequence to be more complex. They find Bronze Age phases A1 and A2 to be non-sequential, but rather have a complex coexistence, possibly reflecting different rates of appropriation of bronze technologies. They propose a revised chronology of diagnostic artefact types, but without Bayesian estimates of type currencies the results are not as strong as they could have been. Also, the terms 'type' and 'chronology' appears to be used interchangeably, introducing a possible danger of circularity in their reasoning (Stockhammer et al. 2015).

On a smaller scale, a recent study by Zavodny et al. (2019) attempts to re-calibrate grave good chronologies from Late Bronze Age Croatia, but results are severely deterred by a low number of available radiocarbon dates. The expected durations of types are simulated in OxCal using a trapezoidal prior model, and the calibrated dates are plotted against these. Besides this, no Bayesian modelling is presented (Zavodny et al. 2019). A few other studies also deserve mentioning here, although no Bayesian modelling is applied. Van Strydonck et al. (2004) have attempted to compare probabilistic distributed radiocarbon dates to art historical date ranges on textiles. The proposed relative date ranges are described as having an introduction phase, a blooming period, and a period of decline. Strydonck et al. adopt a normal distribution for this, with the range as 2-sigma range and the middle

of the range as the median. In OxCal they calculate the difference between this to either single radiocarbon dates or in the case of multiple dates using the interquartile range (middle 50%) and the 95% probability range for a summed probability distribution. They find radiocarbon dating and art historical date ranges to agree within two centuries, except for textiles embroidered in silk that returned older radiocarbon dates, suggesting paintings and similar sources might not provide accurate dates of historical styles (Van Strydonck et al. 2004).

Pottery typology are often included as prior information in chronological site models (Finkelstein and Piasezky 2010), whereas their currencies are ignored, probably because they are regarded as 'fuzzy' and imprecise. Something that is aggravated by studies including large numbers of radiocarbon dates but completely disregarding Bayesian chronological modelling (Woolsey 2020). Exceptions to this is an early study of Bronze Age pottery from Ireland (Brindley 2007), which was also later used in a study of Chalcolithic material culture and funerary practices (Curtis and Wilkin 2012). But more important is a large study by Whittle et al. (2016) building on a number of publications from the 'Time of Their Lives' project. They synchronize typological sequences of pottery from the Neolithic Vinča culture in SE Europe by extracting posterior estimates of key events (as priors) from individual site models and incorporating them in one large model. Using this they model duration of phases, overlap between phases and residence time, but not individual currencies.

Modelling the temporality of change in artefact currencies

Prior information concerning frequency distributions of the artefact currencies is important for the choice of chronological model that is applied to the radiocarbon data in order to investigate the temporality of change. Besides from Zavodny et al. (2019), the studies described above assume artefact types to appear and disappear abruptly and have a uniform distribution, i.e. artefacts of a given type are equally likely to date to any point in between start and end of the type. Computationally these assumptions are certainly easier to model, but they do not address the temporality of change in material culture. Martin Trachsel distinguishes between 'early forms' often found together with artefacts collected over longer time and hence not necessarily chronologically relevant, and 'late forms' that have been in use for longer time than their production time. He sums this up in a theoretical currency model of an artefact type, as the time over which it is in production and in use (Fig. 17) (2004), resulting in a frequency distribution with a steep increase in the beginning and a long tail towards the end (Kneisel 2013).

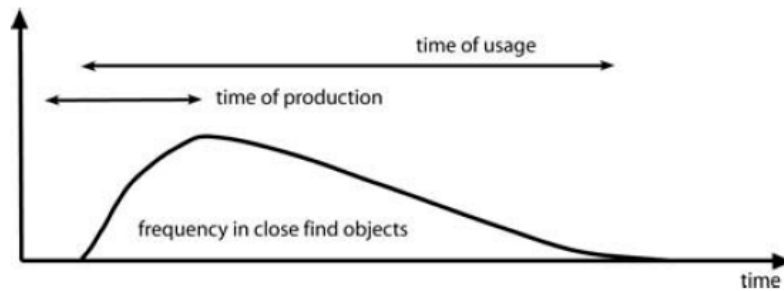


Figure 17: Diagram depicting the frequency of an artefact on relation to time (after Trachsel 2004 and Kneisel 2013).

The occurrence of artefact types has been suggested to be best described by a trapezoidal prior model, which employs different assumptions about the temporal distribution of dates and allows for the possibility of gradual transitions taking a period of time (Brainerd 1951; Karlsberg 2006). This approach allows us to approach the timescales of change in material culture, where there is no a priori way of knowing which cases belong in the introduction, main period of use, and decline (Lee and Bronk Ramsey 2012; Lee et al. 2013).

Returning to Jensen's Pre-Roman Iron Age typo-chronology presented earlier in Part A (2005). Jensen's interpretation of the currency distribution is reflected in how the types are depicted in his typo-chronological system (Figure 5). Here the artefact currencies are placed in their main period of use, but with a line demarcating possible extension into periods before but mainly after. None of the metalwork types have a line before their main period of use, which implies all types had an abrupt introduction, whereas more pottery types are indicated to have prolonged periods of increase and decrease. The currency of the tongue-shaped belt clasp is depicted in four alternative models in Figure 18. Jensen places its main occurrence in period I.1b, but with decrease reaching into the following period I.2a. If this is illustrated in a frequency diagram the currency has an abrupt start, a period of high popularity and a period with decreasing numbers. If instead the actual frequencies counts per burial phase are plotted, this reveals a different frequency distribution with a period of increasing numbers before reaching the maximum. This last density distribution resembles the distribution model proposed by Trachsel (2004), which can be modelled in OxCal using trapezium phase priors (Lee and Bronk Ramsey 2012; Lee et al. 2013).

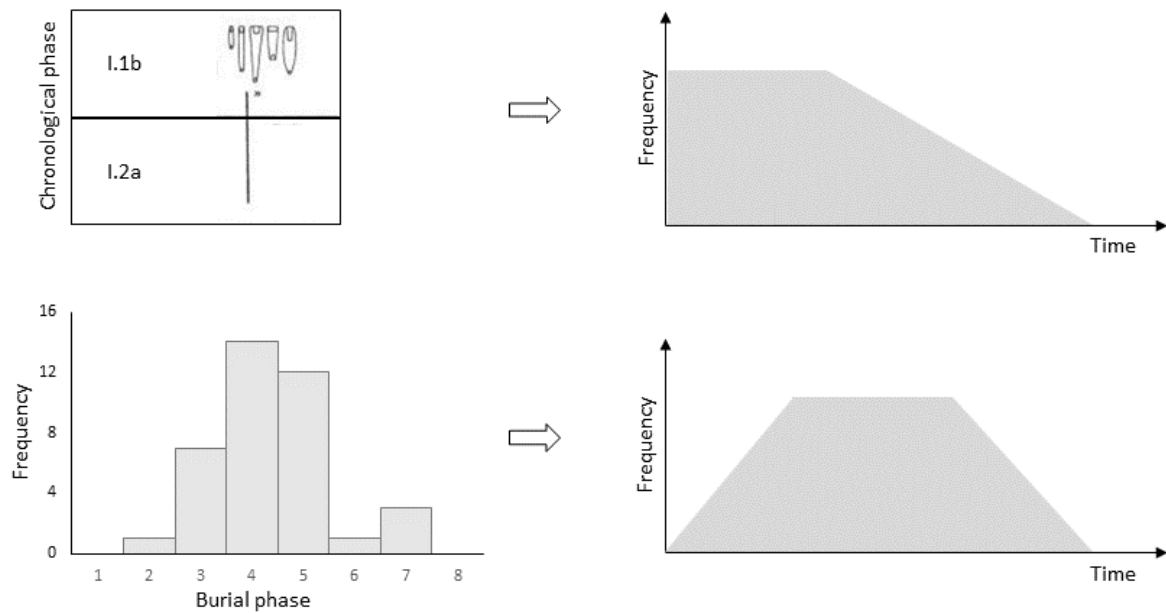


Figure 18: Currency models of the tongue-shaped belt clasp. Top left is how it is depicted in Jensen's typo-chronology (2005), which is depicted in a frequency diagram top right. Lower left is the actual frequency counts per burial phase, which is depicted in a frequency diagram lower right.

Concluding remarks on Bayesian chronological modelling

In this chapter the use of Bayesian chronological modelling in archaeology was presented, something that has been described as the third radiocarbon revolution. The method offers a coherent framework for modelling calendar information in view of our prior beliefs and produces posterior probabilities of events of interest. The basic concepts of model construction in the software OxCal were introduced, including the definition of prior beliefs and model evaluation, which allows testing of the sensitivity of posterior probabilities to the prior beliefs. Special attention was given to the trapezium model because it estimates periods of increase and decrease. As opposed to a uniform distribution model that is applied in the majority of currency studies, i.e. currencies are assumed to have appeared and disappeared abruptly. Finally currency distributions as reflected in the Pre-Roman Iron Age typo-chronology by Jensen were investigated, and it was concluded that the actual artefact frequencies are best modelled in OxCal using the trapezium phase priors.

Part A conclusion

In Part A the archaeological background is introduced, including typo-chronology as a relative dating tool, the Pre-Roman Iron Age in Denmark with its urnfield burial tradition and chronological framework. Radiocarbon dating and Bayesian chronological modelling are introduced as the main methodological tools of this dissertation. The dating of cremated bone is given particular attention and results of an intercomparison study are presented in answer of a dissertation objective. Fortunately it demonstrates that radiocarbon results are reproducible between laboratories and consistent with the expected archaeological chronology. Special attention is also given to the trapezium model that allows the estimation of periods of increase and decrease, and it is demonstrated to be the best chronological model for the Pre-Roman Iron Age artefact currencies under investigation in this dissertation. The concept of wood-age offsets in cremated bone is introduced and factors causing these calendar date offsets between the real cremation events and the radiocarbon dates are examined. It is a research objective to develop a formal method for handling these offsets and it will be the primary aim of the following Part B.

PART B OFFSETS AND OUTLIERS

Modelling offsets and outliers in radiocarbon data

The primary material of this dissertation is cremated bone, which is susceptible to wood-age offsets. This introduces calendar date offsets between the real cremation events and the radiocarbon date, and can significantly affect the research output. It is a research objective to develop a statistical method for formally handling wood-age offsets in cremated bone and Part B is aimed at providing such a model.

In statistics an outlier is an observation that appears to be inconsistent or unrepresentative with the remaining dataset (Barnett and Lewis 1998). Working with radiocarbon dates, an outlier is a date that for some reason does not relate to the dated event in the intended way. If the data is normally distributed, the two sigma rule applies, i.e. roughly 1 in 20 dates will differ more than twice the standard deviation from the mean (Bronk Ramsey 2009b). Outliers can occur by chance in any distribution, but can also be an indication that the dataset has a non-normal distribution or that samples are affected by one or more types of offsets. The precision and accuracy of radiocarbon dates on archaeological material can be affected by a range of errors or offsets, from post-depositional processes to contamination by handling samples on site or in the laboratory (Christen 1994). Much of this is hopefully dealt with by the laboratory sample pretreatment, but four main types of offsets remain (Bronk Ramsey 2009a):

- **Type-s offset:** occurs when the reported radiocarbon measurement uncertainty (1-sigma) is smaller than the real uncertainty. If inevitable measurement scatter is not included measurements will appear over-dispersed.
- **Type-r offset:** occurs when the radiocarbon measurement is correct, but the original ^{14}C ratio of the sample is different from that of the atmosphere. This is due to an admixture of carbon from different sources, e.g. contamination with modern carbon.
- **Type-d offset:** occurs when there is a systematic offset between calibration curve measurements and the sample measurement, e.g. due to differences in growing seasons. If recognized type-d offsets can be corrected using a Delta-R offset.
- **Type-t offset:** occurs when the radiocarbon measurement does not relate to the dated event in the intended way. The ^{14}C measurement is correct, but there is a calendar offset between the ^{14}C event embodied in the sample and the archaeological event with which it is associated.

Identifying outliers is a difficult and essentially subjective procedure. Some samples are known *a priori* to be affected by offsets, e.g. charcoal fragments with potentially large intrinsic ages. Without such prior knowledge, another approach to identifying possible misfit dates is to use the OxCal agreement index, which is a measure of how well the modelled date agrees with the calibrated date (Bronk Ramsey 1995). Dates with indices below the 60% threshold, might not be significant for the overall agreement of a model, but it still demands further query. Once possible outliers have been identified they are often rejected manually, especially if they are interpreted as intrusive in the dated context, but they can also be modelled using formal outlier modelling.⁷ The generic `Outlier_Model` (OM) function was first introduced in OxCal v4.1 (Bronk Ramsey 2009b), and allows dates to be weighted according to a prior probability for how likely they are to be misleading, and allows the user to specify a distribution for potential offsets. OxCal offers default OM, designed specifically to certain types of offsets (see above), e.g. the `General Outlier_Model` drawing offsets from a long-tailed Student's distribution scaled anywhere between 10^0 and 10^4 yr and with a typical prior probability of 0.05. More relevant for this dissertation is the default `Charcoal Outlier_Model`, developed to reduce the impact of wood-age offsets in dates of charcoal, instead of only using them as *terminus post quem*s (as e.g. Garrow et al. 2009). Samples susceptible to intrinsic age, as for example charcoal from trunk wood, are assumed to approximately follow an exponential probability density function, i.e. most samples will date close to the event in question, but a diminishing number of dates will be increasingly older (Nicholls and Jones 2001; Dee and Bronk Ramsey 2014). The Charcoal OM draws offsets from an exponential distribution running from -10 to 0 with a time constant of 1. Offsets can be scaled anywhere between 10^0 and 10^3 yr and are given a prior probability of 1, as all charcoal samples are expected to be affected by wood-age offsets (Bronk Ramsey 2009b). In OxCal the Charcoal OM model is defined as:

$$\text{Outlier_Model ("charcoal", Exp(1, -10, 0), U(0, 3), "t");} \quad (3)$$

And by adding an outlier probability equal to 1 to each charcoal date:

$$\text{Outlier ("Charcoal", 1);} \quad (4)$$

⁷ As it is done in Finkelstein and Piasezky 2010; Olsen et al. 2011; Hornstrup et al. 2012; Alberti 2013; Meadows et al. 2016; Denaire et al. 2017; Dahlström et al. 2018; Fitzpatrick and Jew 2018; Asscher and Boaretto 2019; Edinborough et al. 2020.

A growing number of studies apply the Charcoal OM to dates on charcoal (Nunn and Petchey 2013; Hamilton and Kenney 2015; Higham et al. 2015; Krus et al. 2015; Hanna et al. 2016; Höflmayer et al. 2016a; Höflmayer et al. 2016b; Jakucs et al. 2016; Lulewicz 2018; Manning et al. 2018b).

A bespoke version of the Charcoal OM was suggested by Dee and Bronk Ramsey (2014), allowing a few samples to be younger than the context they represent. The `Charcoal Plus Outlier_Model` takes the standard exponential shape of the Charcoal OM, but also include a very small probability of younger intrusive material. The flexibility of the model allows a realistic reflection of the archaeological scenario at many sites (Dee and Bronk Ramsey 2014; Höflmayer et al. 2016b; Manning et al. 2018b; Manning et al. 2018a; Schmid et al. 2018; Webster et al. 2020). There is limited empirical data available on the scale of wood-age offsets in cremated bone, but it has been suggested to model the offsets using the generic Charcoal OM (Fitzpatrick et al. 2017) or a slightly modified version of this (Garrow et al. 2014). An alternative to outlier modelling is to model individual offsets, tailored to specific samples and their presumed intrinsic ages (Meadows et al. 2012; Torfing 2016; Makarowicz et al. 2018).

Modelling type-r offsets

Radiocarbon laboratories carry out quality assurances by simultaneously measuring internationally agreed standards, but even though great efforts are made to avoid problems, they do occasionally occur. One example of this are the discrepancies of cremated bone dates the radiocarbon laboratory in Groningen experienced in 2017-18 (Paper 3: Rose et al. 2019). PI John Meadows requested that all samples for radiocarbon dating within this dissertation project were split between the Laboratory for Radiocarbon Dating (RICH) in Brussels, the Leibniz Laboratory (KIA) in Kiel, and the Center for Isotope Research (CIO) in Groningen, on the basis that any irregularities might then be easier to discover. This decision turned out to be most fortunate, as four samples that were replicated between the laboratories returned significantly different results, with dates from Groningen being on average 161 ± 40 ^{14}C years younger than dates from Brussels and Kiel. The results from Groningen were also inconsistent with the expected chronology of the Aarupgaard cemetery, whereas results from Brussels and Kiel were in good agreement with each other, and with the expected chronology. An anomaly was suspected in the Groningen dating process, leading to offsets of 100-300 years, and they carried out careful and extensive laboratory testing and identified a relationship between the amount of CO_2 developed and the ^{14}C age. Younger carbon was being added to the samples somewhere and the pretreatment step to remove any sulfur compounds was suspected. The CO_2 was heated with 'Sulfix' particles, which consist of small grains composed of a mixture of Co_3O_4 (catalyst) and Ag_2O . ^{14}C -free

CO₂ was treated in the same way with 'Sulfix' as CO₂ from cremated bone samples, and measured by AMS. The results showed enhanced levels of ¹⁴C, demonstrating that the anomalous radiocarbon dates were due to a contaminated batch of Sulfix. This introduced modern carbon into the CO₂, resulting in a systematic type-r offset, arising from the mixing of carbon reservoirs. The ARTEMIS AMS facility in Saclay in France has experienced a similar situation, probably also involving contamination with modern carbon from a Sulfix product (Zazzo et al. 2013). The contamination problem in Groningen was able to go undiscovered for close to a year (April 2017 -March 2018), because the measurements of background material did not include the entire pretreatment process otherwise applied to cremated bone samples. Following this, the Groningen laboratory protocol was updated and now includes measurement of reference material, replicate measurements and measuring background material including the Sulfix step (see Rose et al. 2019: Supplementary information 1 for further details). Since publication Groningen has changed their laboratory protocol and stopped using Sulfix completely (Sanne Palstra 2020, pers. comm.).

A major challenge when radiocarbon dating collagen in bone and dentine is that consumption of aquatic foods causes type-r dietary reservoir offsets in ¹⁴C ages, as aquatic organisms are depleted in ¹⁴C compared to atmospheric CO₂ (Meadows et al. 2019). Marine organisms have global average ¹⁴C age of c.400yr (Reimer et al. 2013), whereas freshwater foods can have highly variable reservoir offsets (Fischer et al. 2007). Humans (and certain animals) may consume a mixture of terrestrial and aquatic foods, resulting in a mixed carbon signal that requires ¹⁴C age correction (Stuiver et al. 1986). The marine ¹⁴C reservoir offset varies at the regional or even local level, as a function of climate and oceanic circulation, whereas freshwater ¹⁴C reservoir offset primarily varies as a function of calcium carbonate enriched water, e.g. hard water (Philippsen 2013; Cook et al. 2015). Dietary reservoir offsets require offset correction using local ΔR values, defined as the difference between local marine organisms and the global marine calibration model. To calibrate radiocarbon dates on mixed aquatic/terrestrial samples it is necessary to quantitatively reconstruct the individual diet and give realistic estimates of ¹⁴C-depletion in the aquatic species consumed during the period of collagen formation. Dietary stable isotope ratios vary between food groups and species, and their position in the local food web, and paleo-dietary research exploit the fact that these isotopic signals are transferred from diet towards consumer tissues (Fernandes and Jaouen 2017; Meadows et al. 2019). Diet is traditionally reconstructed by measuring stable carbon and nitrogen isotopes (δ¹³C and δ¹⁵N) in collagen, although also oxygen, hydrogen and sulphur are gaining interest, and some laboratories have started to measure isotope signatures in single amino acids and in multiple incremental dentine samples from a single tooth (van der Sluis et al. 2016; van der Sluis et al. 2018).

Case study: Paleo-dietary reconstruction of five individuals from St Alban's Odense⁸

An example of type-r dietary marine reservoir offsets is a medieval multiple grave from St Alban's in Odense (material presented in Part E, Appendix 1). The archaeological excavation information shows the five buried individuals to be contemporaneous, but a combination of their radiocarbon dates is statistically inconsistent ($T = 21.4$, $T'(5\%) = 9.5$, $v = 4$) (Ward and Wilson 1978). The difference between burials x242 and x252 is 125 ± 25 years (5σ), which is highly significant. Both x243 and x241 are also significantly older in ^{14}C age (by $> 2 \sigma$) than x242, and x252's ^{14}C age is significantly older than those of all four of the other burials. The radiocarbon calibration curve is relatively steep in this period, and even small differences in the actual date of dentine formation might lead to differences in ^{14}C ages, but x242 and x252 had the same intrinsic ages (both individuals died at 7–9 years of age). Unless x252 actually pre-dates x242, therefore, their ^{14}C age difference must be due to dietary reservoir effects. Given the archaeological stratigraphic information x252 was the last individual interred in the grave, but it is the oldest in ^{14}C years. Thus, even if a single-event interpretation were to be rejected, dietary reservoir effect corrections would be necessary to reconcile the ^{14}C ages with the sequence of burials.

The percentage marine contribution to the diet in individual samples can be calculated from a straightforward linear interpolation between 100% terrestrial and 100% marine diets, assuming that the stable isotope ratio in collagen only reflects the protein component of the diet (Arneborg et al. 1999; Cook et al. 2015). A linear mixing model was applied to estimate the proportion of marine protein in their diets, using $\delta^{13}\text{C}$ endpoints of -21.7 for 100% terrestrial diets and -10.1 for 100% marine diets. Endpoints are corrected for 1‰ trophic-level shift from diet to consumer and were derived from Mesolithic and Neolithic faunal and marine species from Denmark (Fischer et al. 2007). Endmember values may vary with climate and time period (Millard 2015), but values are not expected to have been significantly different in the medieval period. The linear mixing model estimates the five individuals to have consumed 11.5–24.7% marine protein, with x252 having consumed on average 10% more than the others (Table 3).

⁸ Adapted from Paper 2: Rose et al. 2018.

Table 3: Estimated marine protein consumption, using different dietary models (from Rose et al. 2018: 1554).

Burial	$\delta^{13}\text{C}$ (‰)	$\delta^{15}\text{N}$ (‰)	Linear mixing model	Basic mixing model	Bayesian	Routed Bayesian mixing model
x241	-19.79	12.09	16.5%	7.6 ± 5.6		10.8 ± 5.8
x242	-20.37	11.36	11.5%	4.5 ± 4.1		4.9 ± 3.8
x243	-20.20	10.85	12.9%	4.7 ± 4.0		4.8 ± 3.8
x244	-19.78	10.70	16.6%	6.0 ± 4.8		6.1 ± 4.4
x252	-18.84	12.72	24.7%	13.3 ± 7.5		17.4 ± 6.7

A great disadvantage of the linear mixing model approach, is that it does not provide a clear method for propagating uncertainties. Studies have added 10% uncertainties to estimated marine percentages, but without quantifying why this value should be preferred over others (Cook et al. 2015; Millard 2015). A Bayesian mixing model will attempt to quantify the relative contribution of different food sources and incorporate the uncertainties of their isotopic values. Instead the multi-proxy mixing model FRUITS v3 (Fernandes et al. 2014a) was used to carry out a basic model, assuming protein to be the only carbon source for human collagen. Three distinct food groups were modelled: plants, animal and marine fish. Stable isotope data on cereals (oats, hulled barley, rye) from three medieval sites in Odense (Hammers 2017) were used to estimate parameter values for plant foods. Isotope values for domestic animals (cattle, pig, and sheep) on material from Viking Age Haithabu and medieval Schleswig (Doppler et al. 2010) were used to estimate parameter values for animal foods. Parameter values for plant and animal foods were corrected for -2‰ carbon offset from collagen to protein and a -2‰ nitrogen offset from bulk to protein (Fernandes et al. 2012; Fernandes et al. 2014a). For marine fish (cod, perch, haddock, garfish, plaice, sturgeon), we used isotope values from Haithabu and Schleswig (Doppler et al. 2010). These values are not weighted by species prevalence, and significantly do not include herring. In the Middle Ages, the herring markets in the Øresund exported vast quantities of salted herring to all of Northern Europe, but by the beginning of the 15th century the herring stock started to dwindle and the trade soon lost its importance (Etting 2004). The St Alban's AMS dates point towards a burial event after AD1400, where herring most likely did not contribute significantly to the marine diet and can therefore be ignored. Marine parameter values are corrected by -2‰ carbon and +2‰ nitrogen offsets from collagen to protein (Fischer et al. 2007; Fernandes et al. 2014b). It is difficult to define a specific food group, but from other studies the population of Medieval Odense is expected to have consumed animal products like milk, cheese and eggs, but very little actual flesh, animal or fish (Yoder 2010; Eryvynck et al. 2014). As a consequence, a prior constraint that plant food consumption

will exceed that of animal foods is imposed. A diet to collagen offset of $4.8 \pm 0.5\text{‰}$ for $\delta^{13}\text{C}$ and $4.5 \pm 1.0\text{‰}$ for $\delta^{15}\text{N}$ is assumed (Fernandes et al. 2014a). Table 4 summarizes the parameter values applied in the basic model.

Table 4: Parameter values for three food groups used in Bayesian mixing models (from Rose et al. 2018: 1555).

	Food group	Protein	Energy (lipids, carbohydrates)	Protein $\delta^{15}\text{N}$	Protein $\delta^{13}\text{C}$	Energy $\delta^{13}\text{C}$
Basic model						
	Fish	$70 \pm 5\%$	-	$14.0 \pm 1.0\text{‰}$	$-16.5 \pm 1.0\text{‰}$	-
	Animal	$30 \pm 5\%$	-	$7.0 \pm 0.5\text{‰}$	$-24.0 \pm 0.5\text{‰}$	-
	Plant	$10 \pm 2\%$	-	$4.0 \pm 0.5\text{‰}$	$-25.0 \pm 0.5\text{‰}$	-
Routing model						
	Fish	$70 \pm 5\%$	$30 \pm 5\%$	$14.0 \pm 1.0\text{‰}$	$-16.5 \pm 1.0\text{‰}$	$-24.5 \pm 1.0\text{‰}$
	Animal	$30 \pm 5\%$	$70 \pm 5\%$	$7.0 \pm 0.5\text{‰}$	$-24.0 \pm 0.5\text{‰}$	$-30.0 \pm 0.5\text{‰}$
	Plant	$10 \pm 2\%$	$90 \pm 2\%$	$4.0 \pm 0.5\text{‰}$	$-25.0 \pm 0.5\text{‰}$	$-23.0 \pm 0.5\text{‰}$

The basic Bayesian dietary reconstruction model cannot distinguish plant and animal foods, which given the uncertainty in diet-collagen offsets are too isotopically similar. It is able to identify marine food, as it has more distinct isotopic values, and estimates the five individuals to have consumed 4.5–13.3% marine protein, but with large uncertainty levels, reflecting the combined uncertainties of the model.

A dietary proxy signal does not only reflect the consumed food groups, but more specifically reflects the food group fractions such as e.g. carbohydrates and lipids. These macronutrients do not contribute proportionately to the proxy signal in collagen, which is formed predominantly from dietary protein, but they do have some influence. Dietary routing can be incorporated into a Bayesian routing mixing model to provide more accurate dietary estimates (Fernandes et al. 2014a). A model was constructed that considered both protein and energy macronutrients (carbohydrates and lipids) as food fractions; human collagen is assumed to derive $75 \pm 5\%$ of its carbon from protein, and the balance from energy macronutrients. The same offset values from bulk and collagen to protein values apply as in the model

above, but a -2‰ carbon offset from bulk to energy is added for plant values and likewise from collagen to energy for animal values (Fernandes et al. 2012; Fernandes et al. 2014a). Marine parameter values include a -10‰ $\delta^{13}\text{C}$ offset from collagen to energy (Fischer et al. 2007; Fernandes et al. 2014b). As in the basic model, a diet to collagen fractionation of $4.8 \pm 0.5\%$ for $\delta^{13}\text{C}$ and $4.5 \pm 1.0\%$ for $\delta^{15}\text{N}$ is assumed (Fernandes et al. 2014a). Again the prior constraint that plant food consumption will exceed that of animal foods is imposed, and protein intake is limited to 10–40% of total calories consumed. Table 4 summarizes the parameter values applied in the model. As before, the Bayesian routing mixing model cannot distinguish plant and animal foods, but is able to identify marine food. It estimates the five individuals to have consumed 4.8-17.4% marine calories, again with large uncertainty levels.

Evaluating the fit of dietary reconstruction models

The three dietary reconstruction models report differing intakes of marine food, but not alarmingly so given the large uncertainties. Nevertheless, all models appear to under-estimate the marine contribution to diet, given the ^{14}C -age differences between individuals. If the marine foods had a reservoir effect close to the global marine average, a dietary reservoir effect of > 100 years in individual x252 would require at least 25% of the carbon in this sample's collagen to be derived from marine foods. The linear mixing model provides this, whereas the two Bayesian mixing models calculate more conservative estimates (Table 3). When it is taken into account that the marine offset was slightly higher than the long-term mean in the first decades of the 15th century when the collagen was formed, this could explain some of the apparent underestimation in the Bayesian mixing models. Another factor could be that the preferred plant $\delta^{13}\text{C}$ parameter values in the Bayesian mixing model are too positive, or that there is a more ^{14}C -depleted food source (i.e. freshwater fish). The linear mixing model employs such slightly lower $\delta^{13}\text{C}$ values for terrestrial end-members and slightly higher values for marine end-members, but using actual isotope data for the different food groups is preferable. The Bayesian routing mixing model incorporates more information on food group fractions and isotopic offsets, and better reflects the available knowledge about the potential diets of these individuals. This is the preferred dietary reconstruction model, estimating a consumption of 4.8-17.4% of marine calories, although with large uncertainty levels (Rose et al. 2018)

Modelling type-t offsets

Type-t offsets occur when there are calendar offsets between the radiocarbon measurements and the events of interest, and within this dissertation project such offsets are investigated in dental dentine (Paper 2: Rose et al. 2018), in old wood (Paper 1: Kristiansen et al. forthcoming; Paper 4: Rose et al. 2020), and in cremated bone (Paper 4: Rose et al. 2020). This type of offsets is also present when

radiocarbon dating bone, where a sample will in theory inhibit a mixed radiocarbon signature from the time span between formation and death, but the signal will in effect be close to the turn-over rates in the bone-collagen (Hedges et al. 2007). Bone will, however, re-model at different rates depending on the skeletal element and the age and sex of the individual.

In 2018 the Leibniz Laboratory in Kiel updated their background correction formula for calculating radiocarbon ages in collagen. Although the systematic shift in the type-t offset correction was small, it influences the chronological model for a medieval multiple grave from St Alban's in Odense (Paper 2: Rose et al. 2018). With the former uncertainties it was possible to restrict the grave to a 20-year window *cal AD 1425–1445 (95.4% probability)*, coinciding with two historically documented outbreaks of plague in AD 1427-1428 and AD 1440 (Rose et al. 2018). With the updated uncertainties the grave still has a restricted date range, but now dates to *cal AD 1436-1457 (95.4% probability, Fig. 19)*. The grave no longer coincides with the early plague event in AD 1427-28, but rather introduces another possible event in AD 1450-52 (Bisgaard 2009). Ancient DNA analyses did not detect the presence of *Yersinia pestis* in any of the individuals. Even though the DNA preservation was excellent, there are a variety of reasons why a pathogen may be unable to be detected and thus proving absence is often quite difficult (Katherine Eaton 2019, pers. comm.).⁹

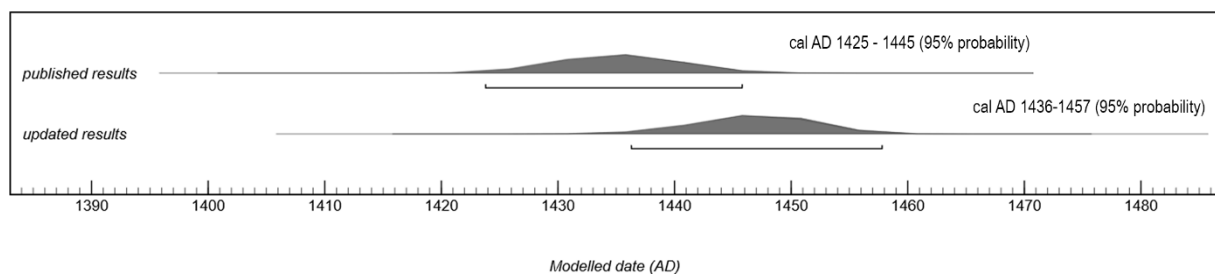


Figure 19: Estimated burial dates of St Alban's grave 156. Published results *cal AD 1425–1445* and updated results *cal AD 1436-1457 (95.4% probability)*.

⁹ Katherine Eaton at the McMaster Ancient DNA Centre, McMaster University in Canada, carried out ancient DNA analysis of the five individuals. They all tested negative for plague (*Y. pestis*) in the separate PCR assay used to target a plague-specific gene (Katherine Eaton 2019, pers. comm.).

Case study: Intrinsic age of collagen¹⁰

Returning to the multiple burial from St Alban's in Odense, where the intrinsic ages of dentine were used as a prior in a chronological model. Unlike bone collagen, collagen in dentine is not re-modelled over time, and thus incorporates a type-t offset equal to the time elapsed between dentine formation and age-at-death (offset range from 5.3 ± 1.0 years to 14.4 ± 1.5 years). A first permanent molar (M1) was sampled from each of the five individuals, and because they had different ages-at-death this ensured that collagen formation in the samples were not exactly contemporaneous and may in fact have spanned a decade. Short-term changes in diet due to e.g. famine will therefore not have affected all five samples. This strategy also aimed to increase the potential dietary differences between individuals, and therefore to maximize potential differences in dietary reservoir effects.

Following the London Atlas, the M1 starts forming dentine at 0.3 ± 0.1 year of age and the crown is complete at 3.5 ± 0.5 years of age (AlQahtani et al. 2010; Beaumont and Montgomery 2015). Applying the quoted variation, a conservative formation period for M1 crown dentine is 0.2–4.0 year of age, with a midpoint of 2.0 ± 0.5 years. Using the midpoint of dentine formation and ages-at-death (see Part E, Appendix 1, St Alban's Odense, Table A1.1) individual age offsets between 5.3 ± 1.0 years and 14.4 ± 1.5 years for the five burials are calculated (Fig. 20).

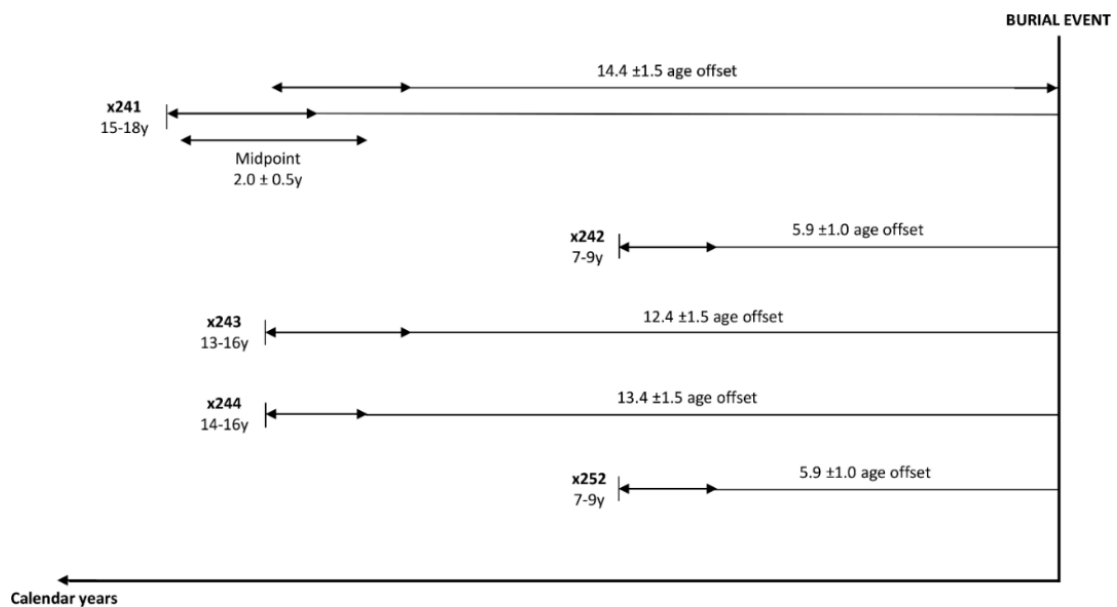


Figure 20: Schematic illustrating of individual age offsets, using age-at-death estimates and midpoint 2.0 ± 0.5 years of M1 crown dentine formation (from Rose et al. 2018: 1551).

¹⁰ Adapted from Paper 2: Rose et al. 2018.

In the chronological model of the grave, the five radiocarbon dates were calibrated with a mix of terrestrial and marine carbon inputs, defined using different dietary models (Table 3). Individual calendar age offsets between 5.3 ± 1.0 years and 14.4 ± 1.5 years were applied. The archaeological excavation information shows the five burials to be contemporaneous, but their combined calibrated dates are statistically inconsistent (see above). When applying the estimated marine consumption given by the linear mixing model, the model estimates a posterior of the burial date to cal AD 1438–1452 (95.4% probability), but with a very poor index of agreement ($A_{\text{model}} = 33.6$), whereby the model is rejected. When applying the estimates from the basic Bayesian mixing model, the model estimates a posterior of the burial date to cal AD 1423–1443 (95.4% probability). The agreement index is satisfactory for the model ($A_{\text{model}} = 78$), but poor for the individual date of x252 ($A = 37$), whose diet-correction is insufficient to fit the single-event model. Finally, when applying the estimates from the routed Bayesian mixing model, the model estimates a posterior of the burial date of the burial date to cal AD 1425–1445 with a mean of $1435 \pm 5\text{yr}$ ($A_{\text{model}} = 92$). Individual x252 ($A = 60$) now has a satisfactory index showing the diet-correction to be sufficient to be compatible with a single event. As mentioned above, the Leibniz Laboratory updated their background correction formula for calculating radiocarbon ages in collagen after Paper 2 was published. With the updated uncertainties the grave now dates to cal AD 1436–1457 (95.4% probability) and no longer coincide with the early plague event in AD 1425–28, but rather introduces another possible event in AD 1450–52 (red vertical line in Fig. 21) (Bisgaard 2009).

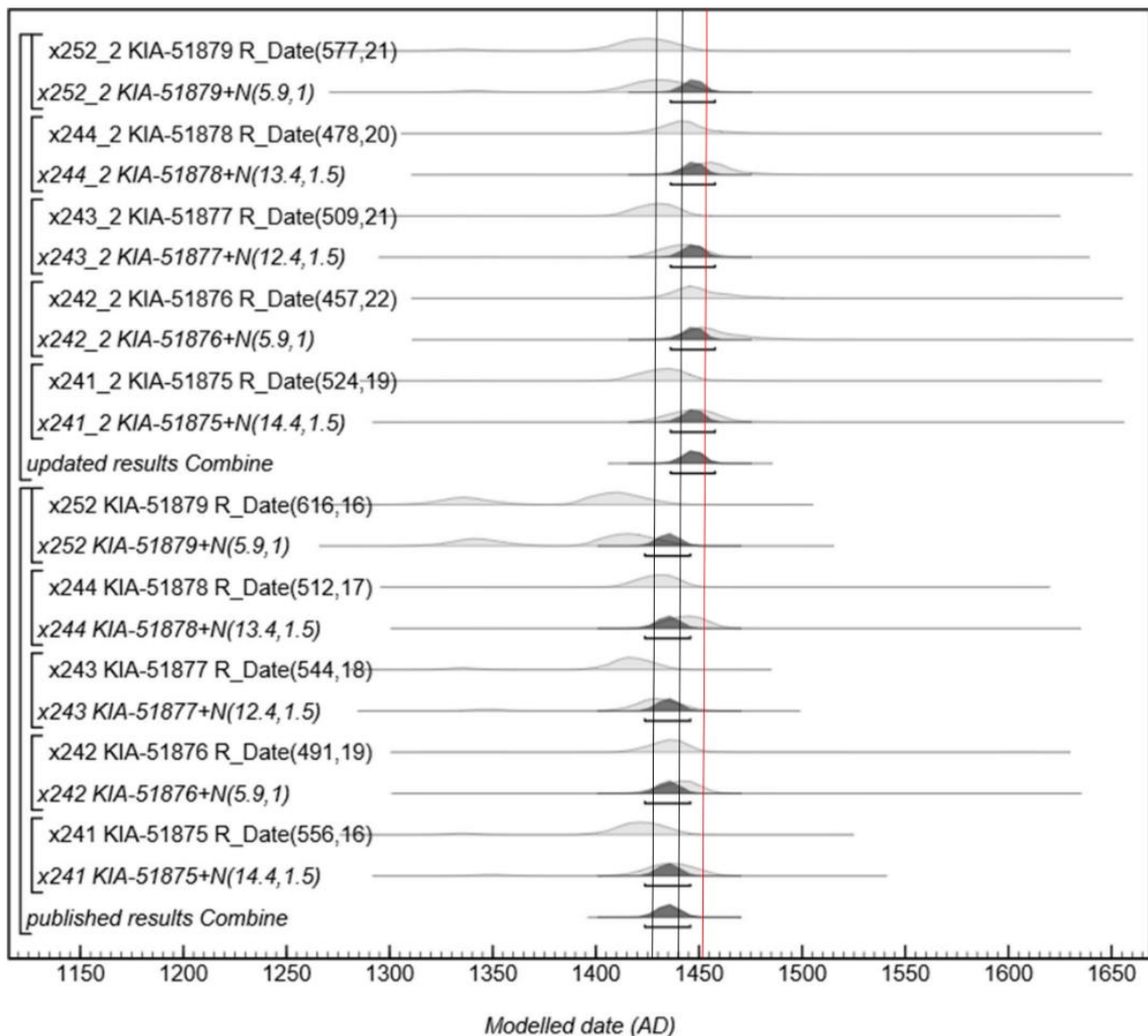


Figure 21: Estimated burial dates of St Alban's grave 156 using a routed Bayesian mixing model and individual calendar age offsets. Black vertical lines indicate coinciding plague events AD 1427–1428 and 1440 according to results published in Rose et al. 2018, and the red line a new possible event in AD 1450-52 introduced after the Leibniz Laboratory updated their background correction formula for calculating radiocarbon ages in collagen.

Case study: Old wood

Modelling dates as *terminus post quem*s (TPQs) in a Bayesian model is often non-informative, but might sometimes be the best alternative to simply omitting dates with large intrinsic ages, i.e. wood-age offsets. In Paper 4 (Rose et al. 2020) samples of cremated bone and context associated organic, including charcoal and short-lived charred plant material (cereal grains and fragments of grass) were radiocarbon dated from 10 individual graves from Aarre urnfield in West Jutland, Denmark (material presented in Part C). Even though the graves were excavated over the last decade and the contents of

the cremation urns were excavated in a controlled indoor environment, several samples of charcoal and cereal grains dated significantly older than the associated cremated bone. These dates were included by using the *After* function in OxCal, i.e. informing the model that these dates pre-date the cremation event. As for grave A99 depicted in Figure 22, where two *Alnus* sp. samples (RICH-25071 and RICH-25066) are probably not much older than the cremation event, but as they are samples of trunk wood they do have a significant intrinsic age. A *Quercus* sp. sample (RICH-25067) might of course have a much larger intrinsic age, but does in this context pre-date the cremation event by up to a millennium.

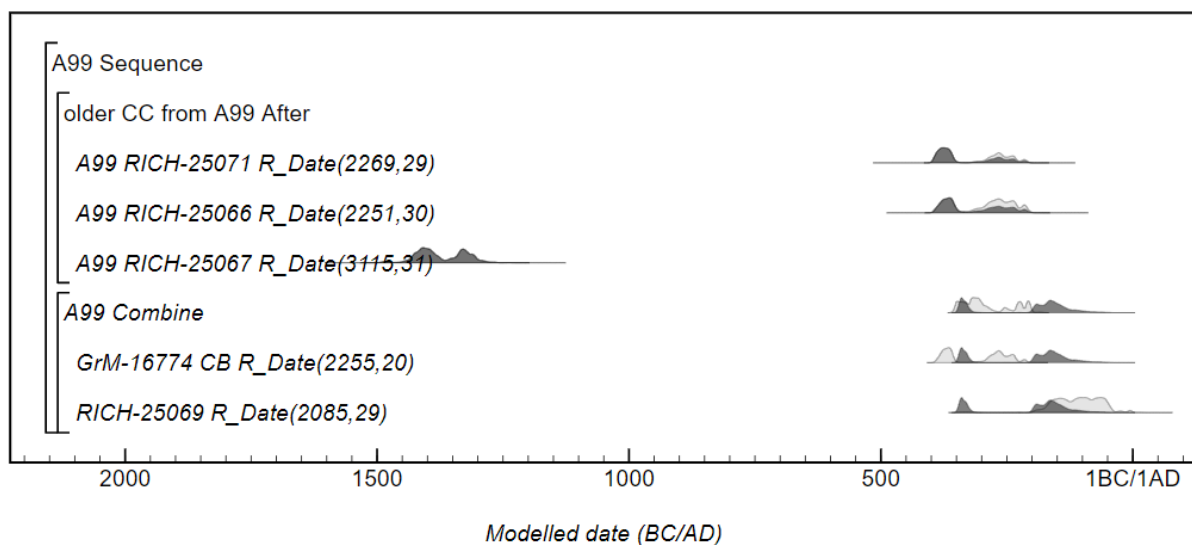


Figure 22: Bayesian chronological model of grave A99 from Aarre urnfield in West Jutland, Denmark. Simple calibrated likelihoods represented by light grey probability distributions, posterior density estimates derived from the model by dark grey probability distributions. Brackets to the left indicate the structure of the model, which is extracted from the larger Model 2 from Rose et al. (2020).

Another approach for including samples with intrinsic age is to model individual offsets, tailored to the specific samples and their accepted intrinsic ages. In Paper 1 (Kristiansen et al. forthcoming) charcoal samples were radiocarbon dated from the Neolithic long barrow Rokaer (material presented in Part E, Appendix 1). This include fragments of *Corylus* sp. and *Quercus* sp. sapwood, which neither have significant intrinsic ages. A bulk sample of *Quercus* sp., probably branch wood fragment with c.20 growth rings,¹¹ two samples of *Alnus* sp. trunk, and a branch fragment do however have moderate

¹¹ Archaeobotanical analysis by Claus Malmros from The Danish National Museum (unpublished report).

intrinsic ages (Claessens et al. 2010; Effenberger 2017a).¹² In a Bayesian chronological model of the long barrow the individual wood-age offsets were estimated based on the lifespan of the specific plant and the sampled section of the plant (Bronk Ramsey 1995; Bronk Ramsey 2009a; Kristiansen et al. forthcoming).

- `R_Date("K-7126 Charcoal ", 4740, 34)+N(20,10);`
A bulk sample of c.20 growth rings of *Quercus* sp., here modelled as falling within a normal distribution range 20 ± 10 yr.
- `R_Date("GrA-69321 x210 Corylus", 4660, 35)+U(0,20);`
Corylus sp. have a low intrinsic age, here modelled as falling within a uniform distribution range 0-20yr.
- `R_Date("KIA-52320 x194a Alnus trunk", 4635, 35)+U(10,50);`
`R_Date("KIA-52321 x194a Alnus trunk", 4740, 35)+U(10,50);`
Alnus sp. trunk wood have moderate intrinsic ages (Claessens et al. 2010), here modelled as falling within a uniform distribution range 10-50yr.

The taphonomic origin of the black burial layer C remains uncertain, but a substantial contribution of peat material cannot be ruled out. This would introduce a potentially very long residence time of the charcoal, besides the intrinsic age offsets already accounted for. In this case, even though the material was deposited at the time of burial interment, the radiocarbon dates do not relate to that event. To handle this, all dates from layer C are treated as *TPQs*, informing the Bayesian model that layer C was deposited any time after the tree-fall dates for individual samples. Layer C was followed by a burial activity phase with dates from mound layer B, where the start event signifies the interment of the burial and the end event the abandonment of the monument (Kristiansen et al. forthcoming).

The satisfactory overall index of agreement ($A_{\text{overall}} > 99$, Fig. 23) indicates that the radiocarbon results are consistent with the structure of the preferred Bayesian chronological model (Bronk Ramsey 1995). Sensitivity testing of the wood-age offsets was carried out, showing only slight changes to the posterior estimates of the burial activity phase chronology. The posterior density estimates derived by the preferred model are given in Figure 23. Initiation of burial activity at Rokaer corresponds to interment of the burial, which we can date to *3467-3336 cal BC (95.4% probability, 68.2%: 3396-3343 cal BC)*.

¹² Also archaeobotanical analyses by Yasmin Dannath and Tim Schroedter from Kiel University (unpublished report).

Duration of the burial activities is estimated to span 0-133yr (95.4% probability, 68.2%: 0-33yr) and the monument is estimated to have been abandoned in 3369-3159 cal BC (95.4% probability, 68.2%: 3358-3315 cal BC). The posterior probability distributions of both start and end boundaries have very long tails, but the model estimates 94% probability that burial activity started after 3450 cal BC and 89% probability that it ended before 3250 cal BC. The Bayesian chronological model of Rokaer long barrow indicates burial activity took place c.3450-3250 cal BC, possibly during only one generation in the 34th century BC. This date is slightly later than the previously suggested 3652-3387 cal BC (95.4%, 68.2%: 3543-3412 cal BC) for the construction and use of the Danish non-megalithic long barrows (Paulsson 2010), but as that study relied on single dates from most sites and did not take account of possible intrinsic ages of charcoal, the estimate is possibly too early. The present Rokaer model relies on more dates from the same site, including dates on material with negligible intrinsic age, and the result is thus regarded as more confident (Kristiansen et al. forthcoming).

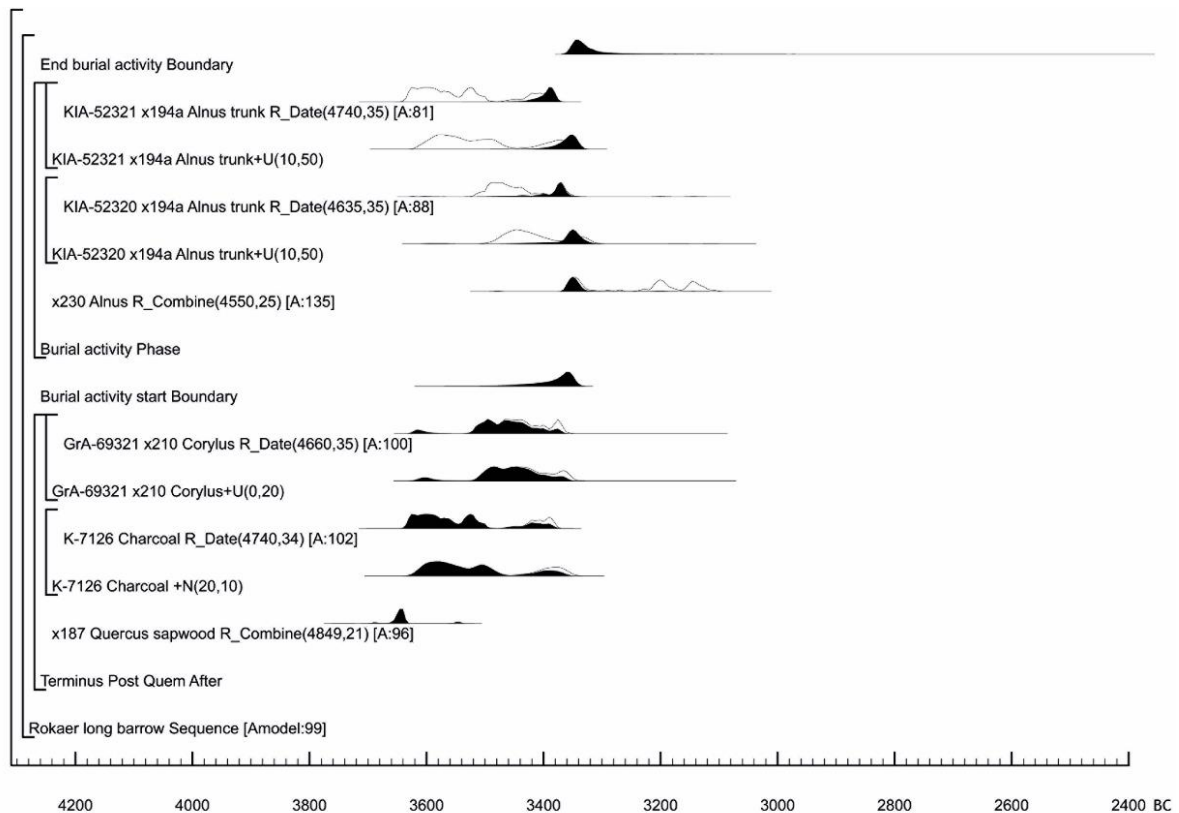


Figure 23: Estimated dates of Rokaer long barrow. Simple calibrated likelihoods represented by white probability distributions, posterior density estimates derived from the Bayesian chronological model by black probability distributions. OxCal indices for individual dates (A) are above the > 60 threshold, indicating satisfactory agreement of individual calibrations with the model (from Kristiansen et al. forthcoming).

Case study: Wood-age offsets in cremated bone¹³

Closely connected with the 'old wood effect' in charcoal is the wood-age offsets introduced to cremated bone during cremation. There is limited empirical data available on the scale of these offsets, although multiple studies report radiocarbon dates on paired cremated bone and charcoal (e.g. (Lanting et al. 2001; Van Strydonck et al. 2005; Olsen et al. 2008; De Mulder et al. 2009; Chatters et al. 2017). As charcoal can itself be affected by variable wood-age offsets, it is instead desirable to focus on associated material with no or limited intrinsic age, e.g. charred twigs or cereal grains. Olsen et al. (2008) reported five pairs of radiocarbon dates on cremated bone and pitch (wood resin with negligible intrinsic age) from the Danish Bronze Age, with a mean difference (cremated bone – pitch ¹⁴C age) of 26 ± 26 ¹⁴C years (ranging from 8-92yr). In another paper, two combined cremated bone ¹⁴C ages were compared to a dendrochronological date, indicating that the cremated bone was 73 ± 26 ¹⁴C years older than the date of cremation (Olsen et al. 2013). In a recent study of a historically attested Buddhist monk from medieval Japan, Minami et al. (2019) radiocarbon dated three samples of fully cremated white bone and a combination of the dates shows them to correspond well with the lifetime of the monk. As wood-age offsets are on the calendar scale (Bronk Ramsey 2009b), these dates require calibration before comparing them using the `Difference` function in OxCal v4.3 (Bronk Ramsey 2009a). All the differences from Olsen et al. (2008; 2013) and Minami et al. (2019) are modelled in a bounded phase starting at zero (i.e. requiring the cremated bone to have a wood-age offset), and the now-constrained wood-age offsets are summarized using the `KDE_Plot` function (Fig. 24) (Bronk Ramsey 2017). Assuming an exponential distribution of wood-age offsets (i.e. applying a `Tau_Boundary` (Bronk Ramsey 2009a) to the end of the bounded phase), the posterior estimates of the offsets have a 22 year median and a 1-sigma range of 32 years. Based on this limited empirical dataset, wood-age offsets in cremated bone appear to be relatively small.

¹³ Adapted from Paper 4: Rose et al. 2020.

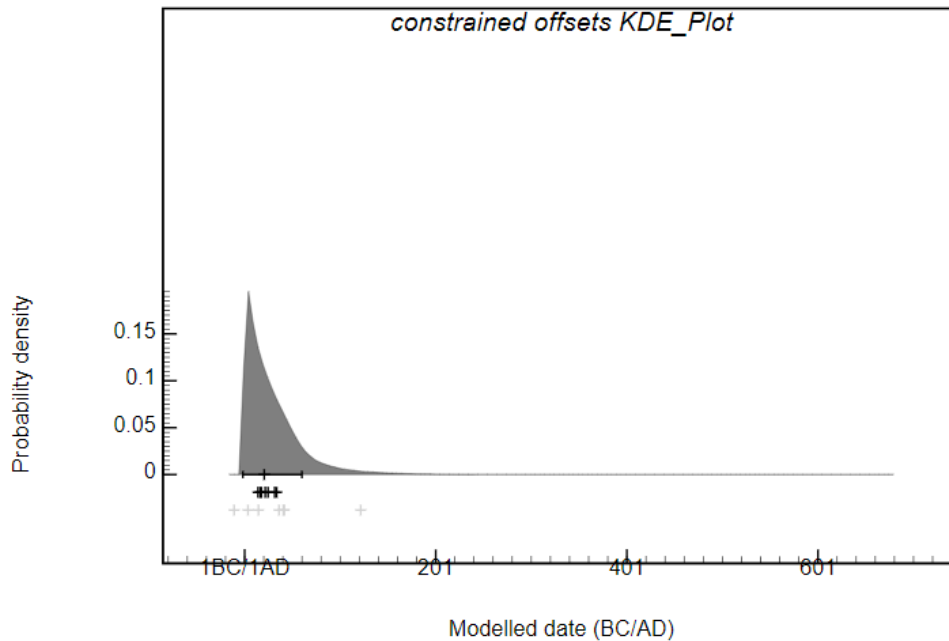


Figure 25: Constrained wood-age offset from Olsen et al. (2008; 2013) and Minami et al. (2019) summarized in a KDE_Plot. Posterior offsets are estimated to -10 years to 52 years (68.2% probability range), with a median of 21 years. The grey crosses are the medians of the likelihood distributions from the radiocarbon measurements, the black crosses are the medians of the posterior distributions estimated by the KDE_Model, and the black bar is the resulting 1-sigma range (from Rose et al. 2020).

Annaert et al. (2020) have in a recent study presented a case study from Broechem, an early Medieval cemetery from the first half of 5th century to the mid-7th century AD in Northern Belgium. They have radiocarbon dated 20 graves with a combination of cremated human bone, cremated animal bone, and charcoal of short-lived and long-lived species. The authors compare the uncalibrated radiocarbon dates on human bone and animal bone, and find the animal bone to date approximately a century older than the human bone. They find the human bone to be consistently too young, whereas the animal bone bones fit the expected chronology based on typo-chronology. The differences between the calibrated radiocarbon results on human bone (HB) and animal bone (AB) are plotted in Figure 25, and there is indeed an obvious trend towards the animal bone dating older than the human bone. Annaert et al. find it unlikely that uptake of old carbon from the wood will cause offsets in the range of a century, but this also cannot explain the consistent differences between human and animal bone dates. They instead focus on the possibility that the human bone are affected by reservoir effects from consumption of fish (marine or terrestrial), whereas the animals had a purely terrestrial diet. They discuss that such a reservoir offset could either be introduced by (human) collagen or bio-apatite. It is unlikely that collagen can cause such a large offset, because even though it might incorporate a

significant amount of protein derived from fish and might contribute to the carbon composition of the pyre atmosphere, it must be burnt out before recrystallization can begin (Snoeck et al. 2014). Cremated bone will incorporate carbon from the bio-apatite, but this is heavily out-weighted by exogenous carbon from the combustion material, as we and others have demonstrated in experimental studies (Hüls et al. 2010; Zazzo et al. 2012; Snoeck et al. 2014; Rose et al. 2020). Bio-apatite incorporates carbonate ions formed through energy production in cells (Lee-Thorp 2008), causing it to reflect a more ‘average’ diet (compared to collagen). If the observed offsets are caused by a reservoir offset in the bio-apatite, this offset would have to be large considered the small uptake of original carbon in cremated bone, which would demand a very large consumption of fish. Annaert et al. recognise that there is no archaeological evidence supporting that the populations of Northern Belgium relied so heavily on fish consumption in this time period.

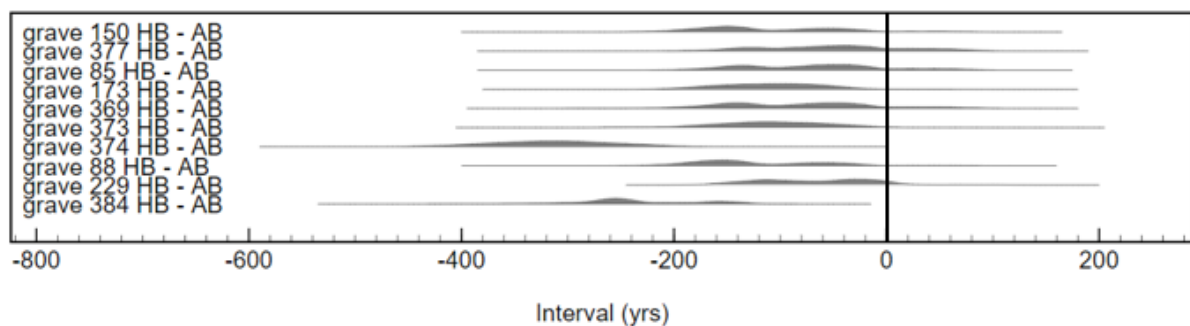


Figure 26: Differences (in years) between calibrated radiocarbon results on cremated human bone (HB) and cremated animal bone (AB) from Broechem cemetery (Annaert et al. 2020). Differences that plot left of the vertical zero line imply that the animal bone is older than the human bone.

Annaert et al. further discuss whether difference in compactness of the cortical bone between humans and animals might cause differential uptake of CO₂ from the pyre atmosphere, but find this to be unlikely based on experimental data from Zazzo et al. (2012). This aspect will need further investigation, considering the experimental cremations included in this dissertation, and particularly with regard to the cattle bone from pyre no. 11 that had a slightly higher mean carbon exchange rate than sheep bone from the same pyre (Rose et al. 2020). Another difference between the human and animal bone is their ages-at-death, where the primarily adult humans have a higher intrinsic carbon age compared to the animals. None of the suggested explanations appear to explain the consistent differences between human and animal bone dates at Broechem cemetery, but the presented data also inhibits any investigations beyond the merely speculative (Annaert et al. 2020). Hopefully future research will reveal whether this same pattern might be present at other sites, and experiments might be designed to target this question by cremating both thick and thin cortical bone.

Wood-age offsets in an experimental dataset

In Paper 4 (Rose et al. 2020) new empirical data was presented on wood-age offsets in experimentally cremated bone (material presented in Part E, Appendix 1). Pyres no. 8 and no. 11 used recent wood and pyres no. 9 and no. 16 used old dendrodated wood (Table 5) (Daly 2011; Daly 2014). To obtain $F^{14}C$ values and ^{14}C ages for the old wood, the mean was calculated of the raw curve points over the dendrodated growth periods in the IntCal13 Northern Hemisphere atmospheric radiocarbon dataset (Reimer et al. 2013). For the recent wood, data from the Bomb13NH1 (AD1650-2010) calibration curve (Hua et al. 2013) was combined with additional data points from the Hammer and Levin datasets of atmospheric ^{14}C activity from Jungfrauoch in the Swiss Alps (Paper 4: Online Supplementary Information 2) (Levin et al. 2013; Hammer and Levin 2017). Wood will have an inhomogeneous ^{14}C signal, but our approach effectively assumes that it was fully homogenized by combustion, and any differences in cremated bone ^{14}C ages from each pyre are therefore due to differential carbon exchange.

Table 5: Pyre fuel for experimental pyres with dendro dates and values of $F^{14}C$ and ^{14}C age (Hua et al. 2013; Levin et al. 2013; Reimer et al. 2013; Hammer and Levin 2017) (from Rose et al. 2020).

Pyre	Fuel	Dendro date	$F^{14}C$	^{14}C age
No. 8	Recent wood (<i>Fraxinus</i> sp.)	AD 1986-2013	1.0954 ± 0.0032	-729 ± 24
No. 9	Old wood (<i>Quercus</i> sp.)	AD 1100-1282	0.8987 ± 0.0013	858 ± 11
No. 11	As pyre no.8	-	-	-
No. 16	Old wood (<i>Quercus</i> sp.)	AD 34-251	0.7926 ± 0.0017	1867 ± 14

Table 6: Animal bone for experimental pyres with slaughter dates and values of $F^{14}C$ and ^{14}C years (from Rose et al. 2020).

Pyre	Bone	Slaughter date	$F^{14}C$	^{14}C age
No. 8	Sheep (<i>Ovis aries</i>), hind limb	2013	1.0231 ± 0.0018	-183 ± 14
No. 9	Cattle (<i>Bos taurus</i>), large diaphysis	2013	1.0231 ± 0.0018	-183 ± 14
No. 11	Sheep (<i>Ovis aries</i>), hind limb	2015	1.0133 ± 0.0019	-106 ± 15
	Cattle (<i>Bos taurus</i>), large diaphysis	2013	1.0231 ± 0.0018	-183 ± 14
No. 16	Sheep (<i>Ovis aries</i>), hind limb	2017	1.0062 ± 0.0013	-50 ± 10

Cuts of cattle (*Bos taurus*) and sheep (*Ovis aries*) reared in Denmark (AD 2013-17) were cooked and defleshed prior to cremation (Table 6). Although it is assumed that prehistoric humans were not defleshed before cremation, skin and flesh will combust at lower temperatures before bio-apatite recrystallization occurs, and thus should not contribute to the carbon composition of the pyre atmosphere (Zazzo et al. 2009; Snoeck et al. 2014). The animals were all young specimens, so the slaughter dates are compared with recent measurements of atmospheric ^{14}C activity to obtain values of $F^{14}\text{C}$ and ^{14}C age before cremation (Levin et al. 2013; Hammer and Levin 2017). No measurements are yet available for 2017, but because the decline in atmospheric ^{14}C in recent years was relatively steady, a value from the trend over the previous decade could be extrapolated. Radiocarbon units were converted using Stuiver and Polach (1977), but as post-bomb ^{14}C data indicative of ^{14}C activity of the atmosphere rather than radioactive decay are reported here, the $F^{14}\text{C}$ convention rather than pMC is preferred (Reimer et al. 2004).

20 new AMS dates were reported, whereof three pyres produced cremated bone with acceptable CI values, but ^{14}C ages from individual pyres are statistically inconsistent (Fig. 26) (Ward and Wilson 1978).¹⁴ The maximum difference between ^{14}C ages from individual pyres are highly significant, ranging from $120 \pm 28\text{yr}$ ($> 4 \sigma$) to $169 \pm 39\text{yr}$ ($> 4 \sigma$). This is an example of how the shape of the radiocarbon calibration curve has an impact on the magnitude of offsets measured in ^{14}C ages. The post-bomb curve is especially steep, thus a small difference in calendar-age offsets between samples will have a large effect on the radiocarbon determinations. It is not possible to reconcile the radiocarbon dates from individual experiments without accounting for wood-age offsets in the cremated bone.

There appears to be no correlation between % carbon exchange and CI values (Fig. 27a), but there is a clear relationship between % carbon exchange and duration of the cremations (hrs) (Fig. 27b). Values of % carbon exchange and $\delta^{13}\text{C}$ appear to be related, but do not suggest a clear linear mixing model between unburned apatite and wood (Fig. 27c) (Rose et al. 2020).

¹⁴ Pyre no. 8: $T' = 18.4$, $T'(5\%) = 7.8$, $v = 3$. Pyre no. 9: $T' = 21.9$, $T'(5\%) = 7.8$, $v = 3$. Pyre no. 11: $T' = 30.4$, $T'(5\%) = 14.1$, $v = 7$. Pyre no. 16: $T' = 880.5$, $T'(5\%) = 7.8$, $v = 3$.

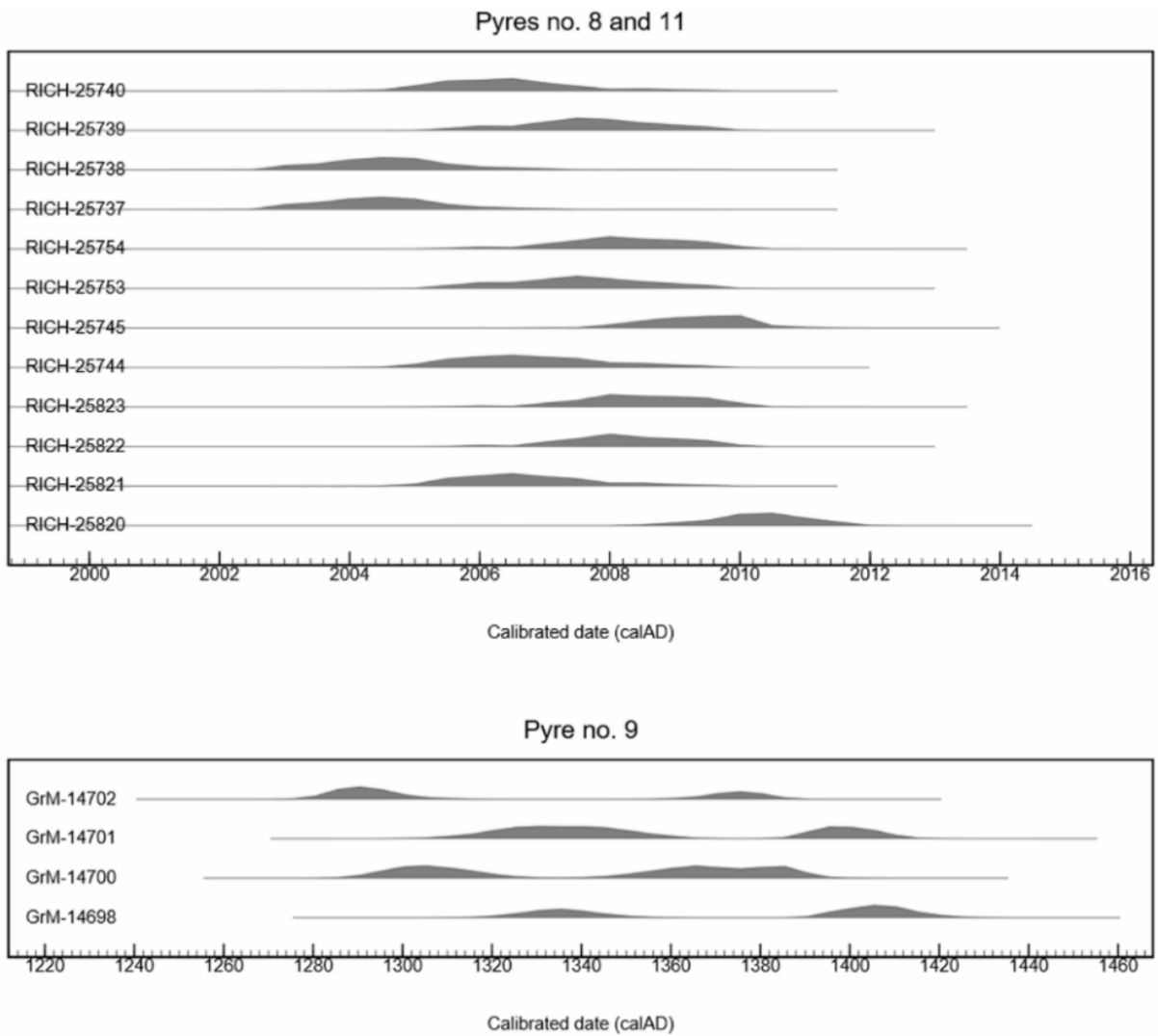


Figure 26: Calibrated radiocarbon results on the experimental dataset. Results from pyre no. 9 are calibrated using the IntCal13 Northern Hemisphere atmospheric radiocarbon dataset (Reimer et al. 2013). Results from Pyres no. 8 and 11 are calibrated using the Bomb13NH1 (AD1650-2010) calibration curve (Hua et al. 2013) with additional data points from the Hammer and Levin datasets of atmospheric ^{14}C activity from Jungfrauoch in the Swiss Alps (Levin et al. 2013; Hammer and Levin 2017).

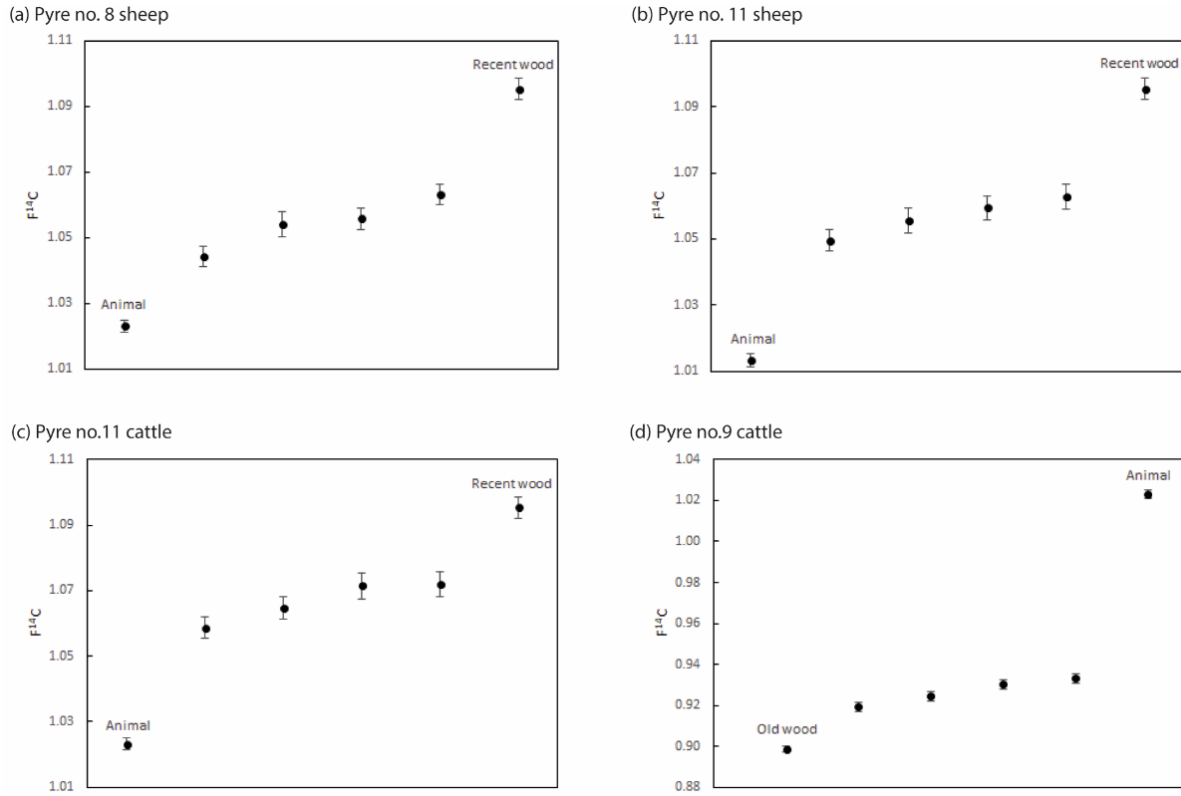


Figure 27: Experimental $F^{14}C$ results with 1σ uncertainties. (a) pyre no. 8 sheep, (b) pyre no. 11 sheep, (c) pyre no. 11 cattle and (d) pyre no. 9 cattle. Endmember values of animal and wood indicated directly in the figures (from Rose et al. 2020).

Calculating carbon exchange

Radiocarbon ages of cremated bone have been shown to plot along or close to a mixing line between the end-members unburned apatite and burning atmosphere ($CO_{2\text{ AIR}} + CO_{2\text{ FUEL}}$) (Hüls et al. 2010; Zazzo et al. 2012). Bone organic matter does not contribute to the cremated bone carbon signal, as it degrades at lower temperatures before apatite recrystallization takes place (Zazzo et al. 2009; Snoeck et al. 2014). The percent carbon exchange between unburned apatite and the pyre atmosphere, as indicated by $F^{14}C$, can be calculated using mass balance equation 1, assuming the $F^{14}C$ content to be evenly distributed throughout the wood and animals.

$$\% \text{carbon exchange} = \frac{F^{14}C_{\text{unburned apatite}} - F^{14}C_{\text{CB}}}{F^{14}C_{\text{unburned apatite}} - F^{14}C_{\text{pyre atmosphere}}} * 100(\%) \quad (5)$$

Where $F^{14}C_{\text{unburned apatite}}$ is the atmospheric $F^{14}C$ when the animal was slaughtered, $F^{14}C_{\text{CB}}$ is the $F^{14}C$ concentration in cremated bone, and $F^{14}C_{\text{pyre atmosphere}}$ is the mean $F^{14}C$ over the period of wood growth, as it will be dominated by CO_2 generated by the wood combustion (Tables 5 and 6) (Zazzo et al. 2012). % carbon exchange uncertainties for individual samples can be calculated using equation 2, where σ_{bone}

is the uncertainty in unburned apatite $F^{14}C$, σ_{CB} is the uncertainty in cremated bone $F^{14}C$, σ_{fuel} is the uncertainty in wood (fuel) $F^{14}C$, and $F^{14}C_{CB}$ is the $F^{14}C$ concentration in cremated bone. The uncertainties are however relatively trivial (c. $\pm 0.5\%$) compared to the observed range of values.

$$\%uncertainty = \frac{\sqrt{\sigma_{bone}^2 + \sigma_{CB}^2 + \sigma_{bone}^2 + \sigma_{fuel}^2}}{F^{14}C_{CB}} * 100(\%) \quad (6)$$

The percent carbon exchange between unburned apatite and the pyre atmosphere ($F^{14}C$ indicated) was calculated and results demonstrate a wide range of carbon exchange from $29.3 \pm 0.5\%$ to $83.5 \pm 0.4\%$ and an overall mean of $58.6 \pm 14.8\%$. Samples cremated using recent wood had a mean exchange of $52.2 \pm 10.9\%$, ranging from $29.3 \pm 0.5\%$ to $67.5 \pm 0.5\%$, whereas samples using old wood had a mean exchange of $77.5 \pm 5.0\%$, with a narrower range from $72.3 \pm 0.4\%$ to $83.5 \pm 0.4\%$. Results are depicted in a density plot in Figure 28, with an added curve depicting 1000 random numbers drawn from a normal distribution, with mean and standard deviation derived from the experimental dataset (from Rose et al. 2020). From this it can be concluded that the distribution of % carbon exchange from the experimental dataset approach a normal distribution.

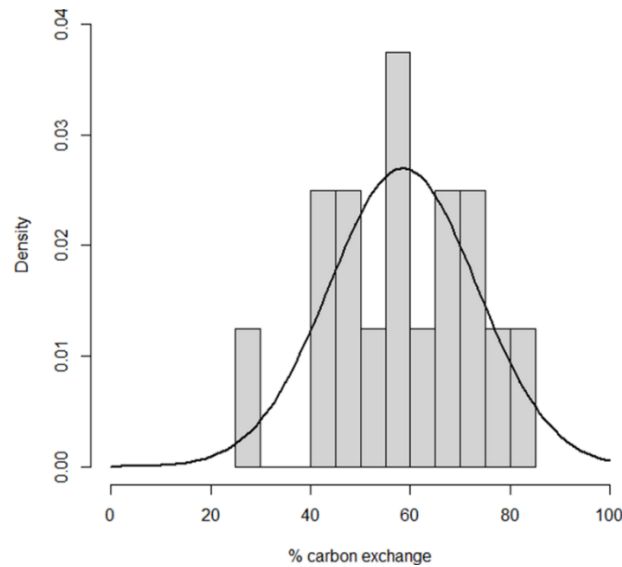


Figure 28: Density plot of % carbon exchange from the experimental dataset (grey bars). The added curve depicts 1000 random numbers drawn from a normal distribution with mean and standard deviation derived from the experimental dataset (from Rose et al. 2020).

The large dispersion of % carbon exchange, even in samples from the same individual (animal cut), is in line with earlier results from laboratory and open-air experimental setups (Hüls et al. 2010; Van Strydonck et al. 2010; Zazzo et al. 2012; Snoeck et al. 2014), and must reflect a differential uptake of exogenous carbon. However, also variations in temperature and CO₂ concentration within a small pyre might play a role, underlining a certain degree of normally distributed dispersion is to be expected when radiocarbon dating cremated bone. Less variation in cremated bone ¹⁴C ages from real prehistoric cremations is to be expected, because the variability in experimentally cremated bone F¹⁴C within each pyre is probably exaggerated due to large differences between the ¹⁴C contents of bones and wood in the experimental pyres (Rose et al. 2020).

Wood-age offsets in an archaeological dataset

In Paper 4 (Rose et al. 2020) the issue of wood-age offsets was approached using an archaeological dataset, although this is difficult as the true cremation dates are not known. The dataset consists of 43 AMS dates measured on 36 unique samples from 10 individual graves from Aarre urnfield in West Jutland, Denmark (material presented in Part C). Both cremated bone and context associated organic samples were dated, including charcoal and short-lived charred plant material (cereal grains and fragments of grass). The graves were excavated over the last decade and the contents of the cremation urns were excavated in a controlled indoor environment. No cremation pyres have been located in or around the cemetery and all graves are secondary deposits (Lorange 2015b). Samples of cremated bone had acceptable CI values (> 5), and values of $\delta^{13}\text{C}$ (mean = $-23.2 \pm 1.9 \delta^{13}\text{C}$) and %C (mean = $0.19 \pm 0.09 \%$ C) fall within expected ranges.

AMS dates are calibrated in OxCal v4.3 using the IntCal13 calibration curve (Bronk Ramsey 2009a; Reimer et al. 2013), and we calculated differences between context associated material and cremated bone (Fig. 29). As expected, differences cluster around zero (indicated by the vertical line), but are strongly skewed towards positive values, i.e. associated samples often date older than the cremated bone. The large majority of charcoal samples are much older than the cremated bone dates, however, and might be derived from residual material relating to documented extensive Bronze Age activities in the area (Lorange 2015b). It is possible that some pyres have been constructed on top of older cooking pits from the Bronze Age, and all kinds of re-use of an area will severely increase the risk of residual material being re-deposited in a younger context, which appears to have occurred frequently in Aarre.

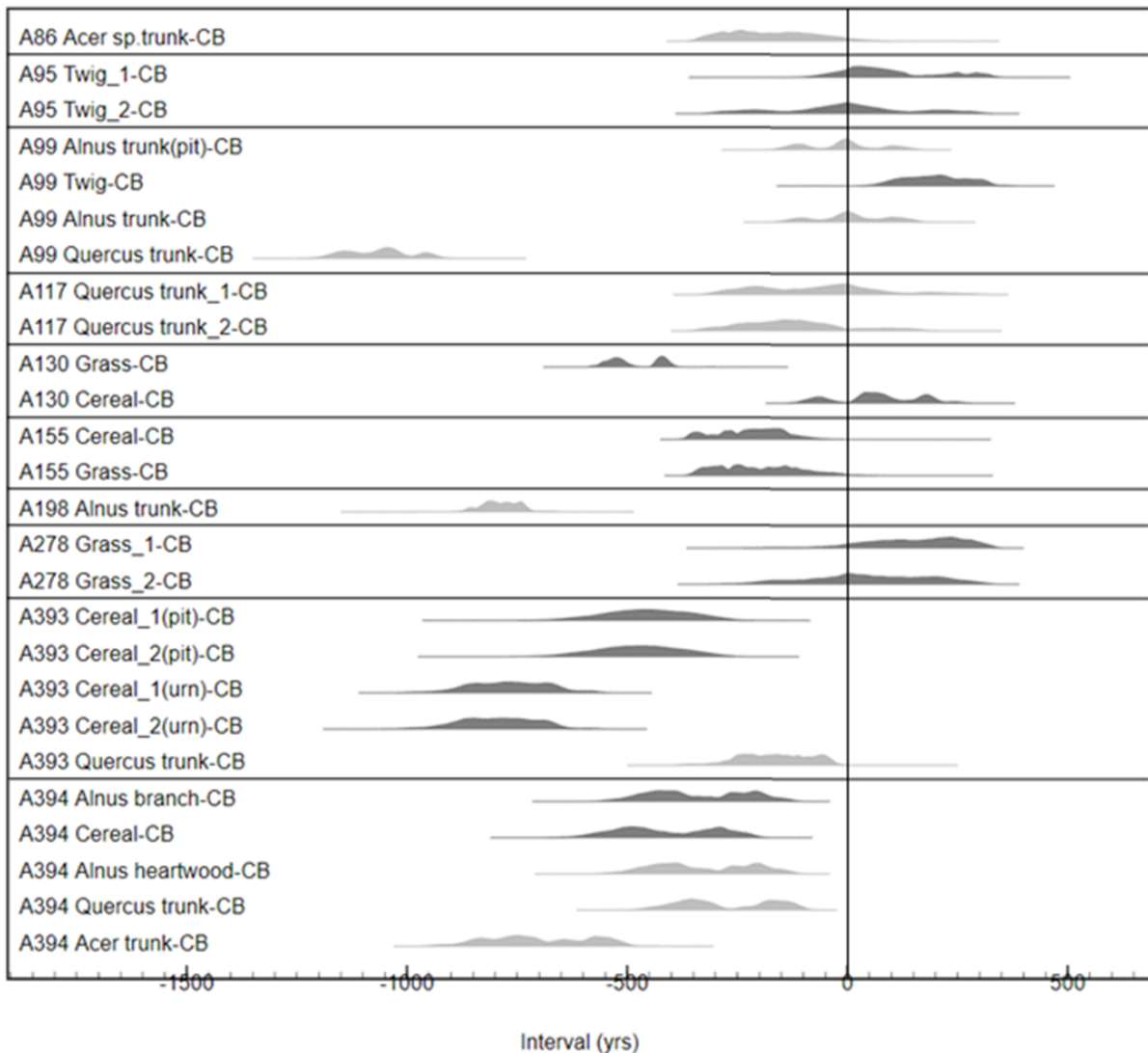


Figure 29: Differences (in years) between calibrated radiocarbon results on context-associated material and cremated bone (CB). Archaeological dataset from Aarre urnfield, grouped by grave. Distributions in black are differences relative to short-lived samples and grey distributions are differences relative to medium - long-lived samples. Differences that plot on or to the right of the vertical zero line imply that a sample is contemporaneous with or more recent than the calibrated date on cremated bone (from Rose et al. 2020).

Single entity, short-lived samples from secure, in situ deposits are in general preferred for radiocarbon dating, but as illustrated in Figure 29 the taphonomic processes might be more complicated than otherwise indicated by the archaeological interpretation, and samples with negligible intrinsic age do not necessarily offer the best estimate of the date of the cremation event. Charcoal samples from oak trunk wood can have considerable intrinsic ages, and even trunk wood samples of shorter-lived alder and maple have an average radiocarbon signal predating the cremation event and can, with a high %

carbon exchange, cause a significant wood-age offset in the cremated bone. Taking a closer look at grave 99, that contains two charcoal samples of alder trunk wood with calibrated dates in agreement with the cremated bone date, whereas a charred twig from the grave dates younger. Another charcoal sample of oak trunk wood from the grave predates the other samples by approximately a millennium and is probably residual and unrelated to the grave. In this scenario the twig with negligible intrinsic age will best reflect the date of the cremation event.

It was decided to focus on graves containing short-lived samples (i.e. with negligible intrinsic age), but ignoring samples dating older than the cremated bone, because wood-age offsets can only make the cremated bone older (unless old bone is cremated with young wood, which is an unlikely archaeological scenario). The calibrated dates similar to or later than the date of the associated cremated bone (i.e. differences plot on or to the right of the zero line in Fig. 29) are regarded as indicators of possible wood-age offsets in the cremated bone samples. Graves A95, A99, A130 and A278 contain material meeting these criteria. The calibrated date differences between cremated bone and short-lived samples are assumed to be exponentially distributed and modelled in a bounded phase starting at zero and ending with a `Tau_Boundary` (Bronk Ramsey 2009a). Results are summarized in a `KDE_Plot` in Figure 30 (Bronk Ramsey 2017). The posterior distribution estimates differences to have a median of *62 years* and a 1-sigma range of *173 years*.

The median offset for the archaeological dataset is larger than the one modelled for combined legacy dates from Bronze Age Denmark and medieval Japan (Fig. 24, median = 22 years, 1-sigma range = 32 years), although they do overlap within 1-sigma ranges (Olsen et al. 2008; Olsen et al. 2013; Minami et al. 2019). It does, however, fall within the 50-100 year offset that has been suggested in the literature, although this now looks to be underestimate the total range (Hüls et al. 2010; Van Strydonck et al. 2010; Zazzo and Saliège 2011; Snoeck et al. 2014). With a high % carbon exchange, as indicated by the experimental dataset, this implies that dating cremated bone is equivalent to or at least close to directly dating the fuel used on the pyre. If the pyre wood has a low intrinsic age, even a high degree of carbon exchange will lead to limited wood-age offsets, but conversely even low degrees of carbon exchange may cause significant wood-age offsets if the wood has a high intrinsic age. Another possible scenario is that the intrinsic age of fuel and bone may be close, causing constant cremated bone ¹⁴C ages, regardless of the degree of carbon exchange (Rose et al. 2020).

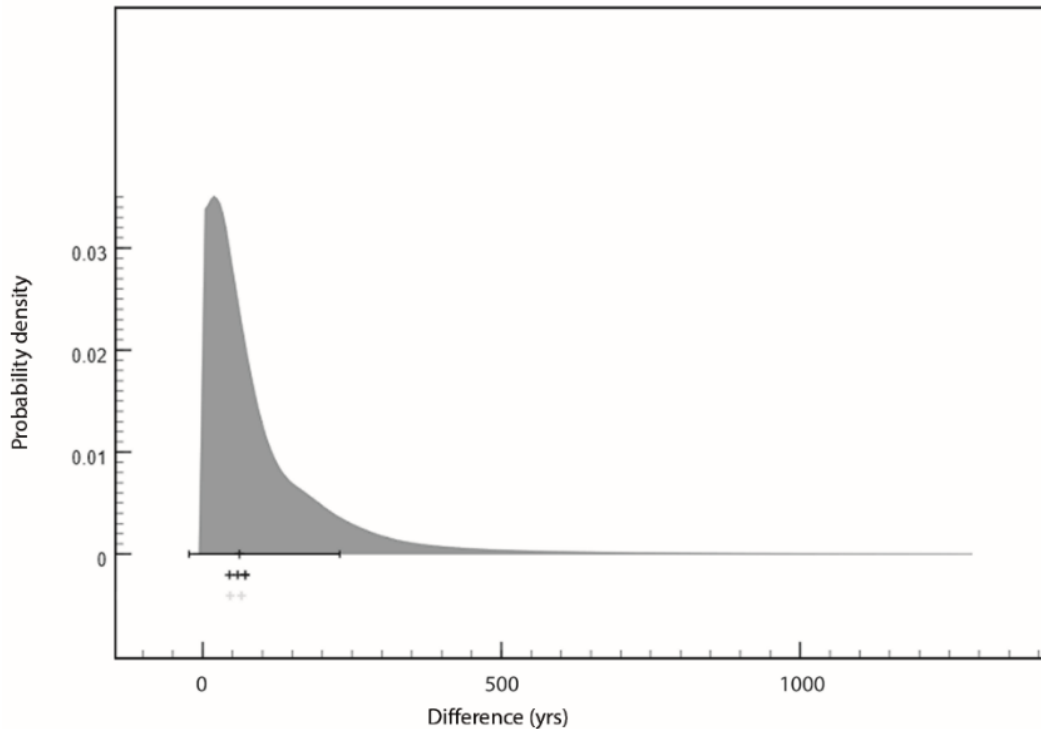


Figure 30: Constrained differences between selected short-lived samples and cremated bone (see text) summarized in a `KDE_Plot`. Differences calculated using weighted means of short-lived samples from grave A95 (2399 ± 19 ^{14}C years, $df = 1$, $T' = 2.8$ (5% = 3.8) and grave A278 (2423 ± 18 ^{14}C years, $df=1$, $T'=1.6$ (5%=3.8)). Median offset of 62 years and a 1-sigma range of 173 years. Grey crosses are medians of the likelihood distributions from the radiocarbon measurements, black crosses are medians of the posterior distributions estimated by the `KDE_Model`, and the black bar is the resulting 1-sigma range (from Rose et al. 2020).

Proposing a new outlier model¹⁵

There are no available proxies (e.g. $\delta^{13}\text{C}$ values) for assessing the scale of type-t wood-age offsets in cremated bone samples, because during cremation isotopic fractionation of carbon takes place as a function of time and temperature (Olsen et al. 2008; Zazzo et al. 2009). Modelling the dates as simple *TPQ* is an unhelpful approach, as this means discarding information about the dates of cremations and will be close to useless in cases where only dates on cremated bone are available. It is here proposed to instead handle dates on cremated bone statistically using the `Outlier_Model` function of OxCal v4.3 (Bronk Ramsey 2009b), which allows dates to be weighted according to a prior probability for how

¹⁵ Adapted from Paper 4: Rose et al. 2020.

likely they are to be misleading, and allows the user to specify a distribution for potential offsets. Calendar age offsets in samples susceptible to intrinsic age are assumed to approximately follow an exponential probability density function, i.e. most samples will date close to the event in question, but a diminishing number of dates will be increasingly older (Nicholls and Jones 2001; Dee and Bronk Ramsey 2014). This assumption can be modelled using the default Charcoal OM (Bronk Ramsey 2009b; Dee and Bronk Ramsey 2014), developed to reduce the impact of wood-age offsets in dates of charcoal, and it has been suggested to also apply this with varying scales to radiocarbon dates on cremated bone (Garrow et al. 2014; Fitzpatrick et al. 2017).

The empirical scale of wood-age offsets was investigated and the underlying distribution of calibrated offsets between cremated bone and selected short-lived samples from the archaeological dataset was found to visually resemble an exponential distribution (Fig. 30) (Rose et al. 2020). This is also the distribution otherwise expected for charcoal dates, i.e. most samples dating close to the event in question, but a diminishing number of samples dating increasingly older (Nicholls and Jones 2001; Dee and Bronk Ramsey 2014). OxCal's default `Charcoal Outlier_Model` (OM) may therefore be a reasonable model for dealing with wood-age offsets in cremated bone. To test this idea, the archaeological results from Aarre urnfield are modelled within a bounded phase of activity (Bronk Ramsey 2009b; Bronk Ramsey 2009a). Individual graves are modelled as phases including dates on cremated bone and selected short-lived samples, except graves A95, A99, A130 and A278 where cremated bone dates are combined with dates on contemporaneous, short-lived samples. Dates of charcoal samples with potentially significant intrinsic ages are modelled as *TPQ* dates. In a *Model 1* (Paper 4: Online Supplementary Information 1, Part 3, Model 1), the Charcoal OM is applied to all cremated bone dates, with a prior probability of 1 (i.e. all cremated bone dates are assumed to be affected by wood-age offsets). The Charcoal OM posterior estimate the cremated bone dates to date *2-91 years* or *0-252 years* older than their cremation events (*68.2% and 95.4% probabilities*), with a median of *55 years*. The offsets agree within the 68.2% probability range with the offsets otherwise indicated by the calibrated differences between selected short-lived material and cremated bone (median *62 years* and 1-sigma range *173 years*), although the Charcoal OM might underestimate the offsets slightly (Rose et al. 2020).

Based on the presented experimental results, the cremated bone dates should always fall between the short-lived sample dates and the average age of charcoal, although individual fragments of charcoal can be younger than the cremated bone. The pyre wood will have an intrinsic age some years older than the cremation event, as will carbon in the unburned bio-apatite. Both are type-t offsets on the

calendar scale. Initially a minimum offset was modelled by incorporating an additional parameter in a Charcoal OM, following the example of Dee and Bronk Ramsey's Charcoal Plus OM (2014). The idea is valid, but was eventually discarded as too complicated and instead different parameter values of the existing exponential OM were tested (as the default Charcoal OM). Moving the upper end of the distribution scale will shift the peak of the OM posterior distribution away from zero (Fig. 31). Changing it from (-10, 0) to (-10, -0.1) ensures the best fit with the wood-age offsets indicated by the presented archaeological results. The constant was changed from the default 1 to 0.9, ensuring a slightly faster exponential decay. Finally the scale parameter was changed from U(0,3) to U(1,3), i.e. offsets can now vary between 10^1 and 10^3 rather than 10^0 - 10^3 years, reducing the chances of sub-decadal offsets. The bespoke `Cremation Outlier_Model` is defined as:

```
Outlier_Model("Cremation", Exp(0.9, -10, -0.1), U(1, 3), "t"); (5)
```

And by adding an outlier probability equal to 1 to each cremated bone date:

```
Outlier("Cremation", 1); (6)
```

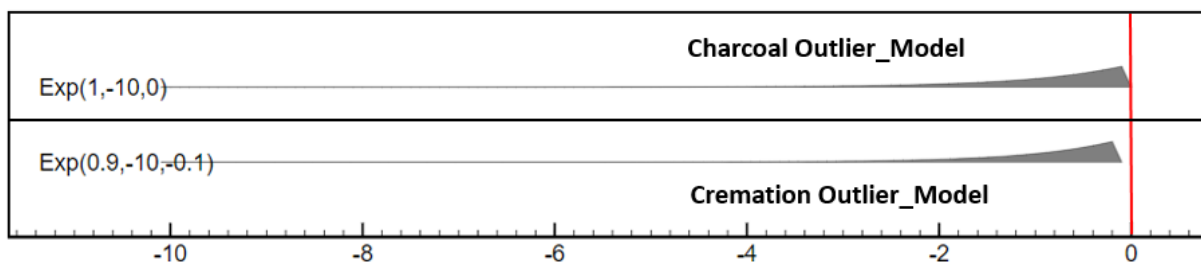


Figure 31: In the upper plot is the likelihood of the default scale in the Charcoal OM, and in the lower plot the adjusted scale parameter of the proposed Cremation OM. Notice that the latter distribution is shifted away from zero as marked by the red vertical line.

In *Model 2* (Fig. 32a) the `Cremation Outlier_Model` is applied to all cremated bone dates, with a prior probability of 1, and otherwise constructed as *Model 1* above (Paper 4: Online Supplementary Information 1, Part 3, Model 2). The Cremation OM estimates the cremated bone dates to date 5-98 years or 2-252 years older than their cremation events (68.2% and 95.4% probabilities), with a median of 61 years (Fig. 32b-d). The Cremation OM estimates larger offsets than the Charcoal OM does and the offset median is very close to the median suggested by the presented archaeological material (Rose et al. 2020).

Next the suitability were tested of both the Charcoal and the Cremation OM for estimating wood-age offsets in the presented experimental dataset using recent wood (pyres no. 8 and no. 11). In a *Model 3* (Paper 4: Online Supplementary Information 1, Part 4, Model 3), the cremated bone dates are treated as representing a bounded phase of activity, and apply a Charcoal OM to the cremated bone dates with a probability of 1. The model estimates activity to start *cal AD 2004-10* and end *cal AD 2008-12* (95.4% probability, $A_{\text{model}} = 96$) and the posterior distribution of the OM estimate the cremated bone dates to date 0-2 years or 0-5 years older than their cremation events (68.2% and 95.4% probabilities). *Model 3* estimates the cremation events to have occurred before the actual event (AD 2013 and 2015), meaning that the Charcoal OM underestimate the wood-age offsets.

Given the short lifespans of the experimental material it will have a shorter residence time of the unburned bio-apatite, compared to the human cremated bone from the archaeological material. The intrinsic age of the pyre wood will however still cause a minimum wood-age offset, why a *Model 4* was created with the same chronological construction as described above. The bespoke Cremation OM was applied to the cremated bone dates, with a prior probability of 1 (Fig. 33a, Paper 4: Online Supplementary Information 1, Part 4, Model 4). The OM takes all adjusted parameters as described for *Model 2*. *Model 4* estimates activity to start *cal AD 2006-14* and end *cal AD 2011-21* (95.4% probability, $A_{\text{model}} = 109$). The posterior distribution of the Cremation OM estimates the cremated bone dates to date 2-7 years or 1-11 years older than their cremation events (68.2% and 95.4% probabilities, Fig. 33b-d). These offsets are larger than calculated by the Charcoal OM and enable *Model 4* to estimate start and end boundaries encompassing the true dates of the cremation events.

It is difficult to assess which OM model is best suited for the archaeological dataset, as the true cremation dates are not known. But it is a convincing argument, that the Cremation OM yields a median offset similar to that suggested by differences between the calibrated dates of short-lived material and associated cremated bone. For the experimental dataset, the Charcoal OM underestimates the observed offsets, whereas the Cremation OM enables the chronological model to accurately date the cremation events. Earlier studies have used outlier modelling to handle wood-age offsets in cremated bone (Garrow et al. 2014; Fitzpatrick et al. 2017), but with new empirical data on the scale and distribution of these offsets it is here suggested that a bespoke Cremation Outlier_Model with a minimum offset is the best suited model for such purposes (Rose et al. 2020).

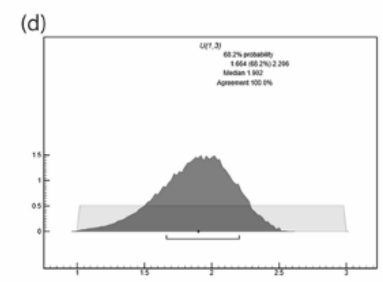
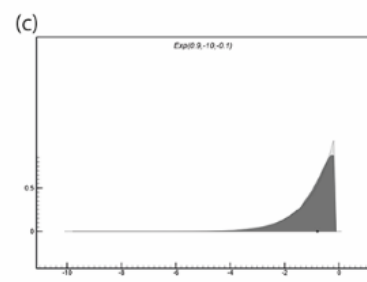
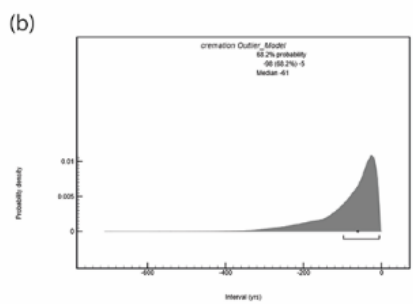
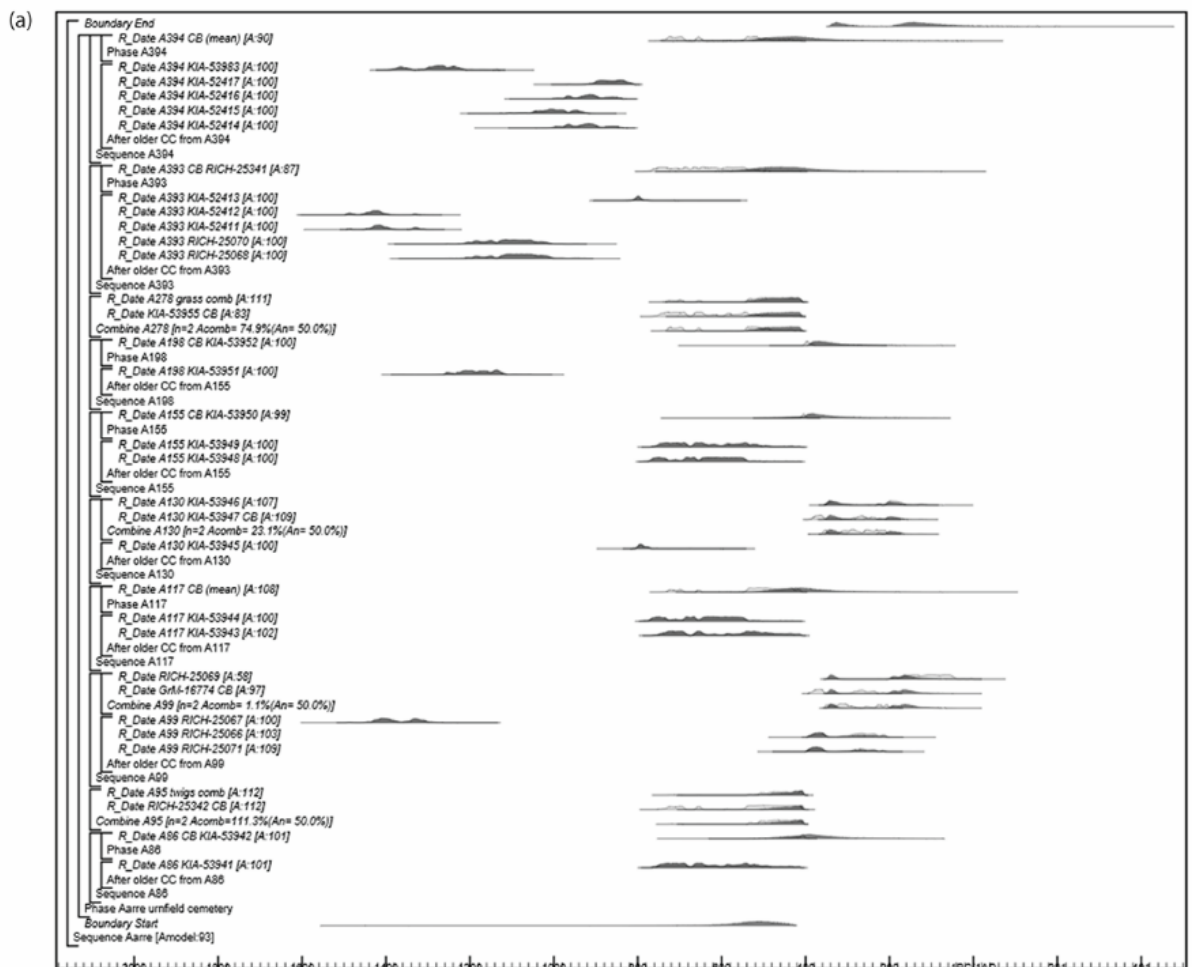


Figure 32: Chronological Model 2 of all radiocarbon results from Aarre urnfield (a) with a bespoke Cremation OM applied to cremated bone dates, (b) is the posterior distribution of the outlier offsets (5-98 years with 68.2% probability), (c) is the effective prior, and (d) the estimated timescale for wood-age offset in cremated bone (posterior distribution in grey and uniform prior shown in outline) (from Rose et al. 2020).

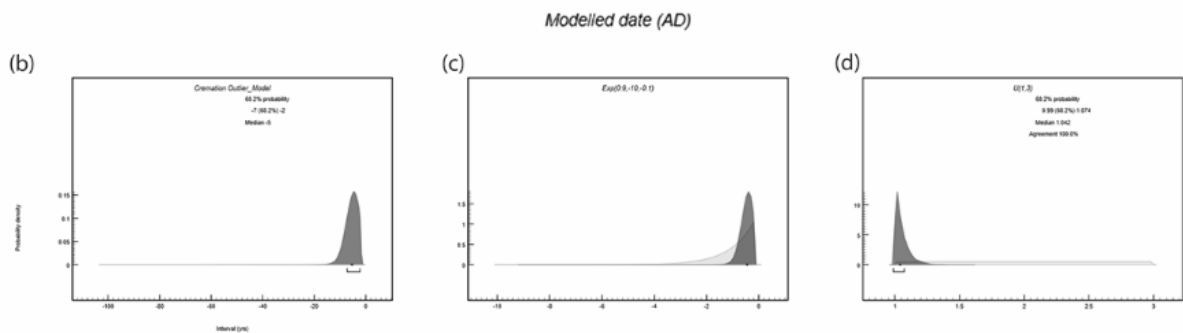
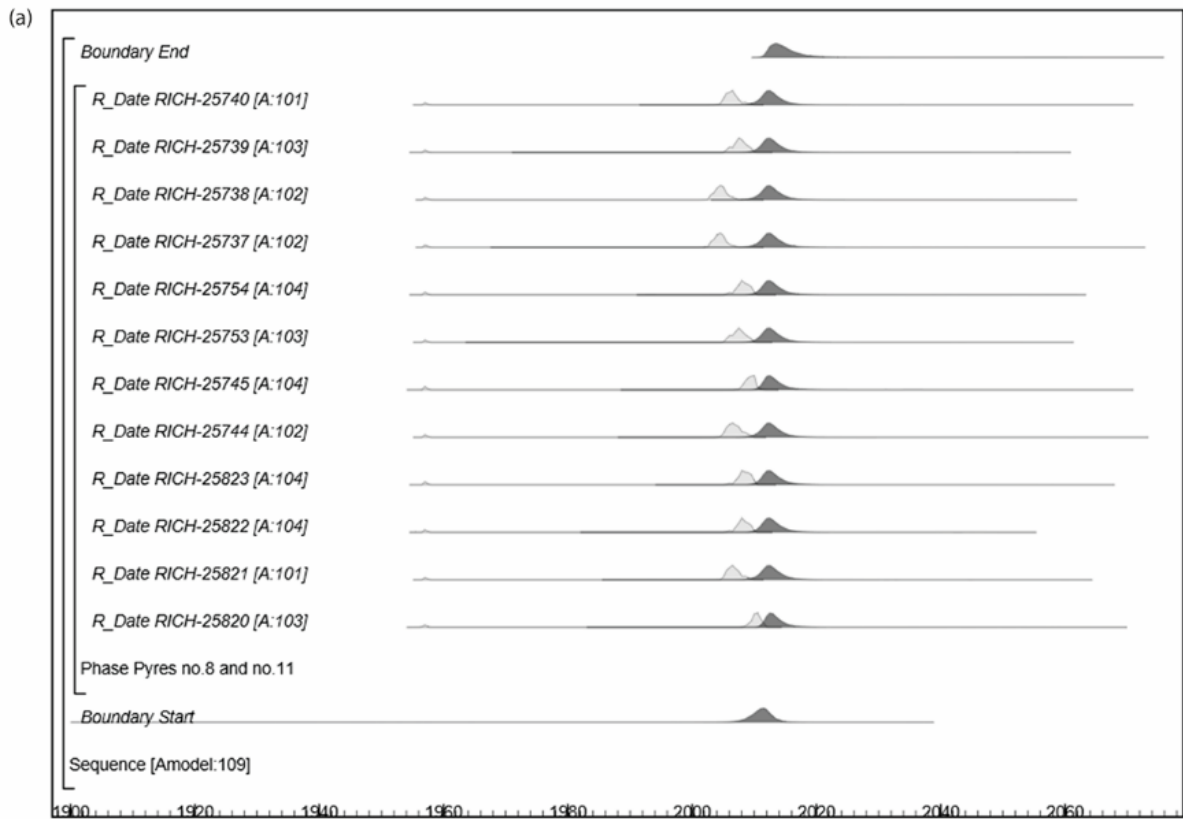


Figure 33: Chronological Model 4 applying a Cremation OM to experimentally cremated bone (a), (b) is the posterior distribution of the outlier offsets (2-7 years with 68.2% probability), (c) is the effective prior, and (d) the estimated timescale for wood-age offset in cremated bone (posterior distribution in grey and uniform prior shown in outline) (from Rose et al. 2020).

Part B conclusion

Radiocarbon outliers do not relate to the dated event in the intended way and Part B provides an introduction to how such outliers might be modelled statistically in OxCal. The different types of offsets that might cause dates to be outliers are presented and the importance of considering intrinsic ages of dated samples and of modelling radiocarbon offsets and outliers using the appropriate statistical models are clearly demonstrated in Part B through a series of case studies. A new statistical model for handling wood-age offsets in cremated bone is proposed in response to a dissertation objective.

Type-r offsets occurs when the carbon in a sample is derived from more carbon sources, such as a contamination issue experienced by the radiocarbon laboratory in Groningen where a contaminated batch of Sulfix was introducing modern carbon to the extracted CO₂ (April 2017- March 2018). The contamination was discovered in the course of this project, when samples replicated between laboratories returned significantly different results (Paper 3: Rose et al. 2019). Another example of type-r offsets can be introduced through the consumption of aquatic foods, such as was the case for a medieval multiple grave from St Alban's Odense where the ¹⁴C dates could not be reconciled with the sequence of burials without correcting for dietary reservoir offsets (Paper 2: Rose et al. 2018). The ¹⁴C dates were also affected by type-t offsets, which is defined as a calendar date offset between the ¹⁴C content of a sample, i.e. its intrinsic age, and the archaeological event with which it is associated. The dates were performed on dentine from the individuals' first molars and individual calendar age offsets were calculated as the difference between dentine formation in early childhood and ages-at-death. The different types of offsets are combined in a Bayesian chronological model and it is possible to date the multiple grave to a 20-year window in the mid-15th century AD. The date was changed slightly following an update of the background correction formula for calculating ¹⁴C ages in collagen at the Leibniz Labor, but enough for it to coincide with different historically documented outbreaks of plague in Denmark.

Another prevalent example of type-t offsets is wood-age offsets in old wood. It is demonstrated how different intrinsic ages of archaeobotanical remains can be modelled as *terminus post quem*s (TPQs) in the case of Aarre urnfield (Paper 4: Rose et al. 2020). In another case study of a Neolithic long barrow from Rokaer individual offsets are tailoring to the intrinsic ages of the specific samples, and by incorporating these offsets it is possible to model an earlier date of the 'Konens Høj' burial type than has previously been suggested (Paper 1: Kristiansen et al. forthcoming). Wood-age offsets is not limited to archaeobotanical remains but can be transferred to cremated bone and it this way cause a

calendar date offset between the real cremation event and the radiocarbon date. There is limited empirical data available on the scale of wood-age offsets, but a literature review conclude that they are relatively small. To remedy this, new empirical data on wood-age offsets in a model experimental dataset is presented (Paper 4: Rose et al. 2020). % carbon exchange is calculated between the unburned apatite and the pyre atmosphere and although the values are widely dispersed they approach a normal distribution with a mean of $58.6 \pm 14.8\%$, reflecting a differential uptake of exogenous carbon. Next the distribution of wood-age offsets are investigated in an archaeological dataset from Aarre urnfield. The calibrated date differences are calculated between the cremated bone and associated, short-lived archaeobotanical remains, such as twigs and cereal grains. The differences are assumed to be exponentially distributed, i.e. most differences will be small but a diminishing number will be larger, and their posterior density distribution has a median of 62 years, which is larger than what has previously been suggested. It is concluded that dating cremated bone is equivalent to, or at least very close to, directly dating the fuel used on the pyre. The size of the wood-age offsets thus primarily depend on the intrinsic age of the wood, but they will always make the cremated bone date older than the true cremation event.

There are no available proxies for assessing the scale of wood-age offsets in samples of cremated bone, but based on the empirical data presented in Part B a new outlier model for formally handling wood-age offsets in cremated bone is proposed (Paper 4: Rose et al. 2020). The model is based on an existing model for charcoal (Bronk Ramsey 2009b; Dee and Bronk Ramsey 2014), but the parameter values are changed to incorporate a minimum offset, a slightly faster exponential decay and reducing the chances of sub-decadal offsets. The bespoke `Cremation Outlier_Model` is tested on the experimental dataset where a chronological model is now able to accurately date the known cremation events, something that was not possible without the outlier model. It is likewise tested on the archaeological dataset from Aarre urnfield where a chronological model estimates median offsets comparable to the offsets suggested by the calibrated date differences between cremated bone and associated, short-lived material. A `Charcoal Outlier_Model` estimates smaller offsets for both datasets and it is concluded that the bespoke `Cremation Outlier_Model` is the best suited model and it is applied to all radiocarbon dates on cremated bone in Part C.

PART C MODELLING ARTEFACT CURRENCIES

Bayesian chronological modelling of Early Iron Age urnfield assemblages from Southern Jutland

In Part C the temporal processes of change in a case study of Early Iron Age urnfield assemblages from Southern Jutland is investigated. A large radiocarbon dataset is combined with prior information concerning site formation processes and artefact typology in a Bayesian framework, and the new statistical model for wood-age offsets is applied to all cremated bone dates. An artefact currency is here defined as a chronological model of when a given type was in production. Modelling artefact currencies in a dynamic way facilitates investigations into the dissertation research questions regarding possible divergent chronological sensitivity of metalwork and pottery types, correlation of typologies and an evaluation of the chronological framework. Also the rate of change, e.g. identifying periods of rapid change in the material record, will be explored and used to improve the current understanding of scales of transformations.

Dating strategy

The dissertation research questions requires that preferably mixed find assemblages of diagnostic pottery and metalwork artefacts are selected and dated. Pottery cannot be ^{14}C dated directly because it is made from fired clay and lack endogenous organic carbon, and although recent research show potential for dating carbon inclusions in iron artefacts the method needs further development (Hüls et al. 2019). Instead the pottery and metalwork artefacts are indirectly dated by associated material that is better suited for radiocarbon dating, which in an urnfield context is cremated human remains and in some cases archaeobotanical remains. If a radiocarbon date on cremated bone is correctly corrected for wood-age offset, it will date the cremation event and the deposition date of the associated artefacts. From an archaeological perspective the cremation is a separate event occurring after death and before burial, but these events are inseparable on a radiocarbon timescale. The production date of an artefact must have occurred sometime before deposition, and for the present purpose it is expected that part of the metalwork might have a discernible residence time, but that the vast majority of funerary urns have a short residence time of less than a decade.

It was difficult to find urnfield graves where combinations of metalwork, pottery and cremated human remains were preserved. Older excavations, such as Becker's excavation of Aarre in the 1950s, provide well-preserved artefacts, but they cannot be included in the dissertation because human remains were

not routinely archived (Becker 1961).¹⁶ During the last four decades, 22 new urnfields from the Pre-Roman Iron Age have been recorded as a direct result of development-led excavations, aerial photography and LiDAR remote sensing, but with a rapidly decreasing state of preservation (Olesen and Schlosser Mauritsen 2015; Møller et al. 2020). Urnfields discovered since the 1980s are often described as only having the lower part of the central cremation urn with a shallow layer of cremated bone preserved, while the rest, including possible artefacts, have been removed by agricultural activity (Mikkelsen and Madsen 1986; Frandsen and Jørgensen 2013; Dollar and Grundvad 2015; Gjerlevsen 2015). This leaves a narrow time frame for urnfield excavations that are likely to provide material for this dissertation, which is even further limited by only about 1/3 of the burials containing metalwork. Aarupgaard urnfield was excavated in the early 1970s and it is the only site to meet all requirements of the dating strategy (Jørgensen 1975). The dating strategy consequently had to be revised in order to increase the dataset. The revised sampling strategy prioritise preserved combinations of metalwork and human remains, whereas preserved pottery is desirable but not necessary. This made it possible to include additional graves from recent excavations at Aarre and Søhale urnfields (Lorange 2015b; Møller et al. 2020).

Table 7: Site specific dating strategy

Aarupgaard urnfield	Graves containing a combination of diagnostic pottery and metalwork and min. 50 g cremated human remains.
Aarre urnfield	Graves containing a combination of diagnostic metalwork and min. 50 g cremated human remains, and in most cases also archaeobotanical remains.
Søhale urnfield	Graves containing a combination of diagnostic metalwork and min. 50 g cremated human remains, and in a few cases also pottery.

¹⁶ No human remains could be located from C.J. Becker's excavations because they were likely never sent to the National Museum of Denmark (Flemming Kaul 2017, pers. comm.).

Material

The three selected urnfields are located in south-west Jutland (Fig. 34) and within the core area of urnfields in present-day Denmark (Møller et al. 2020). This part of the country is characterized by outwash plains with a low-lying topography (Kolstrup 2009). Smaller rivers, lakes and bogs are scattered across the landscape, which to the west is bordered off by the Wadden Sea (part of the North Sea). The climate is temperate and although the primarily sandy soil is nutrient-poor, the area appears to have been relatively densely populated in prehistory. In the Early Iron Age the population lived in relatively dispersed farmsteads, with a subsistence economy based on mixed agriculture (Ethelberg 2003; Webley 2008).



Figure 34: Location of Aarupgaard, Aarre and Søbale urnfields in south-west Jutland, Denmark (map by Ronja Mücke, ZBSA).

Aarupgaard urnfield

Aarupgaard urnfield was first discovered in the late 19th century by the local Reverend Nissen (Gram parish 1888-1899), who excavated several of the small mounds.¹⁷ In 1931 a 72x72m area of the cemetery was declared a protected heritage site, but when an excavation led by H. Neuman was carried out in 1947 it became clear that the site was much larger than expected, with up to 10 acres of it outside of the protected area (Neumann 1947; Jørgensen 1971b). The field was cultivated up until 1970 when the local Haderslev Museum (today Museum of South Jutland) was granted funding to excavate the site in its full extent. Removing large amounts of topsoil by machine was a newly introduced method at this time, and during three field campaigns in the years 1970-72 E. Jørgensen directed the excavation of c. 1300 urn graves (Jørgensen 1971a; Jørgensen 1971b; Jørgensen 1972; Jørgensen 1975). The typology of the intact urns have been analysed by C. K. Jensen (1992; 1996; 2005), and K. Terkildsen (2015) has analysed the social stratification using burial goods and construction details of the burial mounds. In 2018 a project aiming to publish the site in its entirety was initiated and with the help of 'Queen Margrethe II Archaeological Foundation' an initial osteological analysis of the cremated human remains was carried out (Harvig 2019).¹⁸

Aarupgaard urnfield is situated on the western point of a low hill, bordered of by two streams, Gram Å to the north and Gels Å to the south. A large Bronze Age barrow serves as initiation point of burials, and although the barrow was largely destroyed before excavation, three urns typologically dating to the transition period between end Bronze Age and start Iron Age were found in its edges (graves 3330, 3342 and 3869). They are probably among the first burials at the site, and from their position the cemetery expanded along a southbound trajectory over time. This organization of burials can best be described using horizontal stratigraphy. The cemetery covers an area of c.60.000 m², measuring c.100-200 m across (E-W) and c.450 from north to south (Fig. 35). It can be divided into a large western group (red outlines in Fig. 35) and a smaller eastern group (blue outlines in Fig. 35), both starting out from the Bronze Age barrow and in use throughout the chronological sequence of the site, albeit with differing burial tempi. Approximately 1300 graves have been excavated, hereof 94 heritage protected mounds plus an unknown number still within the protected area, reaching a total number of up to 1500 burials. With this, Aarupgaard is by far the largest urnfield in Denmark.

¹⁷ The site is registered under museum no. HAM 1070 and the material is archived at Museum of South Jutland.

¹⁸ Collaborators include Museum of South Jutland, Niels Algren Møller from Museum Thy and the present author.

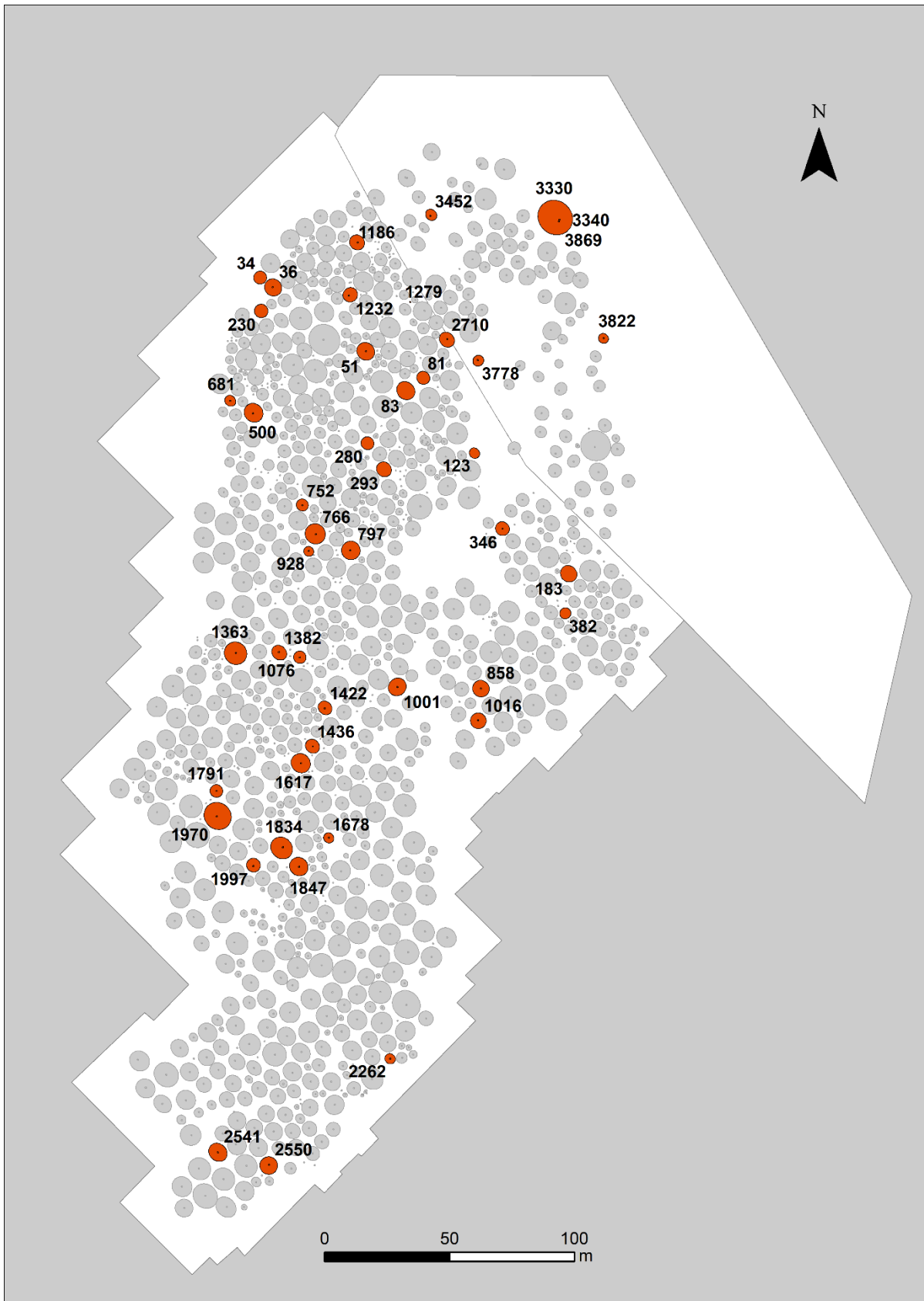


Figure 35: Site plan of Aarupgaard urnfield, 14C dated burials are marked in red. Map by Karin Göbel (ZBSA), based on registrations by Kamilla Terkildsen (Viborg Museum).

The small mounds measuring up to 10 m in diameter are placed in close proximity, but for the large majority without any intercutting. Jørgensen (1975) has described mounds with a diameter of up to 11m, but it has not been possible to confirm this in the museum records. The cremation urns were placed in a small pit in the underground, which was sometimes lined with stones. The majority of urns were covered by a mound and enclosed by a circular ditch. E. Jørgensen (1975) estimated the mounds to have had an original height of 1-2 m. Some mounds were demarcated with kerbstones or wooden posts rammed c.1 m into the ground inside of the circular ditch. The pointed wooden posts measured c.10 cm in diameter and were placed at a distance of 30-40 cm, reaching a total number of 50-60 posts per mound. In the northern part of the cemetery circular ditches have up to six interruptions, whereas in the southern part the ditches only have two interruptions oriented north and south. The shift from more than two to only two interruptions is observed to coincide with the introduction of belt buckles as burial goods (Jørgensen 1971a; Jørgensen 1971b; Jørgensen 1972; Jørgensen 1975; Terkildsen 2015).

Approximately 30% of the graves contained burial goods in the form of dress pins of either iron or bronze, different types of belt buckles, chains and O-rings and a few bronze neck rings. All objects are dress accessories and have accompanied the dead on the pyre, and many are fragmented beyond recognition (Jørgensen 1975; Terkildsen 2015). All graves contain an urn with the cremated human remains, but some graves also have secondary vessels placed either next to the primary urn or in the circular ditch. A few of these also contain a very small amount of cremated bone. The artefacts and cremated human remains are today archived at Museum of Southern Jutland. Based on pin typology, horizontal stratigraphy and number of interruptions of the circular ditches, E. Jørgensen suggested Aarupgaard urnfield had been in use c.500-100 BC and that it could be divided into a number of phases (Jørgensen 1975). C.K. Jensen suggested the site to be divided into three groups based on pottery typology, but refrained from drawing any conclusive boundaries between these (Jensen 1992; Jensen 1996). Building on the earlier works by E. Jørgensen and C.K. Jensen, K. Terkildsen (2015) defined four phases based on diagnostic artefacts and features, corresponding with the chronology put forward by C.K. Jensen (2005).

The majority of urns (c. 70%) contained cremated human remains, but the amount varies from less than 5 g and up to 2600 g, with a mean of c.640 g for all graves, and c. 690 g for graves from mounds with a minimum diameter of 4 m. The difference is not large, but there is a (small) trend of higher amounts of cremated human remains in the very largest mounds (Fig. 36). Three mounds measuring 9 m in diameter contained in average 1450 g cremated human remains, whereas two mounds of 10 m

in diameter contained respectively 75 g and 2600 g each. Probably this trend can be closer described if age and sex of the individuals are also considered.

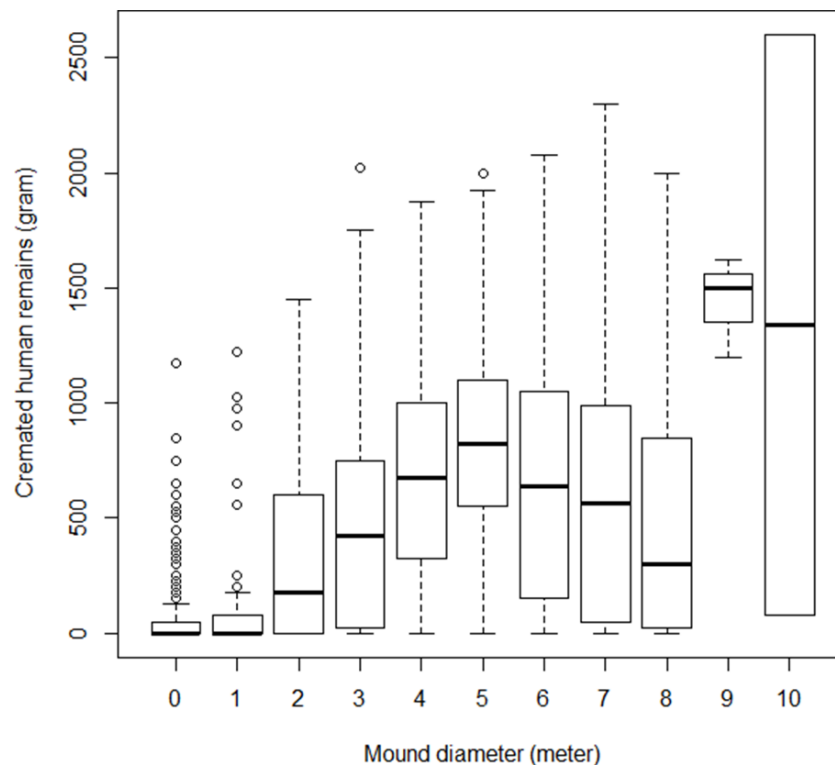


Figure 36: Boxplot of mound diameter against amount of cremated human remains. The boxes represents 50% of the values, the black horizontal line the median, the whiskers the minimum and maximum values, and the open circles the outlier values.

L. Harvig has carried out osteological analyses of cremated human remains from 58 graves, selected to include varying amounts of bone, degree of preservation and from the entire chronological sequence of the site. The results indicate that cremations and subsequent handling of the cremated bone were carried out in a both rigorous and uniform manner, resulting in a very homogenous material. The pyres must have been large and well-constructed in order to burn with a high intensity, fully cremating the bone. The cremated bone is well-preserved and each grave is anatomically representative of a single individual. Overall the material represents a most likely viable demographic population, with individuals of both sexes and from all age groups. It is remarkable that 20 out of 58 graves are estimated to be children, and possibly adding to this number are four graves estimated as 'large child or adult' and 12 graves estimated as 'adult/almost adult'. There are no animal bones in the analysed graves and the cremated bone has probably not been handled beyond transferral from pyre to urn (Harvig 2019).

Aarre urnfield

A. P. Madsen was the first to investigate Aarre urnfield during the early antiquarian registrations, when the small barrows were still visible in the landscape (Madsen and Neergaard 1894).¹⁹ He excavated the central part of c. 250 urnfield barrows over the course of just three weeks, and the material came to play a vital role in the early definition of the Danish Pre-Roman Iron Age. The site was revisited in 1953-54 when C. J. Becker excavated its north-eastern part (Becker 1961). At this point the barrows were no longer visible, but as a new initiative the topsoil was stripped from two-meter-wide excavations trenches at 4 m intervals. Interruptions of the circular ditches could now be observed and the central part of all barrows were excavated to retrieve the urns. C.J. Becker carefully published his results, along with some observations of horizontal stratigraphy in relation to the organization of the cemetery (Becker 1961). C. K. Jensen included C.J. Becker's material in his analysis of the Pre-Roman Iron Age chronology in Southern Scandinavia (Jensen 2005). Most recently, T. Lorange has directed several smaller excavations: the total extent of the cemetery was investigated using trial trenches in 2008 (Frandsen 2008; Lorange 2009); the northern part of the cemetery was excavated in 2010 (Lorange 2010); the central part in 2012 (Frandsen and Jørgensen 2012), and the north-eastern perimeter in 2015 (Lorange 2015a). Several of the graves had already been excavated by C.J. and it was now possible to geo-reference the older excavation (Fig. 37). Approximately half of the original burial ground is assessed to have been archaeologically investigated (Lorange 2015b).

Aarre urnfield is situated on Esbjerg Bakkeø, a low hill island surrounded by wetlands. Three main lines of large burial mounds converge at Aarre, and within the cemetery area are at least 10 Neolithic and Bronze Age barrows (Lorange 2015b; Møller et al. 2020). The earliest urnfields are located around a small group of these barrows, and from here the urnfield cemetery expanded outwards in more directions. The cemetery covers an area of approximately 10,000 m² with originally up to 1000 burials, making Aarre the second largest urnfield in Denmark. The dominant burial form at Aarre is a cremation urn placed either on the ground or in a small pit, covered by a mound and enclosed by a circular ditch. The pit can have a stone lining and a flat stone are occasionally placed on top of the urn as a lid. Some graves contain secondary vessels, either placed next to the primary urn or in the circular ditch. In between the ditches are also single cremation urns and bone-layer graves (German: *Brandgrubengräber*) (Madsen and Neergaard 1894; Becker 1961; Lorange 2009; Lorange 2015b). Approximately 30% of the graves contained burial goods in the form of dress pins of either iron or

¹⁹ The site is registered under museum no. VAM 1600. Artefacts from A.P. Madsen's and C.J. Becker's excavations are archived at the Danish National Museum in Copenhagen, but all material from the more recent excavations is archived at ARKVEST – Arkæologi Vestjylland.

bronze, different types of belt buckles, chains and O-rings. All objects are dress accessories and have accompanied the dead on the pyre, and many are fragmented beyond recognition (Madsen and Neergaard 1894; Becker 1961). Based on typo-chronology of metalwork and pottery (Jensen 2005), Aarre urnfield is estimated to have been in use for 250-300 years, but possibly even longer as the southern part of the cemetery, which is largely unexcavated, might contain younger graves (Lorange 2015b).

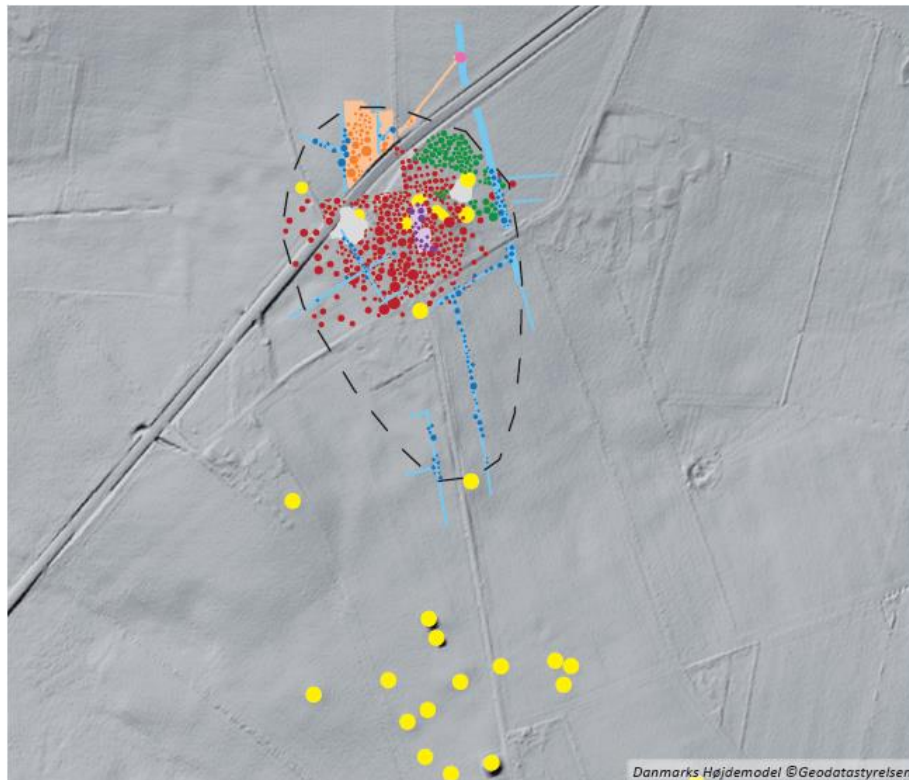


Figure 37: Summary of excavations at Aarre urnfield. Red mounds were investigated by Madsen in 1892, green mounds were excavated by Becker in 1953-54, blue mounds by Lorange in 2008, orange mounds in 2010 and purple in 2012. Large burial mounds are marked in yellow. Results from the field campaign in 2015 is not included (from Lorange 2015b:22).

C.J. Becker (1961) was the first to observe that the cemetery organization could be described using horizontal stratigraphy, which was later confirmed by C.K. Jensen (1996) and J. Martens (1996). The earliest phase of burials at Aarre is characterized by irregular shaped circular mounds and ditches, often merging into larger systems and in one case even capsuling a circular ditch within three larger ones. It remains, however, difficult to documents any direct stratigraphic relationships between the burials. In the following phase the mounds are generally smaller than previous, and both circular ditches and mounds form regular circles and are evenly spaced. Whereas the circular ditches are

uninterrupted in the early phase, in the later phase each grave have two interruptions pointing north and south (Fig. 38) (Lorange 2015b). The circular ditches were still visible at a depth of 25-50 cm in the late 19th century (Madsen and Neergaard 1894), but the recent excavations showed them to be preserved at a depth of only 5-10 cm today (Lorange 2009). No stones or wooden posts demarcating the mounds have been registered at Aarre. A relatively high number of cooking pits and postholes are found in between the circular ditches. These are normal features for the period, but their presence in the landscape where main routes of transport cross, might indicate that besides being a communal burial ground, Aarre was also used for large gatherings. The urnfield burials are part of a very long funerary tradition at Aarre, from the Neolithic to the Roman Iron Age. Burials were not carried out continuously, but the large Neolithic and Bronze Age barrows were visible in the landscape up until the heathland was ploughed in the 19th century (Lorange 2015b).



Figure 38: The part of Aarre urnfield uncovered during the 2010 field campaign. To the south are large and irregular circular ditches from the early phase, and to the north smaller and regular ditches from the later phase (from Lorange 2015b: 27).

Søhale urnfield

Søhale urnfield was excavated in 1996 in advance of gravel extraction and the extent of the burial ground to the west, south and east was documented, whereas a modern road intercuts it to the north (Fig. 39).²⁰ Following excavation the recovered cremation urns were left in museum storage, with their contents still intact, but they were recovered again in 2014. After CT-scanning and excavating of the urns in a controlled indoor environment, the material was analysed as part of a renewed investigation of the Danish urnfield tradition (Møller et al. 2020).

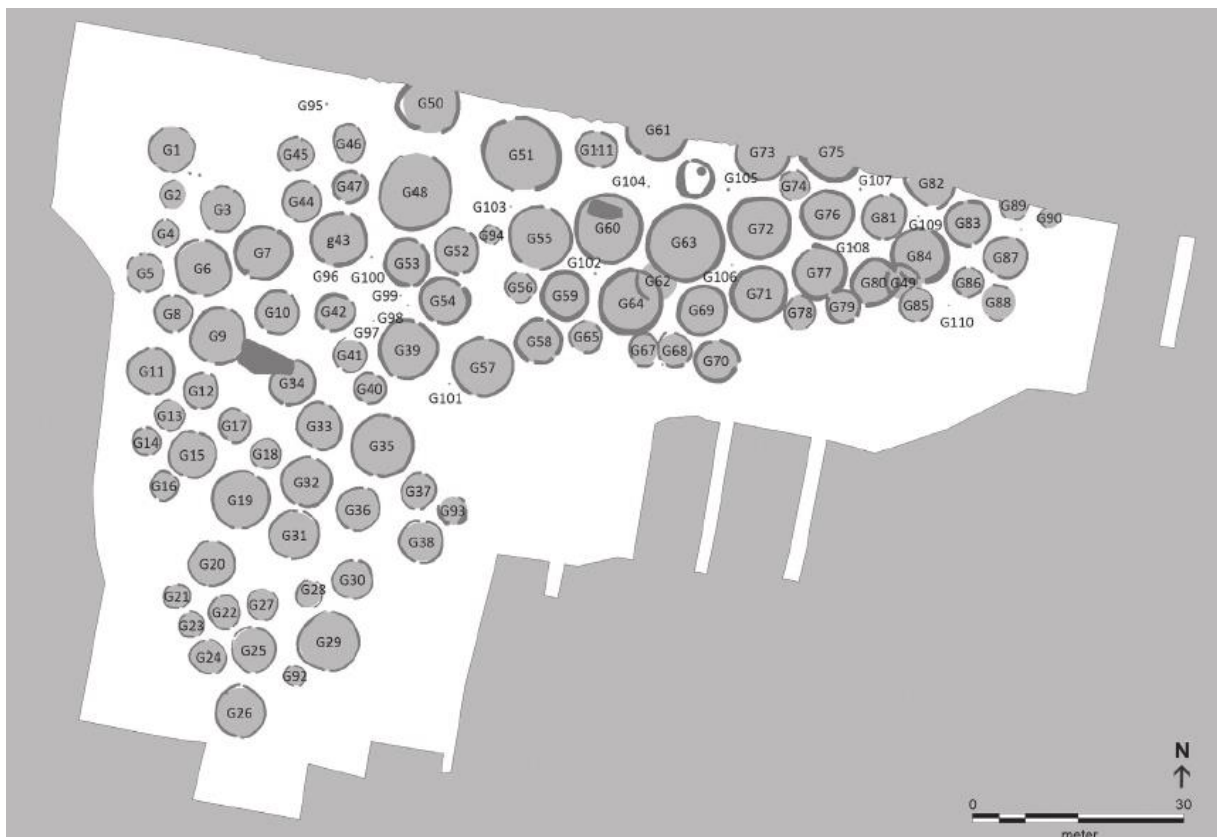


Figure 39: Excavated area of Søhale urnfield (from Møller et al. 2020:22).

Søhale urnfield is situated 10 km inland on a plateau, delimited by streams and wet-lands to the east, north and west. 700 m east of the site is a line of burial mounds demarcating a major transport route. Some 30 m northeast of the site are two large, older barrows that might have served as initiation point, but a modern road prevents further investigation. 93 urnfield mounds were recovered and 73 of these

²⁰ The site is registered under museum no. ESM 2139 and the material is archived at Museum of Southwest Jutland.

contained a centrally placed urn grave enclosed by a circular or slightly oval ditch with a diameter of 2.4 - 9.7 m. Besides the standard urn grave, the local burial tradition also includes bone-layer graves²¹, urn-bone layer graves²², and possible cenotaph graves with and without mound and circular ditch, but no stone lining of the burial pits were observed. The mounds are closely spaced and a few circular ditches overlap, but none of these contained a central burial. The cremation urns were poorly preserved, but 37 out of 103 graves in total contained metalwork in form of dress pins, belt buckles and O-rings. The dress accessories are often very fragmented because they have accompanied the dead on the pyre. Four graves also contained secondary vessels in form of small pots or cups (Møller et al. 2020).

The site chronology has been investigated using metalwork typology and radiocarbon dating of cremated bone (Møller et al. 2020). The earliest group of period I.1a burials are located in the northern part of the cemetery and primarily consists of closely spaced urnfield mounds enclosed by circular ditches without interruptions. Approximately 40 m to the south-west, another burial group was established at the same time or slightly later. This second burial group is characterized by bone-layer graves and circular ditches with two interruptions oriented north and south. The two burial groups merge in period I.2, but each group retains their separate and characteristic burial rites. Møller et al. (2020) interpret this as a cemetery starting out as two separate burial groups differentiated by graves types, and although the burial groups merge over time the differences remain, possibly reflecting different communities sharing the burial ground.

77 out of 103 graves contained cremated bone and L. Harvig has carried out osteological analyses on 67 these. The amount of cremated bone vary from 1 g and up to 1350 g, with a mean of 330 g for children and 770 g for adults. The results reveal highly standardized modus operandi of both cremation and post-cremation handling. The bone is fully cremated with a white to greyish-white colour, reflecting consistent pyre temperatures around 800 °C. There are no signs of wear on the bone, reflecting no further handling besides transferral from pyre to urn. Each burial represents a single individual and individuals across the entire age spectrum have been buried at Søhale, from a neonate no more than a few months old at death to '*maturus*' individuals aged above 35 years. The majority lived to full adulthood, but a remarkable 28% of the graves contained children (Møller et al. 2020),

²¹ German: *Brandgrubengräber*, without a (discernible) container and without substantial amounts of pyre debris.

²² A hybrid burial form containing cremated bone and pottery sherds.

which are otherwise often poorly represented or even missing from archaeological contexts (Ranåker 2009).

Sample selection

Following the defined dating strategy samples of cremated human remains and archaeobotanical remains were sampled for ^{14}C dating from 46 graves from Aarupgaard urnfield, 12 graves from Aarre urnfield and 16 graves from Søhale urnfield. The selection process of graves from Aarupgaard rely on new archival registrations, on published data on pottery by Jensen (2005) and on unpublished registrations by Terkildsen (2005). The urn contents were dry-sieved post-excavation (Marie Louise Stig Sørensen 2017, pers. comm.) and charcoal and other charred archaeobotanical remains were not archived. Cremated human remains were sampled from 46 graves, which span the entire typo-chronological sequence at the site, and in total c. 4% of the recovered burials at Aarupgaard are now radiocarbon dated. The selected graves from Aarre were uncovered in the recent excavations in 2008 and 2010 (Lorange 2010). The material was poorly preserved but fortunately the urns were CT-scanned before they were excavated in a controlled indoor environment. This enable identification of even very fragmented metal artefacts, whereas the urns were too badly damaged (Fig. 40). 10 out of the 12 selected graves from Aarre also contained archaeobotanical remains in form of charcoal, charred cereal grains and grass. The material from Søhale was poorly preserved, but also here the urns had been CT-scanned prior to micro-excavation, making it possible to identify even very fragmented metal artefacts, although the majority of urns were too badly damaged. The pyre debris had at Søhale been carefully sorted before deposition and the urns contained very few archaeobotanical remains and animal bones were completely absent (Møller et al. 2020). Cremated human remains were sampled from 16 graves and adding to these are another 21 graves reported by Møller et al. (2020), but additional analyses of artefact types were carried out. In total c. 36% of the recovered burials at Søhale are now radiocarbon dated.

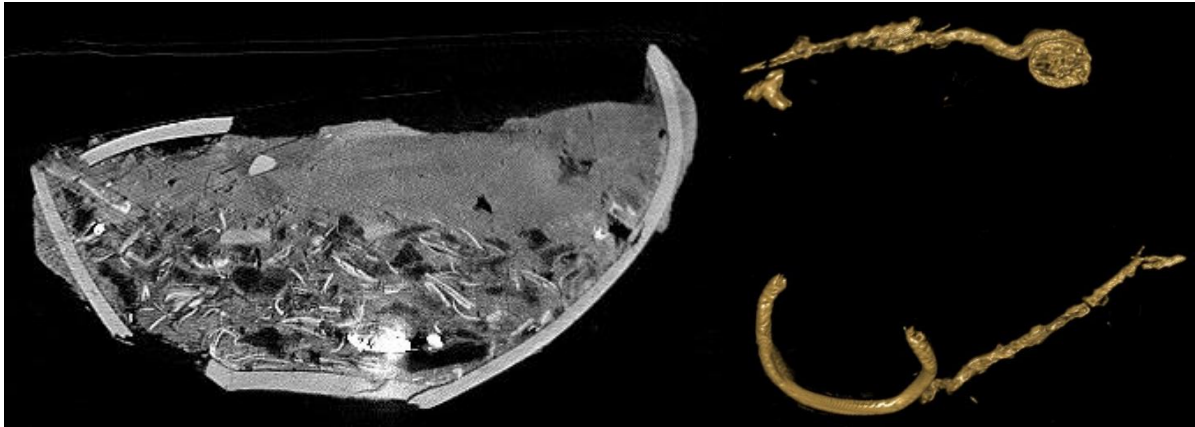


Figure 40: CT scan of urn from grave A278 at Aarre urnfield. To the left is a cross section of the fragmented urn that contain a bottom layer of cremated bone and some fragments of metal. To the right the metal has been isolated and it is possible to determine a bronze ring and two pins with disc-shaped head (pictures by Hjertecenter Vest and ARKVEST).

Laboratory methods

CI values of powdered untreated cremated bone samples were analysed by Fourier-transform infrared spectroscopy (FTIR). All samples had acceptable CI values (> 5), indicating they were fully cremated and suitable for radiocarbon dating. The samples were submitted over several rounds to the Laboratory for Radiocarbon Dating in Brussels, the Leibniz Laboratory in Kiel, and the Center for Isotope Research in Groningen. Samples of charred organics were extracted in Kiel and Brussels following standard acid–alkali–acid procedures (Grootes et al. 2004; Boudin et al. 2015). The laboratories apply different pretreatment methods to cremated bone samples (Brussels (Van Strydonck et al. 2009); Kiel (Hüls et al. 2010); Groningen (Lanting et al. 2001; Dee et al. 2020), but this does not have a measurable influence on the radiocarbon results (Paper 3: Rose et al. 2019). Kiel conducted AMS ^{14}C dating using a HVE 3MV Tandatron 4130 AMS system (Nadeau et al. 1997), Brussels using a Micadas (195.5 kV) AMS system (Boudin et al. 2015), and Groningen using a Micadas (180 kV) AMS system (Dee et al. 2020). All resulting ^{14}C -content was corrected for fractionation using the simultaneously AMS measured $^{14}\text{C}/^{12}\text{C}$ and $^{13}\text{C}/^{12}\text{C}$ isotope ratios (Stuiver and Polach 1977).

Results

Artefact frequencies

Frequencies of metalwork and pottery types from Aarupgaard, Aarre and Søhale urnfields are illustrated in Figure 41. Metalwork has higher frequencies than pottery, because graves from all three sites contain metalwork, but only graves from Aarupgaard contain pottery in larger numbers (metalwork n = 101, pottery n = 46).

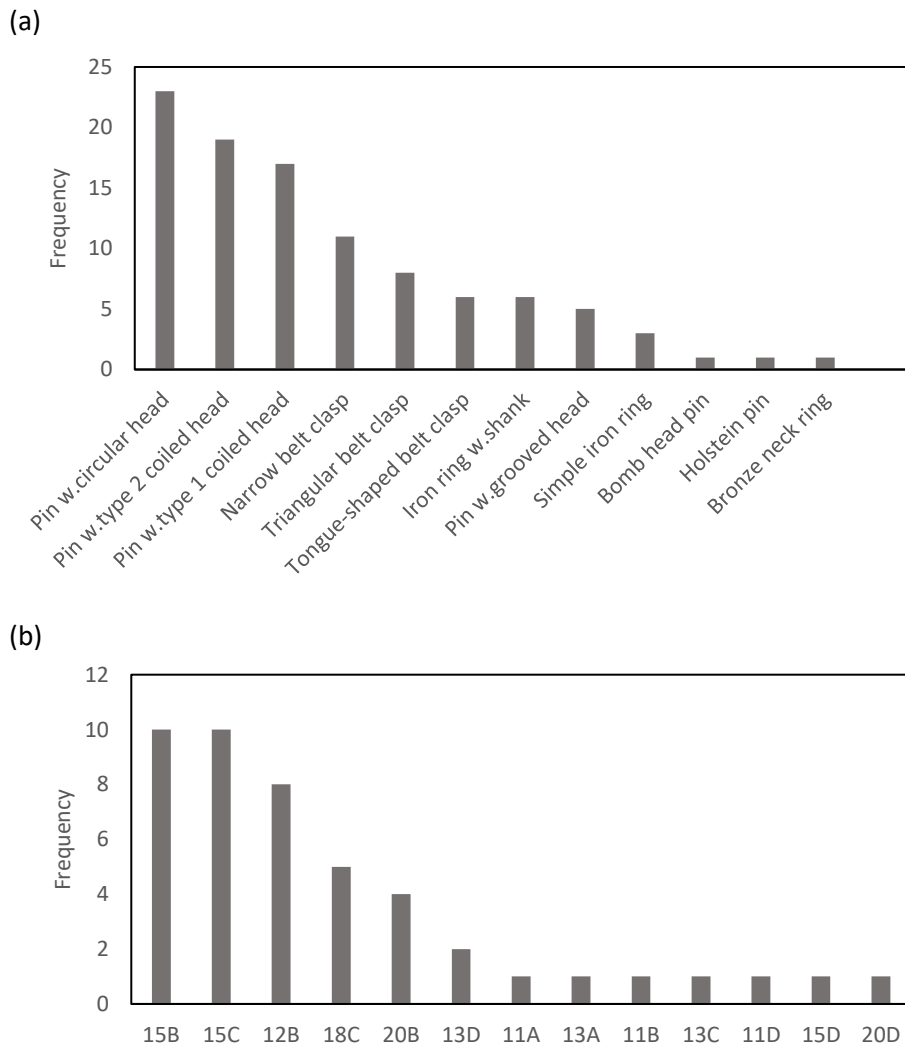


Figure 41: Frequency histogram of artefact types from Aarupgaard, Aarre and Søhale urnfields. Depicting types of (a) metalwork and (b) pottery.

The majority of dated graves are from Aarupgaard urnfield and out of these there are close to equal numbers of graves containing either early pin types (pins with type 1 and 2 coiled head, pins with circular head) or the later occurring belt equipment (iron ring with shanks, all types of belt clasps). The

datasets from Aarre and Søhale are not this equally distributed, mainly because the available material was restricted by preservation, but also because the sites have shorter durations with fewer artefacts from the later part of the typological sequence. This effectively means that the later types are under-represented in the compiled dataset (Fig. 42), with nearly twice the number of graves with early pin types (n = 59) as graves with the later occurring belt equipment (n = 31). Significant changes in burial rates could introduce another bias to the dataset, which will hopefully be investigated further within the Aarupgaard collaborative research project.

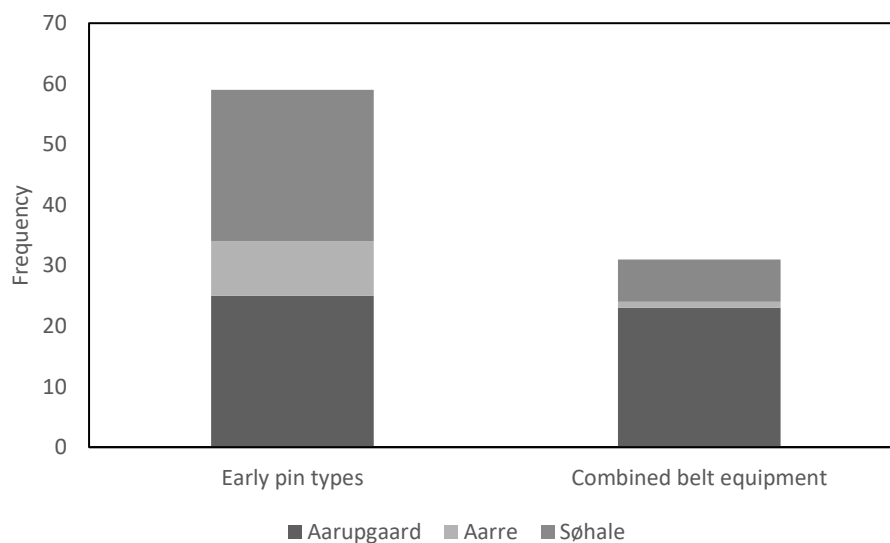


Figure 42: Frequency histogram of early pin types (pins with type 1 and 2 coiled head, pins with circular head) and the later occurring combined belt equipment (iron ring with shanks, all types of belt clasps) divided by site.

Radiocarbon data

The dissertation dataset comprises 131 radiocarbon dates from 74 burials from Aarupgaard, Aarre and Søhale urnfields, including 31 replicate dates on cremated bone samples.²³ 37 dates on cremated bone from 17 graves from Aarupgaard and 43 dates on cremated bone and archaeobotanical remain from 10 graves at Aarre have already been published (Paper 3: Rose et al. 2019; Paper 4: Rose et al. 2020). Here 51 new radiocarbon measurements are reported on 29 graves from Aarupgaard, two graves from Aarre, and 16 graves from Søhale. Additional 22 radiocarbon dates on cremated bone are included

²³ As part of a comparison study (Paper 3: Rose et al. 2019), two cremated bone samples were replicated between Groningen and Kiel. Samples were pretreated in Groningen following the CIO protocol, but subsequently converted to CO₂ and dated in Kiel.

from 21 graves at Søhale published by Møller et al. (2020). These samples were dated at Aarhus AMS Center (Denmark) following pretreatment methods described in Olsen et al. (2008). CI values are not available and it was not possible to replicate any of the dates. There appears to be no systematic difference between the dates measured in Aarhus and the dates measured in Kiel, Groningen and Brussels (Fig. 43). The dissertation dataset in total includes 153 dates on 95 burials from Aarupgaard, Aarre and Søhale urnfields and all dates are reported in Table 8 at the end of Part C.

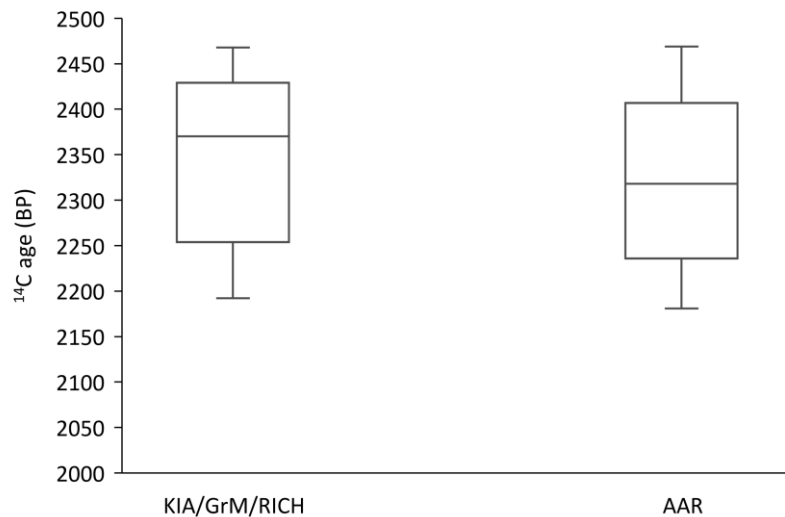


Figure 43: Boxplot of ¹⁴C ages (BP) from Søhale urnfield, comparing dates from Kiel, Groningen and Brussels (KIA/GrM/RICH) to dates from Aarhus (AAR). The boxes represents 50% of the values, the black horizontal line the median, and the whiskers the minimum and maximum values.

Mean values of $\delta^{13}\text{C}$ (Aarupgaard mean = $-23.9 \pm 3.1 \delta^{13}\text{C}$; Aarre mean = $-23.4 \pm 2.1 \delta^{13}\text{C}$; Søhale mean = $-24.8 \pm 2.2 \delta^{13}\text{C}$), and $\%C$ (Aarupgaard mean = $0.19 \pm 0.10 \%$; Aarre mean = $0.18 \pm 0.09\%$; Søhale mean = $0.23 \pm 0.13\%$) fall within expected ranges. Values of $\delta^{13}\text{C}$ are measured by AMS and the results will be affected by fractionation during acid extraction, graphitization and AMS measurement, leading it to be incomparable between laboratories. Neither is $\%C$, because pretreatment methods vary and $\%C$ is calculated at different steps in the process (Rose et al. 2019). Replicate ¹⁴C measurements have been tested for consistency and combined following Ward and Wilson (1978), and all dates are calibrated in OxCal v4.3 using the IntCal13 calibration curve (Bronk Ramsey 2009a; Reimer et al. 2013).

Exploring the radiocarbon dataset

The cumulative distribution of the radiocarbon dataset is explored by summarizing dates on cremated bone from 95 graves from Aarupgaard, Søhale and Aarre urnfields in a KDE_Model with default parameter values (Fig. 44) (Bronk Ramsey 2017). The purpose of this is to assess the overall distribution of dated events, and whether it deviates from the uniform distribution assumption of a standard Bayesian phase model. The resulting kernel density estimation (KDE) has a pronounced peak coinciding with an exceptionally steep part of the radiocarbon calibration curve c.400-350 BC. This raises concern that the KDE might be an artefact of the underlying calibration curve, similar to what might be observed if applying a summed probability distribution (Contreras and Meadows 2014; Torfing 2015).

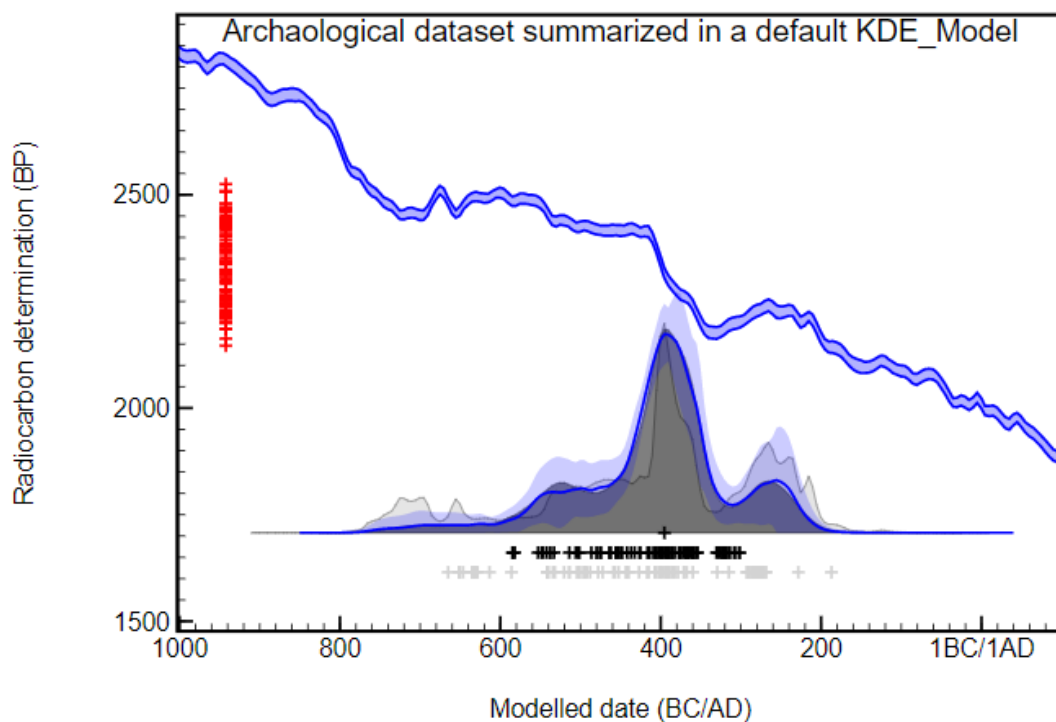


Figure 44: Radiocarbon dates on cremated bone from 95 graves from Aarupgaard, Søhale and Aarre urnfields summarized using a KDE_Model with default parameter values. The dark blue line is the averaged KDE and the light blue band the 1-sigma variability generated from the MCMC sampling. The dark grey distribution is the sampled KDE estimated distribution and the light grey curve is the summed probability distribution. The grey crosses are the medians of the likelihood distributions from the radiocarbon measurements, the black crosses are the medians of the posterior distributions estimated by the KDE_Model. The red crosses to the left are the central values of the radiocarbon dates and the calibration curve is shown for reference.

KDE is implemented in OxCal v4.3.2 as the KDE_Model function and it takes three parameters: a name or label, a kernel (default $N(0,1)$) and a factor or bandwidth (default $U(0,1)$) (Bronk Ramsey 2017). Where the summed probability distribution is simply a superposition of all individually calibrated distributions, the KDE_Model is a hybrid Bayesian/frequentist model where the prior for each dated event is the KDE distribution of all other events in the model. It uses MCMC sampling of the model to generate an averaged kernel density distribution. The default KDE_Model assumes the underlying temporal distribution of events to be normal, but an alternative modelling approach would be to estimate a KDE_Plot within a Bayesian model, which assumes e.g. a uniform temporal distribution of events (Bronk Ramsey 2017).

To test if the KDE in Figure 44 is a realistic estimate of the underlying frequency distribution, 61 radiocarbon dates are simulated at regular 5yr calendar date intervals over the range 500-200 BC and summarize them using a default KDE_Model (Fig. 45a). The modelled date range of the KDE corresponds to the simulated calendar date range, but strongly resembles a normal distribution with a modelled mean coinciding with the younger end of the steep part of the calibration curve. It would appear that the KDE_Model is either not able to fully compensate for the extreme shape of the curve in this specific time period, or that the normal distribution assumption is more influential than expected. Bronk Ramsey has shown it to be possible to estimate realistic density distributions of uniformly distributed dates using the default KDE_Model (Bronk Ramsey 2017), and to test this using the present simulated dataset, the kernel is set to have a uniform distribution ($U(-2,2)$) (Fig. 45b). The resulting KDE has a slightly broader peak than in Figure 45a, but otherwise it still resembles a normal distribution. It is unlikely that it is the distribution assumption causing the observed discrepancies, which leaves the question of whether it is the shape of the calibration curve that is causing the discrepancies. To test this the simulated calendar date range is moved to AD 200-500 and again summarized in a default KDE_Model (Fig. 45c). The KDE is approaching a uniform distribution, although it still has two smaller peaks. The testing of the KDE_Model using simulated dates suggests that the exceptionally steep part of the calibration curve c.400-350 BC constrains the output and causes the observed discrepancies between simulated and modelled dates. In an attempt to handle this the simulated dates are modelled in a uniform phase model (Bronk Ramsey 2009a), and summarized using the KDE_Plot function (Fig. 45d). This provides a realistic estimate of the underlying uniformly distributed simulated dates, indicating that estimating the KDE within a Bayesian model with a strong uniform prior is sufficient in this case to tackle the extreme shape of the calibration curve.

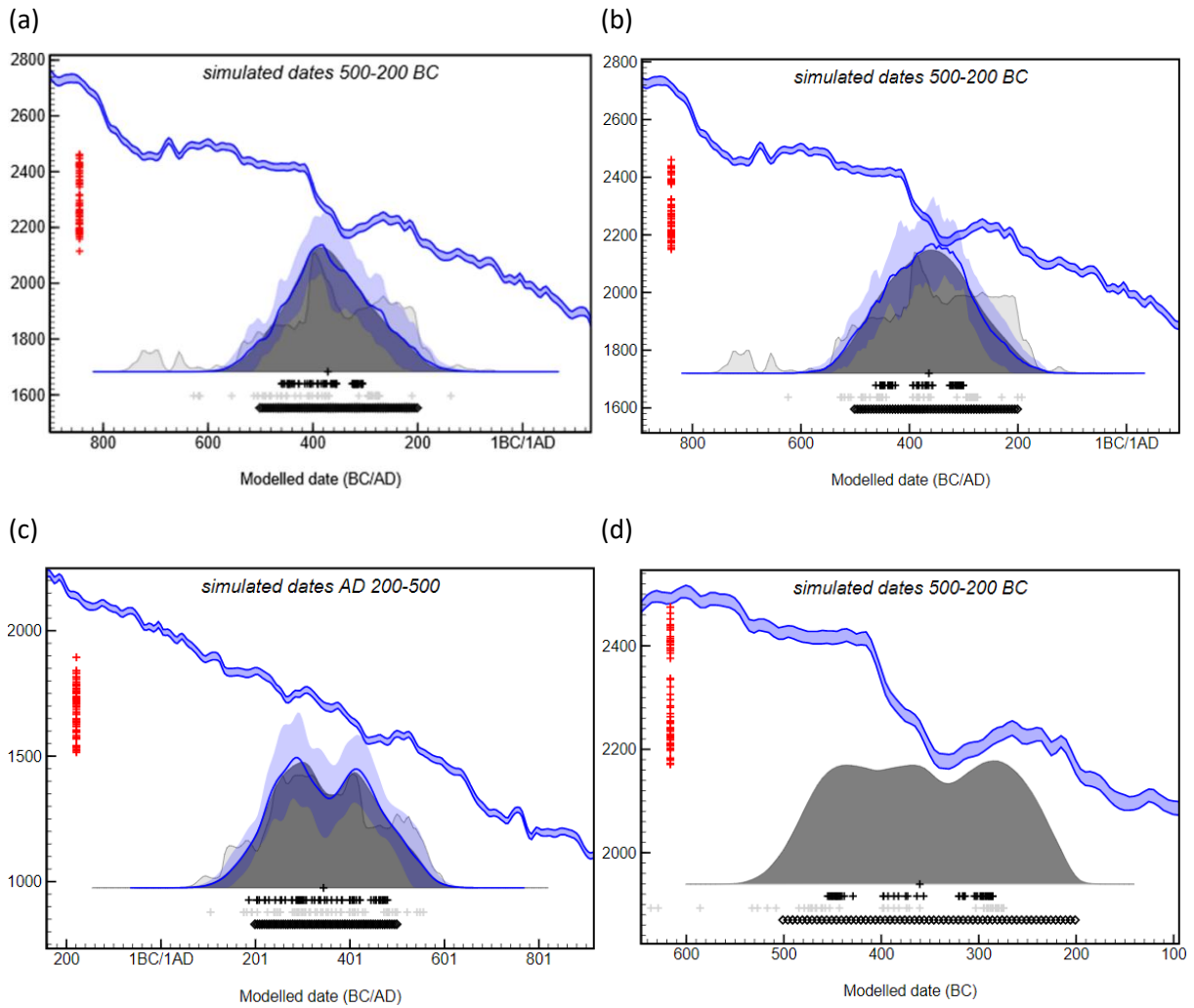


Figure 45: A dataset of 61 simulated radiocarbon dates taken at regular 5yr calendar date intervals and summarized using kernel density estimates, (a) a default KDE_Plot of simulated dates 500-200 BC, (b) a KDE_Model with a uniformly distributed kernel ($U(-2,2)$) of simulated dates 500-200 BC, (c) a default KDE_Model of simulated dates AD 200-500, (d) simulated dates are modelled in an uniform phase model and summarized in a KDE_Plot.

Returning to the archaeological dataset, an alternative KDE is modelled using the same approach as in Figure 45d, i.e. applying a uniform phase model and summarizing the posterior estimated output using the KDE_Plot function (Fig. 46). The modelled data range is close to the range estimated by the KDE_Model in Figure 44, but although the density distributions share some features they are not identical. The KDE in Figure 46 has a uniform distribution from the early 6th century to the late 5th century BC, followed by pronounced peaks in the early 4th century and again in the mid-3rd century BC. The two peaks are related to an inversion of the calibration curve, causing bi-model solutions in the 3rd-4th centuries. Estimating the KDE within a Bayesian model instead of applying a KDE_Model does make a difference for this specific dataset. It is not possible to rule out a peak in burial activity in the

early 4th century and mid-3rd century BC, but the impact is considerably less severe than in Figure 44. It can thus be concluded that the archaeological dataset might not be uniformly distributed, although it cannot be ruled out either.

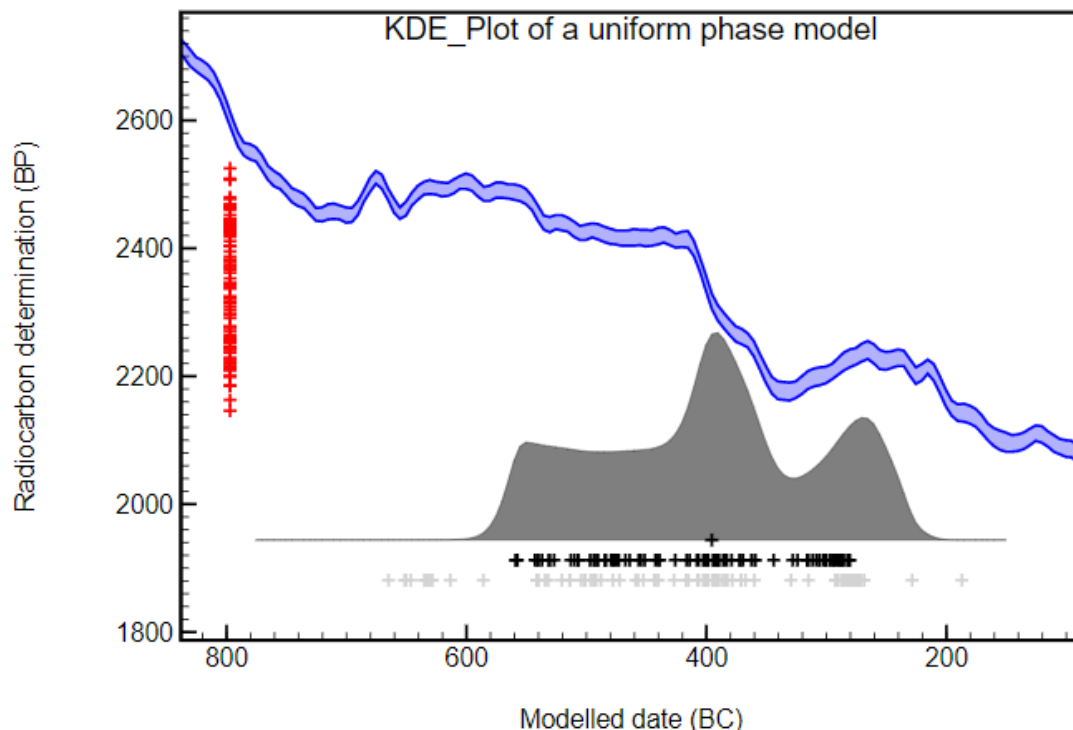


Figure 46: Radiocarbon dates on cremated bone from 94 graves from Aarupgaard, Søhale and Aarre urnfields modelled in a uniform phase model and summarized in a KDE_Plot.

From the same uniform phase model as above, the distribution of individual types of metalwork and pottery with minimum three dated graves are summarized in a number of KDE plots (Fig. 47). Pins with type 1 and 2 coiled heads and simple iron rings largely overlap and were probably still in circulation when pins with circular heads were introduced. The final pin type is pins with grooved head. Belt equipment including iron rings and more types of belt clasps appears to overlap chronologically, making it difficult to distinguish any sequential order. Pottery types 12B and 20B appears to be contemporaneous and early, whereas types 15B and perhaps 15C span a wider range, with both earlier and later examples.

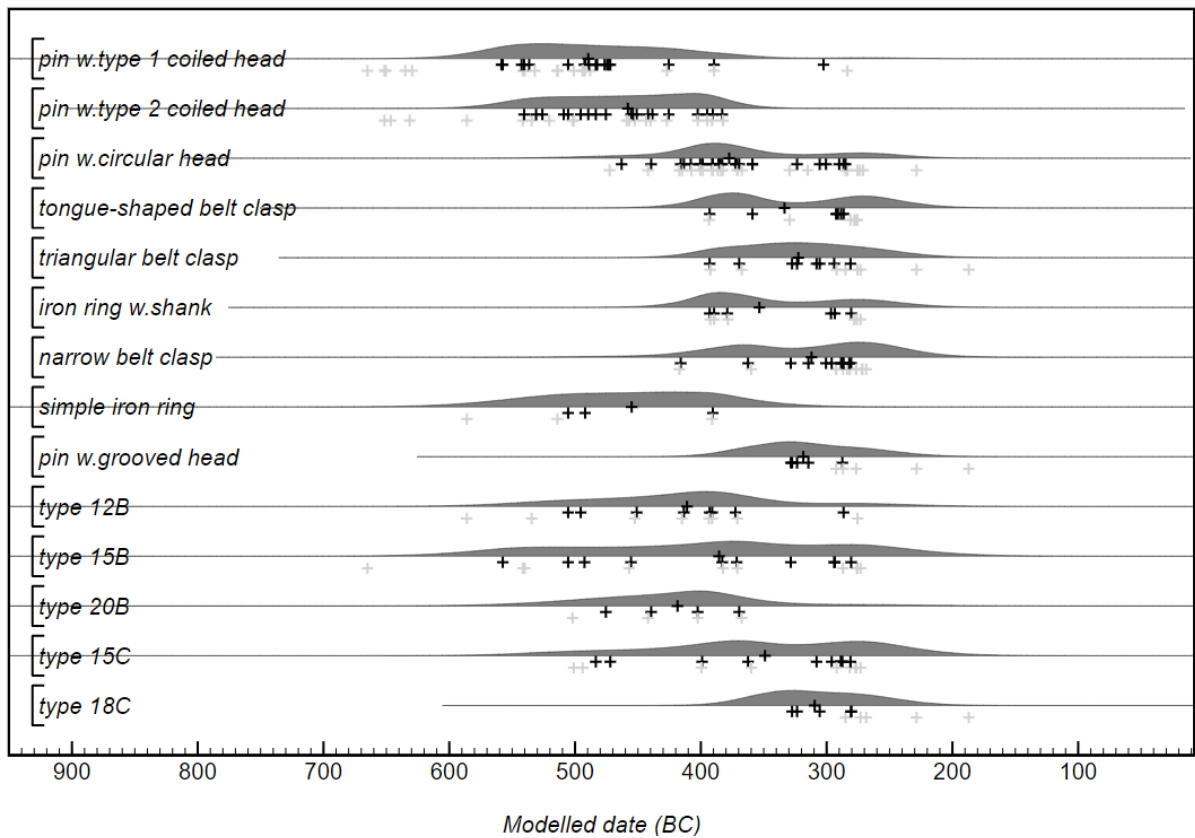


Figure 47: Radiocarbon dates from Aarupgaard, Søhale and Aarre urnfields are modelled in a simple bounded phase, and metalwork and pottery currencies are summarized using *KDE_Plot*. Grey crosses are the median of the unmodelled dates, and the black crosses are the medians of posterior estimated dates.

Chronological modelling

A grand currency model was attempted that incorporate all prior information on site formation processes and artefact typology and with a Cremation Outlier_Model (OM) applied to all cremated bone dates with a prior probability of 1 (Paper 4: Rose et al. 2020). Each dated grave appears multiple times in a grand model, dating both the grave itself and the individual artefacts. For Aarre and Søhale urnfields this result in 1-2 cross references per grave, but up to 3-4 cross references for Aarupgaard urnfield. With proper cross referencing OxCal will create only one independent parameter and evaluate its posterior date every time it appears in the model, whereas neglecting this violates the independence assumption built into OxCal (Bronk Ramsey 2009a). Regardless of what modelling approach was used, the posterior estimated dates all converge on a very narrow time range, i.e. explicitly allowing for the possibility that all graves date to the same event, which is not permitted by the archaeological prior information. It was tested if the over-convergence was caused by the extensive use of cross referencing, but removing these did not solve the problem. It was also tested if the Cremation OM add too much flexibility to the model, but without it the model is unable to account for the inherent scatter in radiocarbon measurements, and inevitably fails. The over-convergence issue necessitated that separate site models for the three urnfields are constructed based on the available prior information on site formation processes, and that metalwork and pottery currencies are modelled in separate models. The same grave is then modelled twice using different prior information, and will as a results end up having two posterior dates that might not agree. Even with this in place it was not possible to include dates from Søhale without the over-convergence issue re-appearing and for this reason *Model A metalwork currencies* only includes dates from Aarupgaard and Aarre, and *Model B pottery currencies* only includes dates from Aarupgaard. This makes the currency models strongly dependent on dates from Aarupgaard urnfield and limits the possibilities to investigate regional differences in rate of change in artefact currencies. It does however also limit the effect of the described sampling bias, because the Aarupgaard dataset has a more balanced number of graves containing early and late types of artefacts than compared to the total dataset.

Currency models

Artefact types of metalwork or pottery are modelled in separate currency models consisting of three parts: Part 1 with legacy dates from Late Bronze Age to help constrain the start of the currencies, Part 2 with a site model for Aarre urnfield that help constrain the Cremation OM, and Part 3 with the actual currency models. Dates of burials with artefacts featuring in more than one of these models are cross-referenced. Artefact types with 1-4 cases are modelled as unbounded phases, types with 5-9 cases as

uniform bounded phases, and types with ≤ 10 cases are modelled using trapezium boundaries. The trapezium boundary start parameter 'start of start' equals the start of production of an artefact type, and 'end of start' equals the start of peak production. The trapezium boundary end parameter 'start of end' equals start of decline of production, and 'end of end' equals the end of production. The mean of the overall 'start' boundary is the midpoint between 'start of start' and 'end of start', which also applies to the overall 'end' boundary (Lee and Bronk Ramsey 2012; Lee et al. 2013). Modelling all the currency models in a uniform bounded phase cause all posterior dates to over-converge and instead `First` and `Last` queries are applied to calculate the first and last dated events of *Model A metalwork currencies* and *Model B pottery currencies*. A Cremation OM is applied to all dates on cremated bone (Rose et al. 2020).

In Part 1 dates from Bronze Age periods V and VI (Olsen et al. 2011) are modelled as a sequence with two contiguous phases. The end boundary ('end BA per.VI') is cross referenced as *terminus post quem* (TPQ) for the start of Part 2 'Site model – Aarre urnfield', and for the start of Part 3 'Currency models'. In Part 2 Aarre urnfield is modelled as a uniform bounded phase of activity, following the boundary TPQ 'end BA per.VI' from Part 1. Individual graves are modelled as phases including dates on cremated bone and selected short-lived samples, except graves A95, A130 and A278 where cremated bone dates are combined with dates on contemporaneous, short-lived samples. Dates of charcoal samples with potentially significant intrinsic age are modelled as TPQ dates.

In Part 3 of *Model A metalwork currencies* from Aarupgaard and Aarre are modelled in an unbounded phase following the boundary TPQ 'end BA per.VI' from Part 1. `First` and `Last` queries are applied to calculate the first and last dated event of the currency model. Dates from Aarre urnfield are cross-referenced to the site model (Part 2). Dates on pin with type 1 coiled head are modelled in a uniform bounded phase, and dates on pins with type 2 coiled head and circular head are modelled in trapezium phases. All pin types are modelled without incorporating the typo-chronological sequence proposed by Jensen (2005). Belt equipment dates are modelled in four contiguous phases (tongue-shaped belt clasp < triangular belt clasp < iron ring with shank < narrow belt clasp) with overall trapezium boundaries. In Part 3 of Model B, pottery currencies from Aarupgaard urnfield are modelled in an unbounded phase following the boundary TPQ 'end BA per.VI', and `First` and `Last` queries are applied to calculate the first and last dated event of the currency model. Pottery types 12B, 15C and 18C are modelled in uniform bounded phases, and type 15B in a trapezium phase. The currencies are modelled without incorporating the typo-chronological sequence proposed by Jensen (2005).

Model A - metalwork currencies

Offsets are applied to five graves from Aarre urnfield, requiring probable heirlooms artefacts to be 50 ± 25 years older than the cremated bone (A89, A99, A278, A393 and A394). A single case of belt equipment from Aarre (grave A130) had to be exempted, as the model would otherwise over-converge, even though the belt clasp does not appear to be an heirloom. The metalwork currencies from Aarupgaard and Aarre are modelled in a phase assuming no chronological order. Pin with type 1 coiled head is modelled in a uniform bounded phase, whereas pin with type 2 coiled head and pin with circular head and the combined group of belt equipment types are modelled in trapezium bounded phases with transition periods for increase and decrease of production. Simple iron ring and pin with grooved head are modelled in phases without boundaries, but all pins with grooved head occur together with belt equipment and dates are cross referenced to these. The model has a good agreement ($A_{\text{overall}} = 71$, Fig. 48, Appendix 2) and the Cremation OM estimates 1-77yr offsets with a mean of 17yr (95.4% probability). The cremated bone dates from graves A89, A278, A393 and A394 from Aarre have agreements < 60 , regardless of the applied heirloom offsets. Grave A130 fails to combine ($T' = 7.7$, $T' (5\%) = 3.8$, $v = 1$), because the offset estimated by the Cremation OM is not large enough to encompass the dates of cremated bone (KIA-53947) and a cereal grain (KIA-53946). The grave is nonetheless kept in the model as it has a significant effects on the posterior estimated OM offsets. The model estimates all metalwork currencies at Aarupgaard and Aarre to have started 695-466 cal BC (95.4% probability), probably 596-491 cal BC (68.2% probability), and ended 256-172 cal BC (95.4% probability), probably 238-198 cal BC (68.2% probability).

The relative order of currencies is tested using the OxCal `Order` function (Bronk Ramsey 1998) and the start of metalwork production is calculated to follow the sequence: pin with type 1 coiled head $<$ pin with type 2 coiled head $<$ pin with circular head $<$ combined belt equipment $<$ pin with grooved head (with the probabilities 53% $<$ 94% $<$ 99% $<$ 87%). The end of production follows the same sequence for pin with type 1 coiled head $<$ pin with type 2 coiled head $<$ pin with circular head (with the probabilities 74% $<$ 87% $<$ 96%), but the order of belt equipment and pin with grooved head is ambiguous. This is not surprising, as all cases of pin with grooved head occur together with belt equipment. A single case of a bomb head pin is contemporary with the early pin types with coiled head, although the date is poorly constrained in the model and date 710-336 cal BC (95.4% probability), probably 498-394 cal BC (68.2% probability). The simple iron ring also appears to belong to the older types, but this is more likely a matter of sampling bias as this type is also found together with later pin types. A single Holstein pin dates to 312-243 cal BC (95.4% probability), probably 290-258 cal BC (68.2%

probability), making it contemporaneous with the belt equipment. The typological sequences proposed by Jensen (2005) is thus confirmed by the radiocarbon evidence.

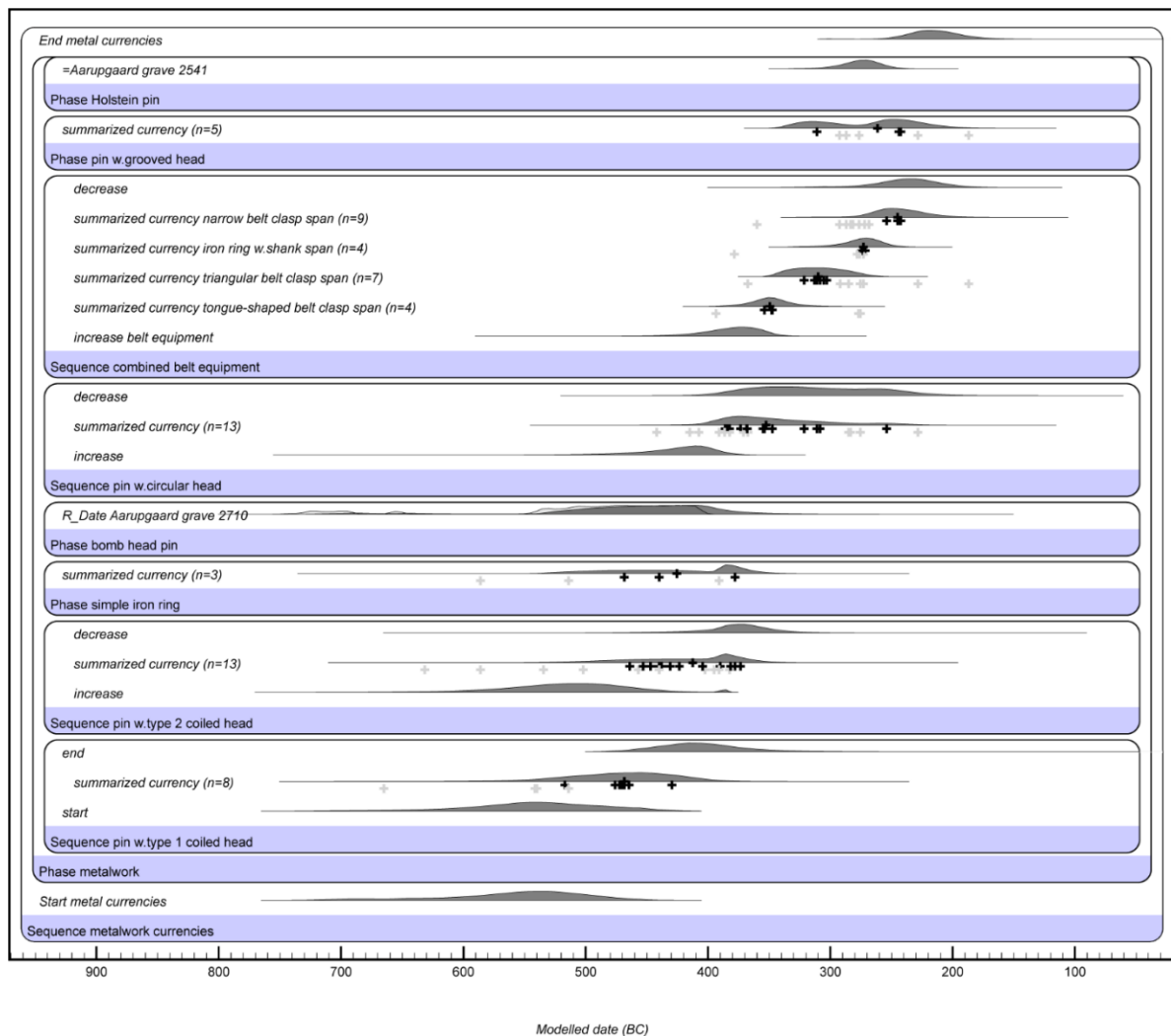


Figure 48: Model A metalwork currencies from Aarupgaard and Aarre urnfields. Summarized plots of the posterior estimated currencies along with estimated periods of production increase and decrease. Simple iron ring and pin with grooved head are plotted without boundaries, as are the single dated cases of bomb head pin and Holstein pin. Grey crosses are the median of the unmodelled dates, and the black crosses are the medians of posterior estimated dates.

Three currencies are modelled using trapezium boundaries, which provide further insight into the periods of production increase and decrease (Fig. 49). Pin with type 2 coiled head has an increase period lasting 0-169yr (95.4% probability), probably 0-69yr (68.2% probability), and a decrease period lasting 0-151yr (95.4% probability), probably 0-54yr (68.2% probability). Increase production of pin with circular head lasts 0-131yr (95.4% probability), probably 0-50yr (68.2% probability), and decrease lasts 0-194yr (95.4% probability), probably 0-140yr (68.2% probability). The combined types of belt

equipment have a period of production increase lasting 0-159yr (95.4% probability), probably 0-95yr (68.2% probability), and decrease lasting 0-119yr (95.4% probability), probably 0-48yr (68.2% probability). It is difficult to assess whether the transition periods of pin with type 2 coiled head and the belt equipment are well defined, as the dates fall on a challenging part of the calibration curve, but pin with circular head is well defined as the currency dates to the particularly steep part around 400-350 cal BC. It appears to have had a relatively rapid introduction period, but with a longer tail towards younger dates.

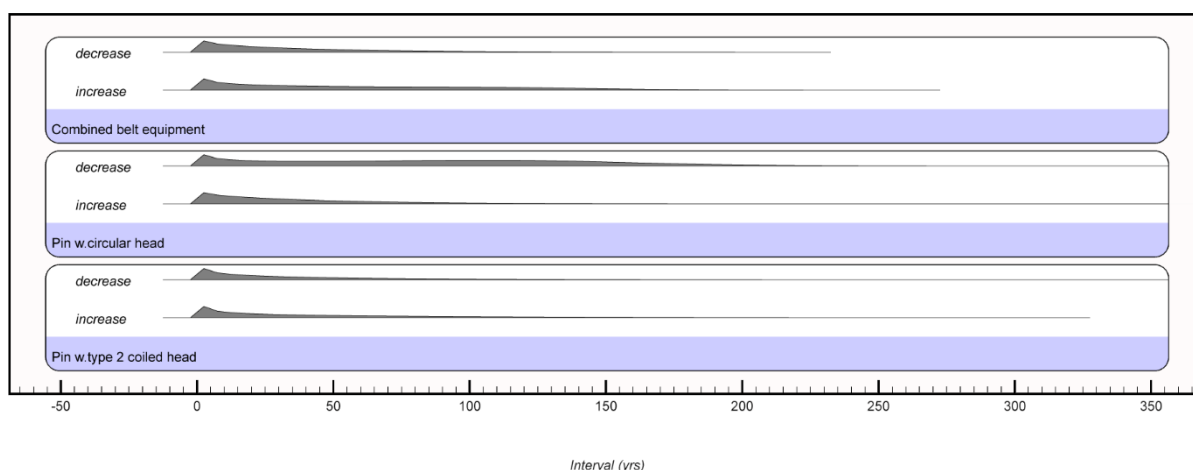


Figure 49: Modelled periods of production increase and decrease for pin with type 2 coiled head, pin with circular head, and the combined belt equipment.

The durations of the currencies are calculated using the OxCal *Difference* function (Fig. 50) (Bronk Ramsey 1998). Pin with type 1 coiled head has the longest potential duration, but this is at least partly due to poor definition of the posterior estimates. Pins with type 2 coiled head and circular head have comparable durations, lasting from a few decades and up to c.250yr (95.4% probability). Pin with grooved head is the pin type with the shortest duration of 39-139yr (95.4% probability), whereas all types of belt equipment have durations shorter than a century. The same function is used to calculate the overlap of the modelled currencies (end of preceding currency – start of succeeding currency; Fig. 50). Pins with coiled head (types 1 and 2) have a large overlap of up to 225yr (95.4% probability), pin with type 2 coiled head and with pin with circular head have an overlap of up to 150yr (95.4% probability). Pin with circular head and pin with grooved head have an overlap of up to 103yr, and pin with circular head and the combined belt equipment have an overlap of up to 140yr (95.4% probability).

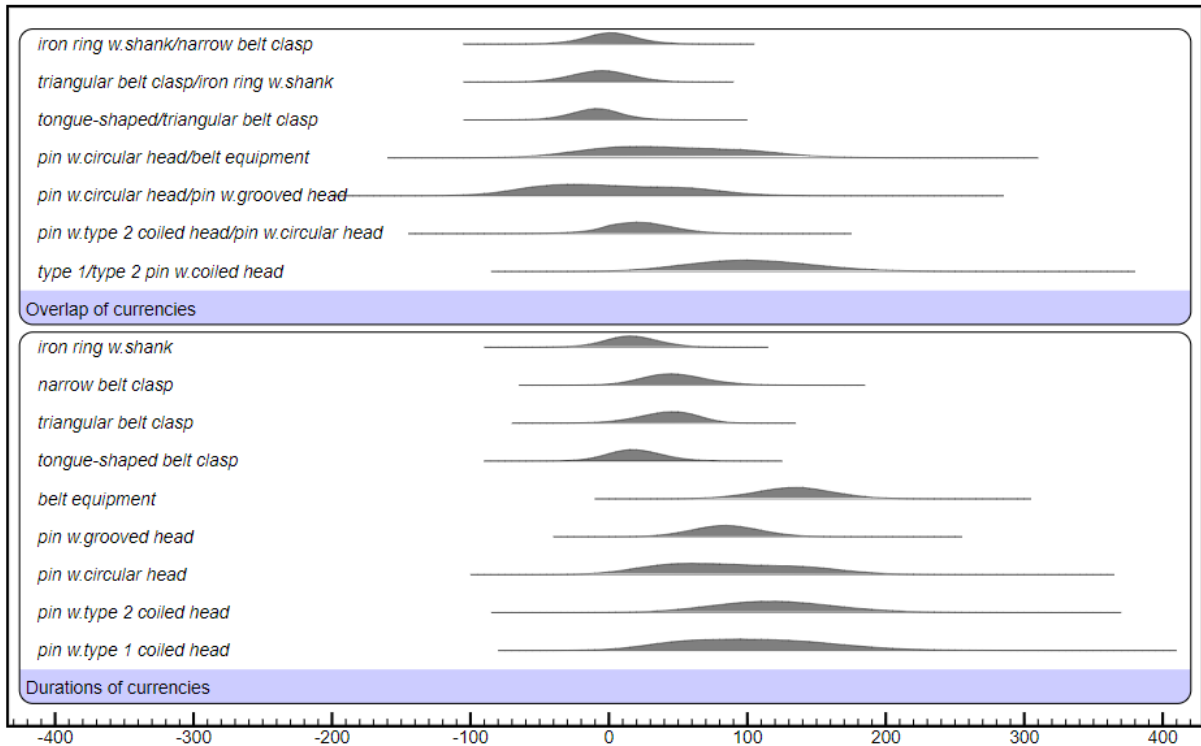


Figure 50: Modelled durations and overlaps of metalwork currencies.

Model B - pottery currencies

The pottery currencies from Aarupgaard urnfield are modelled in a phase assuming no chronological order. Type 15B is modelled in a phase with trapezium boundaries, types 12B, 15B, 15C and 18C are modelled in uniform bounded phases, and the remaining types are modelled in unbounded phases. The model has a good agreement ($A_{\text{overall}} = 79.4$, Fig. 51, Appendix 3), and the Cremation OM estimates 1-71yr offsets with a mean of 15yr (95.4% probability). It estimates all pottery currencies at Aarupgaard to have started 731-534 cal BC (95.4% probability), probably 723-615 cal BC (68.2% probability), and ended 239 cal BC -22 cal AD (95.4% probability), probably 208-108 cal BC (68.2% probability).

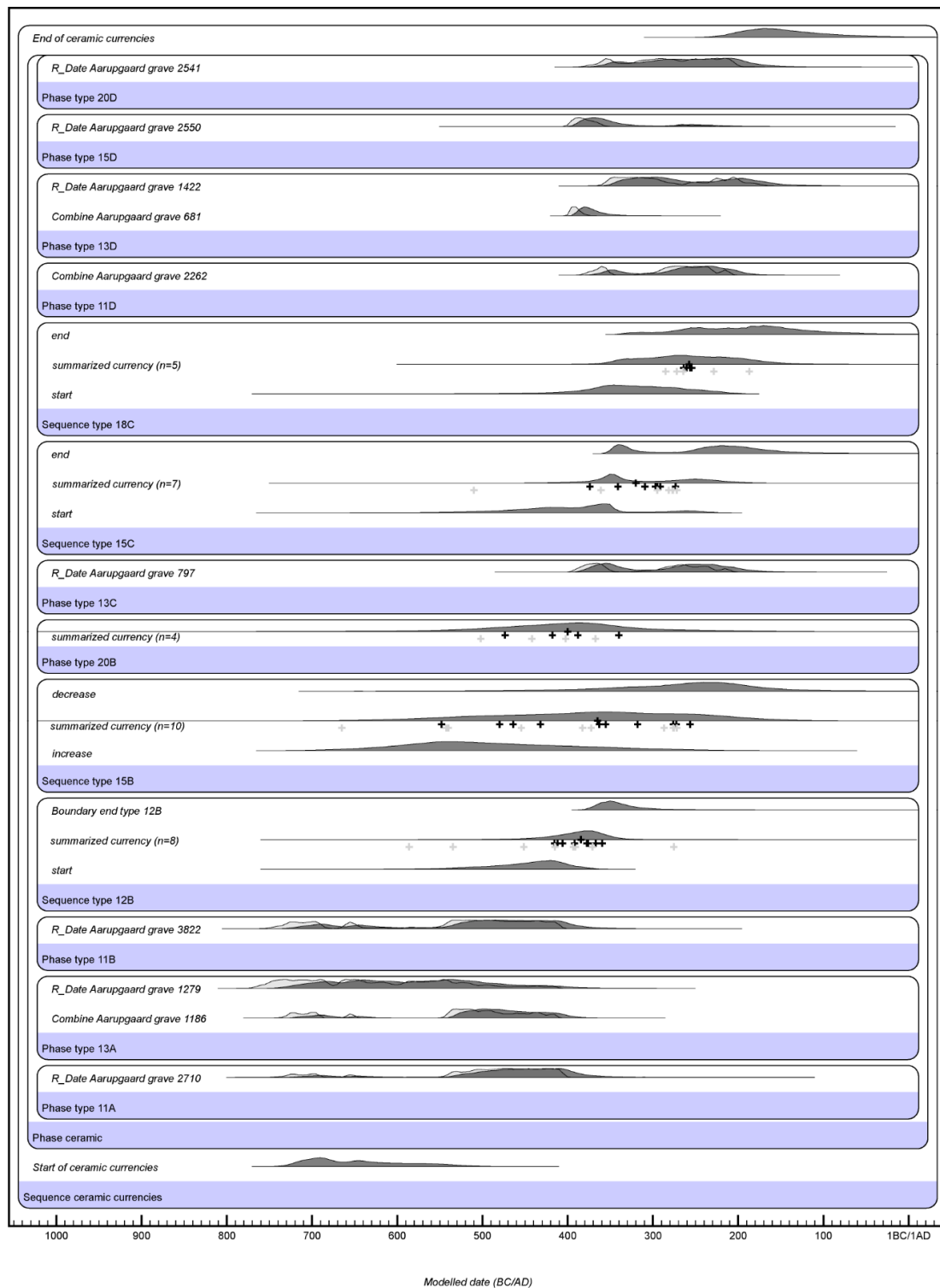


Figure 51: Model B pottery currencies from Aarupgaard urnfield. Summarized plots of the posterior estimated currencies along with estimated periods of production increase and decrease of type 15B, and production start and end of types 12B, 15C and 18C. Remaining types are modelled without boundaries. Grey crosses are the median of the unmodelled dates, and the black crosses are the medians of posterior estimated dates.

The relative order of currencies is tested using the OxCal `Order` function (Bronk Ramsey 1998) and the start of production is calculated to follow the sequence type 15B < type 12B < type 15C < type 18C, with *65% probability* that 15B starts before type 12B, *76% probability* that type 12B starts before type 15C, and *80% probability* that type 15C starts before type 18C. The end of pottery production follows a slightly different sequence 12B < 15B < 15C < 18C, with *80% probability* that type 12B ends before type 15B, *60% probability* that type 15B end before type 15C, and *68% probability* that 15C ends before type 18C. According to Jensen (2005) type 15B was introduced before type 12B, but the radiocarbon evidence demonstrate it to be the other way around and type 15B was probably in use for more than three centuries, covering the entire span of the Early Pre-Roman Iron Age. This can be contextually supported by the associated artefacts that span the typological sequence of metalwork (Fig. 52). The radiocarbon evidence thus demonstrate that the typological sequences proposed by Jensen (2005) are in need of a revision.

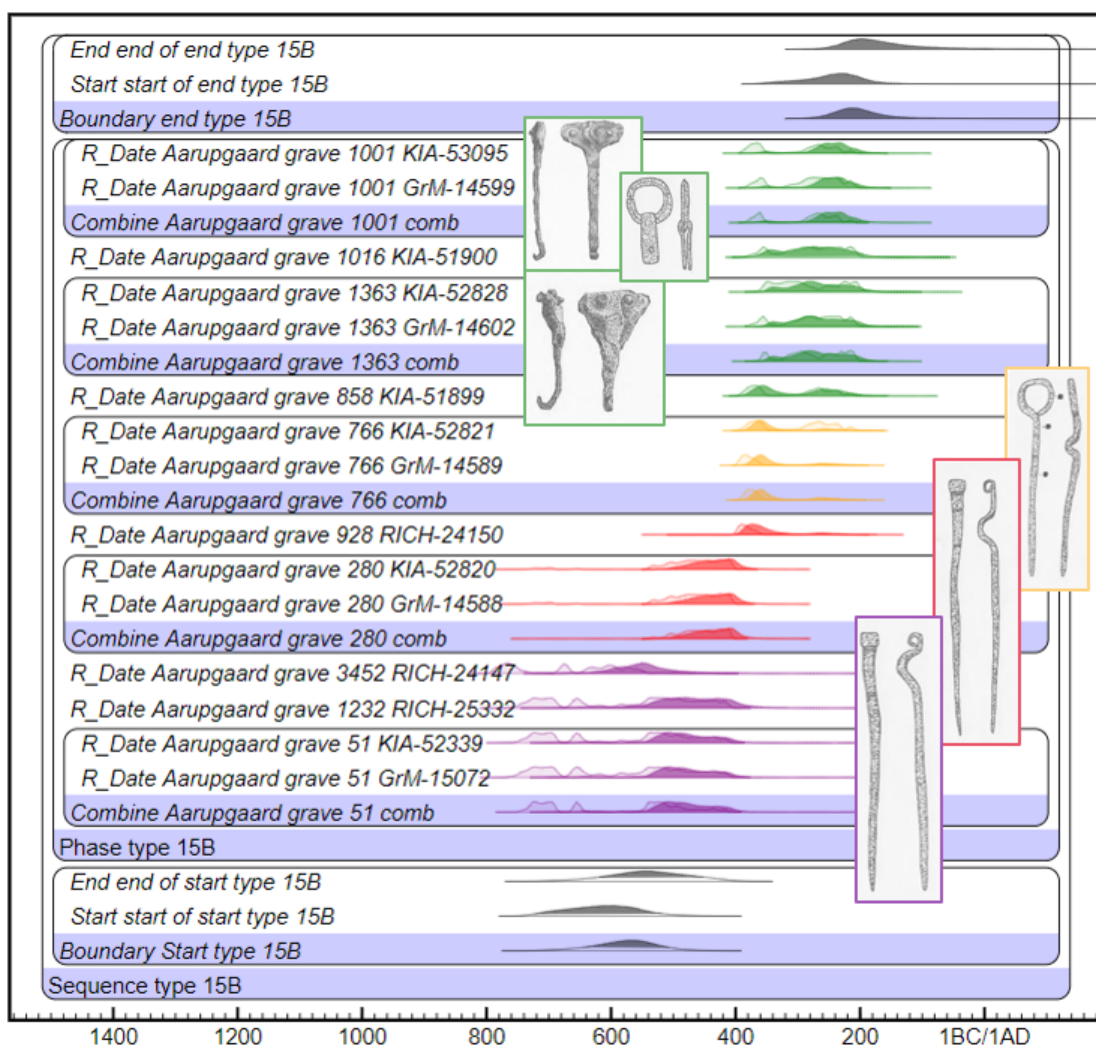


Figure 52: Currency model of pottery type 15B with associated metalwork.

Only type 15B is modelled using trapezium boundaries, but the periods of production increase and decrease are poorly defined and last up to c.350yr. The durations of the currencies are calculated using the OxCal *Difference* function (Fig. 53) (Bronk Ramsey 1998). Type 12B overlaps completely with type 15B and it is also the currency with the shortest duration. Types 15C and 18C have durations around two centuries, whereas type 15B has a very long duration and appears to have been in use at Aarupgaard for most of the Early Pre-Roman Iron Age. The same function is used to calculate the overlap of the modelled currencies (end of preceding currency – start of succeeding currency, Fig. 53). Types 15B and 12B have a large overlap up to 333yr (95.4% probability), agreeing with type 15B both starting and ending before type 12B. Type 15B has an up to 197yr overlap with type 15C, that again has an overlap with type 18C of up to 240yr (95.4% probability).

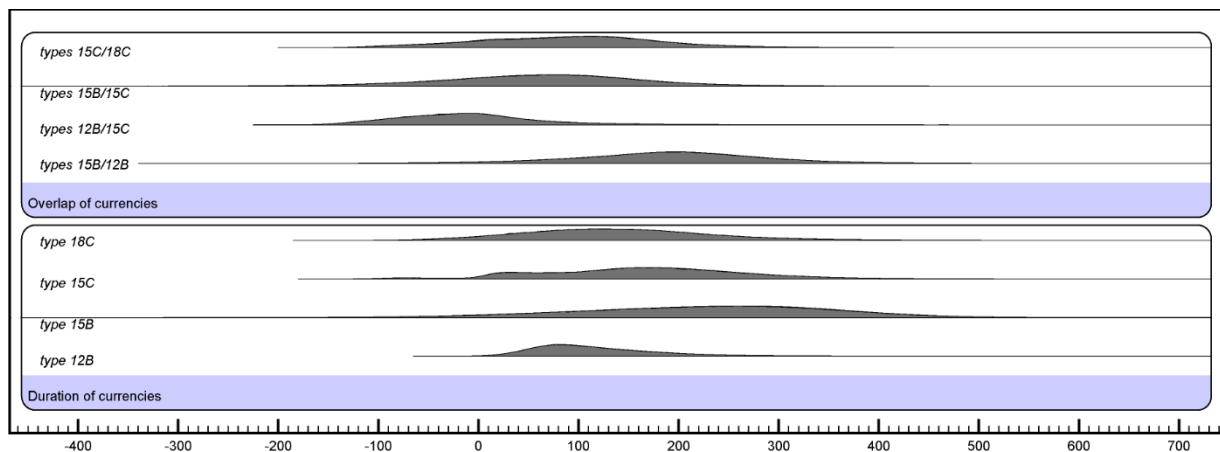


Figure 53: Estimated durations and overlaps of pottery currencies.

Site models

Aarupgaard urnfield

Burial activity at Aarupgaard urnfield is modelled in a bounded sequence with three contiguous phases. The initial 'founding phase' consists of graves 3330, 3340 and 3869 that were interred in a Bronze Age mound. The funerary urns resemble Bronze Age pottery, and although the pins are made of iron, they are typologically closer to Bronze Age types. The boundary 'end BA per.VI' is cross referenced as *TPQ* for the start of the next phase (as done in Part 1 of the currency models, Olsen et al. 2011). The remaining two phases are based on the number of pathways interrupting the circular ditches around the burial mounds, because Jørgensen (1975) has used horizontal stratigraphy and artefact typology to show this to be time-dependent. A phase of graves with 'multiple pathways' is modelled, followed by a final phase with 'two pathways'. The transition between these is modelled with trapezium priors,

allowing it to have a duration. An initial site model only incorporating prior knowledge of site formation processes was accepted, but the younger dates were poorly constrained, with the majority having bimodal distributions. Instead the posterior estimates of metalwork and pottery artefacts from Model A and Model B are incorporated as estimations of the burial events.

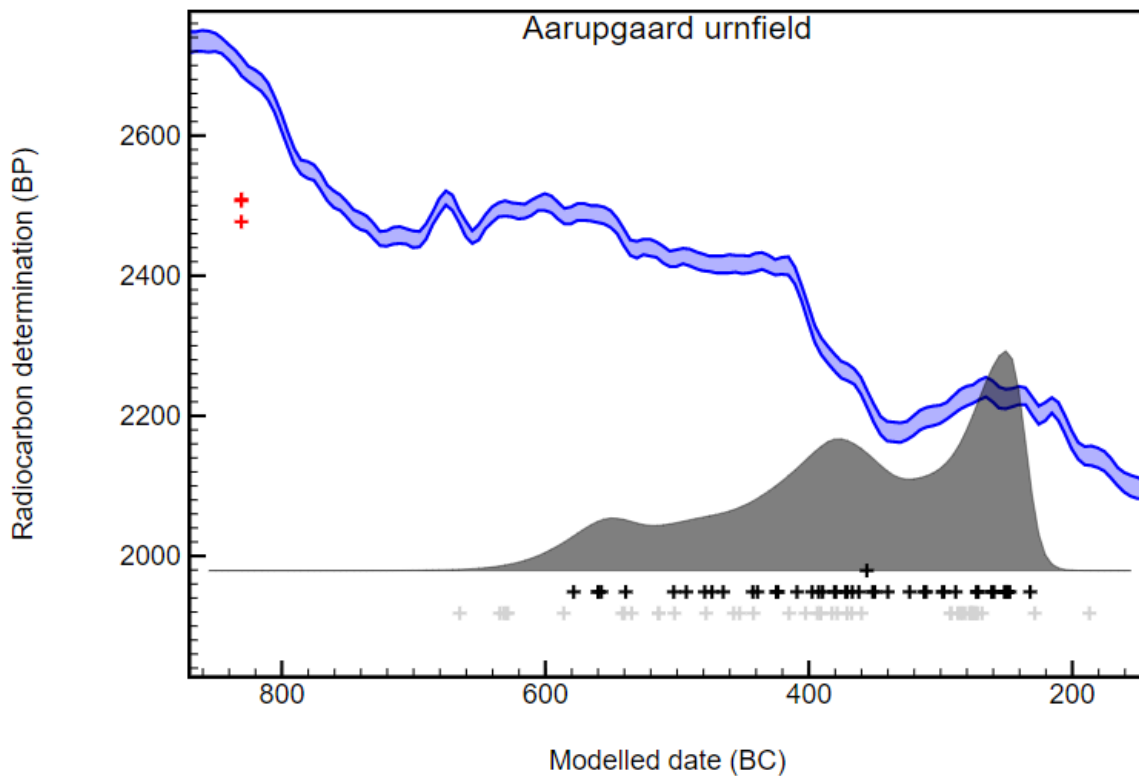


Figure 54: Summarized plot of posterior estimated dates from Aarupgaard urnfield (KDE_Plot). Grey crosses are medians of unmodelled dates and black crosses are medians of posterior estimates. Red crosses are the likelihood medians of the 'founding' graves, not included in the currency models.

The model is accepted ($A_{\text{overall}} = 318$) and show the posterior estimates derived from the currency models to be statistically consistent with the burials. Burials are estimated to have started 622-488 cal BC (95.4% probability), probably 592-530 cal BC (68.2% probability), and ended 251-211 cal BC (95.4% probability), probably 244-225 cal BC (68.2% probability). The duration of the site is summarized using the KDE_Plot function (Fig. 54) and is estimated to have lasted 252-393yr (95.4% probability), probably 294-360yr (68.2% probability). The modelled output agrees with the archaeological prior information, although the dataset only comprises about 4% of the total number of recovered graves with an underrepresentation of the youngest graves at the site. The dataset is thus probably not representative of the entire period of burial activity, and to better estimate the younger part the site chronology it would be necessary to date more graves. The summarized plot in Figure 54 has a pronounced peak in the 3rd century BC, which might be interpreted as a peak in burial activity or even to be related to a

catastrophic event. Through exploring the radiocarbon dataset with synthetic data it is however apparent that the peak might be closely related to an inversion of radiocarbon calibration curve in this period. There might have been a real peak in burial activity at Aarupgaard urnfield, but it cannot be tested any further with the present dataset.

Aarre urnfield

The dataset from Aarre urnfield is relatively large, and even though it only comprises material from 12 graves it also includes a large number of dates on archaeobotanical remains with limited intrinsic ages. The dataset is modelled without information on site formation processes and the stable chronological site model in *Model A metalwork currencies* is preferred. It estimates burial activity at Aarre urnfield to have started 537-414 cal BC (95.4% probability), probably 485-424 cal BC (68.2% probability), and have ended 359-297 cal BC (95.4% probability), probably 351-325 cal BC (68.2% probability). The duration of the site is summarized using the KDE_Plot function (Fig. 55) and is estimated to have lasted 63-174yr (95.4% probability), probably 73-128yr (68.2% probability), agreeing with the archaeological prior information. Bearing in mind that the site is interpreted as originally containing up to 1000 burials (Lorange 2015b), the dataset is not representative of the entire period of burial activity, and it is expected that the youngest phase of burials at the site have not yet been dated.

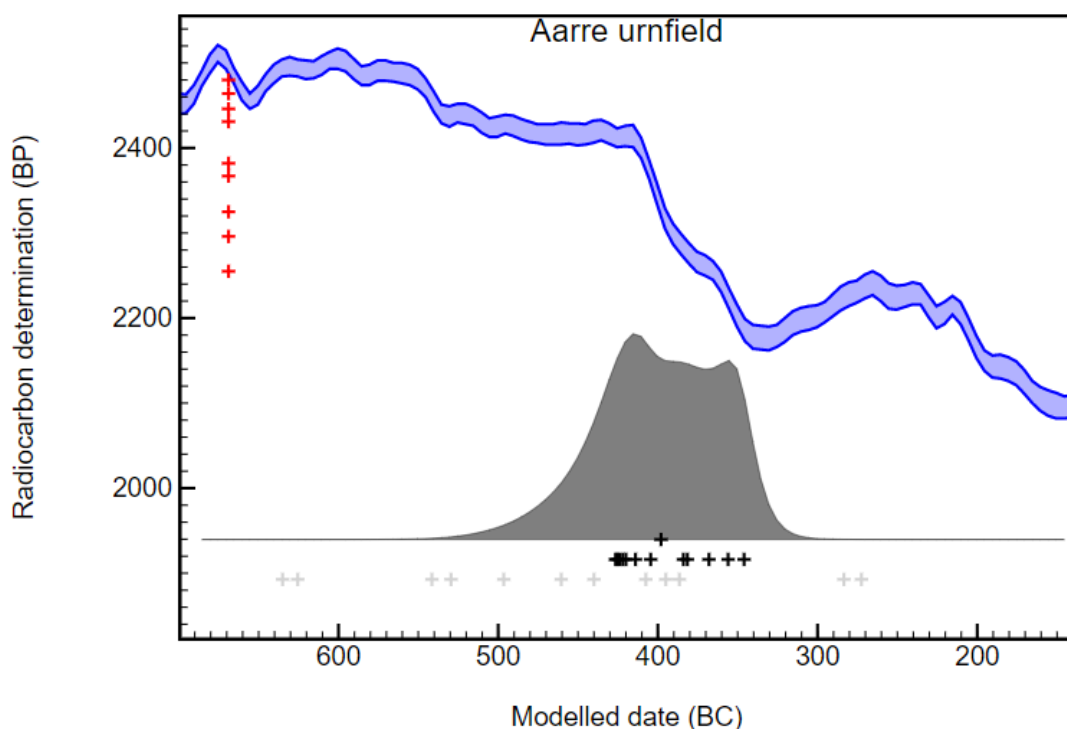


Figure 55: Summarized plot of posterior estimated dates from Aarre urnfield (KDE_Plot). Grey crosses are medians of unmodelled dates and black crosses are medians of posterior estimates.

Søhale urnfield

Burial activity at Søhale urnfield was initially modelled in a uniform bounded phase model with a Cremation OM applied to all dates, but no additional prior information. Although the model was accepted, all posterior dates converge on the steep part of the calibration curve c.400-350 cal BC, and instead the typological sequence derived from *Model A metalwork currencies* was applied in the form of contiguous currency phases. Again the boundary 'end BA per.VI' is cross referenced as *TPQ* for the start of burial activity and graves with no artefacts are included in the overall bounded phase of the site. Grave x65 (AAR-25263) contained two pins with type 1 coiled head and an iron ring with shank, which is at opposite ends of the typological sequence. To allow the older pins to have a residence time an offset scaled 50 ± 25 yr with a normal distribution is applied. This model was however not permitted by the radiocarbon evidence, and it was instead necessary to cross reference the estimated currency boundaries from Model A (which did not contain any dates from Søhale) as start and end of four bounded phases containing dates on pins with coiled head (type 1 and type 2), pin with circular head and combined belt equipment.

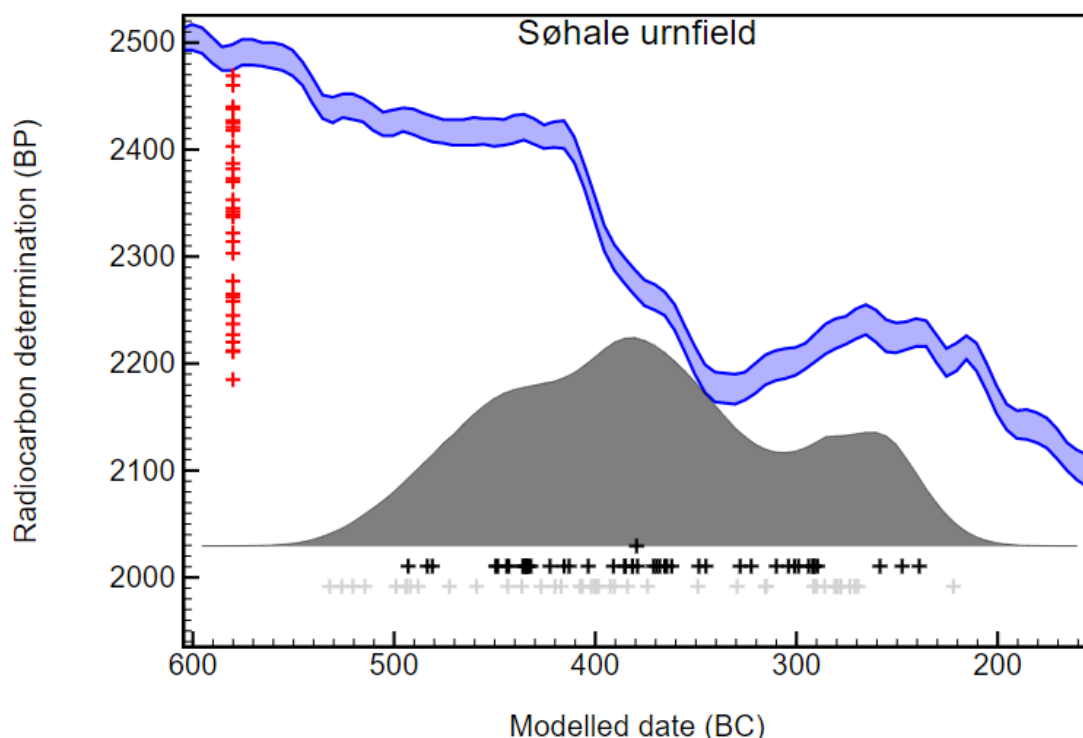


Figure 56: Summarized plot of posterior estimated dates from Søhale urnfield (KDE_Plot). Grey crosses are medians of unmodelled dates and black crosses are medians of posterior estimates.

The model is now accepted ($A_{\text{overall}} = 72$) and the Cremation OM estimates 1-72yr offsets with a mean of 16yr (95.4% probability). Burials are estimated to have started 551-440 cal BC (95.4% probability), probably 522-460 cal BC (68.2% probability), and ended 285-201 cal BC (95.4% probability), probably 260-217 cal BC (68.2% probability). The model estimates the cemetery to have been in use 163-322yr (95.4% probability), probably 204-288yr (68.2% probability, Fig. 56). The Søhale dataset represents a large proportion of the total number of burials at the site, and is probably representative of the period of burial activity. The process of cross referencing posterior estimated currency boundaries from Model A, does however cause the Søhale site model to be heavily dependent on the dataset from Aarupgaard urnfield.

Discussion

Evaluating artefact typologies

24 artefact types of metalwork and pottery are analysed and the relative order of currencies is compared to the typo-chronology of Jensen (2005). The radiocarbon evidence supports the sequence of metalwork types, but it is suggested that the pottery sequence is in need of a revision and that some of the typological definitions are altered.

Pins with type 1 and type 2 coiled heads are typologically distinct and even though type 1 was introduced slightly earlier than type 2, the two types have similar currency distributions with a large overlap of up to 225yr (95.4% probability). In Part A (Fig. 7) it is demonstrated how the head sizes of pins with circular heads are continuously distributed and show no clear typological division. Moreover, there appears to be no correlation of the head size index and the radiocarbon ages, and it can be concluded that the head size is neither typologically relevant nor a time dependant factor (Fig. 57).

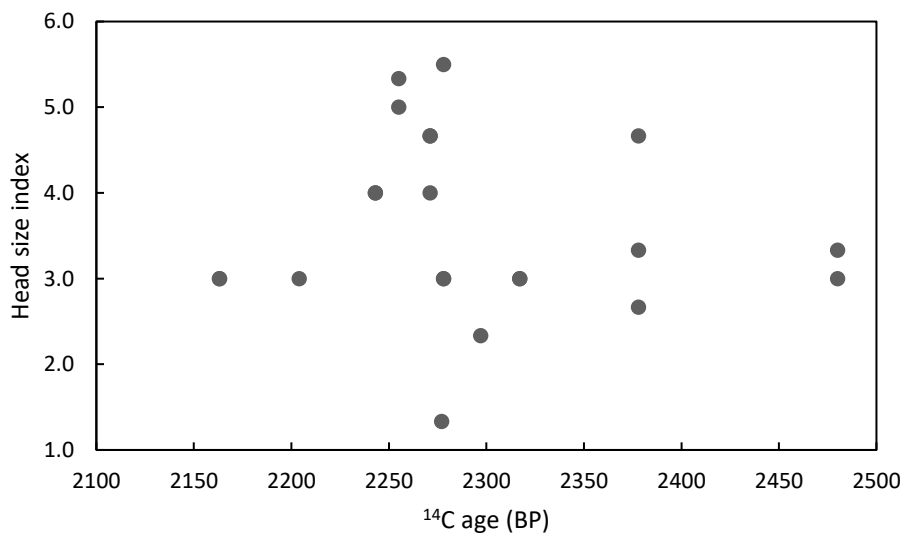


Figure 57: Head size index (inner head diameter divided by pin width) of pins with circular head from Aarupgaard urnfield plotted against uncalibrated radiocarbon ages.

The different types of belt clasps (tongues-shaped belt clasp, triangular belt clasp, narrow belt clasp) have distinct ideal forms, but there is a great deal of ‘fuzziness’ between these which makes it difficult to distinguish them in many instances. It is here proposed to instead distinguish between early types (tongue-shaped and triangular belt clasps) and later types (narrow belt clasp and iron ring with shank) as their respective combined currencies have distinct distributions (Fig. 58). This approach also serves to minimize the risk of misclassifying types of belt clasps.

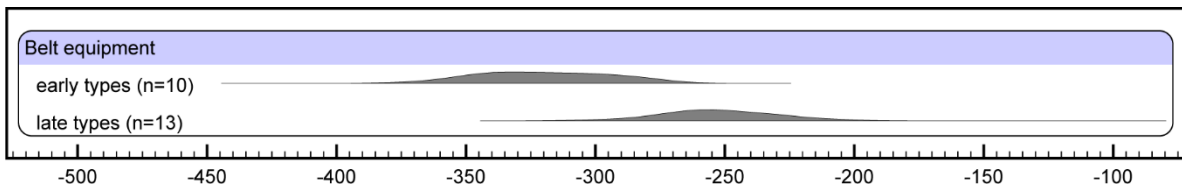


Figure 58: Summarized plots of posterior estimates of early and late occurring types of belt equipment.

An unexpected modelling output is that the shape of the vessels neck appears to be chronologically sensitive and follow the sequence $A < B < C/D$, whereas the shape of the vessel body does not appear to be closely correlated with radiocarbon age (Fig. 59). Vessel shapes 13 and possibly 20 were in use most of the Early Pre-Roman Iron Age, and are thus not particularly chronologically sensitive. This possibly also includes shape 11, but the currency is not well defined with only three cases. Vessel shapes 12, 15, and 18 follow a progressive sequence from lower to higher numbers, showing them to be chronologically sensitive. Jensen (2005) dates type 20B to the Late Pre-Roman Iron Age, but even though the number of dated cases does not allow the currency to be modelled in a bounded phase, the type is evidently introduced earlier (see calibrated dates in Appendix 3). This illustrates that the shape of the vessel neck is of higher chronological importance than the shape of the vessel body, which is most unfortunate as the uppermost part of vessels have often been destroyed by agricultural activities, as is the case at Aarre and Søjhale urnfields.

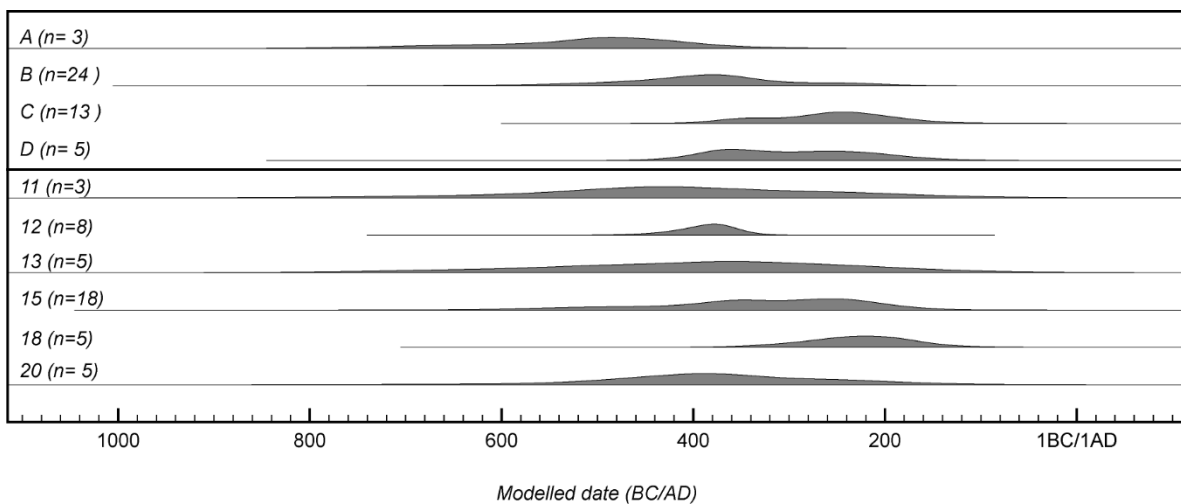


Figure 59: Summarized pottery currencies from Aarupgaard urnfield, divided by vessel neck shape A-D (upper part of plot), and shape 11-20 of vessel body (lower part of plot).

Temporal processes of change in artefact currencies

Chronological models are provided for 9 metalwork currencies and 5 pottery currencies with a minimum of 3 dated cases. The currency models present independent evidence of the chronological distribution of the individual types and provide the needed correlation of metalwork and pottery, regardless of their divergent temporal rates of change.

The modelled metalwork currencies from Aarupgaard and Aarre urnfields depict differing rates of change throughout the investigated period (Fig. 60). There is a marked period of rapid change at the onset of Early Pre-Roman Iron Age with the introduction of pins with type 1 and type 2 coiled heads shortly after one another, together with simple iron rings and bomb head pins. This is followed by a period of relative stability, before another period of rapid change starting in the first half of the 4th century BC, when pins with coiled heads are going out of use, while pins with circular heads and a range of belt equipment are introduced. From then onwards the metalwork is continuously renewed with new types of belt equipment. According to Jensen (2005) the introduction of the later types of belt equipment, pin with grooved head and Holstein pin marks the beginning of the Late Pre-Roman Iron Age, but this is not supported by the radiocarbon evidence that depicts a continuous rate of change from the early 4th century BC and onwards.

The modelled pottery currencies from Aarupgaard urnfield have a low chronological sensitivity marked by long durations, relatively long estimated start and end boundaries, and considerable overlaps of consecutive currencies. It is difficult to identify differing rates of change in the pottery currencies, even though types 12B and 18C appear to be chronologically sensitive, and it is possible that the output would be different if the full pottery repertoire were included in the analysis rather than only the limited selection present in burial contexts. Based on the summarized pottery currencies it is possible to suggest a period of more rapid change starting in the first half of the 4th century BC (Fig. 62), coinciding with rapid change in metalwork as well. Jensen (2005) describes a period of rapid change at the transition from Early to Late Pre-Roman Iron Age, but the modelled currencies suggest this period to occur earlier. It has been suggested that vessel types used in the public domain are more likely to change fast over time, whereas other types appear to have remained more or less unchanged for long periods of time and the large storage vessels often reused as funerary vessels probably belong in the latter category (Whittle et al. 2016). The present finds are instead in line with Hingst (1959), who found the Early Pre-Roman Iron Age pottery from Schleswig-Holstein to be conservative in nature, and to have a limited chronological sensitivity as compared to the metalwork.

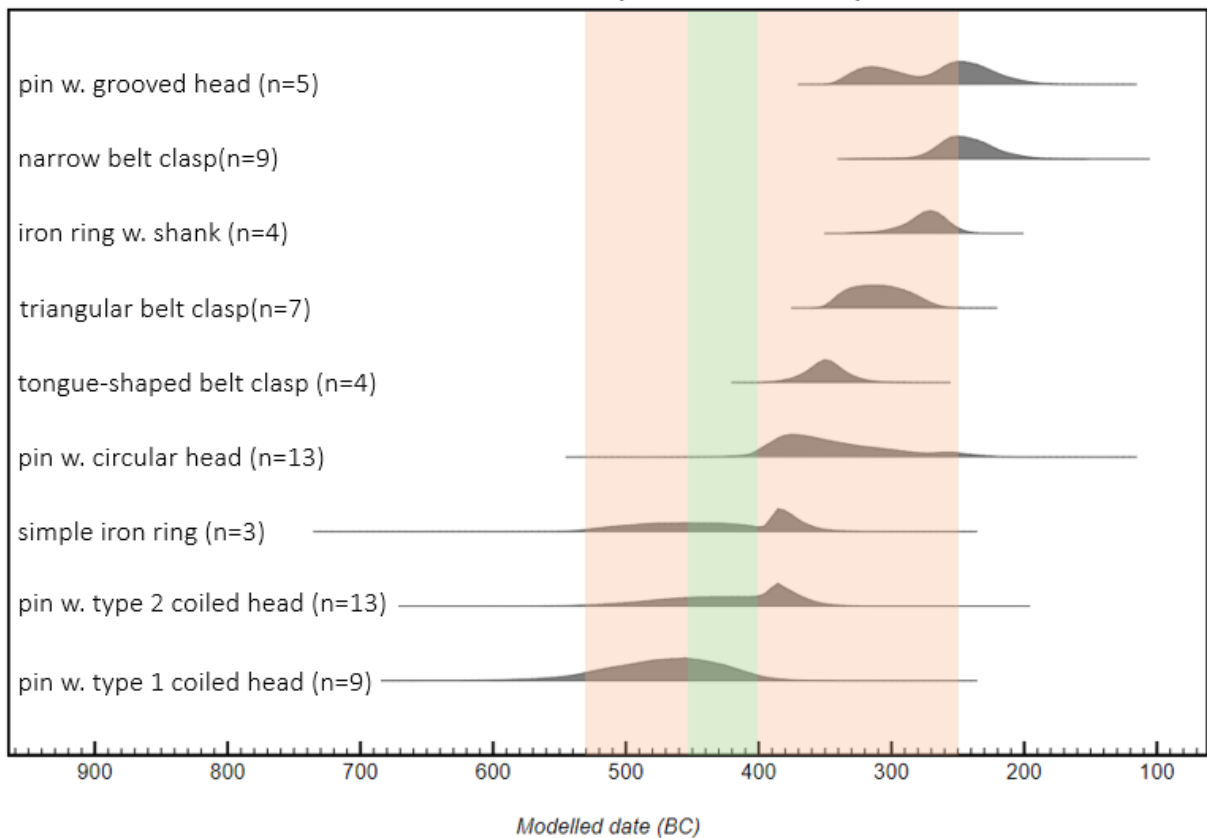


Figure 60: Identified periods with differing rates of change in metalwork currencies.

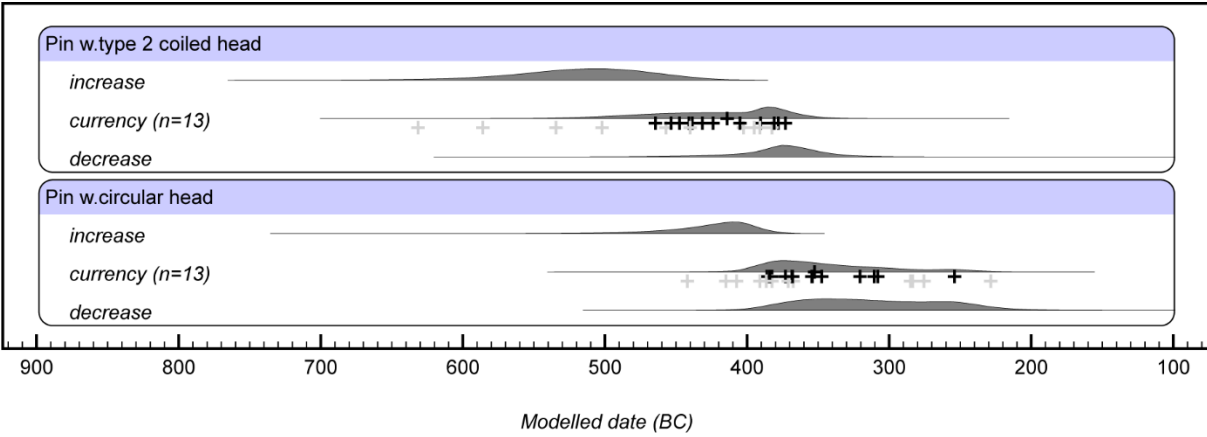


Figure 61: Posterior estimated currencies and periods of production increase and decrease of pin with type 2 coiled head and pin with circular head.

The modelled currencies of pin with type 2 coiled head and pin with circular head similar durations lasting from a few decades and up to c.250yr (95.4% probability), but with differing rates of change in production. It is estimated that type 2 coiled head pin has a rather long period of increase and a shorter

period of decrease, whereas circular head pin has a short period of increase and a longer period of decrease (Fig. 61). This demonstrate that although currencies have comparable durations their underlying patterns of change might differ, meaning that they gained and lost popularity at a non-equal rate. Such comparisons of the temporality of transformations in currencies do however require them to be modelled in trapezium bounded phases that estimates transition periods for the increase and decrease of production.

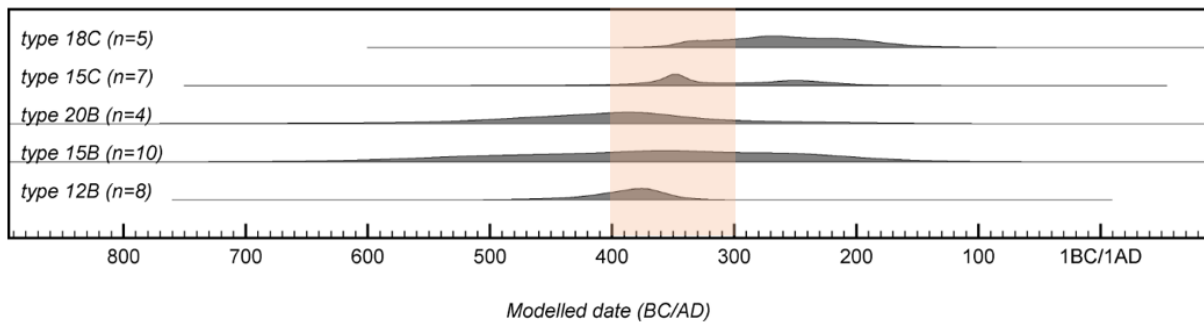


Figure 62: A possible period with higher rates of change in pottery currencies.

Residence time of individual artefacts

The production date and deposition date of an artefact are separate events that can in some instances be greatly removed from each other, i.e. the artefact has a residence time. If older individuals are buried with artefacts they received at a young age those artefacts will have a considerable residence time, which has lead Trachsel (2004) to caution against assigning currency durations shorter than a human lifetime. There is however no available information on the life expectancy in the Pre-Roman Iron Age or at what age individuals would receive dress accessories such as pins and belt clasps. If the artefacts were instead passed down as heirlooms the residence time would increase significantly.

Another important factor when discussing residence time of artefacts is durability of the material in question, and here metalwork generally has a high durability, whereas pottery is more fragile. Jensen (2005) refers to an ethnographic study of the lifecycle of domestic pottery vessels in a Fulani village in Cameroun where smaller vessels were only used for a couple of years before braking, whereas larger vessels used for cooking or storage could have a use-life of up to 12.5yr (David and Hennig 1972). All urns from Sphale urnfield have considerable wear of the bottom and they must have been used for some time prior to being converted to funerary urns, i.e. they have a residence time. No experimental studies have been conducted on the use wear of Pre-Roman Iron Age pottery, but it is plausible that the bottom of a vessel would show signs of use after even a few years. Some of the pottery currencies

are demonstrated to have been produced over a long period, but this does not contradict individual vessels having a short or even negligible residence time. The risk of metalwork having a residence time is considered to be larger and in some instances offsets are applied in allow the currency models to estimate earlier production dates than the deposition dates otherwise estimated by the site model.

A probable case of an heirloom object is a type 1 coiled head pin from grave A99 from Aarre urnfield (Fig. 63). The cremated bone date (GrM-16774) dates the grave to the 4th century BC, which is confirmed by two *TPQ* dates on charcoal from *Alnus* sp. trunk wood from the pit (RICH-25071) and from the funerary urn (RICH-25066). This is considerably later than the currency of the pin type which dates mainly to the 5th century BC and it is for this reason interpreted as an heirloom with a long residence time. The model estimates the pin to have a residence offset of 25-120 years (95.4% probability), which makes it one of the youngest of its type. None of the other graves appear to include artefact with a considerable residence time, but without dates on material with no intrinsic age such is available from Aarre urnfield it would be difficult to identify such, unless the offsets were large.

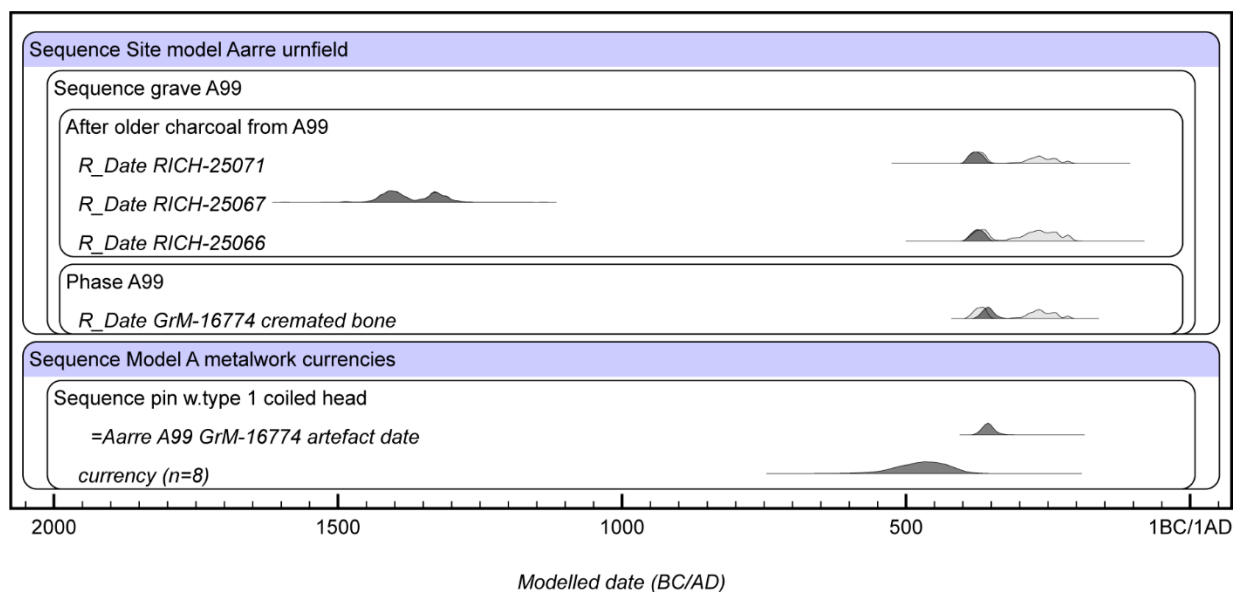


Figure 63: Posterior estimates of grave A99 from Aarre urnfield, from the site model of Aarre urnfield in the upper plot and from the Model A metalwork currencies in the lower plot. The summarized currency of pin with type 2 coiled head is plotted for reference.

Regionality in material culture

Four currencies are tentatively compared between urnfields in order to investigate regionality in material culture (Fig. 64). Results must however be treated with reservation as the currency models

are strongly dependent on dates from Aarupgaard urnfield. The metalwork currencies of pin with type 1 coiled head, pin with type 2 coiled head and pin with circular head are largely contemporaneous at Aarupgaard, Aarre and Søhale urnfield. This is not the case for currencies of pottery type 15C that appear and disappear earlier at Søhale than at Aarupgaard. The currencies are based on very few dated cases and it cannot be excluded that the observed difference is, at least in part, down to a sampling bias. Based on this, it is tentatively suggested that metalwork currencies developed at an equal rate across south-west Jutland, although it cannot be ruled out that introductions might have been slightly staggered across the region. The same cannot be extended to the pottery, although this is based on a single type. The vast majority of pottery were most likely produced locally (Jensen 2005), which might affect the rate of change across the region. There is no information on whether the metalwork was produced locally or in more centralized workshops and this might have changed over the period as the general knowledge of iron technology increased.

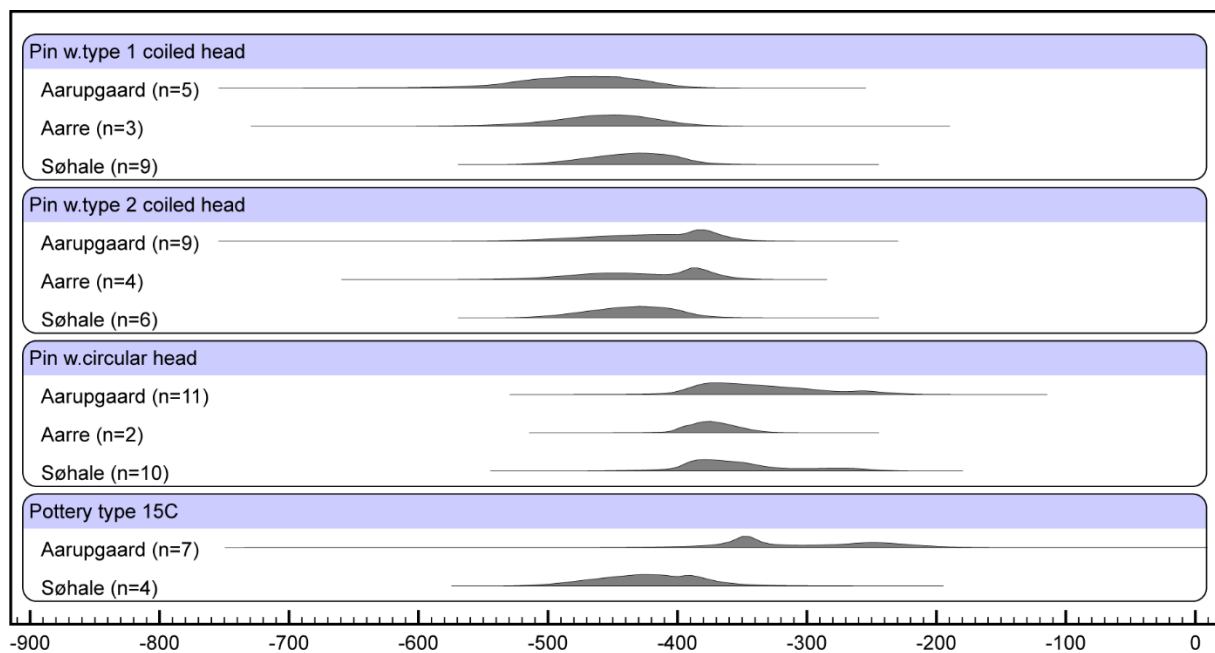


Figure 64: Modelled currencies of pin with type 1 coiled head, pin with type 2 coiled head, pin with circular head and pottery type 15C plotted for Aarupgaard, Søhale and Aarre urnfields respectively.

Evaluating the chronological framework

Change in material culture can be regarded as an indicator of change in a society (Hinz and Müller 2015), but to be classified as a transformation it needs to lead to a substantial and enduring change, visible in different domains of the society and its environment.²⁴ The introduction of iron technology in the Early Iron Age does not by itself constitute a transformation, but in combination with the social structure changing from being kinship based towards more family and village orientated, the introduction of urnfields as a new funerary tradition, and small scale changes in the material culture, it can be qualified as a chronological transformation. Settlement structure and economy remains relatively unchanged until Late Pre-Roman Iron Age, making it difficult to differentiate Late Bronze Age and Early Iron Age settlements (Hedeager 1990; Jensen 1997). Conventionally the transformation from Late Bronze Age to Early Iron Age is set to occur around 500 BC (Vandkilde et al. 1996; Jensen 2005), but Jensen (1997) has suggested it to occur already 530-520 BC, which is supported by a recent study of Søhale urnfield (Møller et al. 2020)

The transformation from Late Bronze Age to Early Iron Age is modelled as the transition period after the end of Bronze Age period VI (Part 1 of the currency models, Olsen et al. 2011), and before the start of burial activity at Aarupgaard, Aarre and Søhale urnfields (individual site models; Fig. 65). The start of Søhale is poorly defined as the model include a substantial number of dates with no typological prior information, but this has no significant effect on the estimated transition period. The Aarupgaard dataset includes three 'founding graves' with artefact assemblages with mixed Bronze Age-Iron Age appearances, producing a significantly earlier start estimate than at Aarre. Without more absolutely dated urnfields it is difficult to assess if Aarupgaard was indeed the earliest cemetery to be established in the region, but its size alone marks as an exceptional site. The end of Bronze Age period VI is estimated to *752-549 cal BC (95.4% probability)*, probably *746-622 cal BC (68.2% probability)*. The transition to Early Iron Age is estimated to occur *734-541 cal BC (95.4% probability)*, probably *691-580 cal BC (68.2% probability)*.

There is an ongoing debate, whether the last Bronze Age period VI does indeed belong in the Bronze Age, or if might instead be viewed as a transitional phase between the Bronze and Iron Ages. The latter model is advocated by Jensen (2005), who finds no clear break in the artefacts types from Bronze Age

²⁴ As defined in in the CRC 1266 collaborative research project. Webpage: <https://www.sfb1266.uni-kiel.de/en> (accessed 23.02.2020).

to Iron Age, and by Kneisel (2013), who demonstrates that a new spectrum of types were introduced in period VI, clearly separating this period from the previous ones. The transformation presented here is earlier than the previously suggested transformation dates and it supports the argument of a longer transitional phase, at least with regard to the material culture. Hopefully more Late Bronze Age dates will become available and reinforce the Bronze Age side of the transformation.

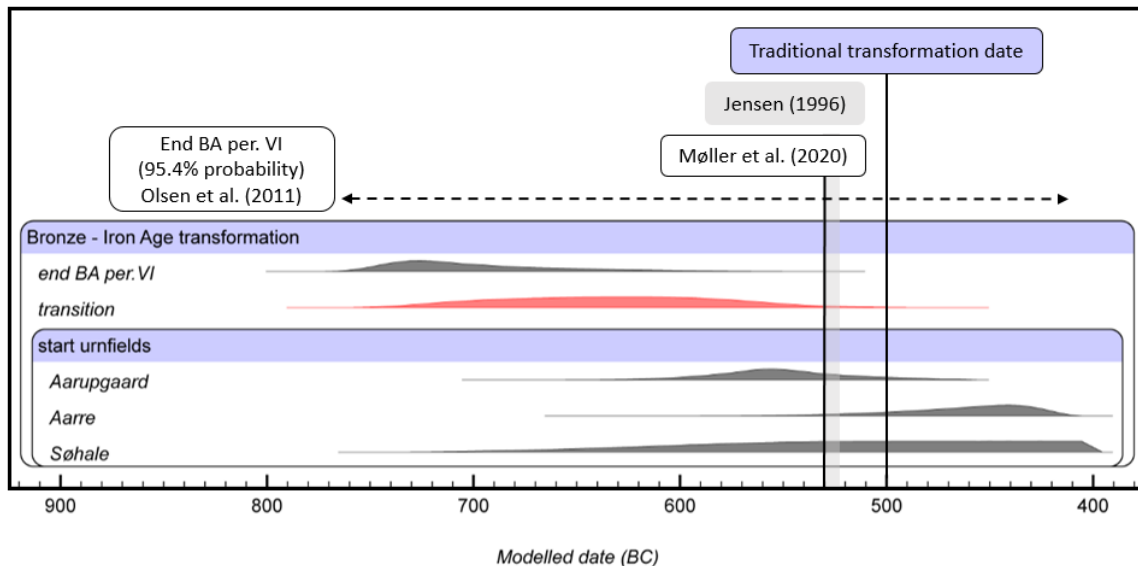


Figure 65: Chronological model of the Bronze-Iron Age transformation. The upper plot depicts the traditional transformation date c.500 BC along with alternative dates suggested by Jensen (1996) and Møller et al. (2020) and the modelled end of Bronze Age period VI by Olsen et al. (2011). The lower plot depicts the modelled end of Bronze Age period VI and start of urnfields at Aarupgaard, Aarre and Søhale estimated by the current study, and the estimated transition period in between with a red distribution.

The transition from period I.1 to period I.2 of the Early Pre-Roman Iron Age coincides with a period of rapid change in metalwork, but without change in other domains it does not qualify as an actual transformation. According to Jensen (2005) the transition in the metalwork sequence occurs after the introduction of pins with type 1 and type 2 coiled head, but before the introduction of pin with circular head. In the pottery sequence it occurs after the introduction of type 12B, but before the introduction of type 18C. The transition is here modelled as an event occurring after a phase containing the posterior estimated start boundaries of type 1 and type 2 pin with coiled head and pottery type 12B, but before a phase containing the posterior estimated start boundaries of pin with circular head, the combined belt equipment, and pottery type 18C (Fig. 66). The transition is estimated to occur 509-386 cal BC (95.4% probability), probably 465-402 cal BC (68.2% probability). This is earlier than 400 BC as suggested by Møller et al. (2020), but unfortunately they do not describe the chronological model and

how the transition is estimated. The modelled transition also provides an additional correlation of the metalwork and pottery sequences.

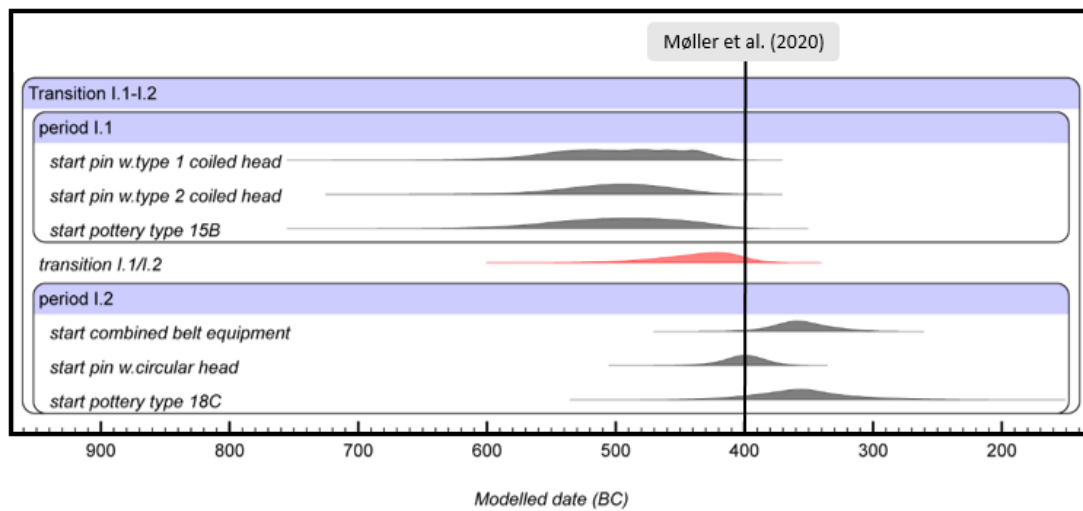


Figure 66: Chronological model of the transition from period I.1 to period I.2 of the Early Pre-Roman Iron Age as defined by the typo-chronology of Jensen (2005). The red distribution is the estimated transition period between periods I.1 and I.2. The vertical line represents the transition date suggested by Møller et al. (2020).

The transformation from Early to Late Pre-Roman Iron Age coincides with a full implementation of the societal changes initiated at the onset of the Iron Age (Hedeager 1990; Jensen 1997). Settlements and burials sites are abandoned across most of western Denmark, including the urnfields (Webley 2008; Møller 2015). Aarupgaard urnfield is one of the very few exceptions to this (Terkildsen 2015). The transformation is conventionally set to occur around 200 BC (Hedeager 1990; Jensen 1997; Jensen 2005), but Martens (1996) suggest it to occur already around 250 BC. This is supported by Møller et al. (2020) who estimate it to occur in the early or middle of the third century BC. According to Jensen (2005) the transformation coincides with the introduction of late types of belt equipment (narrow belt clasp, iron ring with shank), pin with grooved head and Holstein pin. The transformation is here modelled as an event occurring after a phase containing the posterior estimated end boundaries of type 1 and type 2 pin with coiled head and the start boundary of pin with circular head, but before a phase containing the posterior estimated start boundaries of narrow belt clasp, iron ring with shank, pin with grooved head, and Holstein pin. The transition is estimated to occur 390-302 cal BC (95.4% probability), probably 366-321 cal BC (68.2% probability), which is surprisingly early compared to the conventional transition date. An alternative transition date corresponding to the abandonment of Søjale and Aarre urnfields is instead considered (Fig. 67). Burial activity at Aarre urnfield is estimated

to end 359-297 cal BC (95.4% probability), probably 351-325 cal BC (68.2% probability), but this is largely a reflection of the sampling strategy where only a single grave containing belt equipment has been dated, whereas Becker (1961) has published several instances of typologically younger triangular belt clasps from the site. Burial activity at Søhale urnfield is estimated to end 285-201 cal BC (95.4% probability), probably 260-217 cal BC (68.2% probability), which corresponds with the traditional transformation date c.250 BC. It also corresponds with the estimated end of burial activity at Aarupgaard urnfield, although based on typology the site is expected to have been in use into the Late Pre-Roman Iron, and this early end date is probably a reflection of the sampling strategy. Based on this it is concluded that the chronological division of metalwork sequence by Jensen (2005) is in need of a revision.

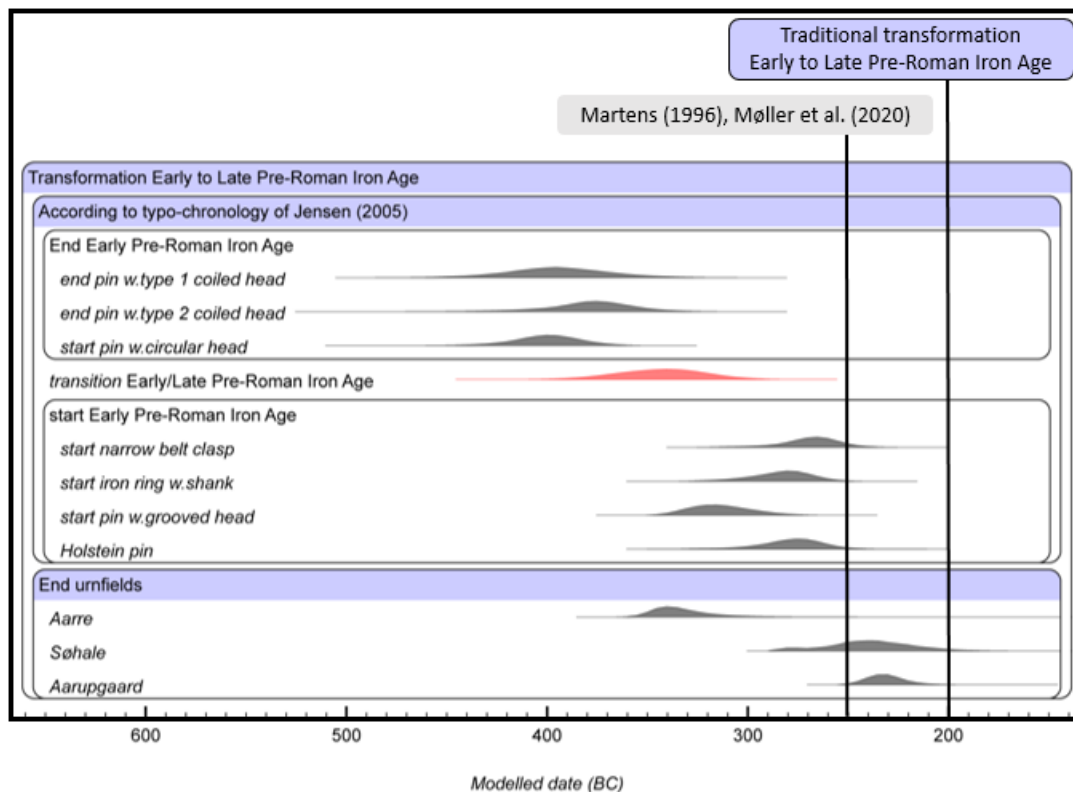


Figure 67: Chronological model of the transformation from Early to Late Pre-Roman Iron Age. The upper plot depicts the transformation as defined by the typo-chronology of Jensen (2005) and the red distribution is the estimated transition period. The lower plot depicts the posterior estimated ends of burial activity at Aarre, Søhale and Aarupgaard urnfields as an alternative model of the transformation. The vertical line at 200 BC represents the traditional transformation date, as suggested by Jensen (2005), and the vertical line at 250 BC represents the transformation date suggested by Marten (1996) and Møller et al. (2020).

The chronological framework of the Pre-Roman Iron Age in Southern Scandinavia are updated using the new posterior estimated transition events between Bronze and Iron Ages, between Jensen's periods I.1 and I.2 and Early and Late Pre-Roman Iron Age (periods I.1/II.1). Figure 68 illustrates clear discrepancies between the conventional, relative dates and the modelled dates of the first two transition events, whereas the conventional date of the last transformation agrees well with the radiocarbon data.

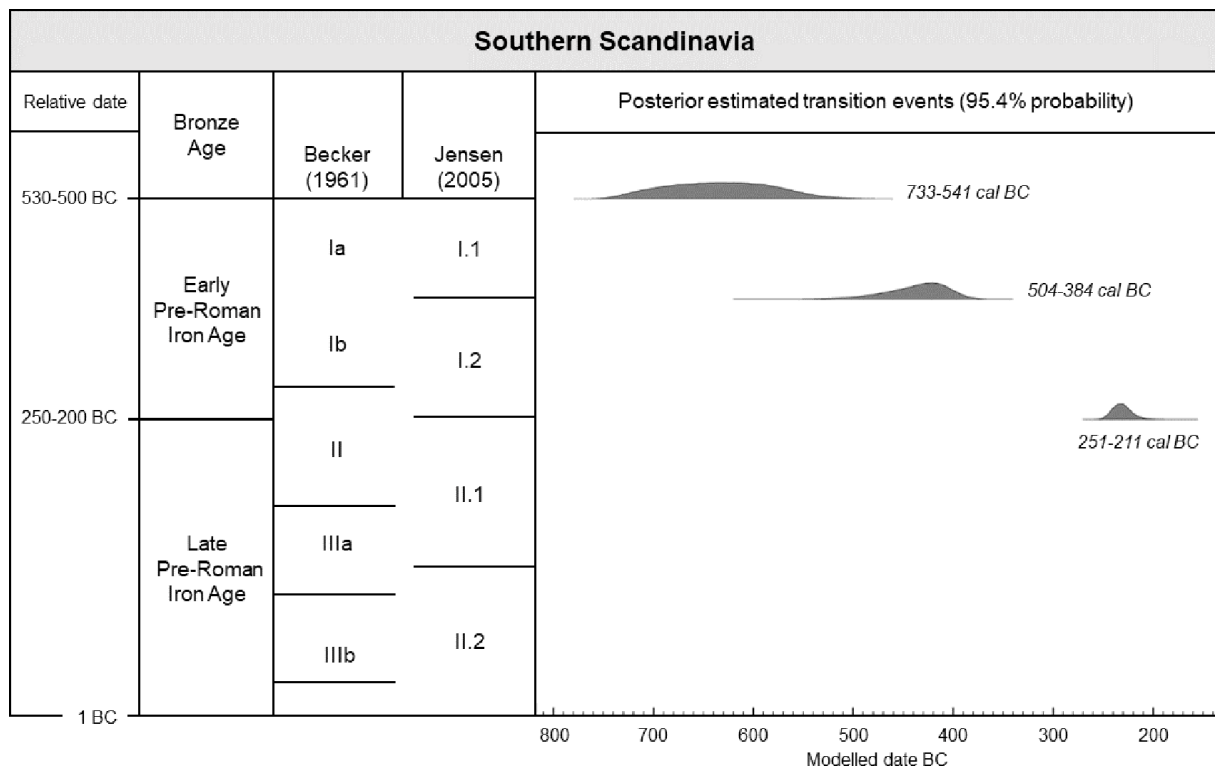


Figure 68: Synchronized version of the relevant chronological systems of the Pre-Roman Iron Age in Southern Scandinavia. Relations between Becker (1961) and Jensen (2005) systems follow Jensen (2005, vol.1: 98). Estimations of key transition events (95.4% probability) follow descriptions above, except for the I.2/II.1 transition that equals the end of burial activity at Aarupgaard urnfield.

Part C conclusion

The question of *when* change occurred is a fundamental aspect of archaeological research and the traditional approach has been to generate typological sequences of artefacts and construct chronological frameworks. Such typo-chronological systems often cover large geographical areas and are essential for interpreting the archaeological record. They do however interpret change across an area as occurring simultaneously and inherently treat transitions between periods as abrupt events. The aim of this dissertation thesis is to investigate the temporality of transformation processes in material culture, specifically in a case study of Early Iron Age urnfield assemblages from Southern Jutland, Denmark. Investigating small-scale transformations, such as occurring in the material culture, is important because it can improve the current understanding of scales of transformations, but also because small-scale transformations can be regarded as an indicator of social and cultural transformations. Existing chronologies for the Early Iron Age in Southern Jutland are based on typo-chronological analysis of primarily metalwork from cremation burials from large urnfield cemeteries, and they are not constrained by scientific dating because the period coincides with a major plateau in the radiocarbon calibration curve (c. 800-400 cal BC). Pottery only plays a secondary role in the chronologies, but because metalwork is practically absent from the contemporary settlements it is difficult to compare funerary and settlement evidence. This dissertation seeks to resolve this and for this purpose 95 burials with mixed find assemblages of diagnostic metalwork and pottery artefacts are selected from three urnfields, Aarupgaard, Aarre and Søhale, located in south-west Jutland. Artefacts are indirectly dated by associated samples of primarily cremated bone, which are corrected for wood-age offsets using the statistical model developed in Part B. To model the temporal processes of change in artefact currencies dynamically a total of 153 radiocarbon dates are combined in a Bayesian framework with prior information on artefact typology and site formation processes, i.e. how the urnfields developed spatially over time or how the graves relate to each other stratigraphically. This research approach enables investigations into the defined research questions regarding divergent chronological sensitivities and correlation of metalwork and pottery, along with a critical evaluation of the chronological framework of Pre-Roman Iron Age in Southern Scandinavia.

The dissertation analyses 24 artefact types of metalwork and pottery and compare the relative order of currencies to the typo-chronology of Jensen (2005). The radiocarbon evidence supports the sequence of metalwork types, but it is suggested that the pottery sequence is in need of a revision and that some of the typological definitions are changed. Pins with circular head are traditionally subdivided into 'pin with small head' and 'pin with large head', but the head size is here demonstrated to be continuously distributed and not correlated with ¹⁴C age. Since the head size is thus not typologically

relevant nor time dependant it is suggested to merge the two sub-types. Four types of belt equipment are analysed, including three types of belt clasps. Although the clasp types have distinct ideal forms, there is a great deal of fuzziness between these. To minimize the risk of misclassification it is suggested to instead distinguish between early types (tongue-shaped belt clasp and triangular belt clasp) and later types (narrow belt clasp and iron ring with shank) because they have distinct chronological distributions.

Chronological models are provided for 9 metalwork currencies and 5 pottery currencies with minimum 3 dated cases, but are limited to dates from Aarupgaard and Aarre due to an over-convergence issue. The currency models present independent evidence of the chronological distribution of the individual types and provide the needed correlation of metalwork and pottery, regardless of their divergent temporal rates of change. A period of rapid change in metalwork currencies is documented to occur at the onset of Early Pre-Roman Iron Age, followed by a period of relative stability, before another period of rapid change occurs in the first half of the 4th century BC. The metalwork currencies have different durations, from less than a century and up to c.250yr, and also to have different temporal patterns of production increase and decrease, which clearly demonstrates that they gained and lost popularity at a non-equal rate. The pottery currencies have a low chronological sensitivity marked by long durations and considerable overlaps of consecutive types. It is however suggested that vessels necks shapes are more chronologically sensitive than vessel body shapes, which is unfortunate with regard to the frequently destruction of these shallow cremation burials due to agricultural activity. A possible period with higher rates of change is identified starting in the first half of the 4th century BC, coinciding with rapid change in metalwork, but overall results support the argument of pottery being more conservative in relation to change as compared to the metalwork (Hingst 1959).

The corrected radiocarbon dates on cremated bone date the cremation event and the deposition of artefacts, which can be greatly removed from the production of those artefact. It is difficult to identify artefacts with minor residence offsets, as expected if an older individual is buried with metalwork received at a young age or if a vessel was used for a longer period before being re-purposed as a cremation urn. If artefacts are passed down as heirlooms they will attain larger residence offsets and such a probable heirloom is identified in grave 99 from Aarre urnfield. To incorporate this possibility the currency model allows the artefact to be older than the burial date in the site model.

The modelled output is strongly dependent on dates from Aarupgaard urnfield and although this limits investigations into possible regional differences in rates of change, four currencies are tentatively compared between the three urnfields. Currencies of pin with type 1 and type 2 coiled head and pin with circular head are large contemporaneous, suggesting that metalwork currencies developed at an equal rate across south-west Jutland. The currency of pottery type 15C has different distributions at Aarupgaard and Søhale, and it is suggested the supposed local production of pottery might affect the rate of change across the region.

Site models are presented for Aarupgaard, Aarre and Søhale urnfields, respectively, and are in agreement with the archaeological prior information. The Aarupgaard model includes three early 'founding graves' with artefacts with a mixed Bronze-Iron Age appearance and burial activity is estimated to have started here first *622-488 cal BC (95.4% probability)*, probably *592-530 cal BC (68.2% probability)*. Activity starts slightly later at Aarre *537-414 cal BC (95.4% probability)*, probably *485-424 cal BC (68.2% probability)*, whereas the start of Søhale *551-440 cal BC (95.4% probability)*, probably *522-460 cal BC (68.2% probability)* is poorly defined because the model includes a substantial number of graves with no prior information on typology. Burial activity is estimated to have first ended at Aarre *359-297 cal BC (95.4% probability)*, probably *351-325 cal BC (68.2% probability)*, followed by Søhale *285-201 cal BC (95.4% probability)*, probably *260-217 cal BC (68.2% probability)*, and Aarupgaard *251-211 cal BC (95.4% probability)*, probably *244-225 cal BC (68.2% probability)*. The summarized of Aarupgaard has a pronounced peak in the 3rd century BC, but it is difficult to interpret this as simulation analysis demonstrates the peak to be closely related to an inversion of the radiocarbon calibration curve in this period.

The dissertation provides probabilistic estimates on key transition events and uses these to synchronize and re-evaluate the chronological framework of the Early Iron Age in Southern Scandinavia. The Bronze-Iron Age transformation is traditionally set to occur around 500 BC, alternative c.530-520 BC, but there is an ongoing debate whether the last Bronze Age period VI does indeed belong in the Bronze Age, or if might instead be viewed as a transitional phase between the Bronze and Iron Ages. This dissertation presents the first probabilistic estimate of such a transition period between Bronze Age period VI and the start of the Pre-Roman Iron Age. Period VI is estimated to end *752-549 cal BC (95.4% probability)*, probably *746-622 cal BC (68.2% probability)* and the transition period is estimated to start *734-541 cal BC (95.4% probability)*, probably *691-580 cal BC (68.2% probability)*. The start of the Pre-Roman Iron Age equals the start of burial activity at the urnfield (see above). The estimated transformation supports the argument of a longer transitional

phase, at least with regard to the material culture, but it is significantly earlier than what has previously been suggested. Hopefully more Late Bronze Age date will become available in the future to investigate this further.

The transition from period I.1 to period I.2 of the Pre-Roman Iron Age is modelled according to the typological sequences of Jensen (2005) and it is estimated to occur *509-386 cal BC (95.4% probability)*, probably *465-402 cal BC (68.2% probability)*. This is slightly earlier than the c.400 BC that has previously been suggested by Møller et al. (2020), but it coincides with a period of rapid change in metalwork and possibly in pottery. The modelled transition also provides a further correlation of metalwork and pottery artefact sequences.

The transformation from Early to Late Pre-Roman Iron Age (period I – period II) is likewise modelled according to the typological sequences of Jensen (2005), which estimates it to occur *390-302 cal BC (95.4% probability)*, probably *366-321 cal BC (68.2% probability)*. This is surprisingly early compared to previously suggested dates of c.250 BC or c.200 BC as Jensen also suggests. An alternative model considers the end of burial activity at Aarupgaard and Aarre urnfields as an estimate of the transformation, and this corresponds well with the traditional transformation date of c.250 BC. Based on the radiocarbon evidence here, it is suggested that Jensen's chronological division of the artefact sequences needs revision.

Table 8: Radiocarbon results and associated artefacts from Aarupgaard, Aarre and Søhale urnfields. Replicate measurements have been tested for consistency and combined following Ward and Wilson (1978).

Lab code	Sample ID	Material	Typology of artefacts	CI	%C of extract	Corrected pMC	AMS $\delta^{13}\text{C}$ (‰VPDB) ¹	¹⁴ C Age (BP)	Reference
Aarupgaard urnfield cemetery (HAM 1070)									
KIA-51892	Urn no. 34	Cremated bone (human)	Urn type 20B, 2 pins with type 2 coiled heads.	6.4	0.24	74.68 ± 0.26	-24.4	2346 ± 28	
KIA-51893	Urn no. 36	Cremated bone (human)	Urn type 20B, 2 pins with type 2 coiled heads.	5.9	0.23	73.81 ± 0.19	-24.6	2439 ± 21	
GrM-15072	Urn no. 51	Cremated bone (human)	Urn type 15B, 2 pins with coiled heads, incomplete neck bends.	5.9	0.11	73.77 ± 0.26	-30.3 ± 0.4	2445 ± 20	Rose et al. (2019)
KIA-52339	Urn no. 51	Cremated bone (human)	-	-	0.38	73.73 ± 0.24	-26.8 ± 0.3	2448 ± 26	Rose et al. (2019)
Weighted mean urn no. 51: $T' = 0.0$, $T' (5\%) = 3.8$, $v = 1$, 2446 ± 16 BP									
GrM-14589	Urn no. 81	Cremated bone (human)	Urn type 12B, 2 pins with type 2 coiled heads, iron chain corroded together with pins.	5.9	0.06	73.93 ± 0.20	-27.5	2425 ± 30	Rose et al. (2019)
KIA-52819	Urn no. 81	Replicate of GrM-14589; apatite pretreated at ClO, CO ₂ extracted and dated at KIA.	-	-	0.19	74.37 ± 0.20	-23.0	2379 ± 22	Rose et al. (2019)
Weighted mean urn no. 81: $T' = 1.5$, $T' (5\%) = 3.8$, $v = 1$, 2395 ± 18 BP									
GrM-15078	Urn no. 83	Cremated bone (human)	Urn type 12B, 2 pins with type 2 coiled heads, pin of unknown type.	6.0	0.06	73.42 ± 0.30	-28.1	2485 ± 30	Rose et al. (2019)
KIA-52825	Urn no. 83	Replicate of GrM-15078; apatite pretreated at ClO, CO ₂ extracted and dated at KIA.	-	-	0.17	74.09 ± 0.25	-20.7	2409 ± 27	Rose et al. (2019)
Weighted mean urn no. 83: $T' = 3.5$, $T' (5\%) = 3.8$, $v = 1$, 2443 ± 21 BP									
KIA-51894	Urn no. 123	Cremated bone (human)	Urn type 20B, triangular belt clasp, pin with circular head.	6.4	0.29	75.32 ± 0.25	-22.6	2277 ± 26	
KIA-51895	Urn no. 183	Cremated bone (human)	Urn type 12B, tongue-shaped belt clasp, 2 pins with circular heads.	6.6	0.21	75.64 ± 0.21	-23.4	2243 ± 23	

Lab code	Sample ID	Material	Typology of artefacts	CI	%C of extract	Corrected pMC	AMS $\delta^{13}C$ (‰VPDB) ¹	¹⁴ C Age (BP)	Reference
GrM-14704	Urn no. 230	Cremated bone (human)	Urn type 12B, 2 pins with circular heads.	5.4	0.07	72.83 ± 0.12	-21.7	2546 ± 19	Rose et al. (2019)
KIA-52826	Urn no. 230	Replicate of GrM-14704; apatite pretreated at ClO, CO2 extracted and dated at KIA.	-	-	0.19	74.53 ± 0.23	-20.9	2362 ± 25	Rose et al. (2019)
<i>Weighted mean urn no. 230: $T' = 34.1$, $T' (5\%) = 3.8$, $v = 1$, 2480 ± 16 BP</i>									
GrM-14588	Urn no. 280	Cremated bone (human)	Urn type 15B, 2 pins with type 2 coiled heads.	6.2	0.08	74.12 ± 0.14	-25.1	2405 ± 20	Rose et al. (2019)
KIA-52820	Urn no. 280	Replicate of GrM-14588; apatite pretreated at ClO, CO2 extracted and dated at KIA.	-	-	0.27	74.16 ± 0.21	-22.7	2402 ± 22	Rose et al. (2019)
<i>Weighted mean urn no. 280: $T' = 0.0$, $T' (5\%) = 3.8$, $v = 1$, 2404 ± 15 BP</i>									
KIA-51896	Urn no. 293	Cremated bone (human)	Urn type 20B, 3 pins with circular heads.	6.9	0.22	74.38 ± 0.21	-22.8	2378 ± 23	
KIA-51897	Urn no. 346	Cremated bone (human)	Urn type 15C, tongue-shaped belt clasp.	6.3	0.18	75.61 ± 0.22	-21.9	2246 ± 24	
GrM-14596	Urn no. 382	Cremated bone (human)	Urn type 15C, narrow belt clasp.	7.3	0.08	75.29 ± 0.14	-24.8 ± 0.2	2280 ± 20	Rose et al. (2019)
KIA-52827	Urn no. 382	Replicate of GrM-14596; apatite pretreated at ClO, CO2 extracted and dated at KIA.	-	-	0.27	75.77 ± 0.24	-22.5 ± 0.3	2229 ± 25	Rose et al. (2019)
<i>Weighted mean urn no. 382: $T' = 2.5$, $T' (5\%) = 3.8$, $v = 1$, 2260 ± 16 BP</i>									
GrM-14705	Urn no. 681	Cremated bone (human)	Urn type 13D, 2 pins with type 2 coiled heads, iron ring.	6.0	0.08	75.01 ± 0.12	-22.3	2310 ± 19	Rose et al. (2019)
KIA-53094	Urn no. 681	Replicate of GrM-14705; apatite pretreated at ClO,	-	-	0.24	75.05 ± 0.19	-22.5	2305 ± 20	Rose et al. (2019)

Lab code	Sample ID	Material	Typology of artefacts	CI	%C of extract	Corrected pMC	AMS $\delta^{13}C$ (‰VPDB) ¹	¹⁴ C Age (BP)	Reference
<i>Weighted mean urn no. 681: $T' = 0.0$, $T' (5\%) = 3.8$, $v = 1$, 2308 ± 14 BP</i>									
RICH-25343	Urn no. 752	Cremated bone (human)	Urn type 12B, 2 pins with circular heads.	5.7	0.28	74.94	-24.2	2317 \pm 26	
GrM-14589	Urn no. 766	Cremated bone (human)	Urn type 15B, 3 pins with circular heads.	5.5	0.16	75.24 \pm 0.14	-26.4	2285 \pm 20	Rose et al. (2019)
KIA-52821	Urn no. 766	Replicate of GrM-14589; apatite pretreated at ClO, CO2 extracted and dated at KIA.	-	-	0.39	75.55 \pm 0.21	-25.2	2252 \pm 23	Rose et al. (2019)
<i>Weighted mean urn no. 766: $T' = 1.2$, $T' (5\%) = 3.8$, $v = 1$, 2271 ± 16 BP</i>									
RICH-24151	Urn no. 797	Cremated bone (human)	Urn type 13C, narrow belt clasp, 2 pins with circular heads.	6.7	0.03	75.53	-27.9	2255 \pm 28	
KIA-51899	Urn no. 858	Cremated bone (human)	Urn type 15B, narrow belt clasp, iron pin with grooved head.	6.2	0.41	75.49 \pm 0.21	-21.5	2258 \pm 23	
RICH-24150	Urn no. 928	Cremated bone (human)	Urn type 15B, pin with type 2 coiled head, pin with circular head.	7.3	0.05	75.13	-20.6	2297 \pm 25	
GrM-14599	Urn no. 1001	Cremated bone (human)	Urn types 18C and 15B, iron ring with shank, pin of unknown type.	6.2	0.08	75.71 \pm 0.14	-23.0	2235 \pm 20	Rose et al. (2019)
KIA-53095	Urn no. 1001	Replicate of GrM-14599; apatite pretreated at ClO, CO2 extracted and dated at KIA.	-	-	0.22	75.54 \pm 0.19	-20.1	2253 \pm 21	Rose et al. (2019)
<i>Weighted mean urn no. 1001: $T' = 0.4$, $T' (5\%) = 3.8$, $v = 1$, 2244 ± 15 BP</i>									
KIA-51900	Urn no. 1016	Cremated bone (human)	Urn type 15B, iron ring with shank.	6.7	0.23	75.85 \pm 0.24	-23.7	2220 \pm 25	
GrM-14592	Urn no. 1076	Cremated bone (human)	Urn type 18C, narrow belt clasp, bronze neck ring.	6.4	0.08	75.47 \pm 0.14	-27.8	2260 \pm 20	Rose et al. (2019)
KIA-52822	Urn no. 1076	Replicate of GrM-14592; apatite	-	-	0.18	76.05 \pm 0.28	-25.3	2199 \pm 29	Rose et al. (2019)

Lab code	Sample ID	Material	Typology of artefacts	CI	%C of extract	Corrected pMC	AMS $\delta^{13}C$ (‰VPDB) ¹	¹⁴ C Age (BP)	Reference
RICH-25340	Urn no. 1076	pretreated at ClO, CO2 extracted and dated at KIA. Cremated bone (human)	-		0.12	76.06 ± 0.26	-25.5	2198 ± 27	Rose et al. (2019)
<i>Weighted mean urn no. 1076: T' = 4.8, T' (5%) = 6.0, v = 2, 2229 ± 15 BP</i>									
GrM-14597	Urn no. 1186	Cremated bone (human)	Urn type 13A, 2 pins with type 1 coiled heads, iron ring.	5.8	0.12	73.58 ± 0.13	-24.7	2465 ± 20	Rose et al. (2019)
KIA-53096	Urn no. 1186	Replicate of GrM-14597; apatite pretreated at ClO, CO2 extracted and dated at KIA.	-	-	0.27	74.10 ± 0.18	-24.1	2408 ± 20	Rose et al. (2019)
<i>Weighted mean urn no. 1186: T' = 4.1, T' (5%) = 3.8, v = 1, 2437 ± 15 BP</i>									
RICH-25332	Urn no. 1232	Cremated bone (human)	Urn type 15B, 2 pins with type 1 coiled heads.	5.8	0.16	73.78	-21.4	2443 ± 27	
RICH-24143	Urn no. 1279	Cremated bone (human)	Urn type 13A, 2 pins with type 2 coiled heads.	5.7	0.21	73.56	-19.6	2467 ± 26	
GrM-14602	Urn no. 1363	Cremated bone (human)	Urn type 15B, triangular belt clasp.	6.5	0.07	75.79 ± 0.14	-30.3	2225 ± 20	Rose et al. (2019)
KIA-52828	Urn no. 1363	Replicate of GrM-14602; apatite pretreated at ClO, CO2 extracted and dated at KIA.	-	-	0.17	76.09 ± 0.23	-27.9	2195 ± 24	Rose et al. (2019)
<i>Weighted mean urn no. 1363: T' = 0.9, T' (5%) = 3.8, v = 1, 2213 ± 16 BP</i>									
RICH-25335	Urn no. 1382	Cremated bone (human)	Urn type 18C, triangular belt clasp, 2 pins with circular heads.	6.8	0.10	76.01	-26.2	2204 ± 27	
RICH-25357	Urn no. 1422	Cremated bone (human)	Urn type 13D, narrow belt clasp, pin with grooved head.	5.9	0.11	76.18	-23.5	2186 ± 26	
RICH-25333	Urn no. 1436	Cremated bone (human)	Urn type 15C, narrow belt clasp.	5.9	0.11	75.55	-25.3	2252 ± 28	

Lab code	Sample ID	Material	Typology of artefacts	CI	%C of extract	Corrected pMC	AMS $\delta^{13}C$ (‰VPDB) ¹	¹⁴ C Age (BP)	Reference
RICH-25334	Urn no. 1617	Cremated bone (human)	Urn type 18C, triangular belt clasp, 2 pins with circular heads, bronze pin with grooved head.	5.4	0.14	76.39	-25.6	2163 ± 28	
KIA-52340	Urn no. 1678	Cremated bone (human)	Urn type 15C, narrow belt clasp.	5.4	0.32	75.64 ± 0.23	-22.3	2243 ± 25	
GrM-15074	Urn no. 1791	Cremated bone (human)	Urn type 15C, triangular belt clasp.	5.7	0.07	75.78 ± 0.26	-30.0	2230 ± 25	Rose et al. (2019)
KIA-52341	Urn no. 1791	Cremated bone (human)	-	-	0.29	76.35 ± 0.23	-29.63	2167 ± 25	Rose et al. (2019)
<i>Weighted mean urn no. 1791: T' = 3.2, T' (5%) = 3.8, v = 1, 2199 ± 18 BP</i>									
GrM-15075	Urn no. 1847	Cremated bone (human)	Urn type 15C, triangular belt clasp.	6.1	0.08	75.53 ± 0.20	-25.4	2255 ± 20	Rose et al. (2019)
KIA-52342	Urn no. 1847	Cremated bone (human)	-	-	0.28	75.78 ± 0.24	-28.9	2228 ± 25	Rose et al. (2019)
<i>Weighted mean urn no. 1847: T' = 0.7, T' (5%) = 3.8, v = 1, 2244 ± 16 BP</i>									
RICH-24144	Urn no. 1834	Cremated bone (human)	Urn type 12B, tongue-shaped belt clasp.	6.5	0.09	74.89	-19.8	2322 ± 25	
KIA-52343	Urn no. 1970	Cremated bone (human)	Urn type 15C, narrow belt clasp, bronze pin with grooved head.	5.9	0.28	75.61 ± 0.22	-22.8	2246 ± 23	
KIA-52344	Urn no. 1997	Cremated bone (human)	Urn type 18C, triangular belt clasp, bronze pin with grooved head.	6.5	0.38	76.36 ± 0.26	-30.6	2167 ± 27	
GrM-14593	Urn no. 2262	Cremated bone (human)	Urn type 11D, narrow belt clasp.	6.5	0.07	75.53 ± 0.16	-20.9	2255 ± 25	Rose et al. (2019)
KIA-52823	Urn no. 2262	Replicate of GrM-14593; apatite pretreated at ClO, CO ₂ extracted and dated at KIA.	-	-	0.24	75.92 ± 0.26	-19.0	2214 ± 28	Rose et al. (2019)
<i>Weighted mean urn no. 2262: T' = 1.2, T' (5%) = 3.8, v = 1, 2237 ± 19 BP</i>									
RICH-24145	Urn no. 2541	Cremated bone (human)	Urn type 20D, iron ring with shank, pin with flat pierced head, Holstein pin.	5.9	0.06	75.89	-22.7	2216 ± 26	
RICH-24146	Urn no. 2550	Cremated bone (human)	Urn type 15D, iron ring with shank.	5.9	0.08	75.18	-22.3	2291 ± 26	

Lab code	Sample ID	Material	Typology of artefacts	CI	%C of extract	Corrected pMC	AMS $\delta^{13}C$ (‰VPDB) ¹	¹⁴ C Age (BP)	Reference
RICH-25355	Urn no. 2710	Cremated bone (human)	Urn type 11A, pin with bomb-shaped head, pin with a pierced hole, pin with bend neck.	5.5	0.12	74.07	-18.9	2411 ± 27	
KIA-52345	Urn no. 3822	Cremated bone (human)	Urn type 11B, 2 pins with type 1 coiled heads.	5.5	0.26	73.87 ± 0.24	-23.9	2433 ± 26	
GrM-14594	Urn no. 3330	Cremated bone (human)	Urn type 15? Iron pin with coiled head, no bend neck.	6.8	0.10	72.96 ± 0.13	-21.0	2535 ± 20	Rose et al. (2019)
KIA-52824	Urn no. 3330	Replicate of GrM-14594; apatite pretreated at ClO, CO ₂ extracted and dated at KIA.	-	-	0.29	73.52 ± 0.24	-21.5	2471 ± 26	Rose et al. (2019)
KIA-51901	Urn no. 3330	Cremated bone (human)	-	-	0.28	73.23 ± 0.24	-21.9	2503 ± 27	Rose et al. (2019)
<i>Weighted mean urn no. 3330: T' = 3.9, T' (5%) = 6.0, v = 2, 2509 ± 14 BP</i>									
RICH-25354	Urn no. 3340	Cremated bone (human)	Urn of Bronze Age period VI type, but side urn is pre-Roman Iron Age in style. Swan neck pin.	5.7	0.35	73.47	-21.5	2477±27	
RICH-24147	Urn no. 3452	Cremated bone (human)	Urn type 15B, 2 pins with type 1 coiled heads.	6.2	0.12	73.03	-19.1	2525 ± 25	
RICH-24148	Urn no. 3778	Cremated bone (human)	Urn type 12B, 2 pins with type 2 coiled heads, iron ring.	5.4	0.12	73.7	-18.1	2452 ± 25	
GrM-15076	Urn no. 3869	Cremated bone (human)	Urn, open with no neck. Iron pin with round head, no neck bend.	6.0	0.09	72.87 ± 0.16	-21.6	2540 ± 20	Rose et al. (2019)
KIA-52346	Urn no. 3869	Cremated bone (human)	-	-	0.21	73.66 ± 0.23	-25.9	2456 ± 25	Rose et al. (2019)
RICH-24152	Urn no. 3869	Cremated bone (human)	-	-	0.20	73.22 ± 0.24	-25.8	2504 ± 26	Rose et al. (2019)
<i>Weighted mean urn no. 3869: T' = 6.9, T' (5%) = 6.0, v = 2, 2507 ± 14 BP</i>									
Aarre urnfield cemetery (VAM 1600)									
KIA-53941	Grave A86, urn, x339	Acer sp. trunk wood charcoal (Ø >10 cm)	-	-	63.96	73.60 ± 0.23	-25.3	2463 ± 25	Rose et al. (2020)

Lab code	Sample ID	Material	Typology of artefacts	CI	%C of extract	Corrected pMC	AMS $\delta^{13}C$ ($\%VPDB$) ¹	¹⁴ C Age (BP)	Reference
KIA-53942	Grave A86, urn, x340	Cremated bone (human)	-	5.4	0.35	74.37 ± 0.24	-19.7	2379 ± 26	Rose et al. (2020)
KIA-53942	Grave A86, urn, X340	Cremated bone (human), replicate	Urn of unknown type. 2 pins with type 2 coiled heads.	-	-	74.31 ± 0.23	-22.8	2385 ± 25	Rose et al. (2020)
<i>Weighted mean x340: T' (5%) = 3.8, v = 1, 2382 ± 19 BP</i>									
RICH-25356	A89, x311	Cremated bone (human)	Urn type 13, 2 pins with type 1 coiled heads.	6.4	0.16	-	-21.18	2464 ± 27	
KIA-53984	Grave A95, urn, x368 no.1	<i>Quercus</i> sp. twig charcoal (ϕ <0.3 cm)	-	-	70.68	74.45 ± 0.23	-28.4	2370 ± 25	Rose et al. (2020)
KIA-53985	Grave A95, urn, x368 no.3	<i>Acer</i> sp. twig charcoal (ϕ <0.5 cm)	-	-	70.49	73.90 ± 0.23	-27.7	2430 ± 26	Rose et al. (2020)
RICH-25342	Grave A95, urn, x369	Cremated bone (human)	Urn type 16?	7.8	0.11	73.90 ± 0.25	-24.3	2428 ± 27	Rose et al. (2020)
RICH-25071	Grave A99, pit, x65 no.2	<i>Alnus</i> sp. trunk wood charcoal (ϕ 8-10 cm)	-	-	60.00	75.39 ± 0.28	-33.3	2269 ± 29	Rose et al. (2020)
RICH-25067	Grave A99, pit, x65 no.3	<i>Quercus</i> sp. trunk wood charcoal (ϕ <10 cm)	-	-	61.00	67.85 ± 0.26	-31.6	3115 ± 31	Rose et al. (2020)
GrM-16774	Grave A99, urn, x345	Cremated bone (human)	Urn of unknown type, pin with type 1 coiled head.	6.5	0.06	75.50 ± 0.17	-26.5	2255 ± 20	Rose et al. (2020)
RICH-25069	Grave A99, urn, x346 no.1	<i>Alnus</i> sp. twig charcoal (ϕ <0.3 cm)	-	-	53.50	77.14 ± 0.28	-31.8	2085 ± 29	Rose et al. (2020)
RICH-25066	Grave A99, urn, x346 no.27	<i>Alnus</i> sp. trunk wood charcoal (ϕ > 10 cm)	-	-	61.60	75.56 ± 0.28	-35.3	2251 ± 30	Rose et al. (2020)
GrM-14604	Grave A117, urn, x762	Cremated bone (human)	Urn type 12, elaborate set of chain and pins.	6.0	0.10	73.75 ± 0.13	-25.7	2445 ± 20	Rose et al. (2019)
KIA-53098	Grave A117, urn, x762	Replicate of GrM-14604; apatite	-	-	0.28	74.03 ± 0.19	-22.1	2416 ± 20	Rose et al. (2019)

Lab code	Sample ID	Material	Typology of artefacts	CI	%C of extract	Corrected pMC	AMS $\delta^{13}C$ (‰VPDB) ¹	¹⁴ C Age (BP)	Reference
<i>Weighted mean x762: T' = 1.1, T' (5%) = 3.8, v = 1, 2431 ± 15 BP</i>									
KIA-53943	Grave A117, urn, x769	<i>Quercus</i> sp. charcoal (ϕ >10 cm) 1 annual ring sampled	-	-	31.21	73.72 ± 0.23	-23.6	2449 ± 25	Rose et al. (2020)
KIA-53944	Grave A117, urn, x774	<i>Quercus</i> sp. charcoal (ϕ >10 cm)	-	-	60.58	73.30 ± 0.22	-25.0	2495 ± 24	Rose et al. (2020)
KIA-53945	Grave A130, urn, x82 no.1	Charred grass stem	Tongue-shaped belt clasp, pin of unknown type.	-	68.30	72.49 ± 0.23	-25.1	2585 ± 25	Rose et al. (2020)
KIA-53946	Grave A130, urn, x82 no.2	<i>Triticum</i> cf. <i>aestivum</i> , charred cereal	-	-	64.19	76.46 ± 0.23	-28.5	2156 ± 24	Rose et al. (2020)
KIA-53947	Grave A130, urn, x217	Cremated bone (human)	-	5.8	0.24	75.57 ± 0.23	-20.9	2250 ± 25	Rose et al. (2020)
KIA-53947	Grave A130, urn, X217	Cremated bone (human), replicate	-	-	-	75.52 ± 0.23	-21.7	2255 ± 25	Rose et al. (2020)
<i>Weighted mean x217: T' = 0.0, T' (5%) = 3.8, v = 1, 2253 ± 18 BP</i>									
KIA-53948	Grave 155, urn, x127 no.1	cf. <i>Triticum</i> sp., charred cereal	-	-	50.00	73.31 ± 0.22	-26.4	2494 ± 24	Rose et al. (2020)
KIA-53949	Grave 155, urn, x127 no.2	<i>Arrhenatherum elatius</i> ssp. <i>Bulbosum</i> , charred grass bulb	-	-	65.52	73.56 ± 0.22	-28.2	2466 ± 24	Rose et al. (2020)
KIA-53950	Grave 155, urn, x281	Cremated bone (human)	Pin with circular head	6.1	0.26	74.55 ± 0.23	-23.6	2359 ± 25	Rose et al. (2020)

Lab code	Sample ID	Material	Typology of artefacts	CI	%C of extract	Corrected pMC	AMS $\delta^{13}C$ (‰VPDB) ¹	¹⁴ C Age (BP)	Reference
KIA-53950	Grave 155, urn, x281	Cremated bone (human), replicate	-	-	-	74.41 \pm 0.23	-24.1	2374 \pm 25	Rose et al. (2020)
<i>Weighted mean x281: T' = 0.2, T' (5%) = 3.8, v = 1, 2367 \pm 18 BP</i>									
KIA-53951	Grave A198, urn, x338	<i>Alnus</i> sp. trunk wood charcoal (\emptyset >10 cm)	-	-	57.02	69.12 \pm 0.21	-24.9	2967 \pm 24	Rose et al. (2020)
KIA-53952	Grave A198, urn, x338 CB	Cremated bone (human)	Urn of unknown type, 2 pins with type 2 coiled heads.	5.9	0.28	74.89 \pm 0.24	-24.9	2323 \pm 26	Rose et al. (2020)
KIA-53952	Grave A198, urn, x338 CB	Cremated bone (human), replicate	-	-	-	74.82 \pm 0.29	-25.9	2330 \pm 35	Rose et al. (2020)
<i>Weighted mean x338 CB: T' = 0.0, T' (5%) = 3.8, v = 1, 2325 \pm 21 BP</i>									
GrM-14707	A281, x484	Cremated bone (human)	Urn type 15, 2 pins with circular heads.	6.2	0.10	74.91 \pm 0.13	-28.0	2320 \pm 20	
KIA-53100	A281, x484	Replicate of GrM-14707; apatite pretreated at ClO, CO ₂ extracted and dated at KIA.		-	0.11	75.37 \pm 0.19	-23.5	2271 \pm 20	
<i>Weighted mean A281, x484: T' = 3.9, T' (5%) = 3.8, v = 1, 2296 \pm 15 BP</i>									
KIA-53953	Grave A278, urn, x782 no.1	Charred grass stem	-	-	74.57	74.17 \pm 0.23	-27.5	2400 \pm 25	Rose et al. (2020)
KIA-53954	Grave A278, urn, x782 no.2	Charred grass, stem and root fragment	-	-	67.11	73.76 \pm 0.23	-26.2	2445 \pm 25	Rose et al. (2020)
KIA-53955	Grave A278, urn, x783	Cremated bone (human)	Urn of unknown type, 2 pins with disc-shaped heads, bronze ring.	5.5	0.20	73.47 \pm 0.24	-22.7	2477 \pm 26	Rose et al. (2020)
KIA-53955	Grave A278, urn, x783	Cremated bone (human), replicate	-	-	-	73.71 \pm 0.23	-22.9	2450 \pm 25	Rose et al. (2020)
<i>Weighted mean x783: T' = 0.6, T' (5%) = 3.8, v = 1, 2463 \pm 19 BP</i>									

Lab code	Sample ID	Material	Typology of artefacts	CI	%C of extract	Corrected pMC	AMS $\delta^{13}C$ (‰VPDB) ¹	¹⁴ C Age (BP)	Reference
RICH-25068	Grave A393, pit, x568 no.1	<i>Triticum dicoccum</i> , charred cereal	-	-	61.10	69.69 ± 0.28	-29.9	2901 ± 32	Rose et al. (2020)
RICH-25070	Grave A393, pit, x568 no.2	<i>Hordeum vulgare nudum</i> , charred cereal	-	-	44.30	69.58 ± 0.28	-27.2	2914 ± 32	Rose et al. (2020)
RICH-25341	Grave A393, urn, x561 CB	Cremated bone (human)	Urn of unknown type, 2 pins with type 1 coiled heads.	6.4	0.16	73.90 ± 0.25	-25.3	2480 ± 27	Rose et al. (2020)
KIA-52411	Grave A393, urn, x561 no.1	<i>Hordeum vulgare nudum</i> , charred cereal	-	-	54.67	67.70 ± 0.21	-24.0	3134 ± 25	Rose et al. (2020)
KIA-52412	Grave A393, urn, x561 no.3	<i>Hordeum vulgare nudum</i> , charred cereal	-	-	32.35	67.57 ± 0.22	-21.9	3150 ± 27	Rose et al. (2020)
KIA-52413	Grave A393, urn, x561 <i>Quercus</i>	<i>Quercus</i> sp. trunk wood charcoal (Ø >10 cm)	-	-	24.78	72.25 ± 0.24	-25.7	2611 ± 27	Rose et al. (2020)
KIA-52414	Grave A394, urn, x556 no.1	<i>Alnus</i> sp. charcoal from branch sapwood (Ø 3-5 cm)	-	-	26.74	70.77 ± 0.23	-24.9	2778 ± 27	Rose et al. (2020)
KIA-53983	Grave A394, urn, x781 no.9	<i>Acer</i> sp. trunk wood charcoal (Ø > 10 cm)	-	-	66.85	68.58 ± 0.21	-27.0	3029 ± 24	Rose et al. (2020)
GrM-14708	Grave A394, urn, x785 CB	Cremated bone (human)	Urn of unknown type, 2 pins with type 2 coiled heads.	6.3	0.10	73.57 ± 0.11	-21.2	2465 ± 18	Rose et al. (2019)
KIA-53099	Grave A394, urn, x785 CB	Replicate of GrM-14708; apatite pretreated at ClO, CO2 extracted and dated at KIA.	-	-	0.14	73.97 ± 0.19	-22.7	2422 ± 20	Rose et al. (2019)
Weighted mean x785 CB: $T' = 2.6$, $T' [5\%] = 3.8$, $v = 1$, 2446 ± 14 BP									

Lab code	Sample ID	Material	Typology of artefacts	CI	%C of extract	Corrected pMC	AMS $\delta^{13}C$ (‰VPDB) ¹	¹⁴ C Age (BP)	Reference
KIA-52415	Grave A394, urn, x785 no.1	<i>Triticum aestivum</i> , charred cereal	-	-	37.76	70.19 ± 0.23	-23.0	2843 ± 26	Rose et al. (2020)
KIA-52416	Grave A394, urn, x785 no.4	<i>Alnus</i> sp. heartwood charcoal (Ø 2-3 cm)	-	-	28.07	70.82 ± 0.23	-27.9	2772 ± 26	Rose et al. (2020)
KIA-52417	Grave A394, urn, x786 no.1	<i>Quercus</i> sp. trunk wood charcoal (Ø >10 cm)	-	-	51.01	71.29 ± 0.24	-25.2	2719 ± 27	Rose et al. (2020)
Søhale urnfield cemetery (ESM 2139)									
AAR-25251	G3, x22	Cremated bone (adult)	Urn of unknown type, unknown iron object.	-	-	75.94 ± 0.26	-25	2211 ± 27	Møller et al. (2020)
AAR-25250	G5, x21	Cremated bone, 25-40yrs (adult), female?	Belt clasp?	-	-	75.5 ± 0.25	-27	2258 ± 27	Møller et al. (2020)
KIA-53937	G7, x37-III	Cremated bone (human)	Urn type 13C, pin with circular head.	5.1	0.38	75.86 ± 0.23	-21.9	2220 ± 20	
KIA-53936	G9, x19-II	Cremated bone (human)	2 pins with large circular heads.	6.2	0.23	75.43 ± 0.24	-25.8	2265 ± 26	
RICH-26501	G10, x23-II	Cremated bone (human)	Urn of unknown type, 2 pins with circular head.	-	0.10	74.97 ± 0.23	-22.8	2314 ± 24	
AAR-25249	G11, x18	Cremated bone, 6-15yrs (infans)	Pin of unknown type, belt clasp of unknown type.	-	-	76.19 ± 0.26	-28	2185 ± 27	Møller et al. (2020)
AAR-25248	G12, x17	Cremated bone (infans-adult)	None	-	-	75.46 ± 0.37	-26	2262 ± 40	Møller et al. (2020)
AAR-25243	G19, x10	Cremated bone, 2-10yrs. (infans)	Urn of unknown type	-	-	75.93 ± 0.29	-24	2212 ± 30	Møller et al. (2020)
AAR-25244	G31, x12/x25A	Cremated bone (adult)	None	-	-	76.22 ± 0.36	-29	2181 ± 38	Møller et al. (2020)
AAR-25245	Grave 31, x12/x25A	Replicate of AAR-25244	None	-	-	75.74 ± 0.32	-24	2232 ± 34	Møller et al. (2020)
Weighted mean G31, x12/x25A: $T' = 1.0$, $T' (5\%) = 3.8$, $v = 1$, 2209 ± 26 BP									

Lab code	Sample ID	Material	Typology of artefacts	CI	%C of extract	Corrected pMC	AMS $\delta^{13}C$ (‰VPDB) ¹	¹⁴ C Age (BP)	Reference
AAR-25246	G32, x14	Cremated bone (infans-adult)	Urn type 15C	-	-	74.74 ± 0.25	-23	2339 ± 26	Møller et al. (2020)
GrM-16770	G34, x40-II	Cremated bone (human)	Urn of unknown type, pin with circular head.	-	0.10	75.79 ± 0.18	-23.5	2227 ± 19	
RICH-26493	G35, x28-II	Cremated bone (human)	Urn of unknown type, tongue-shaped belt clasp.	-	0.26	75.62 ± 0.25	-26.3	2245 ± 27	
AAR-25253	G37, x27	Cremated bone (infans-adult)	None	-	-	75.7 ± 0.28	-24	2237 ± 30	Møller et al. (2020)
RICH-26494	G39, x31-II	Cremated bone (human)	Urn type 15? Pin with circular head, pin with bend neck.	-	0.10	74.76 ± 0.25	-24.6	2337 ± 27	
AAR-25254	G40, x30	Cremated bone (infans-adult)	Eyelet ring with shank, belt clasp of unknown type.	-	-	74.9 ± 0.26	-26	2322 ± 28	Møller et al. (2020)
RICH-26495	G44, x38-II	Cremated bone (human)	Urn type 15, narrow belt clasp.	5.9	0.06	75.54 ± 0.24	-28.8	2254 ± 26	
KIA-53938	G44, x38-II	Replicate of RICH-26495	-	-	0.22	76.12 ± 0.25	-21.5	2192 ± 27	
<i>Weighted mean: G44, x38-II: $T' = 2.7$, $T'(5\%) = 3.8$, $v = 1$, 2224 ± 19 BP</i>									
AAR-25257	G48, x35	Cremated bone, <20yrs (adult), male.	Urn type 12C	-	-	73.54 ± 0.24	-26	2469 ± 26	Møller et al. (2020)
AAR-25258	G51, x47	Cremated bone, <40yrs (matures), male?	Urn type 15, 2 pins with type 1 coiled heads.	-	-	73.98 ± 0.25	-19	2421 ± 27	Møller et al. (2020)
AAR-25256	G52, x33	Cremated bone, <35yrs (matures), male?	Urn of unknown type	-	-	74.61 ± 0.25	-24	2353 ± 27	Møller et al. (2020)
RICH-26502	G53, x34-II	Cremated bone (human)	Urn of unknown type, 2 pins with circular head.	-	0.37	74.71 ± 0.24	-25.8	2342 ± 26	
AAR-25255	G54, x32	Cremated bone, <30yrs (adult)	Urn of unknown type, 2 pins with circular head.	-	-	74.15 ± 0.27	-29	2403 ± 29	Møller et al. (2020)
GrM-16771	G57, x41-V	Cremated bone (human)	Urn 13C, narrow belt clasp, 1 pin with circular head, 1 pin of unknown type.	-	0.09	74.46 ± 0.19	-25.8	2370 ± 20	
GrM-16772	G59, x44-II	Cremated bone (human)	2 pins with coiled head, type 1 and 2.	5.8	0.09	73.60 ± 0.20	-26.5	2465 ± 20	

Lab code	Sample ID	Material	Typology of artefacts	CI	%C of extract	Corrected pMC	AMS $\delta^{13}C$ (‰VPDB) ¹	¹⁴ C Age (BP)	Reference
KIA-53939	G59, x44-II	Replicate of GrM-16772	-	-	0.34	73.55 \pm 0.23	-24.1	2468 \pm 25	
<i>Weighted mean G59, x44-II: T' = 0.0, T' (5%) = 3.8, v = 1, 2466 \pm 16 BP</i>									
GrM-16773	G60, x49-III	Cremated bone (human)	Urn of unknown type, pin with type 1 coiled head, bronze ring with eyelet.	-	0.15	73.92 \pm 0.16	-25.5	2425 \pm 19	
AAR-25260	G63, x51	Cremated bone, <35yrs (maturus), male?	Urn type 15C, pin with type 1 coiled head, pin of unknown type.	-	-	73.8 \pm 0.25	-25	2440 \pm 27	Møller et al. (2020)
KIA-53431	G64, x50-II	Cremated bone (human)	Urn type 15B, pin with type 2 coiled head, fragments of a pin of unknown type.	5.5	0.29	73.82 \pm 0.19	-21.9	2438 \pm 21	
AAR-25261	G69, x52	Cremated bone, 12-18yrs (juvenilis)	Urn type 15C, pin with type 1 coiled head, minimum 2 pins with neck bend.	-	-	74.01 \pm 0.28	-21	2418 \pm 31	Møller et al. (2020)
AAR-25262	G70, x55 II	Cremated bone, <35yrs (maturus), male?	Urn type 13	-	-	74.68 \pm 0.26	-26	2345 \pm 27	Møller et al. (2020)
KIA-53435	G73, x92-III	Cremated bone (human)	Urn of unknown type, pin with type 1 coiled head, pin with bend neck and head, imitation of pin x92-I?	6.0	0.39	73.93 \pm 0.19	-24.2	2427 \pm 21	
AAR-25263	G81, x65	Cremated bone <35yrs (maturus), female?	Urn of unknown type, 2 pins with slightly coiled heads, iron ring with shank.	-	-	74.97 \pm 0.26	-18	2314 \pm 28	Møller et al. (2020)
AAR-25265	G82, x93 II	Cremated bone, <25yrs (adult), male?	Urn type 15, 2 pins, hereof at least one with type 2 coiled head.	-	-	74.3 \pm 0.27	-24	2387 \pm 29	Møller et al. (2020)
AAR-25264	G87, x69	Cremated bone, >25yrs (adult)	Urn of unknown type, pin with circular head, pin with neck bend.	-	-	75.08 \pm 0.27	-26	2303 \pm 28	Møller et al. (2020)
AAR-25252	G93, x26	Cremated bone (infans-adult)	Pin with small circular head, belt clasp of unknown type.	-	-	75.32 \pm 0.36	-20	2277 \pm 38	Møller et al. (2020)
KIA-53434	G105, x76-II	Cremated bone (human)	Urn type 15C, pin with type 2 coiled head, pin with type 1 coiled head.	6.0	0.24	73.86 \pm 0.19	-29.0	2434 \pm 21	
KIA-53940	G105, x76-II	Replicate of KIA-53434	-	-	0.21	73.90 \pm 0.24	-27.4	2429 \pm 26	
<i>Weighted mean G105, x76-II: T' = 0.0, T' (5%) = 3.8, v = 1, 2432 \pm 17 BP</i>									

Lab code	Sample ID	Material	Typology of artefacts	CI	%C of extract	Corrected pMC	AMS $\delta^{13}C$ (‰VPDB) ¹	¹⁴ C Age (BP)	Reference
KIA-53433	G107, x74-II	Cremated bone (human)	Urn of unknown type, pin with type 2 coiled head, pin with type 1 coiled head.	5.9	0.33	74.42 \pm 0.19	-22.6	2373 \pm 21	
KIA-53432	G110, x72-VII	Cremated bone (human)	Urn of unknown type, flat iron ring, 2 pins with type 2 coiled heads.	6.4	0.44	74.34 \pm 0.19	-23.1	2382 \pm 21	
AAR-25259	G111, x48	Cremated bone (adult)	Urn of unknown type	-	-	73.62 \pm 0.27	-26	2460 \pm 30	Møller et al. (2020)

ABSTRACT

The dissertation investigates temporal processes of change in Early Iron Age material culture from Southern Jutland, Denmark (c.500-200 BC). The chronological framework of the period is mainly based on typo-chronological analyses of metalwork, and to a lesser degree of pottery, from large urnfield cemeteries. The chronological framework is unconstrained by scientific dating, which makes it difficult to correlate metalwork and pottery that appear disproportionate in funerary and settlement contexts. The dissertation continues a long tradition of chronological research using artefact assemblages from the urnfields, but it also presents the first large-scale ^{14}C dataset in support of an absolute chronological framework.

The majority of datable material from the urnfields is cremated bone and because ^{14}C dating cremated bone is a relatively new method, it is necessary to investigate methodological aspects relating to laboratory techniques. A laboratory intercomparison demonstrates that differences in pretreatment do not affect the radiocarbon results and that results are reproducible between laboratories (Rose et al. 2019). Another important aspect when dating cremated bone is that it will be affected by wood-age offsets through carbon substitution, effectively causing calendar date offsets between the real cremation events and the radiocarbon dates. The dissertation explores statistical modelling of offsets through additional case studies (Rose et al. 2018; Kristiansen et al. forthcoming), before proposing a new statistical model aimed at wood-age offsets in cremated bone (Rose 2020). The new statistical model is based on the empirical distribution of wood-age offset in an experimental dataset and on archaeological combinations of cremated bone and archaeobotanical remains. The statistical model is applied to all dates on cremated bone from 95 burials from three urnfields, Aarupgaard, Aarre and Sphale, in order to take account of their inherent wood-age offsets. The corrected dates provide indirect dates on the associated artefacts of metalwork and pottery and together with prior information on artefact typology and site formation processes (e.g. how the urnfields developed spatially over time) this is combined in a Bayesian framework aimed at modelling temporal processes of change in the material culture.

24 artefact types are modelled and out of these, nine metalwork and five pottery currencies have sufficient dates to be modelled independently. The models support an existing typological sequence of metalwork, but it also suggests that the ceramic sequence needs to be revised. The models suggest discrepancies in existing ceramic sequences (Jensen 2005), and in contrast to earlier works (Becker

1961; Jensen 2005), it is proposed that pins with circular head is treated as a single type regardless of head size. It is also proposed to divide the different types of belt equipment into an early group and a late group to minimize misclassification. The currency models provide a necessary correlation of metalwork and pottery, but they also offer independent evidence of the temporal processes of change in material culture by demonstrating periods with particularly rapid and slower change of the Early Iron Age material culture. The currency models have inhomogeneous temporal structures, with most metalwork being in use for shorter periods than pottery, but how quickly or slowly a type was introduced, and later abandoned, is very individual. Overall metalwork is found to be chronological sensitive, whereas pottery appears to be more conservative in relation to change.

The dissertation evaluates the chronological framework based on the new ¹⁴C evidence and the transitional from Bronze to Iron Age in Southern Jutland is estimated as a period starting in the early 7th century BC. The Bronze-Iron Age transformation is traditionally considered to occur c.500 BC and to coincide with the introduction of the urnfield phenomenon, but the urnfields are now estimated to start already in the early 6th century BC. The urnfields are abandoned in the last half of the 3rd century BC, which coincides with the traditional transformation from Early to Late Pre-Roman Iron Age c.250-200 BC.

KURZZUSAMMENFASSUNG

Die Dissertation untersucht zeitliche Veränderungsprozesse in der materiellen Kultur der frühen Eisenzeit in Südjütland, Dänemark (ca. 500-200 v. Chr.). Der chronologische Rahmen der Periode basiert auf typo-chronologischen Analysen von Artefakten von großen Urnenfeldern, hauptsächlich Metallobjekten und in geringerem Maße Keramik. Metallobjekte und Keramik treten im Bestattungs- und Siedlungskontext in unterschiedlichen Anteilen auf, aber es ist schwierig, sie zu korrelieren, da der chronologische Rahmen bislang nicht durch wissenschaftliche Datierungen eingegrenzt wird. Die Dissertation setzt eine lange Tradition der chronologischen Forschung unter Verwendung von Materialsammlungen aus den Urnenfeldern fort, präsentiert aber auch den ersten großen Datensatz von Radiokarbonaten zur Unterstützung eines absolut-chronologischen Rahmens.

Verbrannte menschliche Überreste stellen den Großteil des datierbaren Materials aus den Urnenfeldern dar. Da die Radiokarbondatierung von kalzinierten Knochen eine relativ neue Methode ist, müssen methodische Aspekte in Bezug auf Labortechniken untersucht werden. Eine Vergleichsstudie zeigt, dass Radiokarbonaten von kalzinierten Knochen zwischen Radiokarbonlabors reproduzierbar sind, unabhängig von den Unterschieden in den Probenvorbereitungsmethoden (Rose et al. 2019). Als weiterer wichtiger Aspekt bei der Datierung von kalzinierten Knochen ist zu bedenken, dass sich durch Kohlenstoffsubstitution Holzalder-Offsets ergeben, wodurch effektiv Zeitversätze zwischen den tatsächlichen Feuerbestattungsereignissen und den Radiokarbonaten verursacht werden. Die Dissertation untersucht die statistische Modellierung von Zeitversätzen anhand zusätzlicher Fallstudien (Rose et al. 2018; Kristiansen et al. forthcoming), bevor ein neues statistisches Modell vorgeschlagen wird, das auf Holzalder-Offsets in kalzinierten Knochen abzielt (Rose 2020). Das neue statistische Modell basiert auf der empirischen Verteilung des Holzalderversatzes in einem experimentell an kalzinierten Knochen erzeugten Datensatz und auf Kombinationen von archäologischen Funden von kalzinierten Knochen und archäobotanischen Überresten. Das statistische Modell wird auf alle Radiokarbonaten an kalzinierten Knochen aus 95 Bestattungen von drei Urnenfeldern, Aarupgaard, Aarre und Søhale, angewendet, um ihre inhärenten Holzalder-Offsets zu berücksichtigen. Die korrigierten Radiokarbonaten liefern indirekte Daten zu den zugehörigen Artefakten aus Metall und Keramik. Zusammen mit vorliegenden Informationen zur Artefakttypologie und den Prozessen der Fundplatzgenese werden die Daten in einem Bayes'schen Rahmen kombiniert, der auf die Modellierung zeitlicher Veränderungsprozesse in der materiellen Kultur abzielt.

Es werden 24 Artefakttypen modelliert, von denen zu neun Metall- und fünf Keramiktypen genügend Daten vorliegen, um deren Laufzeiten unabhängig voneinander modellieren zu können. Diese Laufzeitmodelle unterstützen die etablierte typologische Abfolge der Metallobjekte, legen jedoch auch nahe, dass die Keramiksequenz überarbeitet werden muss. Die modellierten Laufzeiten deuten auf Diskrepanzen in bestehenden Keramiksequenzen hin (Jensen 2005), und im Gegensatz zu früheren Arbeiten (Becker 1961; Jensen 2005) wird vorgeschlagen, Ringkopfnadeln unabhängig von der Kopfgröße als einen einzigen Typ zu behandeln. Es wird auch empfohlen, die verschiedenen Typen der Gürtelgarnituren in eine frühe und eine späte Gruppe zu unterteilen, um Fehlklassifizierungen zu minimieren. Die Laufzeitmodelle bieten eine notwendige Korrelation zwischen Metallobjekten und Keramik, liefern jedoch auch unabhängige Belege für die zeitlichen Veränderungsprozesse in der materiellen Kultur, indem sie Perioden mit besonders schnellen und langsameren Veränderungen der materiellen Kultur der frühen Eisenzeit demonstrieren. Sie zeigen inhomogene zeitliche Strukturen auf, wobei die meisten Metallobjekte kürzere Laufzeiten als die Keramikformen haben. Wie schnell oder langsam ein Typ eingeführt und später aufgegeben wurde, ist jedoch sehr individuell. Insgesamt erweisen sich Metallobjekte als chronologisch empfindliche Artefakte, während die Keramik in Bezug auf Veränderungen konservativer zu sein scheint.

Die Dissertation bewertet den chronologischen Rahmen auf der Grundlage der neuen Radiokarbondatierungen. Der Übergang von der Bronze- zur Eisenzeit in Südjütland wird auf einen Zeitraum geschätzt, der im frühen 7. Jahrhundert v. Chr. beginnt. Traditionell wird angenommen, dass der Übergang um 500 v. Chr. stattfindet und mit der Einführung des Urnenfeldphänomens zusammenfällt; allerdings ist jetzt davon auszugehen, dass die Urnenfelder bereits im frühen 6. Jahrhundert v. Chr. beginnen. Die Urnenfelder wurden in der letzten Hälfte des 3. Jahrhunderts v. Chr. aufgegeben, was mit der traditionellen Annahme des Übergangs von der älteren zur jüngeren vorrömischen Eisenzeit um 250-200 v. Chr. übereinstimmt.

BIBLIOGRAPHY

- Albrechtsen E. 1956. Albani Torv. *Fynske Minder* 1956:203-19.
- AlQahtani SJ, Hector MP, Liversidge HM. 2010. Brief communication: The London atlas of human tooth development and eruption. *American Journal of Physical Anthropology* 142(3):481-90.
- Annaert R, Boudin M, Deforce K, Eryvnc A, Haneca K, Lentacker A, Snoeck C. 2020. Anomalous radiocarbon dates from the early medieval cremation graves from Broechem (Flanders, Belgium): Reservoir or old wood effects? *Radiocarbon* 62(2):269-88.
- Arentoft E. 1985. Sankt Albani Kirke. *Albani Kirke & Torv. Fynske Studier* XIV:7-59.
- Arneborg J, Heinemeier J, Lynnerup N, Nielsen HL, Rud N, Sveinbjörnsdóttir ÁE. 1999. Change of Diet of the Greenland Vikings Determined from Stable Carbon Isotope Analysis and ¹⁴C Dating of Their Bones. *Radiocarbon* 41(2):157-68.
- Arnold JR, Libby WF. 1949. Age Determinations by Radiocarbon Content: Checks with Samples of Known Age. *Science* 110(2869):678-80.
- Asscher Y, Boaretto E. 2019. Absolute Time Ranges in the Plateau of the Late Bronze to Iron Age Transition and the Appearance of Bichrome Pottery in Canaan, Southern Levant. *Radiocarbon* 61(1):13-37.
- Barnett V, Lewis T. 1998. *Outliers in statistical data*. Chichester: Wiley.
- Bass WM. 1995. *Human osteology: a laboratory and field manual*. Columbia: Missouri Archaeological Society.
- Bayes TR. 1763. An essay towards solving a problem in the doctrine of chances. *Philosophical Transactions of the Royal Society* 53(370-418).
- Bayliss A. 1999. On the taphonomy of charcoal samples for radiocarbon dating. In: Evin J, editor. *Actes du 3ème Congrès International 14C et Archéologie : Lyon 6-10 avril 1998*. Paris: Soc. Préhist. Française. p 51-6.
- Bayliss A, Bronk Ramsey C. 2004. Pragmatic Bayesians: a Decade of Integrating Radiocarbon Dates into Chronological Models. In: E. BC, Millard A, editors. *Tools for Constructing Chronologies: Crossing Disciplinary Boundaries*. London: Springer. p 25-41.
- Bayliss A. 2007. Bayesian Buildings: An Introduction for the Numerically Challenged. *Vernacular Architecture* 38:76–87.
- Bayliss A, Bronk Ramsey C, van der Plicht J, Whittle A. 2007. Bradshaw and Bayes: Towards a Timetable for the Neolithic. *Cambridge Archaeological Journal* 17(S1):1-28.
- Bayliss A. 2009. Rolling Out Revolution: Using Radiocarbon Dating in Archaeology. *Radiocarbon* 51(1):123-47.
- Bayliss A, Hines J, Høilund Nielsen K, McCormac FG, Scull C. 2013a. Anglo-Saxon Graves and Grave Goods of the Sixth and Seventh Centuries AD: A Chronological Framework. J. Hines AB, editor. London: Society for Medieval Archaeology.
- Bayliss A, McGormac G, Thompson M, Hines J. 2013b. Dating Methods and their modelling. In: J. Hines AB, editor. *Anglo-Saxon Graves and Grave Goods of the Sixth and Seventh Centuries AD: A Chronological Framework*. London: Society for Medieval Archaeology. p 33-87.
- Bayliss A. 2015. Quality in Bayesian chronological models in archaeology. *World Archaeology* 47(4):677-700.

- Bayliss A, Beavan N, Hamilton D, Köhler K, Nyerges ÉÁ, Bronk Ramsey C, Dunbar E, Fecher M, Goslar T, Kromer B, Reimer P, Bánffy E, Marton T, Oross K, Osztás A, Zalai-Gaál I, Alasdair W. 2016. Peopling the past: creating a site biography in the Hungarian Neolithic. *Bericht der Römisch-Germanischen Kommission* 94(2013):23-92.
- Beaumont J, Montgomery J. 2015. Oral histories: a simple method of assigning chronological age to isotopic values from human dentine collagen. *Annals of Human Biology* 42(4):407-14.
- Becker CJ. 1961. *Førromersk jernalder i Syd- og Midtjylland*. Kbh.: Nationalmuseet.
- Bisgaard L. 2009. Danish Plague Patterns, 1360-1500. In: Bisgaard L, Søndergaard L, editors. *Living with the Black Death*. Odense: University Press of Southern Denmark. p 85-108.
- Blasco A. 2017. *Bayesian Data Analysis for Animal Scientists: The Basics*. Cham: Springer International Publishing.
- Boozer AL. 2015. The tyranny of typologies: evidential reasoning in Romano-Egyptian domestic archaeology. In: Chapman R, Wylie A, editors. *Material Evidence: Learning from archaeological practice*. London: Routledge. p 92– 109.
- Boudin M, Van Strydonck M, van den Brande T, Synal H-A, Wacker L. 2015. RICH – A new AMS facility at the Royal Institute for Cultural Heritage, Brussels, Belgium. *Nuclear Instruments and Methods in Physics Research Section B: Beam Interactions with Materials and Atoms* 361:120-3.
- Brainerd GW. 1951. The Place of Chronological Ordering in Archaeological Analysis. *American Antiquity* 16(4):301-13.
- Brindley AL. 2007. *The Dating of Food Vessels and Urns in Ireland*. Galway: Department of Archaeology, National University of Ireland.
- Bronk Ramsey C. 1995. Radiocarbon Calibration and Analysis of Stratigraphy : The OxCal Program. *Radiocarbon* 37(2):425-30.
- Bronk Ramsey C. 1998. Probability and Dating. *Radiocarbon* 40(1):461-74.
- Bronk Ramsey C. 2000. Comment on 'The use of Bayesian statistics for C-14 dates of chronologically ordered samples: A critical analysis'. *Radiocarbon* 42(2):199-202.
- Bronk Ramsey C. 2008a. Deposition models for chronological records. *Quaternary Science Reviews* 27(1):42-60.
- Bronk Ramsey C. 2008b. Radiocarbon Dating: Revolutions in Understanding. *Archaeometry* 50(2):249-75.
- Bronk Ramsey C. 2009a. Bayesian Analysis of Radiocarbon Dates. *Radiocarbon* 51(1):337-60.
- Bronk Ramsey C. 2009b. Dealing with Outliers and Offsets in Radiocarbon Dating. *Radiocarbon* 51(3):1023-45.
- Bronk Ramsey C, Lee S. 2013. Recent and Planned Developments of the Program OxCal. *Radiocarbon* 55(2):720-30.
- Bronk Ramsey C. 2017. Methods for summarizing radiocarbon datasets. *Radiocarbon* 59:1809-33.
- Buck C, Christen A, James GN, Cardiff U. 1999. BCal: an on-line Bayesian radiocarbon calibration tool. *Internet Archaeology*(7).
- Buck CE, Kenworthy JB, Litton CD, Smith AFM. 1991. Combining archaeological and radiocarbon information: a Bayesian approach to calibration. *Antiquity* 65(249):808-21.
- Buck CE, Litton CD. 1991. A computational Bayes approach to some common archaeological problems. In: Rahtz S, Lockyear K, editors. *Computer Applications and Quantitative Methods in Archaeology 1990*. Oxford: *Tempus Reparatum*. p 92-9.

- Buck CE, Litton CD, Smith AFM. 1992. Calibration of radiocarbon results pertaining to related archaeological events. *Journal of Archaeological Science* 19(5):497-512.
- Buck CE, Christen JA, Kenworthy JB, Litton CD. 1994a. Estimating the duration of archaeological activity using ¹⁴C determinations. *Oxford Journal of Archaeology* 13(2):229-40.
- Buck CE, Litton CD, Scott EM. 1994b. Making the most of radiocarbon dating: some statistical considerations. *Antiquity* 68(259):252-63.
- Buck CE, Cavanagh WG, Litton CD. 1996. Bayesian approach to interpreting archaeological data. Chichester: Wiley.
- Buck CE, Christen JA. 1998. A Novel Approach to Selecting Samples for Radiocarbon Dating. *Journal of Archaeological Science* 25(4):303-10.
- Buck CE, Meson B. 2015. On being a good Bayesian. *World Archaeology* 47(4):567-84.
- Buck CE, Juarez M. 2017. Bayesian radiocarbon modelling for beginners. Sheffield University.
- Chatters JC, Brown JW, Hackenberger S, McCutcheon P, Adler J. 2017. Calcined bone as a reliable medium for radiocarbon dating: a test using paired North American samples. *American Antiquity* 82(3):593-608.
- Childe VG. 1950. Prehistoric migrations in Europe. Oslo.
- Christen JA. 1994. Summarizing a Set of Radiocarbon Determinations: A Robust Approach. *Journal of the Royal Statistical Society. Series C (Applied Statistics)* 43(3):489-503.
- Christen JA, Buck CE. 1998. Sample Selection in Radiocarbon Dating. *Journal of the Royal Statistical Society. Series C (Applied Statistics)* 47(4):543-57.
- Christensen J, Bjerregaard M. 2017. Albani Kirke og kirkegård. In: Runge M, Hansen J, editors. *Knuds Odense - Vikingernes By*. Odense. p 116-27.
- Christensen JT. 1999. Døden skiller – om kirkegårdsskel og -skik under Skt. Knuds Plads. *Fynske Minder* 1999:83-92.
- Claessens H, Oosterbaan A, Savill P, Rondeux J. 2010. A review of the characteristics of black alder (*Alnus glutinosa* (L.) Gaertn.) and their implications for silvicultural practices. *Forestry: An International Journal of Forest Research* 83(2):163-75.
- Contreras DA, Meadows J. 2014. Summed radiocarbon calibrations as a population proxy: a critical evaluation using a realistic simulation approach. *Journal of Archaeological Science* 52:591-608.
- Cook GT, Ascough PL, Bonsall C, Hamilton WD, Russell N, Sayle KL, Scott EM, Bownes JM. 2015. Best practice methodology for ¹⁴C calibration of marine and mixed terrestrial/marine samples. *Quaternary Geochronology* 27:164-71.
- Cooper LP, Jarvis W, Bayliss A, Beamish MG, Bronk Ramsey C, Browning J, Brettell R, Cook G, Evans A, Heron C, Macphail R. 2017. Making and Breaking Microliths: A Middle Mesolithic Site at Asfordby, Leicestershire. *Proceedings of the Prehistoric Society* 83:43-96.
- Curtis N, Wilkin N. 2012. The Regionality of Beakers and Bodies in the Chalcolithic of North-east Scotland. In: Allen MJ, Gardiner J, Sheridan A, editors. *Is there a British Chalcolithic? People, place and polity in the later 3rd millennium*. 4 ed. London: The Prehistoric Society and Oxbow Books. p 237-56.
- Daly A. 2011. Dendrochronological analysis of timbers from a well at Odense Adelige Jomfrukloster, Fyn. OBM137 unpublished report: Dendro.dk.

- Daly A. 2014. Dendrochronological analysis of timbers from a well at Skovgård, Sdr. Nærrå, Fyn. OBM 1613. unpublished report: Dendro.dk.
- David N, Hennig H. 1972. The Ethnography of Pottery; a Fulani Case Seen in Archaeological Perspective. Addison-Wesley modular publications module 21.
- De Mulder G, Van Strydonck M. Radiocarbon dates of two urnfields at Velzeke (Zottegem, East-Flanders, Belgium). In: Higham T, Bronk Ramsey C, Owen C, editors. Oxford University School of Archaeology Monograph; 2004 9-14 April 2002; Oxford. p 247-62.
- De Mulder G, Van Strydonck M, Boudin M, Leclercq W, Paridaens N, Warmenbol E. 2007. Re-Evaluation of the Late Bronze Age and Early Iron Age Chronology of the Western Belgian Urnfields Based on ¹⁴C Dating of Cremated Bones. Radiocarbon 49(2):499-514.
- De Mulder G, Van Strydonck M, Boudin M. 2009. The Impact of Cremated Bone Dating on the Archaeological Chronology of the Low Countries. Radiocarbon 51(2):579-600.
- De Mulder G, Van Strydonck M, De Clercq W. 2013. ¹⁴C Dating of "Brandgrubengraber" from the Bronze Age to the Roman Period in Western Flanders (Belgium). Radiocarbon 55(3):1233-45.
- De Mulder G, Creemers G, Van Strydonck M. 2014. Challenging the Traditional Chronological Framework of Funerary Rituals in the Meuse-Demer-Scheldt Region: ¹⁴C Results from the Site of Lummen-Meldert (Belgium). Radiocarbon 56(2):461-8.
- De Mulder G, Van Strydonck M, Boudin M, Bourgeois I. 2017. Unraveling the occupation history of the cremation cemetery at Wijnegem/Blikstraat (Belgium). Radiocarbon 59(6):1645-56.
- De Reu J, De Mulder G, Van Strydonck M, Boudin M, Bourgeois J. 2012. ¹⁴C Dates and Spatial Statistics: Modeling Intrasite Spatial Dynamics of Urnfield Cemeteries in Belgium Using Case Study of Destelbergen Cemetery. Radiocarbon 54(3-4):635-48.
- de Vries H. 1958. Variation in Concentration of Radiocarbon with Time and Location on Earth: Akademie Van Wet.
- Dean JS. 1978. Independent Dating in Archaeological Analysis. Advances in Archaeological Method and Theory 1:223-55.
- Dee MW, Bronk Ramsey C. 2014. High-precision Bayesian modeling of samples susceptible to inbuilt age. Radiocarbon 56(1):83-94.
- Dee MW, Palstra SWL, Aerts-Bijma AT, Bleeker MO, de Bruijn S, Ghebru F, Jansen HG, Kuitens M, Paul D, Richie RR, Spriensma JJ, Scifo A, van Zonneveld D, Verstappen-Dumoulin BMAA, Wietzes-Land P, Meijer HAJ. 2020. Radiocarbon dating at Groningen: New and updated chemical pretreatment procedures. Radiocarbon 62(1):63-74.
- Deetz J, Dethlefsen E. 1965. The Doppler Effect and Archaeology: A Consideration of the Spatial Aspects of Seriation. Southwestern Journal of Anthropology 21(3):196-206.
- Denaire A, Lefranc P, Wahl J, Bronk Ramsey C, Dunbar E, Goslar T, Bayliss A, Beavan N, Bickle P, Whittle A. 2017. The Cultural Project: Formal Chronological Modelling of the Early and Middle Neolithic Sequence in Lower Alsace. Journal of Archaeological Method and Theory 24(4):1072-149.
- Desor É. 1865. Les palafittes ou constructions lacustres du Lac de Neuchâtel. Paris.
- Dollar SRD, Grundvad L. 2015. Tiesbøl. En tuegravplads ved Brørup fra ældre førromersk jernalder. In: Foss P, Møller NA, editors. De dødes landskab. Grav og gravskik i ældre jernalder i

- Danmark. Ribe: SAXO-instituttet, Københavns Universitet. p 15-20.
- Effenberger H. 2017a. Report about the results of the charcoal analysis and selection of datable material for the sites HOM and VAM1600. unpublished report: Effenberger Archäobotanik.
- Eliassen K, Johannsen BB, Johannsen H, Vedsø M. 2001. †S. Albani Kirke. Danmarks Kirker IX(3):1729-48.
- Eriksen BV. 2017. Fascinating flint artefacts from Rokær. Jahresbericht Zentrum für Baltische und Skandinavische Archäologie 2017:49.
- Ervynck A, Boudin M, van den Brande T, Van Strydonck M. 2014. Dating Human Remains from the Historical Period in Belgium: Diet Changes and the Impact of Marine and Freshwater Reservoir Effects. Radiocarbon 56(2):779-88.
- Ethelberg P, Hardt N, Poulsen B, Sørensen AB. 2003. Det Sønderjyske landbrugs historie : jernalder, vikingetid og middelalder. Haderslev: Museum Sønderjylland - Arkæologi Haderslev.
- Ethelberg P. 2003. Gården og landsbyen i jernalder og vikingetid (500 f.Kr. - 1000 e.Kr.). In: Madsen LS, Madsen O, editors. Det Sønderjyske landbrugs historie : jernalder, vikingetid og middelalder. Haderslev: Haderslev Museum and Historisk Samfund for Sønderjylland. p 123-373.
- Etting V. 2004. Queen Margrete I (1353-1412) and the founding of the Nordic Union. Leiden: Brill.
- Fernandes R, Nadeau M-J, Grootes PM. 2012. Macronutrient-based model for dietary carbon routing in bone collagen and bioapatite. Archaeological and Anthropological Sciences 4(4):291-301.
- Fernandes R, Millard AR, Brabec M, Nadeau M-J, Grootes P. 2014a. Food Reconstruction Using Isotopic Transferred Signals (FRUITS): A Bayesian Model for Diet Reconstruction. PLOS ONE 9(2):e87436.
- Fernandes R, Meadows J, Dreves A, Nadeau M-J, Grootes P. 2014b. A preliminary study on the influence of cooking on the C and N isotopic composition of multiple organic fractions of fish (mackerel and haddock). Journal of Archaeological Science 50:153-9.
- Fernandes R, Jaouen K. 2017. Isotopes in archaeology. Archaeological and Anthropological Sciences.
- Finkelstein I, Piasezky E. 2010. Radiocarbon dating the Iron Age in the Levant: a Bayesian model for six ceramic phases and six transitions. Antiquity 84(324):374-85.
- Fischer A, Olsen J, Richards M, Heinemeier J, Sveinbjörnsdóttir ÁE, Bennike P. 2007. Coast-inland mobility and diet in the Danish Mesolithic and Neolithic: evidence from stable isotope values of humans and dogs. Journal of Archaeological Science 34(12):2125-50.
- Fitzpatrick AP, Hamilton WD, Haselgrove CC. 2017. Radiocarbon dating and Bayesian modelling of the Late Iron Age cremation burial cemetery at Westhampnett, West Sussex, GB. Archaeologisches Korrespondenzblatt 47:359-81.
- Fokkens H. 1997. The genesis of urnfields: economic crisis or ideological change? Antiquity 71(272):360-73.
- Fowler C. 2017. Relational Typologies, Assemblage Theory and Early Bronze Age Burials. Cambridge Archaeological Journal 27(01):95-109.
- Frandsen L. 2008. Årets udgravninger. Årre. Opdatering 2008:60-1.
- Frandsen L, Jørgensen PK. 2012. Årets udgravninger. Årre. Opdatering 2012:123.

- Frandsen L, Jørgensen PK. 2013. Årets udgravninger. Billumvad. Opdatering 2013:152-53.
- Garrow D, Gosden C, Hill JD, Bronk Ramsey C. 2009. Dating Celtic Art: a Major Radiocarbon Dating Programme of Iron Age and Early Roman Metalwork in Britain. *Archaeological Journal* 166(1):79-123.
- Garrow D, Meadows J, Evans C, Tabor J. 2014. Dating the Dead: a High-Resolution Radiocarbon Chronology of Burial Within an Early Bronze Age Barrow Cemetery at Over, Cambridgeshire. *Proceedings of the Prehistoric Society* 80:207-36.
- Gelman A. 2004. Bayesian data analysis. Boca Raton: Chapman & Hall.
- Gjerlevsen S. 2015. Udgravningsberetning for ARV 113 Årre, Tingvejen. unpublished report: ARKVEST - Arkæologi Vestjylland. 1-26 p.
- Godwin H. 1962. Half-life of Radiocarbon. *Nature* 195(4845):984.
- Gräslund B. 1974. Relativ datering. Om kronologisk metod i nordisk arkeologi.
- Griffiths S. 2014. Simulations and Outputs. *Radiocarbon* 56(2):871-6.
- Grootes PM, Nadeau M-J, Rieck A. 2004. 14C-AMS at the Leibniz-Labor: radiometric dating and isotope research. *Nuclear Instruments and Methods in Physics Research Section B: Beam Interactions with Materials and Atoms* 223–224:55-61.
- Hamilton WD, Haselgrove C, Gosden C. 2015. The impact of Bayesian chronologies on the British Iron Age. *World Archaeology* 47(4):642-60.
- Hamilton WD, Kenney J. 2015. Multiple Bayesian modelling approaches to a suite of radiocarbon dates from ovens excavated at Ysgol yr Hendre, Caernarfon, North Wales. *Quaternary Geochronology* 25:72-82.
- Hamilton WD, Krus AM. 2018. The myths and realities of Bayesian chronological modeling revealed. *American Antiquity* 83(02).
- Hammer S, Levin I. 2017. Monthly mean atmospheric D¹⁴CO₂ at Jungfrauoch and Schauinsland from 1986 to 2016. *heiDATA Dataverse*.
- Hanna JA, Graham E, Pendergast DM, Hoggarth JA, Lentz DL, Kennett DJ. 2016. A New Radiocarbon Sequence from Lamanai, Belize: Two Bayesian Models from One of Mesoamerica's Most Enduring Sites. *Radiocarbon* 58(4):771-94.
- Harris EC. 1989. Principles of Archaeological Stratigraphy. London: Academic Press.
- Harvig L, Frei KM, Price TD, Lynnerup N. 2014a. Strontium isotope signals in cremated petrous portions as indicator for childhood origin. *PloS one* 9(7):e101603.
- Harvig L, Runge MT, Lundø MB. 2014b. Typology and function of Late Bronze Age and Early Iron Age cremation graves - a micro-regional case study. *Danish Journal of Archaeology* 3(1):3-18.
- Harvig L. 2019. Osteologisk undersøgelse af brændt skeletmateriale fra tuegravfeltet Aarupgaard, 500-100 f.Kr. Unpublished report: Museum of South Jutland.
- Hedeager L. 1990. Danmarks jernalder: mellem stamme og stat [Doctoral dissertation]. Aarhus: Aarhus Universitetsforlag: Aarhus University
- Hedges REM, Clement JG, Thomas CDL, O'Connell TC. 2007. Collagen turnover in the adult femoral mid-shaft: Modeled from anthropogenic radiocarbon tracer measurements. *American Journal of Physical Anthropology* 133(2):808-16.
- Henriksen MB. 2016. Brændt, men ikke altid begravet? Vikingetidens ligbrændingssteder og brandgrave. In: Ulriksen J, Lyngstrøm H, editors. Død

- og begravet – i vikingetiden. Copenhagen University: Forhistorisk arkæologi, SAXO-instituttet ved Københavns Universitet. p 2-12.
- Higham CFW, Douka K, Higham TFG. 2015. A New Chronology for the Bronze Age of Northeastern Thailand and Its Implications for Southeast Asian Prehistory. *PLOS ONE* 10(9):e0137542.
- Higham T, Jacobi R, Basell L, Ramsey CB, Chiotti L, Nespoulet R. 2011. Precision dating of the Palaeolithic: A new radiocarbon chronology for the Abri Pataud (France), a key Aurignacian sequence. *Journal of Human Evolution* 61(5):549-63.
- Hillson S. 1996. *Dental Anthropology*. Cambridge: Cambridge University Press.
- Hingst H. 1959. *Vorgeschichte des Kreises Stormarn*. Neumünster: Wachholtz.
- Hingst H. 1980. *Neumünster-Oberjörn. Ein Urnenfriedhof der vorrömischen Eisenzeit am Oberjörn und die vor- and frühgeschichtliche Besiedlung auf dem Neumünsteraner Sander*. Neumünster: Wachholtz.
- Hingst H. 1986. *Urnenfriedhöfe der vorrömischen Eisenzeit aus dem östlichen Holstein und Schwansen*. Neumünster: Wachholtz.
- Hinz M, Müller J. 2015. The Absolute Speed of Change: Multidimensional Scaling and Innovation Rates. *Archaeometry* 57(3):560-81.
- Höflmayer F, Kamlah J, Sader H, Dee MW, Kutschera W, Wild EM, Riehl S. 2016a. New Evidence for Middle Bronze Age Chronology and Synchronisms in the Levant: Radiocarbon Dates from Tell el-Burak, Tell el-Dab'a, and Tel Ifshar Compared. *Bulletin of the American Schools of Oriental Research* 375(375):53-76.
- Höflmayer F, Yasur-Landau A, Cline EH, Dee MW, Lorentzen B, Riehl S. 2016b. New radiocarbon dates from Tel Kabri support a high Middle Bronze Age chronology. *Radiocarbon* 58(3):599-613.
- Holden JL, Phakey PP, Clement JG. 1995. Scanning electron microscope observations of heat-treated human bone. *Forensic Science International* 74(1):29-45.
- Hornstrup KM, Olsen J, Heinemeier J, Thrane H, Bennike P. 2012. A new absolute Danish Bronze Age chronology as based on radiocarbon dating of cremated bone samples from burials. *Acta Archaeologica* 83(1):9-53.
- Housley R, Gamble C, Street M, Pettitt P. 1997. Radiocarbon evidence for the Lateglacial human recolonisation of Northern Europe. *Proceedings of the Prehistory Society* 63:25-54.
- Hua Q, Barbetti M, Rakowski AZ. 2013. Atmospheric Radiocarbon for the Period 1950–2010. *Radiocarbon* 55(04):2059-72.
- Hüls CM, Erlenkeuser H, Nadeau MJ, Grootes PM, Andersen N. 2010. Experimental Study on the Origin of Cremated Bone Apatite Carbon. *Radiocarbon* 52(2):587-99.
- Hüls CM, Meadows J, Rau A. 2019. Interpreting ¹⁴C Measurements on 3rd–4th Century AD Iron Artifacts from Nydam, Denmark. *Radiocarbon* 61(5):1517-29.
- Ion A. 2017. How interdisciplinary is interdisciplinarity? Revisiting the Impact of aDNA Research for the Archaeology of Human Remains. *Current Swedish Archaeology* 25:177–98.
- Jakucs J, Bánffy E, Oross K, Voicsek V, Bronk Ramsey C, Dunbar E, Kromer B, Bayliss A, Hofmann D, Marshall P, Whittle A. 2016. Between the Vinča and Linearbandkeramik Worlds: The Diversity of Practices and Identities in the 54th–53rd Centuries cal BC in

- Southwest Hungary and Beyond. *Journal of World Prehistory* 29(3):267-336.
- Jensen CK. 1992. Om behovet for en nyvurdering af den førromerske kronologi. *Lag* 3:53-73.
- Jensen CK. 1996. Chronologische Probleme der Vorrömische Eisenzeit Dänemarks. *Praehistorische Zeitschrift* 1996(2):194-216.
- Jensen CK, Højlund Nielsen K. 1997. Burial & society : the chronological and social analysis of archaeological burial data. Aarhus: Aarhus University Press.
- Jensen CK. 2005. Kontekstuel kronologi : en revision af det kronologiske grundlag for førromersk jernalder i Sydsandinavien. Højbjerg: Kulturlaget.
- Jensen J. 1997. Fra Bronze - til Jernalder. En kronologisk undersøgelse. København: Det Kongelige Nordiske Oldskriftselskab.
- Jensen J. 2006. Danmarks oldtid. Kbh.: Gyldendal.
- Jones M, Nicholls G. 2002. New Radiocarbon Calibration Software. *Radiocarbon* 44(3):663-74.
- Jørgensen E. 1971a. Liden Tue. *Skalk* 1971(2):3-7.
- Jørgensen E. 1971b. Tuegravpladsen ved Årupgård. *Haderslev Amts Museum* 13(2):73-7.
- Jørgensen E. 1972. Tuegravpladsen ved Årupgård II. *Haderslev Amts Museum* 13(3):105-9.
- Jørgensen E. 1975. Tuernes Mysterier. *Skalk* 1975(1):3-10.
- Karlsberg AJ. 2006. Flexible Bayesian methods for archaeological dating [Doctoral thesis]. Sheffield: University of Sheffield.
- Keller F. 1858. Pfahlbauten : zweiter Bericht. 12(3).
- Kieffer-Olsen J. 1993. Grav og gravskik i det middelalderlige Danmark : 8 kirkegårdsudgravninger [Doctoral dissertation]. Højbjerg: Aarhus University.
- Kneisel J. 2013. New chronological research of the late Bronze Age in Scandinavia. *Danish Journal of Archaeology* 2(2):95-111.
- Knorr F. 1910. Friedhöfe der älteren Eisenzeit in Schleswig-Holstein, Teil I. Kiel: Schleswig-Holsteinisches Museum vaterländischer Altertümer.
- Kolstrup E. 2009. Vegetational and environmental history during the Holocene in the Esbjerg area, west Jutland, Denmark. *Vegetation History and Archaeobotany* 18(5):351-69.
- Kootker LM, Geerdink C, van der Broeke PW, Kars H, Davies GR. 2018. Breaking Traditions: An Isotopic Study on the Changing Funerary Practices in the Dutch Iron Age (800–12 bc). *Archaeometry* 60:594– 611.
- Kristiansen AM. 2000. Langhøjen ved Rokær-variation over et tema. In: Hvass S, editor. *Vor skjulte kulturarv. Arkæologien under overfladen.*: Det kongelige nordiske oldskriftselskab Jysk arkæologisk selskab. p 44-5.
- Kristiansen AM. 2016. Rokær – an early Neolithic long barrow from Eastern Jutland, Denmark. *Jahresbericht Zentrum für Baltische und Skandinavische Archäologie* 2016:66-7.
- Kristiansen AM, Eriksen BV, Rose HA. forthcoming. Rokaer – an early Neolithic long barrow from East Jutland.
- Krus AM, Cook R, Hamilton D. 2015. Bayesian Chronological Modeling of SunWatch, a Fort Ancient Village in Dayton, Ohio. *Radiocarbon* 57(5):965-77.
- Lanos P, Philippe A. 2015. Event model: a robust Bayesian tool for chronological modeling. HAL id <hal-01241720>.

- Lanos P, Philippe A. 2017. Hierarchical Bayesian modeling for combining Dates in archaeological context. *Journal de la Société Française de Statistique* 158(2):72-88.
- Lanos P, Philippe A. 2018. Event date model: a robust Bayesian tool for chronology building. *Communications for Statistical Applications and Methods* 25(2):131-57.
- Lanos P, Dufresne P. 2019. ChronoModel version 2.0: Software for Chronological Modelling of Archaeological Data using Bayesian Statistics.
- Lanting JN, Aerts-Bijma AT, van der Plicht J. 2001. Dating of Cremated Bones. *Radiocarbon* 43(2A):249-54.
- Lee-Thorp JA. 2008. On isotopes and old bones. *Archaeometry* 50(6):925-50.
- Lee S, Bronk Ramsey C. 2012. Development and Application of the Trapezoidal Model for Archaeological Chronologies. *Radiocarbon* 54(1):107-22.
- Lee S, Bronk Ramsey C, Mazar A. 2013. Iron Age Chronology in Israel: Results from Modeling with a Trapezoidal Bayesian Framework. *Radiocarbon* 55(2):731-40.
- Lekson SH. 2015. The Chaco meridian : one thousand years of political and religious power in the ancient Southwest. Van Dyke RM, Tuwaletsiwa P, Fowles S, editors. Lanham, Maryland: Rowman & Littlefield.
- Levin I, Kromer B, Hammer S. 2013. Atmospheric $\Delta^{14}\text{CO}_2$ trend in Western European background air from 2000 to 2012. *Tellus B: Chemical and Physical Meteorology* 65(1):20092.
- Libby WF. 1952. Radiocarbon dating. Chicago: University of Chicago Press.
- Litton CD, Leese MN. 1991. Some statistical problems arising in radiocarbon calibration. In: Rahtz S, Lockyear K, editors. *Computer Applications and Quantitative Methods in Archaeology* 1990. Oxford: Tempus Reparatum. p 101-9.
- Lorange T. 2009. Gensyn med tuegravpladsen ved Årre. *Opdatering* 2009:97-105.
- Lorange T. 2010. Full-body CT-scan af nogle gamle vestejyder : udgravning af urner fra tuegravpladsen ved Årre. *Opdatering* 2010:139-45.
- Lorange T. 2015a. Årets udgravninger. Årre, tuegravpladsen. *Opdatering* 2015:217.
- Lorange T. 2015b. Det sakrale landskab ved Årre. Landskabets hukommelse gennem 4.000 års gravriter. In: Foss P, Møller NA, editors. *De dødes landskab. Grav og gravskik i ældre jernalder i Danmark*. Ribe: SAXO-instituttet, Københavns Universitet. p 21-36.
- Lulewicz J. 2018. Radiocarbon Data, Bayesian Modeling, and Alternative Historical Frameworks: A Case Study From the US Southeast. *Advances in Archaeological Practice* 6(1):58-71.
- Lyman RL, Harpole JL. 2002. A. L. Kroeber and the Measurement of Time's Arrow and Time's Cycle. *Journal of Anthropological Research* 58(3):313-38.
- Madsen A, Neergaard C. 1894. Jydske gravpladser fra den førromerske jernalder. *Aarbøger for Nordisk Oldkyndighed og Historie* 1894:165-212.
- Makarowicz P, Goslar T, Niebieszcański J, Cwaliński M, Kochkin IT, Romaniszyn J, Lysenko SD, Ważny T. 2018. Middle Bronze Age societies and barrow line chronology. A case study from the Bukivna 'necropolis', Upper Dniester Basin, Ukraine. *Journal of Archaeological Science* 95:40-51.
- Malmer MP. 1984. Arkeologisk positivism. *Fornvännen* 79:260-8.

- Manning SW, Smith AT, Khatchadourian L, Badalyan R, Lindsay I, Greene A, Marshall M. 2018a. A new chronological model for the Bronze and Iron Age South Caucasus: radiocarbon results from Project ArAGATS, Armenia. *Antiquity* 92(366):1530-51.
- Manning SW, Birch J, Conger MA, Dee MW, Griggs C, Hadden CS, Hogg AG, Bronk Ramsey C, Sanft S, Steier P, Wild EM. 2018b. Radiocarbon re-dating of contact-era Iroquoian history in northeastern North America. *Science Advances* 4(12):eaav0280.
- Martens J. 1996. Die vorrömische Eisenzeit in Südkandinavien. Probleme und Perspektiven. *Praehistorische Zeitschrift* 71(217-243).
- Martens J. 2014. Jastorf and Jutland. In: Brandt J, Rauchfuss B, editors. Internationalen Tagung zum einhundertjährigen Jubiläum der Veröffentlichung der "Ältesten Urnenfriedhöfe bei Uelzen und Lüneburg" durch Gustav Schwantes. Bad Bevensen: Archäologisches Museum Hamburg. p 245-66.
- Martens J. 2017. Settlement Pottery of the Kraghede Group. In: Meyer M, Łuczkiwicz P, Rauchfuss B, editors. Eisenzeitliche Siedlungskeramik der Przeworsk-Kultur. Berlin: Universität Berlin und der Humboldt-Universität zu Berlin. p 153-98.
- McKinley JI. 1994. Bone Fragment Size in British Cremation Burials and its Implications for Pyre Technology and Ritual. *Journal of Archaeological Science* 21(3):339-42.
- McLaughlin TR. 2019. On Applications of Space–Time Modelling with Open-Source 14C Age Calibration. *Journal of Archaeological Method and Theory* 26:479–501.
- Meadows J. 2012. From scientific dating to chronology. *Jahresbericht Zentrum für Baltische und Skandinavische Archäologie* 2011:110-1.
- Meadows J, Martinelli N, Pignatelli O, Cester R, Fozzati L, Kromer B. 2012. Keeping the Sea Out: Early Medieval Structures at ca'Foscari University, Venice, Italy. *Radiocarbon* 54(3-4):567-79.
- Meadows J, Bērziņš V, Legzdīņa D, Lübke H, Schmölcke U, Zagorska I, Zariņa G. 2018. Stone-age subsistence strategies at Lake Burtnieks, Latvia. *Journal of Archaeological Science: Reports* 17:992-1006.
- Meadows J, Lozovskaya O, Bondetti M, Drucker DG, Moiseyev V. 2019. Human palaeodiet at Zamostje 2, central Russia: Results of radiocarbon and stable isotope analyses. *Quaternary International*.
- Mestorf J. 1886. *Urnenfriedhöfe in Schleswig-Holstein*. Hamburg.
- Mikkelsen DK, Madsen IP. 1986. Beretning for VKH 979. Mørup. Nørup s. Sb 123. Vejle. 1-44 p.
- Millard A. 2015. *Palace Green Library excavations 2013 (PGL13): Chronology of the burials*. Durham: Department of Archaeology, Durham University.
- Minami M, Mukumoto H, Wakaki S, Nakamura T. 2019. Effect of crystallinity of apatite in cremated bone on carbon exchanges during burial and reliability of radiocarbon dating. *Radiocarbon* 61(6):1823-34.
- Miyake F, Nagaya K, Masuda K, Nakamura T. 2012. A signature of cosmic-ray increase in AD 774-775 from tree rings in Japan. *Nature* 486(7402):240-2.
- Miyake F, Masuda K, Nakamura T. 2013. Another rapid event in the carbon-14 content of tree rings. *Nature communications* 4(1):1748.
- Møller NA. 2013. Tuegravpladsen ved Jernvedlund. *Levende viden* Årg. 1 nr. 1 (2013):100-11.

- Møller NA. 2015. Døde i de levendes verden. Vestjyske gravfund i kontekst. In: Foss P, Møller NA, editors. De dødes landskab. Grav og gravskik i ældre jernalder i Danmark. Ribe: SAXO-insitutttet, Københavns Universitet. p 215-36.
- Møller NA, Harvig LL, Grundvad B. 2020. The Iron Age urnfield tradition of southwestern Jutland, Denmark. *Acta Archaeologica* 91(1):11-80.
- Mook W, Streurman H. Physical and chemical aspects of radiocarbon dating; 1983. Council of Europe. p 31-55.
- Naylor JC, Smith AFM. 1988. An Archaeological Inference Problem. *Journal of the American Statistical Association* 83(403):588-95.
- Naysmith P, Scott EM, Cook GT, Heinemeier J, Van der Plicht J, Van Strydonck M, Bronk Ramsey C, Grootes PM, Freeman SPHT. 2007. A Cremated Bone Intercomparison Study. *Radiocarbon* 49(2):403-8.
- Needham S, Bronk Ramsey C, Coombs D, Cartwright C, Pettitt P. 1997. An Independent Chronology for British Bronze Age Metalwork: The Results of the Oxford Radiocarbon Accelerator Programme. *Archaeological Journal* 154(1):55-107.
- Neergaard C. 1892. Jernalderen. Aarbøger for Nordisk Oldkyndighed og Historie(1892).
- Neergaard C. 1916. Sønderjyllands Jernalder Aarbøger for Nordisk Oldkyndighed og Historie 1916:227-302.
- Neergaard C. 1931. Nogle sønderjydske Fund fra den ældre jernalder. Fra Nationalmuseets Arbejdsmark 1931:63-80.
- Neumann H. 1947. Tuegravpladsen på Årupgårds mark, Gram sogn. Haderslev Amts Museum 1947:6-7.
- Nicholls G, Jones M. 2001. Radiocarbon Dating with Temporal Order Constraints. *Journal of the Royal Statistical Society. Series C (Applied Statistics)* 50(4):503-21.
- Nilsson B. 1987. Död och begravning. Begravningskicket i Norden. Tanke och tro. Aspekter på medeltidens tankevärld och fromhetsliv. *Studier til det medeltida Sverige* 3:133-50.
- Niu M, Heaton TJ, Blackwell PG, Buck CE. 2013. The Bayesian Approach to Radiocarbon Calibration Curve Estimation: The IntCal13, Marine13, and SHCal13 Methodologies. *Radiocarbon* 55(04):1905-22.
- Normark J. 2010. Involutions of Materiality : Operationalizing a Neo-materialist Perspective through the Causeways at Ichmul and Yo'okop. *Journal of Archaeological Method and Theory* 17(2):132-73.
- Nunn P, Petchey F. 2013. Bayesian re-evaluation of Lapita settlement in Fiji: radiocarbon analysis of the Lapita occupation at Bourewa and nearby sites on the Rove Peninsula, Viti Levu Island. *Journal of Pacific Archaeology* 4(2):21-34.
- O'Shea JM. 1984. Mortuary variability: an archaeological investigation. Orlando: Academic Press.
- Olesen LH, Schlosser Mauritsen E. 2015. Fortiden Set fra Himlen. Luftfotoarkæologi i Danmark. Holstebro: Holstebro Museum.
- Olsen J, Heinemeier J, Bennike P, Krause C, Margrethe Hornstrup K, Thrane H. 2008. Characterisation and blind testing of radiocarbon dating of cremated bone. *Journal of Archaeological Science* 35(3):791-800.
- Olsen J, Margrethe Hornstrup K, Heinemeier J, Bennike P, Thrane H. 2011. Chronology of the Danish Bronze Age Based on 14C

- Dating of Cremated Bone Remains. *Radiocarbon* 53(2):261-75.
- Olsen J, Heinemeier J, Hornstrup KM, Bennike P, Thrane H. 2013. 'Old wood' effect in radiocarbon dating of prehistoric cremated bones? *Journal of Archaeological Science* 40(1):30-4.
- Olsen TB. 2016. Antropologisk rapport OBM3183, Albani Torv. unpublished report: Retsmedicinsk Institut, Antropologisk Afdeling, ADBOU, Syddansk Universitet.
- Parzinger H. 1989. *Chronologie der Späthallstatt- und Frühlatène-Zeit : Studien zu Fundgruppen zwischen Mosel und Save*. Weinheim: VCH, Acta Humaniora.
- Paulsson BS. 2010. Scandinavian Models: Radiocarbon Dates and the Origin and Spreading of Passage Graves in Sweden and Denmark. *Radiocarbon* 52(3):1002-17.
- Pearson MP. 1999. *The archaeology of death and burial*. Stroud: Sutton.
- Pedersen K, Bjerregaard MM. 2016. Sygdom, død og begravelse på Albani Kirkegård. Observationer fra en igangværende arkæologisk udgravning. *Bibliotek for Læger* 208:158-77.
- Person A, Bocherens H, Saliège J-F, Paris F, Zeitoun V, Gérard M. 1995. Early Diagenetic Evolution of Bone Phosphate: An X-ray Diffractometry Analysis. *Journal of Archaeological Science* 22(2):211-21.
- Philippe A, Vibet M-A. 2018. A note on the Bayesian modeling of the stratigraphic chronology of Canimar Abajo, Cuba. *Radiocarbon*:1-11.
- Philippsen B. 2013. The freshwater reservoir effect in radiocarbon dating. *Heritage Science* 1(1):24.
- Plog S, Hantman JL. 1990. Chronology Construction and the Study of Prehistoric Culture Change. *Journal of Field Archaeology* 17(4):439-56.
- Ranåker M. 2009. Flerpersonsgravar uder medeltid. Västerhus kyrkogård belyst av andra begravningsplatser. In: Iregren E, Alexandersen V, Redin L, editors. *Västerhus. Kapell, kyrkogård och befolkning: Kungl. Vitterhets Historie och Antikvitets Akademien*. p 26-39.
- Rasmussen KL. 2000. Danske arkæologiske 14C-dateringer. *Arkæologiske udgravninger i Danmark 2000*:329-32.
- Reimer PJ, Brown TA, Reimer RW. 2004. Discussion: Reporting and Calibration of Post-Bomb 14C Data. *Radiocarbon* 46(3):1299-304.
- Reimer PJ, Bard E, Bayliss A, Beck JW, Blackwell PG, Bronk Ramsey C, Buck CE, Cheng H, Edwards RL, Friedrich M, Grootes PM, Guilderson TP, Hafflidason H, Hajdas I, Hatté C, Heaton TJ, Hoffmann DL, Hogg AG, Hughen KA, Kaiser KF, Kromer B, Manning SW, Niu M, Reimer RW, Richards DA, Scott EM, Southon JR, Staff RA, Turney CSM, van der Plicht J. 2013. IntCal13 and Marine13 Radiocarbon Age Calibration Curves 0–50,000 Years cal BP. *Radiocarbon* 55(04):1869-87.
- Reinecke P. 1924. Zur Chronologischen Gliederung der süddeutschen Bronzezeit. *Germania* 8:43-4.
- Renfrew C, Bahn P. 2001. *Archaeology: theories methods and practice*. London: Thames & Hudson.
- Rindel PO. 2015. Tuegravpladserne fra førromersk jernalder ved Grøntoft. In: Foss P, Møller NA, editors. *De dødes landskab. Grav og gravskik i ældre jernalder i Danmark*. Ribe: SAXO-insituttet, Københavns Universitet. p 37-50.
- Roberts BW, Uckelmann M, Brandherm D. 2013. Old Father Time: The Bronze Age Chronology of Western Europe. In: Fokkens H, Harding A, editors. *The Oxford handbook of the European Bronze Age*. Oxford: Oxford University Press. p 17-46.

- Rose HA, Meadows J, Bjerregaard M. 2018. High-Resolution Dating of a Medieval Multiple Grave. *Radiocarbon* 60(5):1547-59.
- Rose HA, Meadows J, Palstra SWL, Hamann C, Boudin M, Huels M. 2019. Radiocarbon Dating Cremated Bone: A Case Study Comparing Laboratory Methods. *Radiocarbon* 61(5):1581-91.
- Rose HA. 2020. Bayesian chronological modelling of the Early Iron Age in Southern Jutland, Denmark [Doctoral thesis]. Kiel: Kiel University.
- Rose HA, Meadows J, Henriksen MB. 2020. Bayesian modeling of wood-age offsets in cremated bone. *Radiocarbon* 62(2):379-401.
- Sacken Ev. 1868. *Das Grabfeld von Hallstadt in Oberösterreich und dessen Alterthümer*. Wien.
- Scheuer L, Black S. 2000. *Developmental juvenile osteology*. San Diego, Calif: Academic Press.
- Schmid MME, Dugmore AJ, Foresta L, Newton AJ, Vésteinsson O, Wood R. 2018. How ¹⁴C dates on wood charcoal increase precision when dating colonization: The examples of Iceland and Polynesia. *Quaternary Geochronology* 48:64-71.
- Schuur EAG, Trumbore SE, Druffel ERM, Southon JR, Steinhof A, Taylor RE, Turnbull JC. 2016. Radiocarbon and The Global Carbon Cycle. In: Schuur EAG, Druffel ERM, Trumbore SE, editors. *Radiocarbon and Climate Change. Mechanisms, Applications and Laboratory Techniques*: Springer. p 1-19.
- Schwantes G. 1911. *Die älteste Urnenfriedhöfe bei Uelzen und Lüneburg*. Schuchhardt C, editor. Hannover.
- Snoeck C, Brock F, Schulting RJ. 2014. Carbon Exchanges between Bone Apatite and Fuels during Cremation: Impact on Radiocarbon Dates. *Radiocarbon* 56(2):591-602.
- Snoeck C, Lee-Thorp J, Schulting R, Jong J, Debouge W, Mattielli N. 2015. Calcined bone provides a reliable substrate for strontium isotope ratios as shown by an enrichment experiment. *Rapid Communications in Mass Spectrometry* 29(1):107-14.
- Snoeck C, Schulting RJ, Lee-Thorp JA, Lebon M, Zazzo A. 2016a. Impact of heating conditions on the carbon and oxygen isotope composition of calcined bone. *Journal of Archaeological Science* 65:32-43.
- Snoeck C, Pouncett J, Ramsey G, Meighan IG, Mattielli N, Goderis S, Lee-Thorp JA, Schulting RJ. 2016b. Mobility during the Neolithic and Bronze Age in Northern Ireland explored using strontium isotope analysis of cremated human bone. *American Journal of Physical Anthropology* 160(3):397-413.
- Snoeck C, Pouncett J, Claeys P, Goderis S, Mattielli N, Parker Pearson M, Willis C, Zazzo A, Lee-Thorp JA, Schulting RJ. 2018. Strontium isotope analysis on cremated human remains from Stonehenge support links with west Wales. *Scientific Reports* 8(1):10790.
- Stig Sørensen ML. 2015. 'Paradigm lost' – on the State of Typology within Archaeological Theory. In: Kristiansen K, Šmejda L, Turek J, editors. *Paradigm found. Archaeological Theory. Present, Past And Future*. Oxford. p 84-94.
- Stiner MC, Kuhn SL, Weiner S, Bar-Yosef O. 1995. Differential Burning, Recrystallization, and Fragmentation of Archaeological Bone. *Journal of Archaeological Science* 22(2):223-37.
- Stockhammer PW, Massy K, Knipper C, Friedrich R, Kromer B, Lindauer S, Radosavljević J, Wittenborn F, Krause J. 2015. Rewriting the Central European Early Bronze Age Chronology: Evidence from Large-Scale Radiocarbon Dating. *PLOS ONE* 10(10):e0139705.

- Strien H-C. 2019. 'Robust chronologies' or 'Bayesian illusion'? Some critical remarks on the use of chronological modelling. *Documenta Praehistorica* 46(0):204-15.
- Stuiver M, Polach HA. 1977. Discussion Reporting of 14C Data. *Radiocarbon* 19(3):355-63.
- Stuiver M, Reimer PJ. 1986. A Computer Program for Radiocarbon Age Calibration. *Radiocarbon* 28(2B):1022-30.
- Stuiver M, Pearson GW, Braziunas T. 1986. Radiocarbon Age Calibration of Marine Samples Back to 9000 Cal Yr BP. *Radiocarbon* 28(2B):980-1021.
- Stuiver M, Reimer PJ. 1993. Extended 14C Database and revised CALIB 3.014C Age Calibration Program. *Radiocarbon* 35(1):215-30.
- Suess HE. 1967. Bristlecone pine calibration of the radiocarbon time scale from 4100 BC to 1500 BC. *Radio-active Dating and Methods of Low-Level Counting*:143-51.
- Taylor RE. 2016. Radiocarbon Dating: Development of a Nobel Method. In: Schuur EAG, Druffel ERM, Trumbore SE, editors. *Radiocarbon and Climate Change. Mechanisms, Applications and Laboratory Techniques*: Springer. p 21-44.
- Terkildsen KF. 2005. En vurdering af social stratifikation i førromersk jernalder med udgangspunkt i Årupgaard gravpladsen.
- Terkildsen KF. 2015. Gravpladsen Årupgård som kilde til social stratifikation i førromersk jernalder. In: Foss P, Møller NA, editors. *De døde landskab. Grav og gravskik i ældre jernalder i Danmark*. Ribe. p 51-70.
- Thomsen CJ. 1836. *Ledetraad til Nordisk Oldkyndighed*. Kbh.
- Torring T. 2015. Neolithic population and summed probability distribution of 14C-dates. *Journal of Archaeological Science* 63(Supplement C):193-8.
- Torring T. 2016. A new time: Bayesian models of an Early Neolithic enclosure in North-Western Denmark. *Danish Journal of Archaeology* 4(2):109-24.
- Trachsel M. 2004. *Untersuchungen zur relativen and absoluten Chronologie der Hallstattzeit*. Bonn: Habelt.
- Trumbore SE, Sierra CA, Hicks Pries CE. 2016. Radiocarbon Nomenclature, Theory, Models, and Interpretations: Measuring Age, Determining Cycling Rates, and Tracing Source Pools. In: Schuur EAG, Druffel ERM, Trumbore SE, editors. *Radiocarbon and Climate Change. Mechanisms, Applications and Laboratory Techniques*: Springer. p 45-82.
- Undset I. 1881. *Jernalderens begyndelse i Nord-Europa : en Studie i sammenlignende forhistorisk Arkæologi*. Kristiania: Alb. Cammermeyer.
- van der Sluis LG, Reimer PJ, Lynnerup N. 2016. Investigating Intra-Individual Dietary Changes and 14C Ages Using High-Resolution $\delta^{13}\text{C}$ and $\delta^{15}\text{N}$ Isotope Ratios and 14C Ages Obtained from Dentine Increments. *Radiocarbon* 57(4):665-77.
- van der Sluis LG, Reimer PJ, Ogle N. 2018. Adding Hydrogen to the Isotopic Inventory-Combining $\delta^{13}\text{C}$, $\delta^{15}\text{N}$ and $\delta^2\text{H}$ Stable Isotope Analysis for Palaeodietary Purposes on Archaeological Bone: Combining $\delta^{13}\text{C}$, $\delta^{15}\text{N}$ and $\delta^2\text{H}$ stable isotope analysis on bone. *Archaeometry* 61:720-49.
- Van Strydonck M, De Moor A, Bénazeth D. 2004. 14C Dating Compared to Art Historical Dating of Roman and Coptic Textiles from Egypt. *Radiocarbon* 46(1):231-44.
- Van Strydonck M, Boudin M, Hoefkens M, De Mulder G. 2005. 14C-dating of cremated bones, why does it work?

- Lunula. *Archaeologia protohistorica* XIII:3-10.
- Van Strydonck M, Boudin M, De Mulder G. 2009. 14C Dating of Cremated Bones: The Issue of Sample Contamination. *Radiocarbon* 51(2):553-68.
- Van Strydonck M, Boudin M, Mulder GD. 2010. The Carbon Origin of Structural Carbonate in Bone Apatite of Cremated Bones. *Radiocarbon* 52(2):578-86.
- Vandkilde H, Rahbek U, Rasmussen KL. 1996. Radiocarbon dating and the chronology of Bronze Age Southern Scandinavia. *Acta Archaeologica* 67:183-98.
- Vedel E. 1872. *Den ældre Jernalders Begravelser paa Bornholm*. Kjøbenhavn.
- Veil S, Breest K, Grootes P, Nadeau M-J, Hüls M. 2012. A 14 000-year-old amber elk and the origins of northern European art. *Antiquity* 86(333):660-73.
- Ward GK, Wilson SR. 1978. Procedures for Comparing and Combining Radiocarbon Age Determinations: a Critique. *Archaeometry* 20(1):19-31.
- Webley L. 2008. Iron Age households : structure and practice in Western Denmark, 500 BC-AD 200. Højbjerg: Jutland Archaeological Society.
- Webster L, Streit K, Dee M, Hajdas I, Höflmayer F. 2020. New radiocarbon-based assessment supports the prominence of Tel Lachish during Late Bronze Age IB-IIA. *Radiocarbon* 61(6):1711-27.
- Whittle A, Bayliss A, Barclay A, Gaydasrka B, Bánffy E, Borić D, Draşovean FD, Jakucs J, Marić M, Orton D, Pantović I, Schier W, Tasić N, Vander Linden M. 2016. A Vinča potscape: formal chronological models for the use and development of Vinča ceramics in south-east Europe. *Documenta Praehistorica* 43:1-60.
- Wilhelmson H, Ahlström T, Department of A, Ancient H, Institutionen för arkeologi och antikens h, Lund U, Historisk O, Lunds u, Historisk o. 2015. Iron Age migration on the island of Öland: Apportionment of strontium by means of Bayesian mixing analysis. *Journal of Archaeological Science* 64:30-45.
- Wilhelmson H, Price TD. 2017. Migration and integration on the Baltic island of Öland in the Iron Age. *Journal of Archaeological Science: Reports* 12:183-96.
- Willis C, Marshall P, McKinley J, Pitts M, Pollard J, Richards C, Richards J, Thomas J, Waldron T, Welham K, Pearson MP. 2016. The dead of Stonehenge. *Antiquity* 90(350):337-56.
- Wood R. 2015. From revolution to convention: the past, present and future of radiocarbon dating. *Journal of Archaeological Science* 56:61-72.
- Woolsey CA. 2020. A direct-dated ceramic AMS sequence from the Gaspereay Lake Reservoir site complex, Maine-Maritimes region, northeastern North America. *Radiocarbon* 62(2):419-37.
- Worsaae JJA. 1859. *Nordiske Oldsager i Det Kongelige Museum i Kjøbenhavn*. Copenhagen.
- Yoder C. 2010. Diet in medieval Denmark: a regional and temporal comparison. *Journal of Archaeological Science* 37(9):2224-36.
- Zavodny E, Culleton BJ, McClure SB, Kennett DJ, Balen J. 2019. Recalibrating grave-good chronologies: new AMS radiocarbon dates from Late Bronze Age burials in Lika, Croatia. *Antiquity* 93(367):113-27.
- Zazzo A, Saliège JF, Person A, Boucher H. 2009. Radiocarbon Dating of Calcined Bones: Where Does the Carbon Come from? *Radiocarbon* 51(2):601-11.
- Zazzo A, Saliège JF. 2011. Radiocarbon dating of biological apatites: A review.

Palaeogeography, Palaeoclimatology,
Palaeoecology 310(1):52-61.

Zazzo A, Saliège J-F, Lebon M, Lepetz S, Moreau
C. 2012. Radiocarbon Dating of
Calcined Bones: Insights from
Combustion Experiments Under

Natural Conditions. Radiocarbon 54(3-
4):855-66.

Zazzo A, Lebon M, Chiotti L, Comby C, Delqué-
Količ E, Nespoulet R, Reiche I. 2013.
Can we Use Calcined Bones for ^{14}C
Dating the Paleolithic? Radiocarbon
55(3):1409-21.

APPENDICES

Appendix 1 Additional case studies

It is a research objective to propose a statistical model for handling wood-age offsets in cremated bone and this necessitates the inclusion of additional case studies that provide important insight into the different types of offsets that might affect radiocarbon dates and how these might be modelled statistically. Three case studies are selected from the Danish area (Fig. 69), based on the criteria that they provide opportunities to model types of offsets that are not otherwise possible with the urnfield assemblages. Rokaer long barrow is included because it offer an opportunity to model wood-age offsets in charcoal with varying intrinsic ages (Paper 1: Kristiansen et al. forthcoming). St Alban's Odense is included because it offer an opportunity to model dietary offsets and individual offsets tailored to specific material (Paper 4: Rose et al. 2020). A modern experimental case study is included because it offer an opportunity to investigate the scale and scatter of empirical wood-age offsets in cremated bone with a known-age. The experience gained through the additional case studies played a significant role for the development of a new outlier model for wood-age offsets in cremated bone (Paper 4: Rose et al. 2020).



Figure 69: Location of Aarupgaard, Aarre and Søhale urnfields and the additional archaeological case studies Rokaer long barrow and St Alban's Odense (map by Ronja Mücke, ZBSA).

Rokaer long grave

Rokaer is a non-megalithic long barrow from Eastern Jutland, excavated by Horsens Museum in 1998 (Fig. 70).²⁵ The barrow had prior to this been partly destroyed by agricultural activity, but the bottom of a single-phased grave monument remained (Kristiansen 2000). The barrow is SW-NE oriented and preserved in a 12.5 x 15-18 m area, at a depth of c. 30 cm. It is demarcated by a zig-zag line of postholes along the long sides, and to the east by a 6m long façade ditch with vertical planks. The western façade was only preserved as a double set of postholes. The barrow contained a single centrally placed grave covered by a 2 x 3 m stone packing. Underneath three layers of stones (layer B) was a thin layer of compact, burned material (burial layer C) (Kristiansen 2016). On top of the stone packing were grave goods in form of two polished thin butted flint axes and a 16 cm long polished flint dagger (Eriksen 2017) and more than 200 amber beads from a complex chain (Fig. 71) (Kristiansen 2016). Underneath the grave at each end were two postholes (brown circles in Fig. 71), revealing the grave to be of the ‘Konens Høj’ type and dating to the Early Neolithic (ENII) (Kristiansen 2016).



Figure 70: Plan of Rokaer long barrow (from Kristiansen 2016: 66).

²⁵ The site is registered under museum no. HOM 1151.

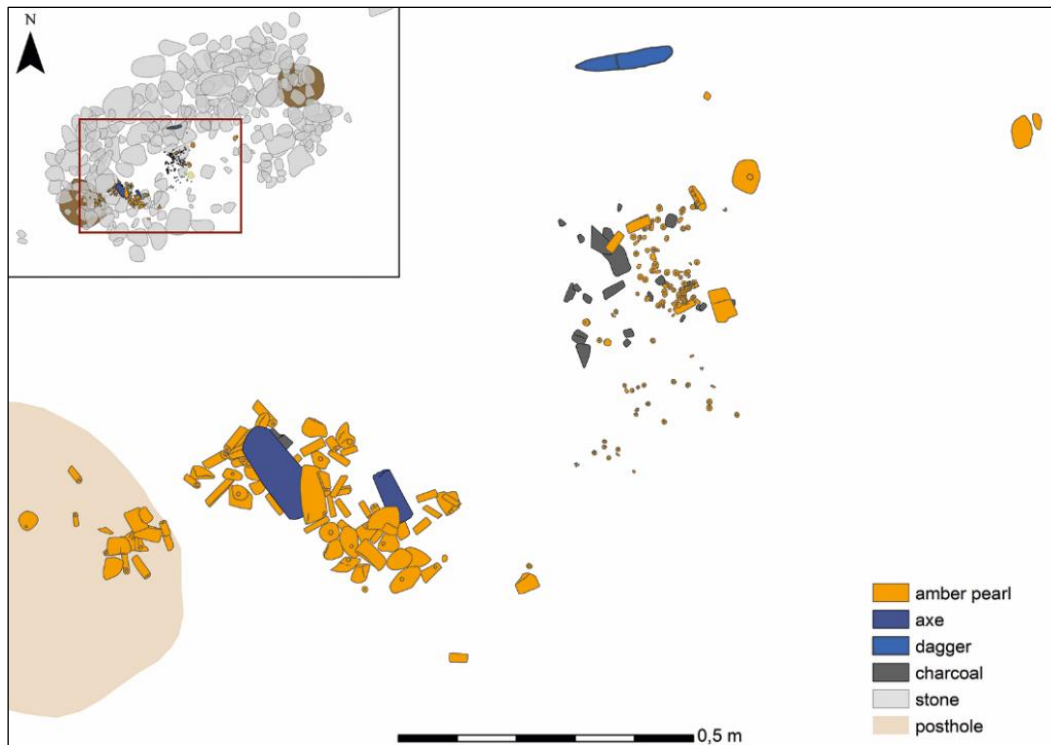


Figure 71: The central grave in Rokaer long barrow with grave goods (from Kristiansen 2016: 67).

Sample Selection²⁶

A single charcoal sample had already been radiocarbon dated (Rasmussen 2000), but it was decided to date another seven charcoal samples. From the black burial layer C were dated two new samples of charcoal; a fragment of *Corylus* sp. (hazel) and a fragment of *Quercus* sp. (oak) sapwood in duplicate. Neither of these have significant intrinsic ages (wood-age offsets) that need to be accounted for here. The original radiocarbon date was measured on a bulk sample of *Quercus* sp. charcoal from the same layer and judging from the archaeobotanical analysis, it probably consisted primarily of a branch wood fragment with c. 20 growth rings.²⁷ From in between the stones in mound layer B were dated three samples of charcoal; two fragments of *Alnus* sp. (alder) trunk (diameter larger than 10 cm), possibly originating from the same tree, and an *Alnus* sp. branch fragment with two annual rings; the latter was dated in duplicate. Trunk wood from *Alnus* sp. is expected to have a moderate intrinsic age (Claessens et al. 2010; Effenberger 2017a).²⁸

²⁶ Aapted from Paper 1: Kristiansen et al. forthcoming.

²⁷ Archaeobotanical analysis by Claus Malmros from The Danish National Museum (unpublished report).

²⁸ Also archaeobotanical analyses by Yasmin Dannath and Tim Schroedter from Kiel University (unpublished report).

St Alban's Odense²⁹

Odense is situated on the island of Funen in central Denmark. During the medieval period, Odense was an important commercial town and a clerical centre, with its own bishopric and numerous churches and monasteries. St Alban's Church is believed to be one of the first churches on Funen, and is possibly identical to a church mentioned in AD 988. After having been used as consecrated burial ground for around 500 years, the church was abandoned in the wake of the Lutheran reformation in AD 1536 and demolished in the 1540s (Eliassen et al. 2001). A series of archaeological excavations has been carried out by Odense City Museums, most recently in 2015–2016 (Albrechtsen 1956; Arentoft 1985; Christensen 1999; Pedersen and Bjerregaard 2016). Vital parts of the church and cemetery were destroyed in the 1950s when an underground carpark was constructed, but the excavations provide a rough idea of the building history of the church and the boundaries of the church yard (Eliassen et al. 2001; Christensen and Bjerregaard 2017). The latest excavation has revealed c. 360 individuals buried east and north of the church.³⁰ A group of graves with brick-built coffins are typologically dated to the mid-12th century to 13th century, while the remaining graves are only dated stratigraphically to AD 1100–1500. Following medieval burial practice, the large majority of the graves contained a single individual, but a handful of graves held two or more individuals (Fig. 72) (Pedersen and Bjerregaard 2016).



Figure 72: Grave 156 with multiple individuals being excavated by archaeologists from Odense City Museums in November 2015 (picture by Odense City Museums).

²⁹ Adapted from Paper 2: Rose et al. 2018.

³⁰ The excavation is registered under museum no. OBM 3183.

Multiple graves have been observed in medieval cemeteries throughout Scandinavia, most often containing juveniles and only more rarely adults (Ranåker 2009). These graves reflect the contemporaneous death of the interred individuals, as burials in the Middle Ages usually took place within one or two days after death (Nilsson 1987). We know little of the belief system behind this custom, but incidents of multiple deaths within a short period of time, caused by e.g. violence, accidents or epidemics, could lead to communal graves being dug in haste (Ranåker 2009; Millard 2015).

About 25 m east of the St Alban's church, a multiple grave containing five juveniles received special attention during the 2015–2016 excavation. Because of the heavily mixed burial soil it was not possible to define the edges of grave 156, but based on the buried individuals it must have been minimum 1 m wide × 1.7 m long. The grave was intercut by younger graves to the east. No coffin remains were found, but the presence of small bronze pin fragments next to burial x244 indicates it might have been wrapped in a shroud for burial, as is often the case for medieval burials. The five juveniles were placed partly overlapping in a supine position orientated roughly E–W, with the heads towards west. The internal stratigraphy in the grave was as follows; burials x241 and x243 placed side by side, partly overlain by burials x242 and x244, which in turn were overlain by burial x252 (Fig. 73).

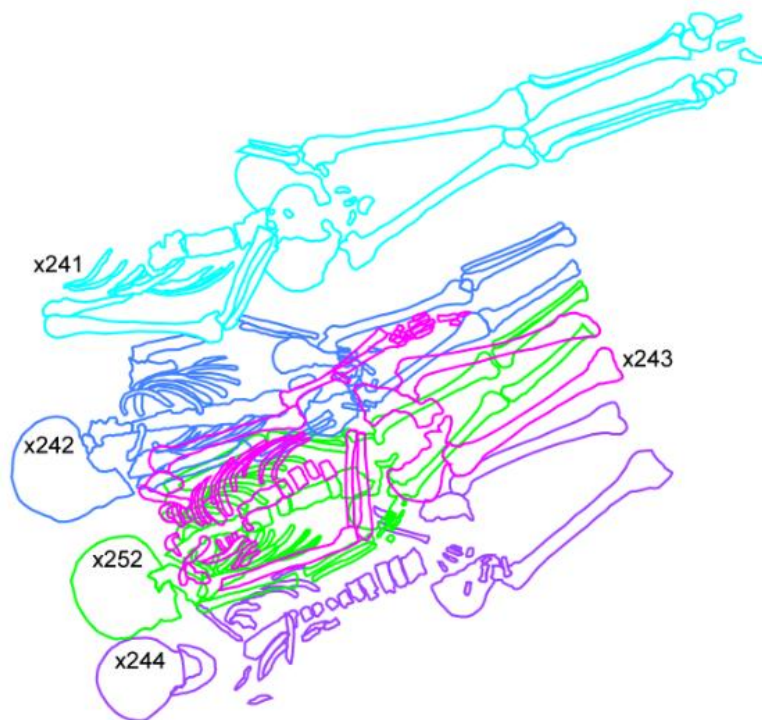


Figure 73: Multiple grave 156, St Alban's Odense (from Rose et al. 2018: 1548).

A study of long-term trends in medieval inhumation practices (Kieffer-Olsen 1993) found that in the earliest Christian burials, the arms were positioned beside the body (position A); in later burials, the hands were folded in the pelvic area (position B), and subsequently folded across the lower stomach (position C). In the latest burials, both hands were folded across the chest (position D). Arm positions therefore provide relative dates for the use of a burial ground, but may be misleading at the individual level, as the different positions overlap in time. The individuals buried in grave 156 had the arms placed in position B, indicating a possible date between mid-13th to mid-15th centuries, but it was not possible to confirm this stratigraphically.

Osteology

The osteological analysis of grave 156 builds on an unpublished museum report from ADBOU, the Unit of Anthropology at Southern Denmark University (Olsen 2016) and on analyses carried out by the present author. Age determinations of juveniles rely on dental development and eruption, length of long bones, and ossification of epiphyses (Bass 1995; Scheuer and Black 2000). Sex determination is only possible when the primary pelvic bones (ilium, ischium, and pubis) have completely ossified around the age of 16 (Bass 1995). The preservation of the skeletons was medium-good, compared to the norm of Danish medieval human material. No clear cause-of-death or signs of violent trauma were recognized. Osteological information, given in Table 9, is inconclusive, but it is possible that the five individuals were killed by an acute infectious disease.

Table 9: Osteological results from grave 156, St Alban's Odense (from Rose et al. 2018: 1550).

Burial	Sex	Age-at-death	Preservation	Preservation and pathologies
x241	Male?	15-18 years	Well	Indistinct signs of pathology on skull.
x242	?	7-9 years	Medium	-
x243	?	13-16 years	Medium	-
x244	?	14-16 years	Well	Severe growth deficiencies are visible in the enamel of all permanent teeth. Indistinct signs of pathology on skull.
x252	?	7-9 years	Medium	Indistinct signs of pathology on skull.

Sample Selection

A lower first permanent molar (M1) was sampled from each of the five primary burials from grave 156, disregarding any stray teeth. Using a dentist's drill, the tooth was separated from the root with a horizontal cut just beneath the enamel-dentine junction. The crown was divided into two with a vertical cut down the middle. Next, using an abrasive drill bit, all the dentine was pulverized and removed as a bulk sample. Because of the individuals' young ages-at-death, secondary dentine formation could be disregarded (Hillson 1996).

Experimental material³¹

Mogens Bo Henriksen from Odense City Museums has carried out open-air cremation experiments over the period 2014-17, in order to produce material for investigating empirical wood-age offsets in cremated bone. The experiments were designed to mimic a prehistoric cremation pyre, albeit in a scaled down version using an iron brazier, which protected the fire from the wind and ensured the bones were in close contact with the fuel until the fires burned down after 2-2.5 hours (Fig. 74). This did not allow close control of environmental parameters (Henriksen 2016). Cuts of cattle (*Bos taurus*) and sheep (*Ovis aries*) reared in Denmark (AD 2013-17) were cremated on four separate experimental pyres using recent wood (*Fraxinus* sp., AD 1986-2013) or old dendro-dated wood (*Quercus* sp., AD 1100-1282; AD 34-251) (Daly 2011; Daly 2014). Snoeck et al. (2014) conducted similar experiments, but our new contribution was the dating of multiple bone fragments from the same pyre, thereby documenting variable uptake of exogenous carbon during cremation (Rose et al. 2020).



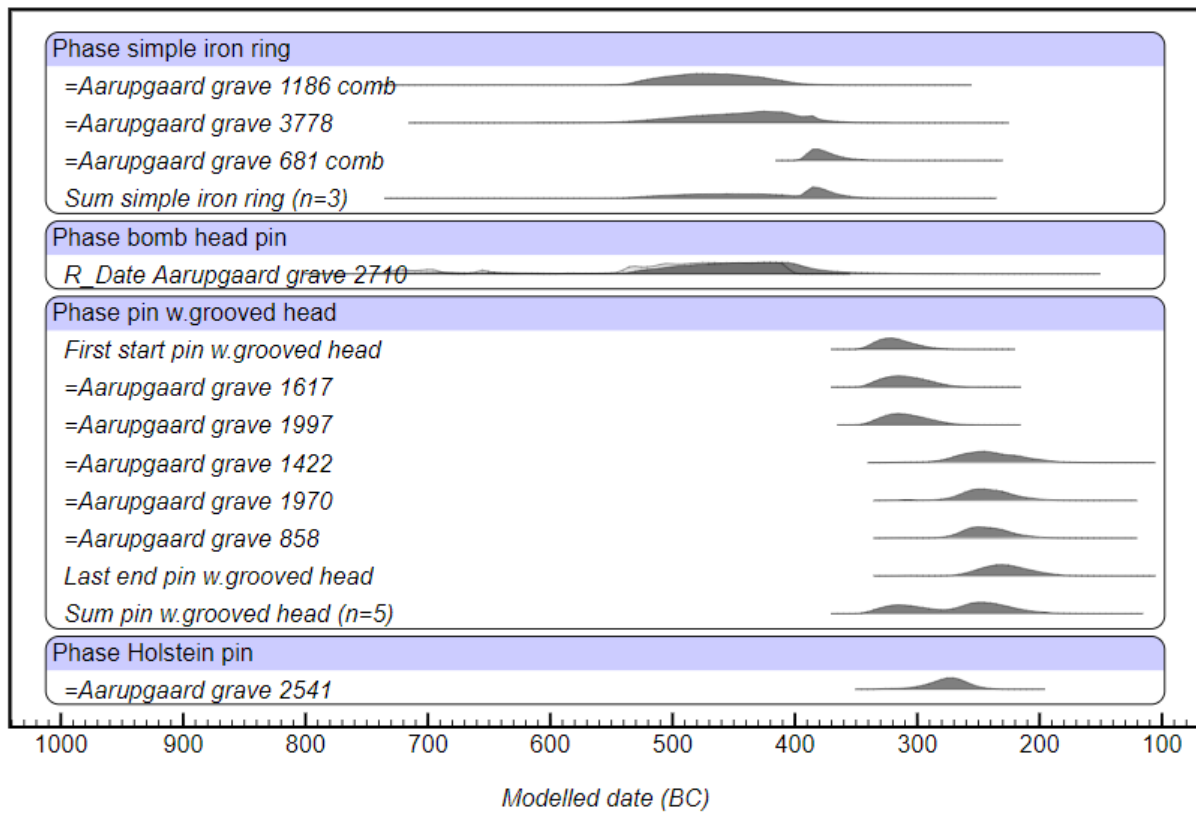
Figure 74: The left picture is from experimental pyre no.11 before ignition, the right picture is from experimental pyre no. 16 during cremation (pictures by Mogens Bo Henriksen, Odense City Museums).

³¹ Adapted from Paper 4: Rose et al. 2020.

Appendix 2 Metalwork currencies

Posterior estimated output from *Model A metalwork currencies*

Chronological model of metalwork types modelled in unbounded phases

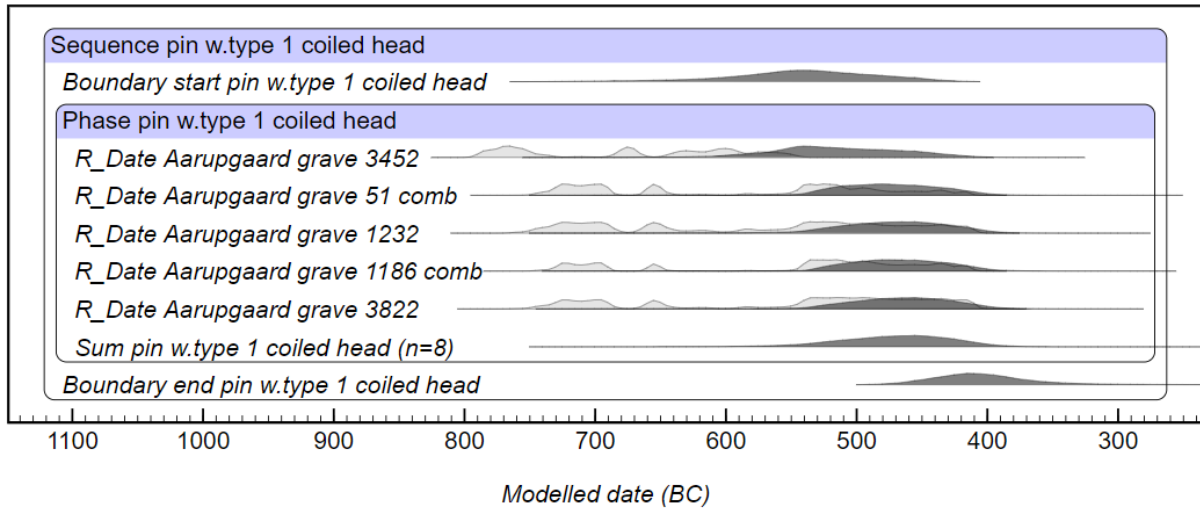


Currency model of pin with type 1 coiled head

Start boundary: 588-479 cal BC (68.2% probability), 661-432 cal BC (95.4% probability)

End boundary: 447-377 cal BC (68.2% probability), 481-321 cal BC (95.4% probability)

Duration of currency: 50-150yr (68.2% probability), 9-212yr (95.4% probability)

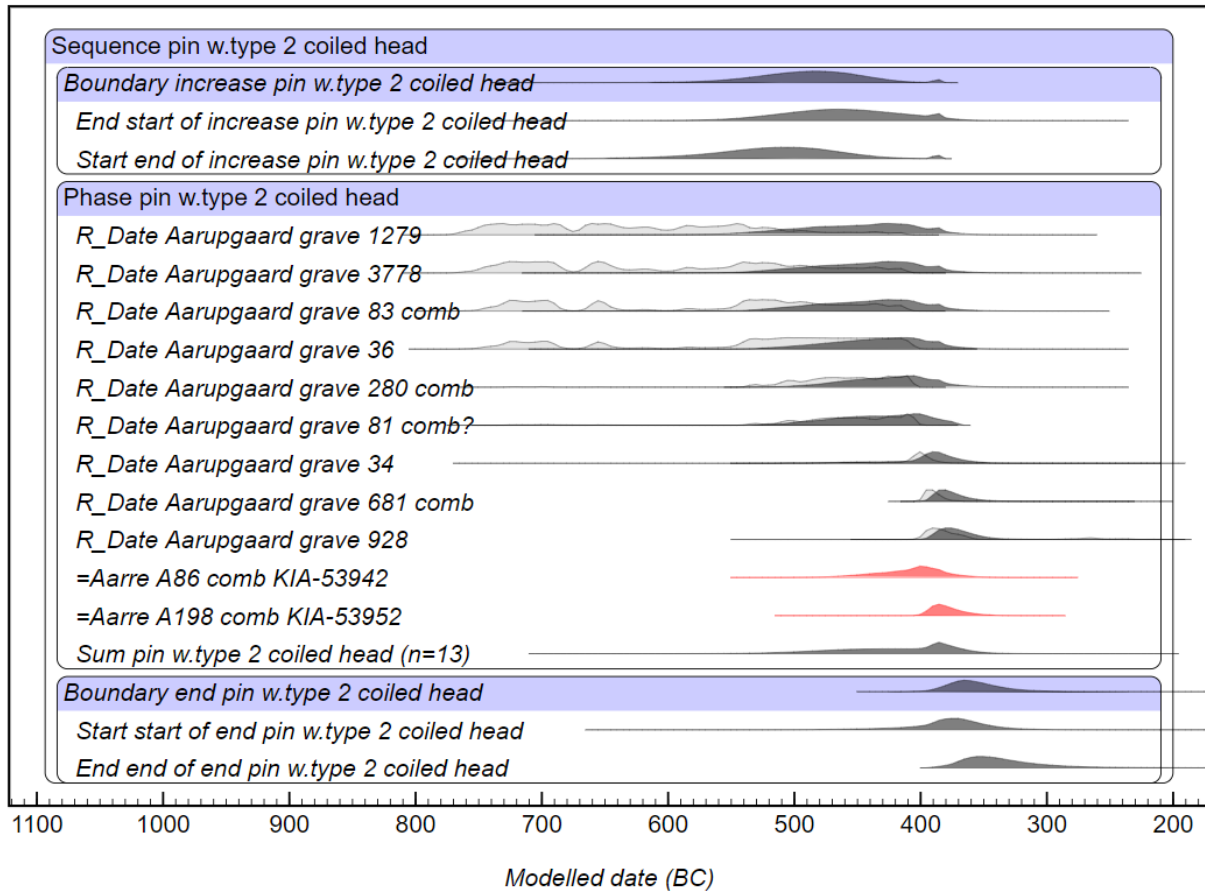


Currency model of pin with type 2 coiled head

End of increase: 560-446 cal BC (68.2% probability), 621-383 cal BC (95.4% probability)

Start of decrease: 398-346 cal BC (68.2% probability), 459-314 cal BC (95.4% probability)

Duration of currency: 79-165yr (68.2% probability), 40-215yr (95.4% probability)

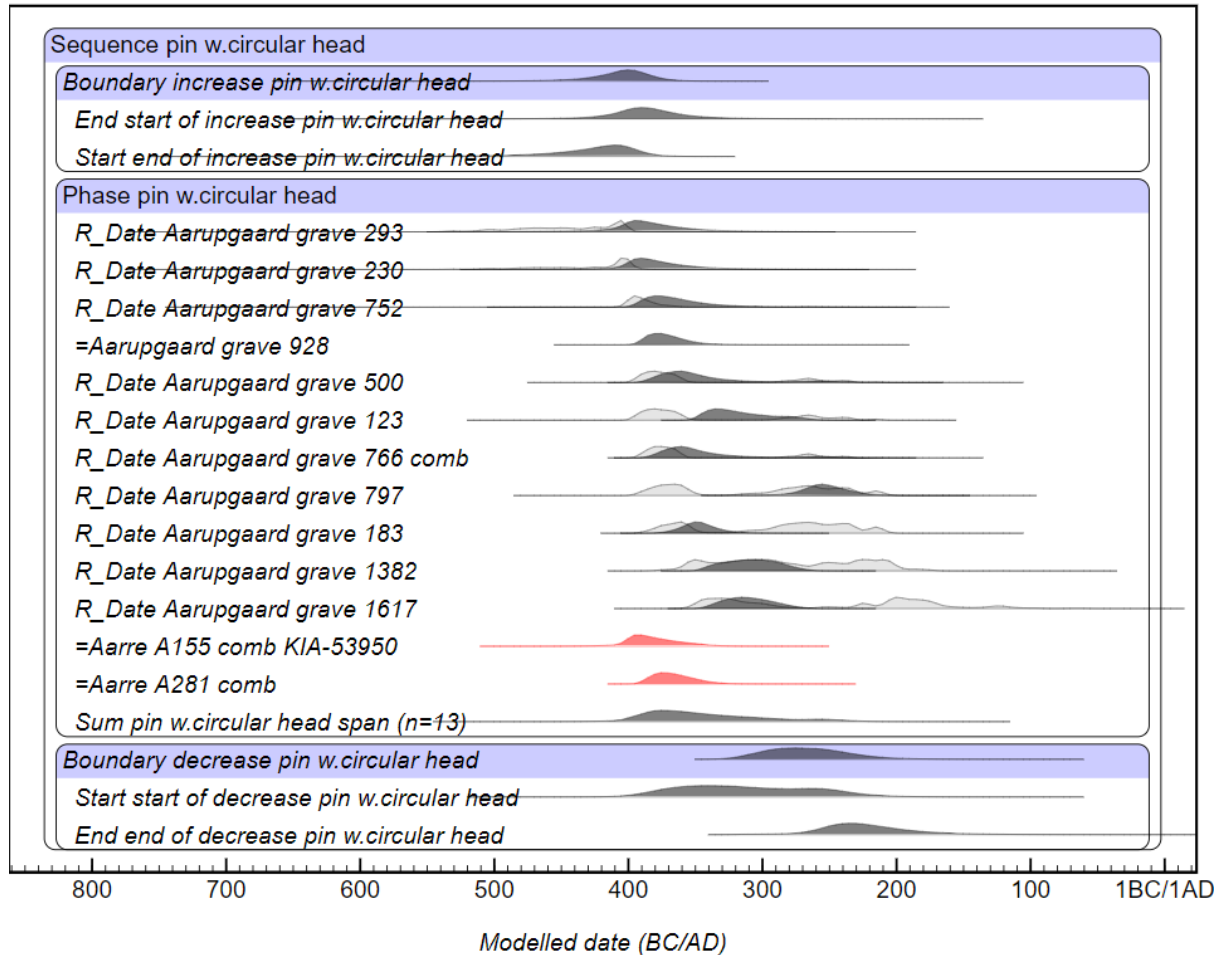


Currency model of pin with circular head

End of increase: 445-391 cal BC (68.2% probability), 503-373 cal BC (95.4% probability)

Start of decrease: 373-257 cal BC (68.2% probability), 397-222 cal BC (95.4% probability)

Duration of currency: 30-140 (68.2% probability), -3-186yr (95.4% probability)

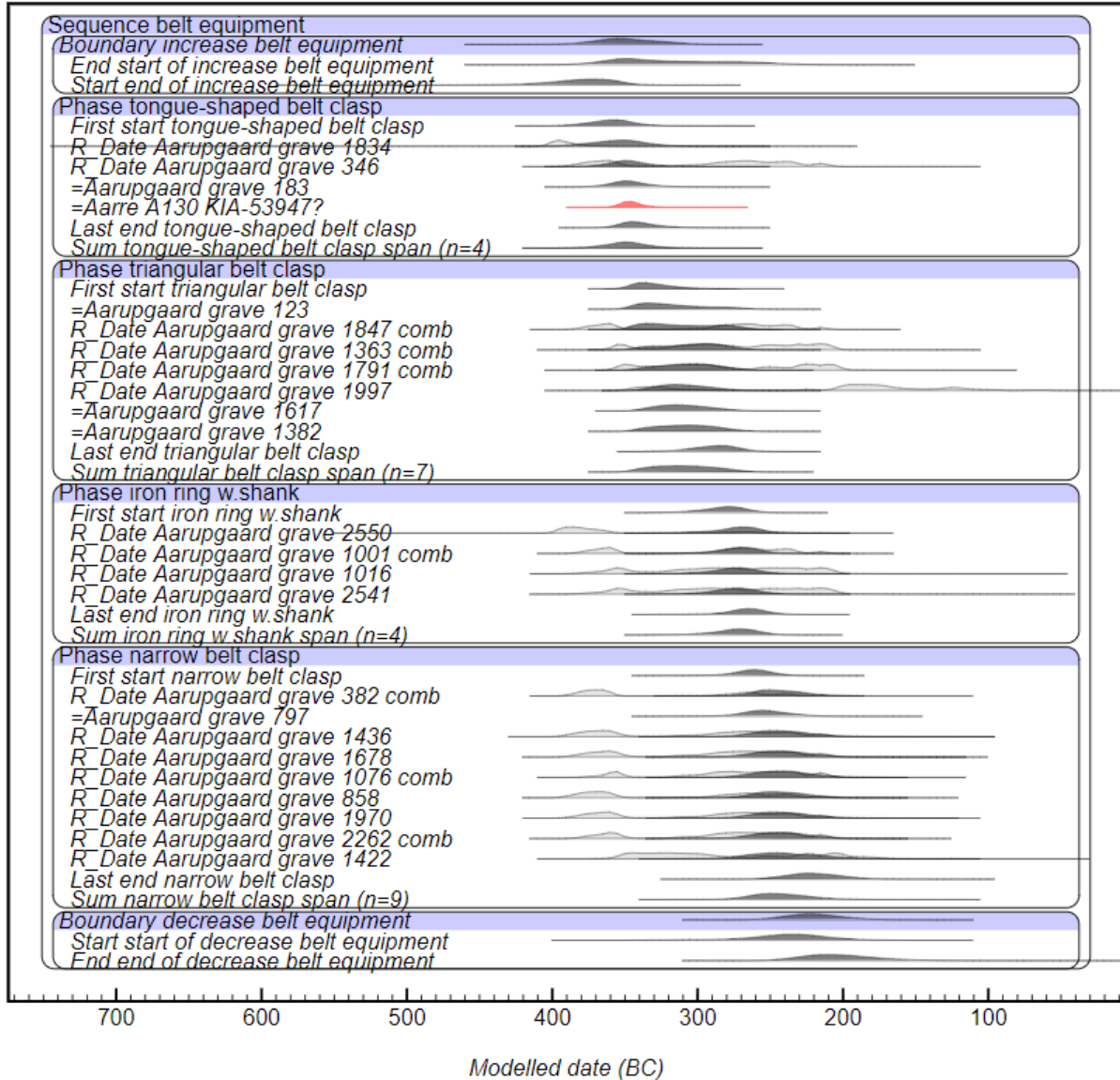


Currency model of combined belt equipment

End of increase: 398-354 cal BC (68.2% probability), 431-341 cal BC (95.4% probability)

Start of decrease: 262-210 cal BC (68.2% probability), 310-184 cal BC (95.4% probability)

Duration of currency: 105-162yr (68.2% probability), 74-190yr (95.4% probability)



Appendix 3 Pottery currencies

Posterior estimated output from *Model B* pottery currencies

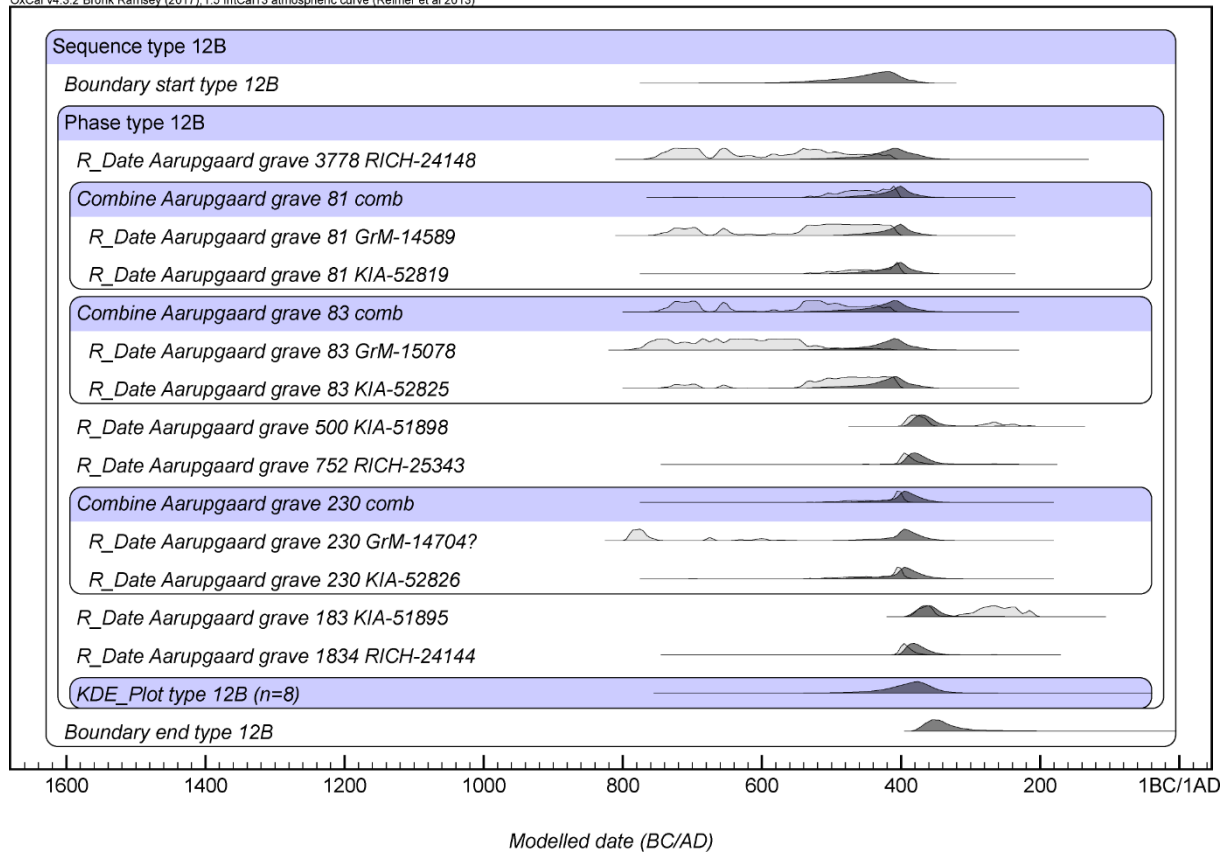
Currency model of pottery type 12B

Start boundary: 481-396 cal BC (68.2% probability), 559-371 cal BC (95.4% probability)

End boundary: 371-326 cal BC (68.2% probability), 384-243 cal BC (95.4% probability)

Duration of currency: 28-118yr (68.2% probability), 0-197yr (95.4% probability)

OxCal v4.3.2 Bronk Ramsey (2017); r.5 IntCal13 atmospheric curve (Reimer et al 2013)



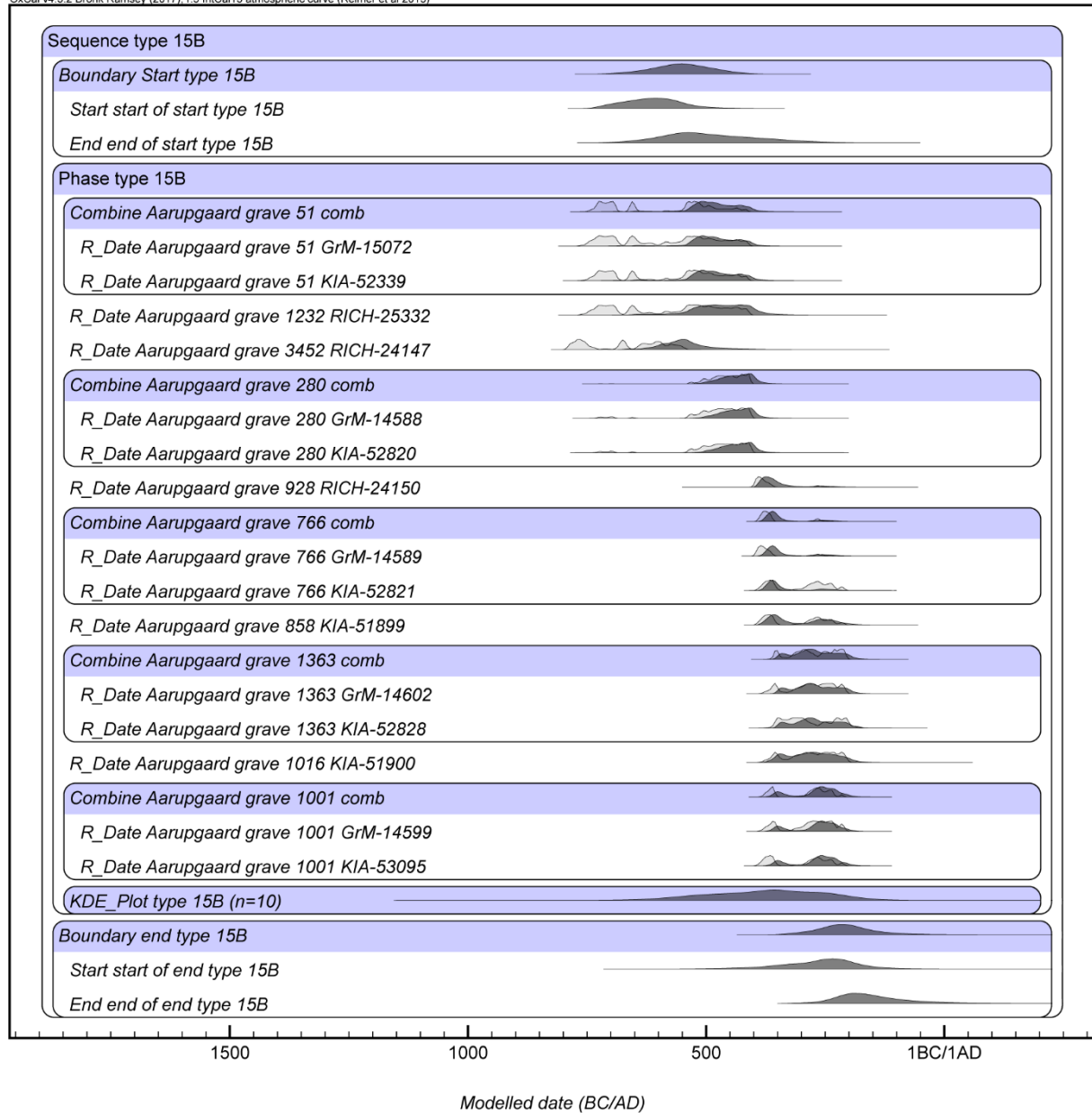
Currency model of pottery type 15B

End of start boundary: 606-408 cal BC (68.2% probability), 671-280 cal BC (95.4% probability)

Start of end boundary: 332-177 cal BC (68.2% probability), 466-101 cal BC (95.4% probability)

Duration of currency: 269-378yr (68.2% probability), 198-443yr (95.4% probability)

OxCal v4.3.2 Bronk Ramsey (2017), r.5 IntCal13 atmospheric curve (Reimer et al 2013)



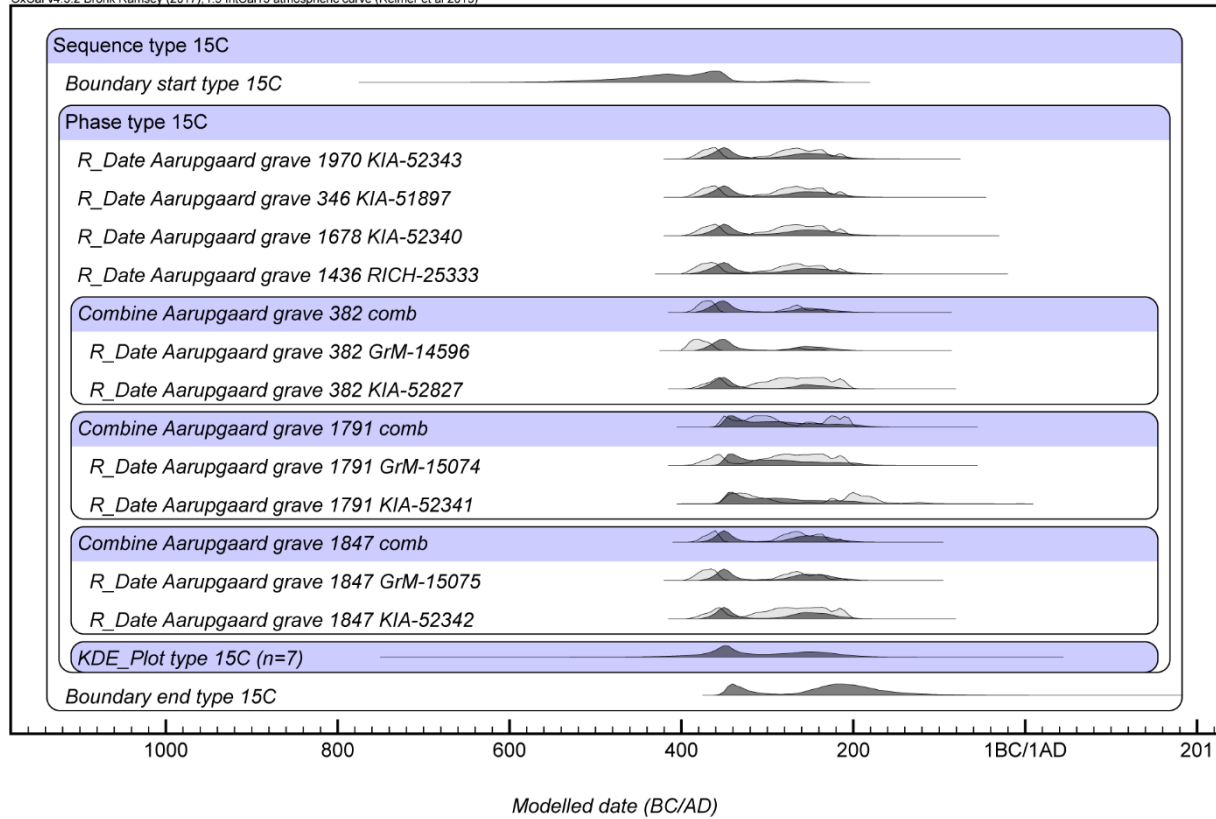
Currency model of pottery type 15C

Start boundary: 463-345 cal BC (68.2% probability), 554-229 cal BC (95.4% probability)

End boundary: 350-172 cal BC (68.2% probability), 356-111 cal BC (95.4% probability)

Duration of currency: 0-219yr (68.2% probability), 0-259yr (95.4% probability)

OxCal v4.3.2 Bronk Ramsey (2017), r.5 IntCal13 atmospheric curve (Reimer et al 2013)



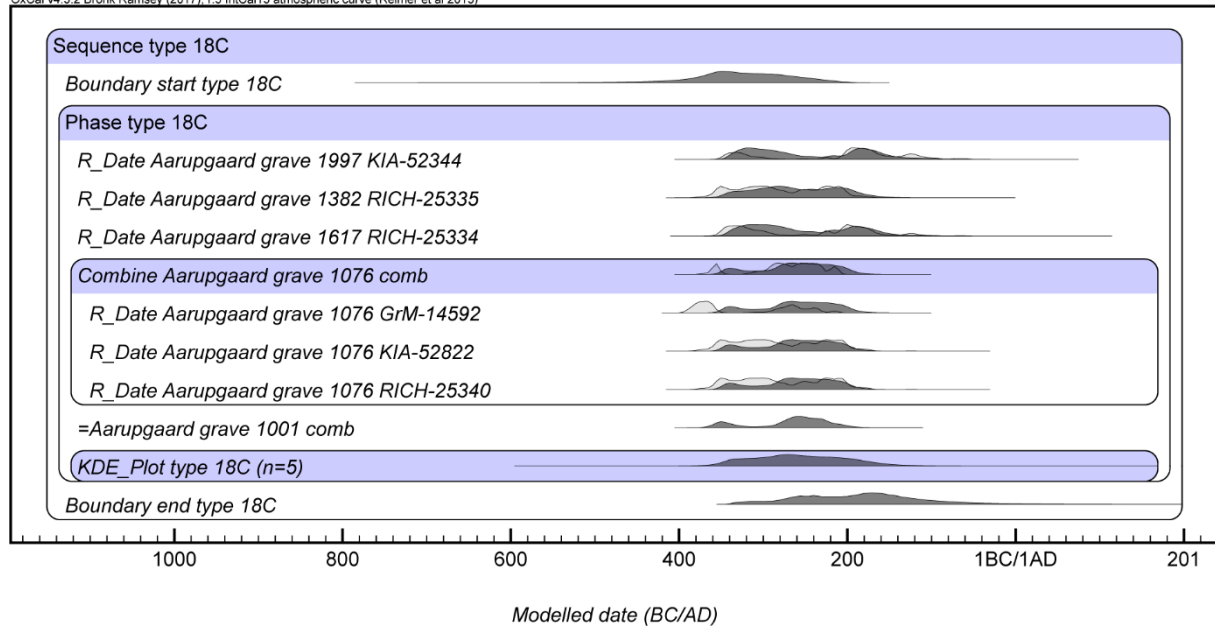
Currency model of pottery type 18C

Start boundary: 376-261 cal BC (68.2% probability), 461-201 cal BC (95.4% probability)

End boundary: 271-125 cal BC (68.2% probability), 339-21 cal BC (95.4% probability)

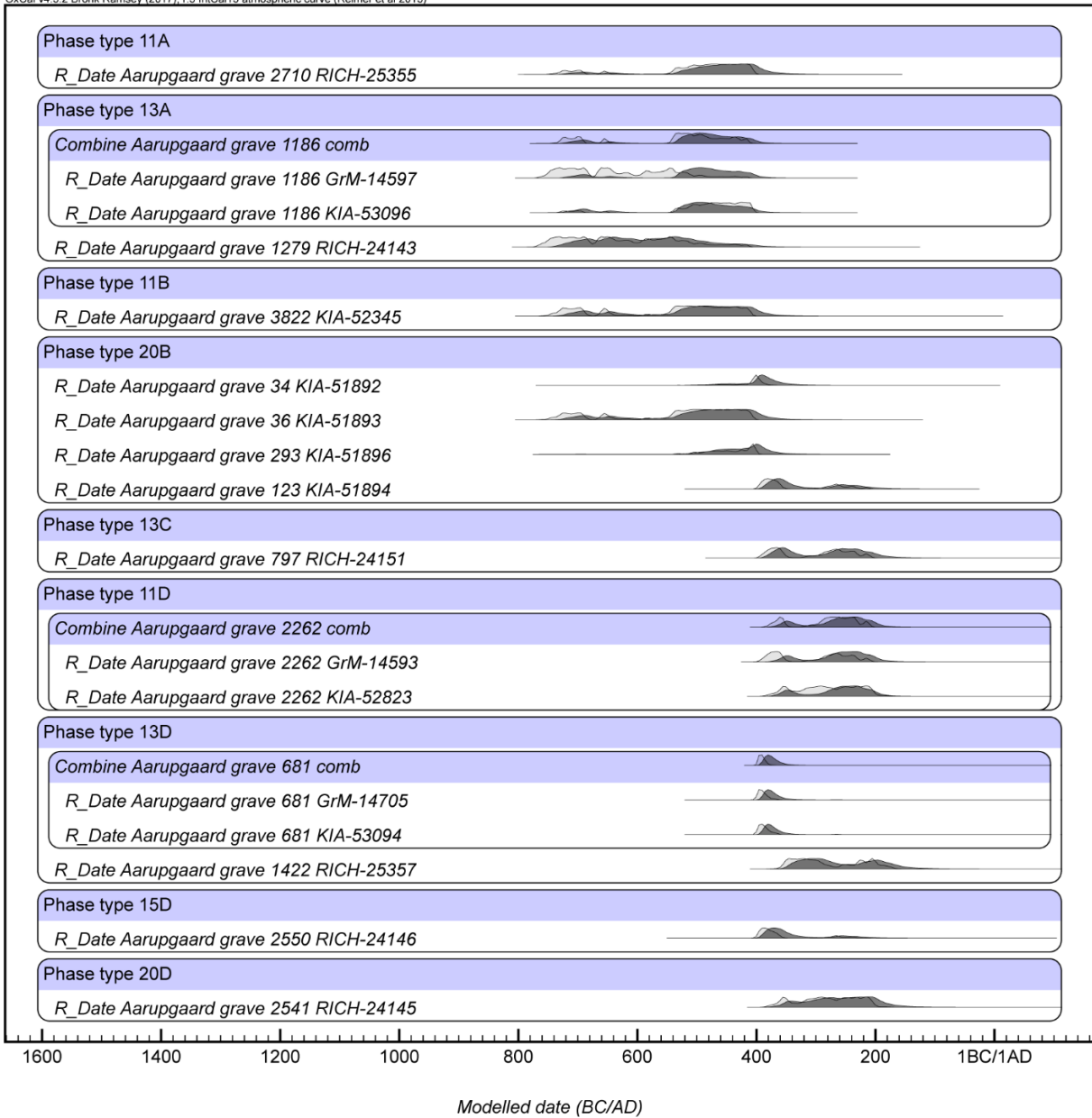
Duration of currency: 0-110yr (68.2% probability), 0-187yr (95.4% probability)

OxCal v4.3.2 Bronk Ramsey (2017), r.5 IntCal13 atmospheric curve (Reimer et al 2013)



Chronological model of pottery types modelled in unbounded phases

OxCal v4.3.2 Bronk Ramsey (2017), r.5 IntCal13 atmospheric curve (Reimer et al 2013)



Appendix 4 Paper 1

Rokaer – an early Neolithic long barrow from East Jutland

Authors: Kristiansen, A. M., Eriksen, B. V., & Rose, H. A.

Publication forthcoming

Rokaer – a Neolithic long barrow

Anne Mette Kristiansen, Berit Valentin Eriksen and Helene Agerskov Rose

Radiocarbon dating

By Helene Agerskov Rose

A single charcoal sample was radiocarbon dated in 2000 by at the then Copenhagen ¹⁴C Dating Laboratory (DK) (Rasmussen 2000), presumably using the gas proportional counting system described by Rasmussen et al. (Rasmussen et al. 1999). When calibrated, the date (K-7126, 4740±34) has a multimodal probability range of c.3600-3400 BC (95% probability). For the current publication it was decided to date another seven charcoal samples; two of these were duplicate measurements of single fragments (Table 1).

From the black burial layer C were dated two new samples of charcoal; a fragment of *Corylus* sp. (hazel) and a fragment of *Quercus* sp. (oak) sapwood in duplicate. Neither of these have significant intrinsic ages (wood-age offsets) that need to be accounted for here. The original radiocarbon date was measured on a bulk sample of *Quercus* sp. charcoal from the same layer, judging from the archaeobotanical analysis, it probably consisted primarily of a branch wood fragment with c.20 growth rings¹. From in between the stones in mound layer B were dated three samples of charcoal; two fragments of *Alnus* sp. (alder) trunk (diameter larger than 10 cm), possibly originating from the same tree, and an *Alnus* sp. branch fragment with two annual rings; the latter was dated in duplicate. Trunk wood from *Alnus* sp. is expected to have a moderate intrinsic age² (Claessens et al. 2010).

Table 1. Radiocarbon results from Rokaer long barrow.

Lab code	Sample ID	Context	Description	δ ¹³ C (‰)	Corrected pMC	¹⁴ C age BP
KIA-52320	x194a	Layer B	<i>Alnus</i> sp. trunk, single fragment	-27.2	56.16 ± 0.23	4635 ± 35
KIA-52321	x194b	Layer B	<i>Alnus</i> sp. trunk, single fragment	-27.3	55.43 ± 0.23	4740 ± 35
GrA-69320	x230	Layer B	<i>Alnus</i> sp. single fragment, 2 growth rings	-27.0	57.07 ± 0.26	4505 ± 35
KIA-52293	X230	Layer B	Replicate of GrA-69320	-25.7	56.45 ± 0.23	4595 ± 35
GrA-69322	x187	Layer C	<i>Quercus</i> sp. sapwood, single fragment	-24.3	55.04 ± 0.25	4795 ± 35
KIA-51925	X187	Layer C	Replicate of GrA-69322	-23.7	54.48 ± 0.17	4635 ± 35
GrA-69321	x210	Layer C	<i>Corylus</i> sp. single fragment	-25.0	55.99 ± 0.25	4660 ± 35
K-7126 ³	X190	Layer C	<i>Quercus</i> sp. bulk sample	-23.0	-	4740 ± 34

The samples were dated by Accelerator Mass Spectrometry (AMS) radiocarbon dating at the Leibniz Laboratory in Kiel (D) and at the Centre for Isotope Research in Groningen (NL). Laboratory methods

¹ Archaeobotanical analysis by Claus Malmros from The Danish National Museum (unpublished report).

² Archaeobotanical analyses by Yasmin Dannath and Tim Schroedter at Kiel University and by Henrike Heffenberger (unpublished reports).

³ Rasmussen KL. 2000. Danske arkæologiske 14C-dateringer. Arkæologiske udgravninger i Danmark 2000:329-32.

followed standard published procedures in Kiel; (Nadeau et al. 1998; Grootes et al. 2004) and in Groningen; (Mook and Streurman 1983; Aerts-Bijma et al. 1997). Measured ^{14}C concentrations were corrected for fractionation using measurements of stable isotope $\delta^{13}\text{C}$ obtained by AMS (Stuiver and Polach 1977). Results are reported in Table 1. Where more than one radiocarbon result is available for the same charcoal fragment, they are first combined following the method given by Ward and Wilson (Ward and Wilson 1978).

When there are more radiocarbon results available from the same site, we can reduce the uncertainties of the calibrated dates using Bayesian chronological modelling. It is a statistical method that although mathematically rigorous, is fundamentally subjective, but that also forces us to evaluate how we interpret the archaeological information. We construct a Bayesian chronological model analogous to a Harris matrix, incorporating both absolute and relative dating evidence, i.e. the calibrated radiocarbon dates (with any applicable offsets) and the sequence of events implicit in archaeological observations, such as stratigraphic relationships between samples. Stratigraphic relationships can be misleading, as even a freshly-deposited sample can have an inbuilt age, e.g. charcoal reflecting the tree-fall date rather than the archaeological event of deposition. It is therefore essential to understand the taphonomy of samples and possibly apply an offset function to inform the Bayesian model of any inbuilt ages of these. Given the information we provide the model with, it produces *posterior density estimates* of the dates of events of interest, including events not directly sampled like start or end of activities at a site. Because the radiocarbon calibration curve is wiggly, these estimates are not normally distributed and need to be expressed as intervals with a specified probability of including the true date of the event concerned. The length of these depending on the precision of the AMS measurement, how steep the relevant part of the calibration curve is and the amount of information included in the Bayesian model. A more detailed introduction to radiocarbon dating and Bayesian chronological modelling can be found in Bayliss et al. (2013).

A model of the Rokaer long barrow was created in OxCal (v.4.3) (Bronk Ramsey 1995; Bronk Ramsey 2009) using the IntCal13 dataset to convert the radiocarbon ages to calendar dates (Reimer et al. 2013). All available dates are on charcoal, which is susceptible to in-built age offsets. Individual wood-age offsets were therefore estimated based on the lifespan of the specific plant and the sampled section of the plant (e.g. heartwood or branch) (Bronk Ramsey 2009).

The taphonomic origin of the black burial layer C remains unresolved, but a substantial contribution of peat material cannot be ruled out. This would introduce a potentially very long residence time of the charcoal, besides the intrinsic age offsets already accounted for. In this case, even though the material was deposited at the time of burial interment, the radiocarbon dates do not relate to that event. To handle this, all dates from layer C are treated as *termini post quos* (TPQs), informing the Bayesian model that layer C was deposited any time after the tree-fall dates for individual samples. Layer C was followed by a burial activity phase with dates from mound layer B, where the start event signifies the interment of the burial and the end event the abandonment of the monument.

The satisfactory overall index of agreement ($A_{\text{overall}} > 99$, Fig. 1) indicates that the radiocarbon results are consistent with the structure of the preferred Bayesian chronological model (Bronk Ramsey 1995). Sensitivity testing of the wood-age offsets was carried out, showing only slight changes to the posterior estimates of the burial activity phase chronology. The posterior density estimates derived by the preferred model are given in Figure 1. Initiation of burial activity at Rokaer corresponds to interment of the burial, which we can date to 3467-3336 BC (95% probability, 68%: 3396-3343 BC). Duration of the burial activities is estimated to span 0-133yr (95% probability, 68%: 0-33yr) and the monument is estimated to have been abandoned in 3369-3159 BC (95% probability, 68%: 3358-3315 BC). The posterior probability distributions of both start and end boundaries have very long tails, but the model estimates 94% probability that burial activity started after 3450 BC and 89% probability that it ended before 3250 BC.

The Bayesian chronological model of Rokaer long barrow indicates burial activity took place c.3450-3250 BC, possibly during only one generation in the 34th century BC. This date is slightly later than the previously suggested 3652-3387 BC (95%, 68%: 3543-3412 BC) for the construction and use of the Danish non-megalithic long barrows (Paulsson 2010), but as that study relied on single dates from most sites and did not take account of possible intrinsic ages of charcoal, the estimate is possibly too early. Our Rokaer model relies on more dates from the same site, including dates on material with negligible intrinsic age, and we are thus confident of the result.

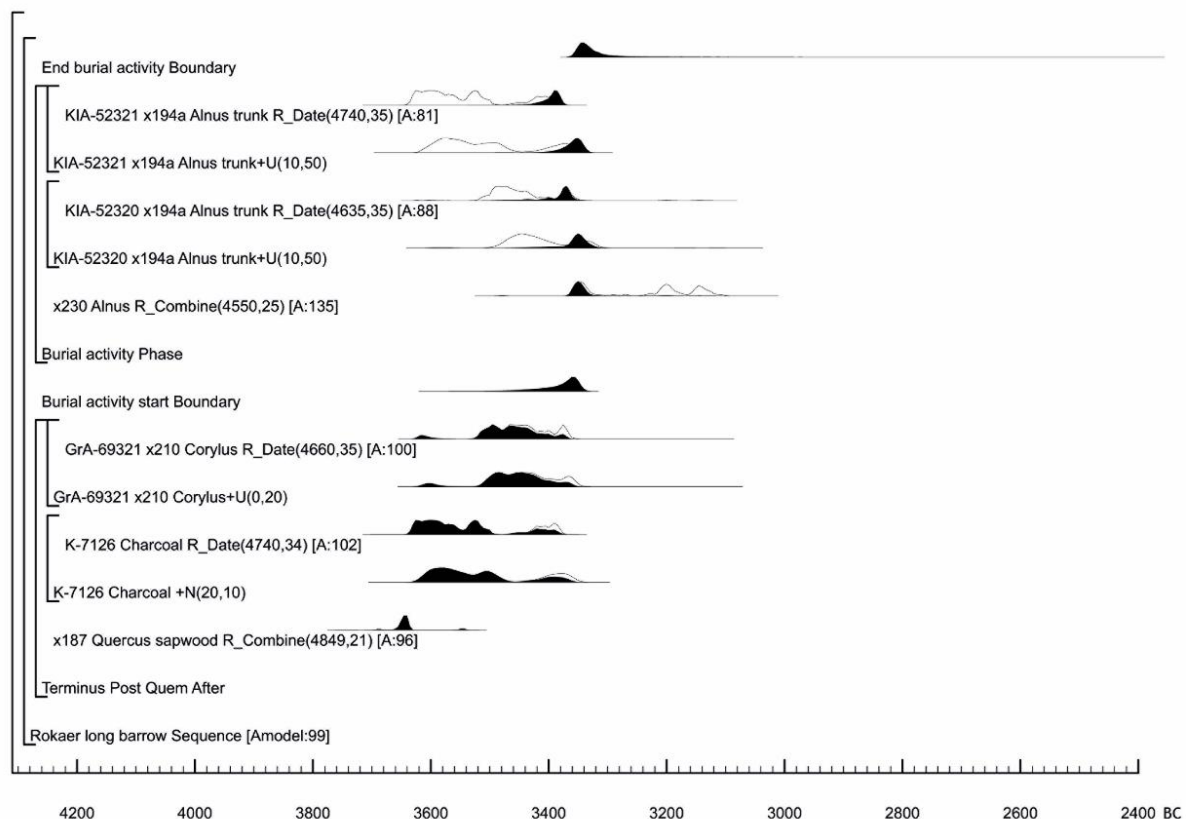


Figure 1: Estimated dates of Rokaer long barrow. Simple calibrated likelihoods represented by white probability distributions, posterior density estimates derived from the Bayesian chronological model by black probability distributions. OxCal indices for individual dates (A) are above the > 60 threshold, indicating satisfactory agreement of individual calibrations with the model.

References

- Aerts-Bijma AT, Meijer H, Van der Plicht J. 1997. AMS sample handling in Groningen. *Nuclear Instruments and Methods in Physics Research Section B: Beam Interactions with Materials and Atoms* 123(1-4):221-5.
- Bayliss A, McGormac G, Thompson M, Hines J. 2013. Dating Methods and their modelling. In: J. Hines AB, editor. *Anglo-Saxon Graves and Grave Goods of the Sixth and Seventh Centuries AD: A Chronological Framework*. London: Society for Medieval Archaeology. p 33-87.
- Bronk Ramsey C. 1995. Radiocarbon Calibration and Analysis of Stratigraphy : The OxCal Program. *Radiocarbon* 37(2):425-30.
- Bronk Ramsey C. 2009. Bayesian Analysis of Radiocarbon Dates. *Radiocarbon* 51(1):337-60.
- Claessens H, Oosterbaan A, Savill P, Rondeux J. 2010. A review of the characteristics of black alder (*Alnus glutinosa* (L.) Gaertn.) and their implications for silvicultural practices. *Forestry: An International Journal of Forest Research* 83(2):163-75.
- Grootes PM, Nadeau M-J, Rieck A. 2004. 14C-AMS at the Leibniz-Labor: radiometric dating and isotope research. *Nuclear Instruments and Methods in Physics Research Section B: Beam Interactions with Materials and Atoms* 223–224:55-61.
- Mook W, Streurman H. *Physical and chemical aspects of radiocarbon dating*; 1983. Council of Europe. p 31-55.
- Nadeau M-J, Grootes P, Schleicher M, Hasselberg P, Rieck A, Bitterling M. 1998. Sample throughput and data quality at the Leibniz-Labor AMS facility. *Radiocarbon* 40(1):239-45.
- Paulsson BS. 2010. Scandinavian Models: Radiocarbon Dates and the Origin and Spreading of Passage Graves in Sweden and Denmark. *Radiocarbon* 52(3):1002-17.
- Rasmussen KL, Tauber H, Bonde N, Christensen K, Theodórsson P. 1999. A 23-year retrospective blind check of accuracy of the Copenhagen radiocarbon dating system. *Radiocarbon* 41(1):9-15.
- Rasmussen KL. 2000. Danske arkæologiske 14C-dateringer. *Arkæologiske udgravninger i Danmark 2000*:329-32.
- Reimer PJ, Bard E, Bayliss A, Beck JW, Blackwell PG, Ramsey CB, Buck CE, Cheng H, Edwards RL, Friedrich M, Grootes PM, Guilderson TP, Haflidason H, Hajdas I, Hatté C, Heaton TJ, Hoffmann DL, Hogg AG, Hughen KA, Kaiser KF, Kromer B, Manning SW, Niu M, Reimer RW, Richards DA, Scott EM, Southon JR, Staff RA, Turney CSM, van der Plicht J. 2013. IntCal13 and Marine13 Radiocarbon Age Calibration Curves 0–50,000 Years cal BP. *Radiocarbon* 55(04):1869-87.
- Stuiver M, Polach HA. 1977. Discussion Reporting of 14C Data. *Radiocarbon* 19(3):355-63.
- Ward GK, Wilson SR. 1978. Procedures for Comparing and Combining Radiocarbon Age Determinations: a Critique. *Archaeometry* 20(1):19-31.

OxCal code

```
Plot()
{
  Sequence("Rokaer long barrow")
  {
    After("Terminus Post Quem")
    {
      R_Combine("x187 Quercus sapwood")
      {
        R_Date("GrA-69322 x187 Quercus sapwood", 4795, 35);
        R_Date("KIA-51925 x187 Quercus sapwood", 4879, 26);
      };
      R_Date("K-7126 Charcoal ", 4740, 34)+N(20,10);
      R_Date("GrA-69321 x210 Corylus", 4660, 35)+U(0,20);
    };
    Boundary ("Burial activity start");
    Phase("Burial activity")
    {
      //two annual rings, so no offset needed
      R_Combine("x230 Alnus")
      {
        R_Date("GrA69320 x230 Alnus", 4505, 35);
        R_Date("KIA-52293 x230 Alnus", 4595, 35);
      };
      R_Date("KIA-52320 x194a Alnus trunk", 4635, 35)+U(10,50);
      R_Date("KIA-52321 x194a Alnus trunk", 4740, 35)+U(10,50);
      Span("Duration burial activities");
    };
    Span ("Duration overall");
    Boundary("End burial activity");
  };
  Order("burial begins after 3450 BC")
  {
    C_Date("3450 BC", -3450, 0);
    Date("=Burial activity start");
  };
  Order("burial ends before 3250 BC")
  {
    C_Date("3250 BC", -3250, 0);
    Date("=End burial activity");
  };
};
```


Appendix 5 Paper 2

High-Resolution Dating of a Medieval Multiple Grave

Authors: Rose, H. A., Meadows, J., & Bjerregaard, M.

Published 2018 in *Radiocarbon*; 60(5), 1547-1559. doi:10.1017/RDC.2018.43

To view supplementary material for this article, please visit <https://doi.org/10.1017/RDC.2019.70>

Printed with permission by Cambridge University Press

HIGH-RESOLUTION DATING OF A MEDIEVAL MULTIPLE GRAVE

Helene Agerskov Rose^{1*} • John Meadows¹ • Mikael Bjerregaard²

¹Center for Baltic and Scandinavian Archaeology, Stiftung Schleswig-Holsteinische Landesmuseen, Schlossinsel 1, Schloss Gottorf, D-24837 Schleswig, Germany.

²Odense City Museums, Archaeology, Overgade 48, DK-5000 Odense C, Denmark.

ABSTRACT. Multiple burial in medieval burial grounds are often interpreted as a result of disease, but it is difficult to test such hypotheses, as most acute infectious diseases leave no visible evidence on skeletal material. Scientific dating can potentially associate multiple burials with historically documented epidemics, but the precision required to exclude alternative explanations would normally be attainable only by dendrochronology. Here, we argue that by combining archaeological, osteological and paleodiet research in a Bayesian framework, we can exploit differences in dietary reservoir effects to refine the dates of multiple burials, and potentially date such events to within a range of <20 years. We present new radiocarbon (¹⁴C) and stable isotope ($\delta^{13}\text{C}$, $\delta^{15}\text{N}$) results from a medieval multiple grave at St Alban's Odense, on the island of Funen in central Denmark. We show the ca. 150-yr spread in ¹⁴C ages of the five juveniles is compatible with differences in the amount of fish they consumed. Our chronological model, which combines marine reservoir effect correction with calendar age offsets based on osteological evidence, dates the multiple burial to *cal AD 1425–1445* (95% probability), an interval in which two plague epidemics took place in Denmark.

KEYWORDS: Bayesian chronological modeling, marine reservoir effect, medieval, multiple burial, paleodiet.

INTRODUCTION

Medieval and historical archaeology has sometimes viewed radiocarbon (¹⁴C) dating as a last resort, as stratigraphy, artifact typology, and written and pictorial sources can often date samples more precisely than the most precise ¹⁴C measurements. This is particularly the case with human remains, which may be subject to unknown offsets affecting both calendar dates and ¹⁴C ages. Offsets on the calendrical timescale stem from uncertainties in the collagen turnover rate in the skeletal element sampled, which are amplified by uncertainty in an individual's age-at-death. Additional ¹⁴C age offsets are caused by dietary reservoir effects, which can only be estimated, based on quantitative reconstruction of individual diet and realistic estimates of ¹⁴C-depletion in the aquatic species consumed during the period of collagen formation. Our understanding of reservoir effects on ¹⁴C dates, dietary analyses using stable light isotopes and the employment of Bayesian chronological modeling in the interpretation of ¹⁴C dates have progressed over the last two decades, and studies are beginning to readdress this view (Millard 2015). In this study, we aim to show that by combining archaeological, osteological, and paleodiet research in a Bayesian framework, it is now possible to ¹⁴C date a medieval event very precisely, opening up new research questions and the possibility to better relate archaeological finds with historically documented events.

St Alban's Odense

Odense is situated on the island of Funen in central Denmark. During the medieval period, Odense was an important commercial town and a clerical center, with its own bishopric and numerous churches and monasteries. St Alban's Church is believed to be one of the first churches on Funen, and is possibly identical to a church mentioned in AD 988. After having been used as consecrated burial ground for around 500 years, the church was abandoned in the wake of the Lutheran reformation in AD 1536 and demolished in the 1540s (Eliassen et al. 2001). A series of archaeological excavations were carried out by Odense City Museums, most recently in 2015–2016 (Albrechtsen 1956; Arentoft 1985; Christensen 1999; Pedersen and Bjerregaard 2016). Vital parts of the church and cemetery were destroyed in the 1950s when an underground carpark was

*Corresponding author. Email: Helene.rose@schloss-gottorf.de.

constructed, but the excavations have given a rough idea of the building history of the church and the boundaries of the church yard (Eliassen et al. 2001; Christensen and Bjerregaard 2017). The recent excavation (OBM3183) has revealed ca. 360 individuals buried east and north of the church. A group of graves with brick-built coffins are typologically dated to the mid-12th century to 13th century, while the remaining graves are only dated stratigraphically to AD 1100–1500. Following medieval burial practice, the large majority of the graves contained a single individual, but a handful of graves held two or more individuals (Pedersen and Bjerregaard 2016). Multiple graves have been observed in medieval cemeteries throughout Scandinavia, most often containing juveniles and only more rarely adults (Ranåker 2009). These graves reflect the contemporaneous death of the interred individuals, as burials in the Middle Ages usually took place within one or two days after death (Nilsson 1987). We know little of the belief system behind this custom, but incidents of multiple death in a short period of time, caused by e.g. violence, accidents or epidemics, could lead to communal graves being dug in haste (Ranåker 2009; Millard 2015).

About 25 m east of the church, a multiple grave containing five juveniles received special attention during the 2015–2016 excavation. Because of the heavily mixed burial soil it was not possible to define the edges of grave 156, but based on the buried individuals it must have been minimum 1 m wide \times 1.7 m long. The grave was intercut by younger graves to the east. No coffin remains were found, but the presence of small bronze pin fragments next to burial x244 indicates it might have been wrapped in a shroud for burial, as is often the case for medieval burials. The five juveniles were placed partly overlapping in a supine position orientated roughly E–W, with the heads towards west. The internal stratigraphy in the grave was as follows; burials x241 and x243 placed side by side, partly overlain by burials x242 and x244, which in turn were overlain by burial x252 (Figure 1).

A study of long-term trends in medieval inhumation practices (Kieffer-Olsen 1993) found that in the earliest Christian burials, the arms were positioned beside the body (position A); in later

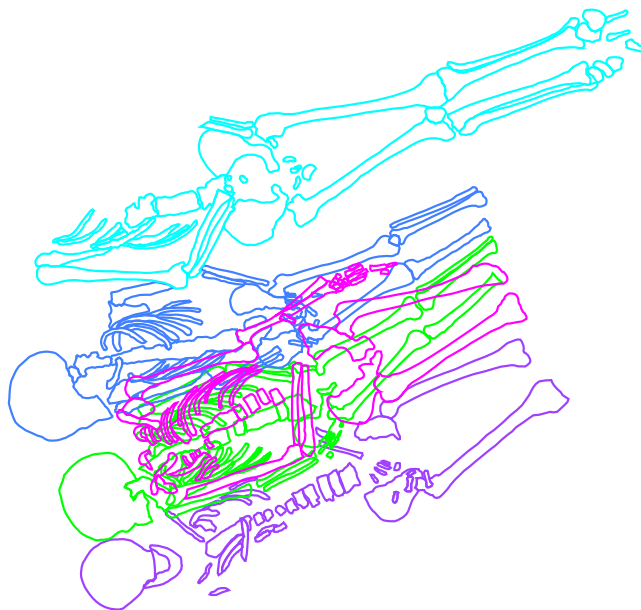


Figure 1 Multiple grave 156, St Alban's Odense.

burials, the hands were folded in the pelvic area (position B), and subsequently folded across the lower stomach (position C). In the latest burials, both hands were folded across the chest (position D). Arm positions therefore provide relative dates for the use of a burial ground, but at an individual level may be misleading, as the different positions overlap in time. The individuals buried in grave 156 had the arms placed in position B, indicating a possible date between mid-13th to mid-15th centuries, but it was not possible to confirm this stratigraphically.

Establishing Plague as Cause-of-Death

Paleopathology is a long-established interdisciplinary science, combining medicine, osteology and archaeology, yet it often struggles to establish a cause-of-death. Many diseases only affect the soft tissues, rendering it practically impossible to establish a cause-of-death based only on visual inspection of bones (Waldron 2009).

Acute infectious diseases such as common pneumonia, measles or smallpox could be fatal, but the great killer in the medieval period was the plague. It swept across Europe AD 1347–1352 and reappeared several times over the next centuries. The plague had a devastatingly high mortality rate, yet caused no visible pathological change of the skeleton (Roberts and Manchester 2005). Thus, plague victims could only be identified from written sources, or their burial in known epidemic cemeteries, such as East Smithfield in London (DeWitte 2010). This situation is changing, with on-going research into ancient DNA of *Yersinia pestis* (Luhmann et al. 2017). Another approach could be to date potential plague victims precisely, and try to relate them to historically documented plague events.

Historian Lars Bisgaard (2009) attempted to track Danish plague patterns from AD 1360–1500, hypothesizing that a plague epidemic would have caused a sudden increase in the number of “deeds of gift.” These gift letters, which usually have an exact date, concern endowments for perpetual masses and testaments and are connected with the general preparation for death, although not exclusively connected to the actual time-of-death. Deeds of gift would often be established as the rumor of a coming plague epidemic spread or afterward on behalf of the newly deceased, causing a spread of dates around the actual epidemic event. The preserved written records from Denmark are fragmentary, but it was possible to isolate peaks in the annual number of deeds, which could to varying degrees be confirmed as plague epidemics through documented references from neighbouring countries. Bisgaard was able to define 15 plausible plague epidemics in the period AD ca. 1350–1500, pointing to a decadal plague cycle.

MATERIAL AND METHODOLOGY

Sample Selection

It was decided to sample a lower first permanent molar (M1) from each of the five primary burials, disregarding any stray teeth. Using a dentist’s drill, the tooth was separated from the root with a horizontal cut just beneath the enamel-dentine junction. The crown was divided into two with a vertical cut down the middle. Next, using an abrasive drill bit, all the dentine was pulverized and removed as a bulk sample. Because of the individuals’ young ages-at-death, secondary dentine formation could be disregarded.

Laboratory Methods

All five samples were extracted and dated at the Leibnitz-Labor, Kiel, Germany. Dentine powder was ultrasonicated for 30 min in 10 mL acetone to remove any grease, then rinsed 5 × with demineralized water. Samples were then demineralized in HCl (ca. 1%) at room

temperature. Next they were treated with 1% NaOH (20°C, 1 hr) to remove mobile humic acids and finally again with 1% HCl (20°C, 1 hr). Collagen was gelatinized overnight in demineralized water at 85°C at pH = 3, filtered through a 0.45 µm pore silver filter to remove insoluble particles, and freeze-dried before analysis (Grootes et al. 2004).

For AMS ¹⁴C dating, an aliquot of collagen was combusted with copper oxide and silver wool at 900°C in pre-combusted quartz tubes. The obtained CO₂ was reduced with H₂ over about 2 mg of Fe powder as catalyst, and pressed into a target holder for AMS measurement. Background and known-age bones were extracted and dated concurrently, with satisfactory results.

An aliquot of collagen from each sample was sent to Aarhus AMS Center, Denmark, for duplicate measurements of %C, %N, δ¹³C, and δ¹⁵N using a continuous-flow IsoPrime IRMS coupled to an Elementar PyroCube elemental analyzer. δ¹³C and δ¹⁵N values are normalized to the VPDB and AIR scale respectively using an in-house gelatin standard, GelA. Repeated measurement (n = 15) of the GelA standard yielded a standard deviation for δ¹³C < 0.2‰ and for δ¹⁵N < 0.4‰.

RESULTS AND DISCUSSION

Osteology

The osteological analysis of grave 156, St Alban's Odense, builds on an unpublished museum report from ADBOU, the Unit of Anthropology at Southern Denmark University (Olsen 2016) and on analyses carried out by the first author. Age determinations of juveniles rely on dental development and eruption, length of long bones, and ossification of epiphyses (Bass 1995; Scheuer and Black 2000). Sex determination is only possible when the primary pelvic bones (ilium, ischium, and pubis) have completely ossified around the age of 16 yr (Bass 1995). The preservation of the skeletons was medium-good, compared to the norm of Danish medieval human material. No clear cause-of-death or signs of violent trauma were recognized. Osteological information, given in Table 1, is inconclusive, but it is possible that the five individuals were killed by an acute infectious disease.

Unlike bone collagen, collagen in dentine is not remodeled over time. Following the London Atlas the M1 starts forming dentine at 0.3 ± 0.1 yr and the crown is complete at 3.5 ± 0.5 yr (AlQahtani et al. 2010; Beaumont and Montgomery 2015). Applying the quoted variation, a conservative formation period for M1 crown dentine is 0.2–4.0 yr of age, with a midpoint of 2.0 ± 0.5 yr. Using the midpoint of dentine formation and ages-at-death (Table 1) we calculated individual age offsets between 5.3 ± 1.0 yr and 14.4 ± 1.5 yr for the five burials (Figure 2).

Table 1 Osteological results.

Burial	Sex	Age-at-death (yr)	Preservation	Pathology
x241	Male?	15–18	Good	Indistinct signs of pathology on skull
x242	?	7–9	Medium	—
x243	?	13–16	Medium	—
				A severe growth deficiency is visible in the enamel of all permanent teeth
x244	?	14–16	Good	Indistinct signs of pathology on skull
x252	?	7–9	Medium	Indistinct signs of pathology on skull

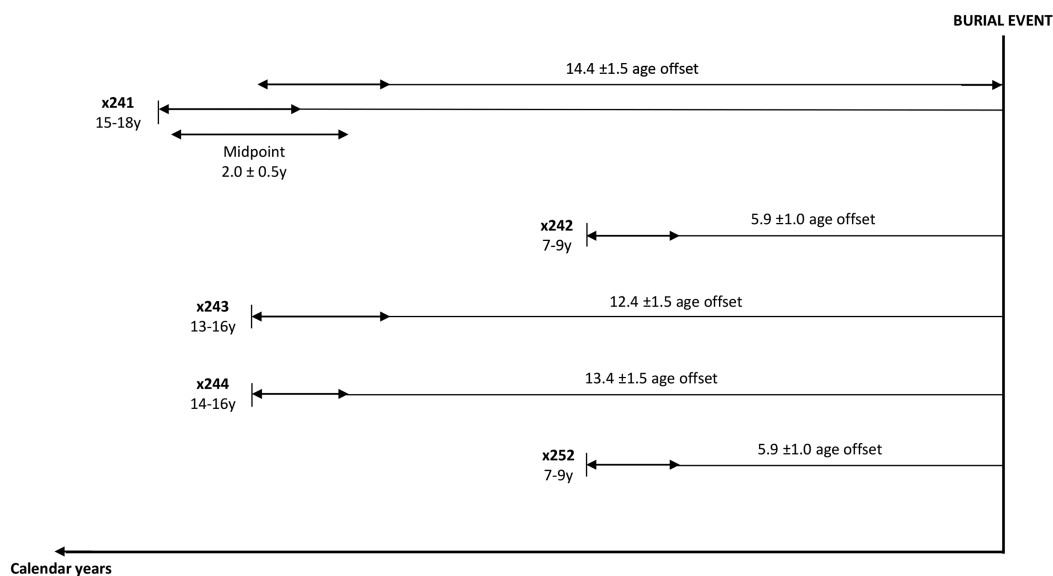


Figure 2 Schematic illustrating of individual age offsets, using age-at-death estimates and midpoint 2.0 ± 0.5 yr of M1 crown dentine formation.

The offsets between dentine formation and age-at-death are needed to estimate the date of the burial event, given the ^{14}C events embodied in the samples. By sampling the same tooth in individuals with different ages-at-death, we ensured that collagen formation in our samples was not exactly contemporaneous (and in fact may have spanned a decade). Short-term changes in diet due to e.g. famine will therefore not have affected all five individuals. This strategy aimed to increase the potential dietary differences between individuals, and therefore to maximize potential differences in dietary reservoir effects.

Isotopic Results

Samples from all five individuals had acceptable collagen yields of 2.1–2.9% and satisfactory atomic C/N ratios, well within the commonly quoted range of 2.9–3.6 (DeNiro 1985). Details of AMS and EA-IRMS results for grave 156 are given in Table 2.

The five AMS dates are conventional ^{14}C ages and corrected for fractionation using $\delta^{13}\text{C}$ measured by AMS (Stuiver and Polach 1977). A combination of the dates show them to be statistically inconsistent [$T = 21.4$, $T'(5\%) = 9.5$, $\nu = 4$] (Ward and Wilson 1978). The difference between burials x242 and x252 is 125 ± 25 yr (5σ), which is highly significant. Both x243 and x241 are also significantly older in ^{14}C age (by $>2\sigma$) than x242, and x252's ^{14}C age is significantly older than those of all four of the other burials. The ^{14}C calibration curve is relatively steep in this period, and even small differences in the actual date of dentine formation might lead to differences in ^{14}C ages, but x242 and x252 had the same intrinsic ages (both individuals died at 7–9 years of age). Unless x252 actually pre-dates x242, therefore, their ^{14}C age difference must be due to dietary reservoir effects. Given the archaeological stratigraphic information (see above), x252 was the last individual interred in the grave, but it is the oldest in ^{14}C years. Thus, even if a single-event interpretation were to be rejected, dietary reservoir effect corrections would be necessary to reconcile the ^{14}C ages with the sequence of burials.

Table 2 AMS and EA-IRMS results.

Burial	Element	Sample ID	Yield (wt.%)	AMS $\delta^{13}\text{C}$ (‰)	IRMS $\delta^{13}\text{C}$ (‰ VPDB)	$\delta^{15}\text{N}$ (‰ air)	Atomic C/N	Corr. pMC	Conven. ^{14}C age
x241	Lower 1st perm. molar, left	KIA-51875	2.4	-20.52	-19.79 ± 0.02	12.09 ± 0.03	3.1	93.31 ± 0.19	556 ± 16
x242	Ditto, right	KIA-51876	2.1	-21.09	-20.37 ± 0.14	11.36 ± 0.23	3.1	94.08 ± 0.22	491 ± 19
x243	Ditto, right	KIA-51877	2.9	-21.41	-20.20 ± 0.18	10.85 ± 0.33	3.1	93.46 ± 0.21	544 ± 18
x244	Ditto, left	KIA-51878	2.9	-20.07	-19.78 ± 0.07	10.70 ± 0.06	3.1	93.83 ± 0.20	512 ± 17
x252	Ditto, left	KIA-51879	2.5	-19.23	-18.84 ± 0.11	12.72 ± 0.15	3.2	92.62 ± 0.19	616 ± 16

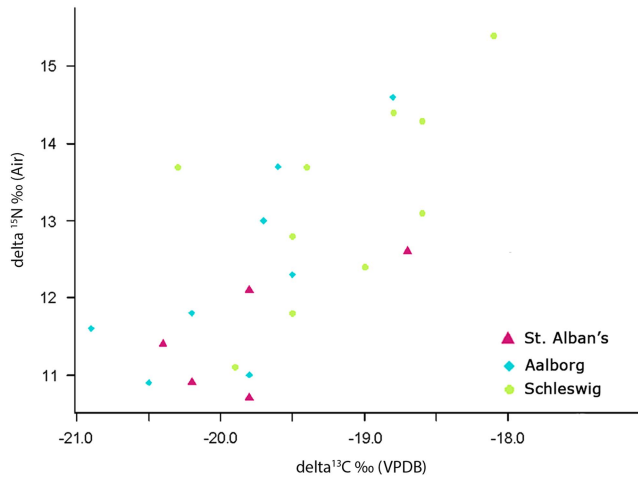


Figure 3 Stable isotope values from St Alban's Odense, Aalborg Northern Jutland (van der Sluis et al. 2016) and Schleswig Northern Germany (Grupe et al. 2013).

The IRMS analyses were carried out in duplicate, only the IRMS $\delta^{13}\text{C}$ values were used for dietary analysis. Reported measurement uncertainties were small ($\delta^{13}\text{C} \pm 0.1$, $\delta^{15}\text{N} \pm 0.2$) and the repeated measurement standard errors are consistent with the reported uncertainties ($\delta^{13}\text{C}$ 0.2, $\delta^{15}\text{N}$ 0.3). Burials x243 and x244 died at similar ages and show comparable ^{14}C ages and stable isotope values. This might be a case of twins, but as aDNA analyses have not been performed it is not possible to test whether they were indeed related.

Stable isotope values for St Alban's and two other medieval populations of comparable age-at-death are shown in Figure 3: eight juveniles from Aalborg, Northern Jutland (mean age = 2.9 yr) (van der Sluis et al. 2016) and 10 juveniles from the late phase at Rathausmarkt in Schleswig, Northern Germany (mean age = 1.6 yr) (Grupe et al. 2013). The overall pattern approximates a mixing line between marine (higher $\delta^{13}\text{C}$ and $\delta^{15}\text{N}$) and terrestrial diets. The St Alban's individuals mainly cluster in the bottom left part of the plot, suggesting marine food might have played less of a role in medieval Odense than in contemporary Aalborg and Schleswig.

A single outlier from Schleswig has a significantly elevated $\delta^{15}\text{N}$ signal, relative to its $\delta^{13}\text{C}$ value, probably due to delayed weaning. When a child is breastfed, its $\delta^{15}\text{N}$ values will become elevated, one trophic level higher than the mother, and gradually come down when other food sources are introduced. The duration and termination of this transition can vary between populations (Richards et al. 2002; Burt 2013). Although it is possible that the Odense individuals were weaned within the period of M1 dentine formation, we expect any breastfeeding effect in our samples to be blurred and hard to detect as a result of bulk sampling (compared to incremental dentine samples: van der Sluis et al. 2016). However, the Odense $\delta^{15}\text{N}$ values are relatively low compared to Aalborg and Schleswig, and give no indication of nursing effects.

DIETARY ANALYSIS

Human consumption of marine foods causes ^{14}C age offsets, as marine organisms have global average ^{14}C age of ca. 400 yr (Reimer et al. 2013). The actual marine offset is defined by the difference between the marine and terrestrial calibration curves at any given point in time, which compared to the long-term average increased during the first half of the 15th century (Reimer et al. 2013). To estimate the size of the offsets in individual samples, we need to

Table 3 Estimated marine fish consumption, using different dietary models.

Burial	$\delta^{13}\text{C}$ (‰)	$\delta^{15}\text{N}$ (‰)	Linear mixing model (%)	FRUITS model, protein only (%)	FRUITS model, routed (%)
x241	-19.79	12.09	16.5	7.6 ± 5.6	10.8 ± 5.8
x242	-20.37	11.36	11.5	4.5 ± 4.1	4.9 ± 3.8
x243	-20.20	10.85	12.9	4.7 ± 4.0	4.8 ± 3.8
x244	-19.78	10.70	16.6	6.0 ± 4.8	6.1 ± 4.4
x252	-18.84	12.72	24.7	13.3 ± 7.5	17.4 ± 6.7

quantitatively reconstruct the individual diet and give realistic estimates of ^{14}C -depletion in the aquatic species consumed during the period of collagen formation. The ^{14}C ages are correlated with the stable isotope values, and the dietary reservoir effects in our samples can therefore be attributed to high ^{15}N and ^{13}C foods. We would not expect this pattern if they had consumed significant amounts of freshwater fish from this region (Grupe et al. 2013), which is why we choose not to consider ^{14}C freshwater reservoir effects. Our focus is on dating the burials correctly, not on reconstructing the diet in great detail¹.

Linear Mixing Model

We applied a linear mixing model to estimate the proportion of marine protein in the diet (Arneborg et al. 1999), using $\delta^{13}\text{C}$ endpoints of -21.7 for 100% terrestrial and -10.1 for 100% marine diets (Fischer et al. 2007). Endpoints are corrected for 1‰ trophic-level shift from diet to consumer. These values were derived from Mesolithic and Neolithic faunal and marine species from Denmark, but we do not expect baseline values to have been significantly different in the medieval period. The linear mixing model approach does not provide a clear method for the propagation of uncertainties.

The linear mixing model estimates the five individuals to have consumed 11.5–24.7% marine protein; with x252 having consumed on average 10% more than the others (Table 3).

Bayesian Dietary Reconstruction

Next, a Bayesian dietary reconstruction model was applied to estimate the proportion of marine protein in the diet. We used the multi-proxy mixing model FRUITS (vers.3.), which allows us to consider the contribution of each food group to each isotope value and to incorporate the uncertainty in their isotopic values (Fernandes et al. 2014a).

Our basic model assumes that three food groups were significant: plants, animals, and marine fish, and that protein was the only carbon source for human collagen. Stable isotope data on cereals (oats, hulled barley, rye) from three medieval sites in Odense (Hammers 2017) are used to estimate parameter values for plant foods. Isotope values for domestic animals (cattle, pig, sheep) on material from Viking Age Schleswig and medieval Schleswig (Doppler et al. 2010) are used to estimate parameter values for animal foods. Parameter values for plant and animal foods are corrected for -2‰ carbon offset from collagen to protein and a -2‰ nitrogen offset from bulk to protein (Fernandes et al. 2012, 2014a).

For marine fish (cod, perch, haddock, garfish, plaice, sturgeon), we used isotope values from Haithabu and Schleswig (Doppler et al. 2010). These values are not weighted by species

¹A more detailed diet reconstruction was hampered by low collagen yields, which did not allow measurements of $\delta^{34}\text{S}$.

Table 4 Parameter values for three food groups used in FRUITS models.

	Food group	Protein	Energy (lipids, carbohydrates)	Protein $\delta^{15}\text{N}$	Protein $\delta^{13}\text{C}$	Energy $\delta^{13}\text{C}$
Protein only						
	Fish	$70 \pm 5\%$	—	$14.0 \pm 1.0\text{‰}$	$-16.5 \pm 1.0\text{‰}$	—
	Animal	$30 \pm 5\%$	—	$7.0 \pm 0.5\text{‰}$	$-24.0 \pm 0.5\text{‰}$	—
	Plant	$10 \pm 2\%$	—	$4.0 \pm 0.5\text{‰}$	$-25.0 \pm 0.5\text{‰}$	—
Dietary routing						
	Fish	$70 \pm 5\%$	$30 \pm 5\%$	$14.0 \pm 1.0\text{‰}$	$-16.5 \pm 1.0\text{‰}$	$-24.5 \pm 1.0\text{‰}$
	Animal	$30 \pm 5\%$	$70 \pm 5\%$	$7.0 \pm 0.5\text{‰}$	$-24.0 \pm 0.5\text{‰}$	$-30.0 \pm 0.5\text{‰}$
	Plant	$10 \pm 2\%$	$90 \pm 2\%$	$4.0 \pm 0.5\text{‰}$	$-25.0 \pm 0.5\text{‰}$	$-23.0 \pm 0.5\text{‰}$

prevalence, and significantly do not include herring. In the Middle Ages, the herring markets in the Øresund exported vast quantities of salted herring to all of Northern Europe, but by the beginning of the 15th century the herring stock started to dwindle and the trade soon lost its importance (Etting 2004). The St Alban's AMS dates point towards a burial event after AD 1400, where herring most likely did not contribute significantly to the marine diet and can therefore be ignored. Marine parameter values are corrected by -2‰ carbon and $+2\text{‰}$ nitrogen offsets from collagen to protein (Fischer et al. 2007; Fernandes et al. 2014b).

It is difficult to define a specific food group, but from other studies we expect the population of Medieval Odense to have consumed animal products like milk, cheese and eggs, but very little actual flesh, animal or fish (Yoder 2010; Erynck et al. 2014). As a consequence the prior constraint that plant food consumption will exceed that of animal foods is imposed. A diet to collagen offset of $4.8 \pm 0.5\text{‰}$ for $\delta^{13}\text{C}$ and $4.5 \pm 1.0\text{‰}$ for $\delta^{15}\text{N}$ is assumed (Fernandes et al. 2014a). Table 4 summarizes the parameter values applied in our basic model.

The Bayesian dietary reconstruction model cannot distinguish plant and animal foods, which given the uncertainty in diet-collagen offsets are too isotopically similar. It is able to identify marine food as it has more distinct isotopic values, and estimates the five individuals to have consumed 4.5–13.3% marine protein, but with large uncertainty levels, reflecting the combined uncertainties of the model.

Dietary Routing

A dietary proxy signal not only reflects the consumed food groups, but more specifically the food group fractions such as e.g. carbohydrates and lipids. These macronutrients do not contribute proportionately to the proxy signal in collagen, which is formed predominantly from dietary protein, but they do have some influence. Dietary routing can be incorporated in FRUITS to provide more accurate dietary estimates (Fernandes et al. 2014a).

We constructed a model considering both protein and energy macronutrients (carbohydrates and lipids) as food fractions; human collagen is assumed to derive $75 \pm 5\%$ of its carbon from protein, and the balance from energy macronutrients. The same offset values from bulk and collagen to protein values apply as in the model above, but a -2‰ carbon offset from bulk to energy is added for plant values and likewise from collagen to energy for animal values (Fernandes et al. 2012; Fernandes et al. 2014a). Marine parameter values include a -10‰ $\delta^{13}\text{C}$ offset from collagen to energy (Fischer et al. 2007; Fernandes et al. 2014b). As above the model

assumes a diet to collagen fractionation of $4.8 \pm 0.5\text{‰}$ for $\delta^{13}\text{C}$ and $4.5 \pm 1.0\text{‰}$ for $\delta^{15}\text{N}$ (Fernandes et al. 2014a). Again the prior constraint that plant food consumption will exceed that of animal foods is imposed, and protein intake is limited to 10–40% of total calories consumed. Table 4 summarizes the parameter values applied in the model.

As before, the dietary routing model cannot distinguish plant and animal foods, but is able to identify marine food. It estimates the five individuals to have consumed 4.8–17.4% marine calories, again with large uncertainty levels.

The three dietary reconstruction models report differing intakes of marine food, but not alarmingly so given the large uncertainties. Nevertheless, all models appear to under-estimate the marine contribution to diet, given ^{14}C -age differences between individuals. If the marine foods had a reservoir effect close to the global marine average, a dietary reservoir effect of >100 yr in individual x252 would require at least 25% of the carbon in this sample's collagen to be derived from marine foods. The linear mixing model provides this, whereas the two FRUITS models give more conservative estimates (Table 3). When we take into account that the marine offset was slightly higher than the long-term mean in the first decades of the 15th century when the collagen was formed, this could explain some of the apparent underestimation in the FRUITS model. Another factor could be that our preferred plant $\delta^{13}\text{C}$ parameter values in the FRUITS model are too positive, or that there is a more ^{14}C -depleted food source (i.e. freshwater fish). The linear mixing model employs such slightly lower $\delta^{13}\text{C}$ values for terrestrial end-members and slightly higher values for marine end-members, but we are more confident using actual isotope data for the different food groups. The dietary routing model incorporates more information on food group fractions and isotopic offsets, and better reflects what we know about the potential diets of these individuals.

Diet and Dating: OxCal Model for Grave 156, St Alban's Odense

We use OxCal v4.3.2 and the IntCal13 and Marine13 international calibration curves with the resolution set to one year (Bronk Ramsey 2009; Reimer et al. 2013). The five ^{14}C dates are calibrated with a mix of terrestrial and marine carbon inputs, defined by the FRUITS dietary routing model (Table 4 and footnote²). Individual calendar age offsets between 5.3 ± 1.0 yr and 14.4 ± 1.5 yr are applied.

The marine ^{14}C age varies at the regional level and requires offset correction using local ΔR values. It was difficult to determine the geographical origin of the consumed marine food and thereby finding an appropriate ΔR value for our OxCal model. A new ancient DNA study of cod from Viking-age Haithabu has revealed its origin to be Arctic, probably caught at Lofoten and traded as dried fish as far as Northern Germany (Star et al. 2017). The mean of the nearest 100 ΔR data points to Odense on Chrono Marine Reservoir Database³, which cover the Baltic, eastern North Sea and the Norwegian Sea, was statistically no different from zero (32 ± 18 SE) and it was therefore decided not to include a local ΔR correction. The marine component was therefore calibrated using the global marine calibration model (Reimer et al. 2013).

²OxCal code using dietary routing estimates:

```
Curve("terrestrial", "Intcal13.14c"); Curve("Marine", "Marine13.14c"); Combine("Burial")
{Mix_Curves("x241", "terrestrial", "Marine", 10.8, 5.8); R_Date("x241 KIA-51875", 556, 16) + N(14.4, 1.5);
Mix_Curves("x242", "terrestrial", "Marine", 4.9, 3.8); R_Date("x242 KIA-51876", 491, 19) + N(5.9, 1);
Mix_Curves("x243", "terrestrial", "Marine", 4.8, 3.8); R_Date("x243 KIA-51877", 544, 18) + N(12.4, 1.5);
Mix_Curves("x244", "terrestrial", "Marine", 6.1, 4.4); R_Date("x244 KIA-51878", 512, 17) + N(13.4, 1.5);
Mix_Curves("x252", "terrestrial", "Marine", 17.4, 6.7); R_Date("x252 KIA-51879", 616, 16) + N(5.9, 1); }
```

³URL: <http://calib.org/marine/>.

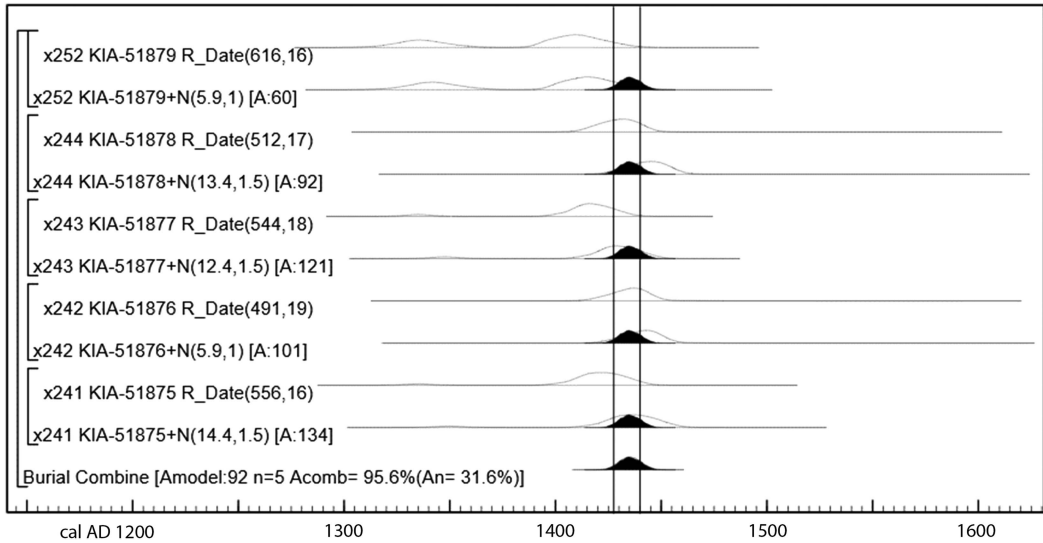


Figure 4 Estimated burial date of St Alban's grave 156 using the routed diet reconstruction proposed in this paper (above). OxCal indices for individual dates (A) are at or above the >60 threshold, indicating satisfactory agreement of individual calibrations assuming the five individuals are contemporary. Vertical lines indicate plague events AD 1427–1428 and 1440 discussed in this paper (below).

The archaeological excavation information shows the five burials to be contemporaneous, but their combined calibrated dates are statistically inconsistent (see above). When applying the estimated marine consumption given by the linear mixing model, the OxCal output gives a 95.4% probability of the burial date to be AD 1438–1452, but with a very poor index of agreement ($A_{\text{model}} = 33.6$), whereby the model is rejected. When applying the estimates from the FRUITS protein-only model, the OxCal output gives a 95% probability of the burial date to be AD 1423–1443 ($A_{\text{model}} = 78$). The index is satisfactory for the model, but poor for the individual date of x252 (A: 37), whose diet-correction is insufficient to fit the single-event model. We therefore choose to reject this model as well. Finally when applying the estimates from the dietary routing model, the OxCal output gives a 95% probability of the burial date to be AD 1425–1445 with a mean of 1435 ± 5 ($A_{\text{model}} = 92$, Figure 4). Individual x252 (A: 60) has a satisfactory index showing the diet-correction to be sufficient to be compatible with a single event and we accept the model.

The archaeological context of the grave provides very little prior information besides the five individuals being buried with an arm position B, which has a wide date range between mid-13th to mid-15th centuries. Few arm position B are expected to date to the 15th century, but given the large chronological overlap of positions, the archaeological information does not contradict our proposed date of the burial.

Given the results above we can now try to relate the burial event to the historical information on plague epidemics in Denmark. Bisgaard mentions two events possibly coinciding with St Alban's grave 156; AD 1427–1428 and 1440. He states the first event to be uncertain although not improbable, whereas the latter event is reasonably certain (Bisgaard 2009). The 95% probability range of our FRUITS routed dietary model overlap both events, making it difficult to decide which is more likely.

Given the ^{14}C -age differences of the individuals we expected a dietary reservoir effect of >100 yr in individual x252 (i.e., at least 25% of the carbon in x252's collagen should be from marine foods). The model estimated x252 to have consumed 17.4% marine protein, which appears to underestimate the marine contribution to the diet. Increasing the marine contribution would make the burial younger, which is why we believe the real calendrical date of the burial is likely somewhere in the younger part of the range. Accordingly we find the younger plague event AD 1440 to be the most plausible. Whether the five individuals were indeed plague victims or instead died from some other epidemic disease around the same time is impossible to ascertain given our current understanding.

CONCLUSION

We have shown, by exploiting differences in dietary reservoir effects it is possible to refine the dates of multiple burials, and potentially date such events to within a range of <20 years. By combining archaeological, osteological and paleodiet research in a Bayesian framework we were able to date St Alban's grave 156 to AD 1425–1445 (95% probability), an interval in which two plague epidemics took place in Denmark. It was not possible to establish a positive link between the grave and a plague event, as to do so would require aDNA analyses.

ACKNOWLEDGMENTS

Analyses were funded through the Center for Baltic and Scandinavian Archaeology (ZBSA)'s Man and Environment research theme, including subproject G1: *Timescales of Change - Chronology of cultural and environmental transformations* of the Collaborative Research Center Scales of Transformation: *Human-environmental Interaction in Prehistoric and Archaic Societies* (DFG-SFB 1266). The authors would like to thank Odense City Museum for giving access and permission to sample the teeth. We would also like to thank the anonymous reviewers for their constructive comments and valuable input on the manuscript.

REFERENCES

- Albrechtsen E. 1956. Albani Torv. *Fynske Minder* 1956:203–19.
- AlQahtani SJ, Hector MP, Liversidge HM. 2010. Brief communication: the London atlas of human tooth development and eruption. *American Journal of Physical Anthropology* 142(3): 481–90.
- Arentoft E. 1985. Sankt Albani Kirke. Albani Kirke & Torv. *Fynske Studier* XIV:7–59.
- Arneborg J, Heinemeier J, Lynnerup N, Nielsen HL, Rud N, Sveinbjörnsdóttir ÁE. 1999. Change of diet of the Greenland Vikings determined from stable carbon isotope analysis and ^{14}C dating of their bones. *Radiocarbon* 41(2):157–68.
- Bass WM. 1995. *Human Osteology: A Laboratory and Field Manual*. Columbia (MO): Missouri Archaeological Society.
- Beaumont J, Montgomery J. 2015. Oral histories: a simple method of assigning chronological age to isotopic values from human dentine collagen. *Annals of Human Biology* 42(4):407–14.
- Bisgaard L. 2009. Danish Plague Patterns, 1360–1500. In: Bisgaard L, Søndergaard L, editors. *Living with the Black Death*. Odense: University Press of Southern Denmark. p 85–108.
- Bronk Ramsey C. 2009. Bayesian analysis of radiocarbon dates. *Radiocarbon* 51(1):337–60.
- Burt NM. 2013. Stable isotope ratio analysis of breast-feeding and weaning practices of children from medieval Fishergate House York, UK. *American Journal of Physical Anthropology* 152(3):407–16.
- Christensen JT. 1999. Døden skiller – om kirkegårdsskel og -skik under Skt. Knuds Plads. *Fynske minder* 1999:83–92.
- Christensen JT, Bjerregaard MM. 2017. Albani Kirke og kirkegård. In: Runge M, Hansen J, editors. *Knuds Odense - Vikingernes By*. Odense. p 116–27.
- DeNiro MJ. 1985. Postmortem preservation and alteration of in vivo bone collagen isotope ratios in relation to palaeodietary reconstruction. *Nature* 317(6040):806–9.
- DeWitte SN. 2010. Age patterns of mortality during the Black Death in London, A.D. 1349–1350. *Journal of Archaeological Science* 37(12): 3394–400.
- Doppler S, Vohberger M, von Carnap-Bornheim C, Heinrich D, Peters J, Grupe G. 2010. Biodiversity of archaeological fauna in the estuarine palaeoecosystem of the Schlei Fjord, northern Germany:

- isotopic evidence. *Documenta Archaeobiologiae* 8:21–70.
- Eliassen K, Johannsen BB, Johannsen H, Vedsø M. 2001. †S. Albani Kirke. *Danmarks Kirker* IX(3): 1729–48.
- Ervynck A, Boudin M, van den Brande T, van Strydonck M. 2014. Dating human remains from the historical period in Belgium: diet changes and the impact of marine and freshwater reservoir effects. *Radiocarbon* 56(2):779–88.
- Etting V. 2004. *Queen Margrete I (1353–1412) and the Founding of the Nordic Union*. Leiden: Brill.
- Fernandes R, Nadeau M-J, Grootes PM. 2012. Macronutrient-based model for dietary carbon routing in bone collagen and bioapatite. *Archaeological and Anthropological Sciences* 4(4):291–301.
- Fernandes R, Millard AR, Brabec M, Nadeau M-J, Grootes P. 2014a. Food reconstruction using isotopic transferred signals (FRUITS): a Bayesian model for diet reconstruction. *PLOS ONE* 9(2): e87436.
- Fernandes R, Meadows J, Dreves A, Nadeau M-J, Grootes P. 2014b. A preliminary study on the influence of cooking on the C and N isotopic composition of multiple organic fractions of fish (mackerel and haddock). *Journal of Archaeological Science* 50:153–9.
- Fischer A, Olsen J, Richards M, Heinemeier J, Sveinbjörnsdóttir ÁE, Bennike P. 2007. Coast-inland mobility and diet in the Danish Mesolithic and Neolithic: evidence from stable isotope values of humans and dogs. *Journal of Archaeological Science* 34(12):2125–50.
- Grootes PM, Nadeau M-J, Rieck A. 2004. ¹⁴C-AMS at the Leibniz-Labor: radiometric dating and isotope research. *Nuclear Instruments and Methods in Physics Research B* 223–224:55–61.
- Grupe G, Von Carnap-Bornheim C, Becker C. 2013. Rise and fall of a medieval trade centre: economic change from viking Haithabu to medieval Schleswig revealed by stable isotope analysis. *European Journal of Archaeology* 16(1):13–66.
- Hammers NM. 2017. Assessing cultivation conditions and variation through stable isotope analysis (delta13C and delta15N) on cereal crops from medieval Odense (Denmark). Radiocarbon and Diet 2 Conference. Aarhus University.
- Kieffer-Olsen J. 1993. Grav og gravskik i det mid delalderlige Danmark: 8 kirkegårdsudgravninger. Højbjerg: Afd. for Middelalder- og renaissancearkæologi.
- Luhmann N, Doerr D, Chauve C. 2017. Comparative scaffolding and gap filling of ancient bacterial genomes applied to two ancient *Yersinia pestis* genomes. *Microbial Genomics* 3:1–11.
- Millard A. 2015. *Palace Green Library Excavations 2013 (PGL13): Chronology of the Burials*. Durham: Department of Archaeology, Durham University.
- Nilsson B. 1987. Död och begravning. Begravningskicket i Norden. Tanke och tro. Aspekter på medeltidens tankevärld och fromhetsliv. *Studier til det medeltida Sverige* 3:133–50.
- Olsen TB. 2016. Antropologisk rapport OBM3183, Albani Torv. Retsmedicinsk Institut, Antropologisk Afdeling, ADBOU, Syddansk Universitet.
- Pedersen K, Bjerregaard MM. 2016. Sygdom, død og begravelse på Albani Kirkegård. Observationer fra en igangværende arkæologisk udgravning. *Bibliotek for Læger* 208:158–77.
- Ranåker M. 2009. Flerpersonsgravar uder medeltid. Västerhus kyrkogård belyst av andra begravningsplatser. In: Iregren E, Alexandersen V, Redin L, editors. *Västerhus. Kapell, kyrkogård och befolkning: Kungl. Vitterhets Historie och Antikvitets Akademien*. p 26–39.
- Reimer PJ, Bard E, Bayliss A, Beck JW, Blackwell PG, Ramsey CB, Buck CE, Cheng H, Edwards RL, Friedrich M, Grootes PM, Guilderson TP, Hafliadason H, Hajdas I, Hatté C, Heaton TJ, Hoffmann DL, Hogg AG, Hughen KA, Kaiser KF, Kromer B, Manning SW, Niu M, Reimer RW, Richards DA, Scott EM, Southon JR, Staff RA, Turney CSM, van der Plicht J. 2013. IntCal13 and Marine13 radiocarbon age calibration curves 0–50,000 years cal BP. *Radiocarbon* 55(4):1869–87.
- Richards MP, Mays S, Fuller BT. 2002. Stable carbon and nitrogen isotope values of bone and teeth reflect weaning age at the Medieval Wharram Percy site, Yorkshire, UK. *American Journal of Physical Anthropology* 119(3):205–10.
- Roberts C, Manchester K. 2005. *The Archaeology of Disease*. Ithaca (NY): Cornell University Press.
- Scheuer L, Black S. 2000. *Developmental Juvenile Osteology*. San Diego (CA): Academic Press.
- Star B, Boessenkool S, Gondek AT, Nikulina EA, Hufthammer AK, Pampoulie C, Knutsen H, André C, Nistelberger HM, Dierking J, Peterleit C, Heinrich D, Jakobsen KS, Stenseth NC, Jenstoft S, Barrett JH. 2017. Ancient DNA reveals the Arctic origin of Viking Age cod from Haithabu, Germany. *Proceedings of the National Academy of Sciences* 114(34):9152–7.
- Stuiver M, Polach HA. 1977. Discussion: reporting of ¹⁴C data. *Radiocarbon* 19(3):355–63.
- van der Sluis LG, Reimer PJ, Lynnerup N. 2016. Investigating intra-individual dietary changes and ¹⁴C ages using high-resolution $\delta^{13}\text{C}$ and $\delta^{15}\text{N}$ isotope ratios and ¹⁴C ages obtained from dentine increments. *Radiocarbon* 57(4):665–77.
- Waldron T. 2009. *Palaeopathology*. Cambridge: Cambridge University Press.
- Ward GK, Wilson SR. 1978. Procedures for comparing and combining radiocarbon age determinations: a critique. *Archaeometry* 20(1):19–31.
- Yoder C. 2010. Diet in medieval Denmark: a regional and temporal comparison. *Journal of Archaeological Science* 37(9):2224–36.

Appendix 6 Paper 3



Radiocarbon Dating Cremated Bone: A Case Study Comparing Laboratory Methods

Authors: Rose, H. A., Meadows, J., Palstra, S. W. L., Hamann, C., Boudin, M., & Huels, M.

Published 2019 in *Radiocarbon*: 61(5), 1581-1591. doi:10.1017/RDC.2019.70

Printed with permission by Cambridge University Press

RADIOCARBON DATING CREMATED BONE: A CASE STUDY COMPARING LABORATORY METHODS

Helene Agerskov Rose^{1*}  • John Meadows^{1,2} • Sanne W L Palstra³ • Christian Hamann² • Mathieu Boudin⁴ • Matthias Huels² 

¹Center for Baltic and Scandinavian Archaeology (ZBSA), Schleswig-Holstein State Museums Foundation, Schlossinsel 1, Schleswig 24837, Germany

²Christian-Albrechts-Universitaet zu Kiel, Leibniz-Labor für Altersbestimmung und Isotopenforschung, Kiel, Germany

³University of Groningen, Center for Isotope Research, Groningen, The Netherlands

⁴Royal Institute for Cultural Heritage, Laboratory for Radiocarbon Dating, Brussels, Belgium

ABSTRACT. Radiocarbon (¹⁴C) results on cremated bone are frequently published in high-ranking journals, but ¹⁴C laboratories employ different pretreatment methods as they have divergent perceptions of what sources of contaminants might be present. We found pretreatment protocols to vary significantly between three laboratories (Brussels [RICH], Kiel [KIA], and Groningen [CIO]), which all have a long history of dating cremated bone. We present a case study of 6 sets of replicate dates, to compare laboratory pretreatment protocols, and a further 16 sets of inter-laboratory replicate measurements, which compare specific steps of the conversion and measuring process. The ¹⁴C results showed dates to be reproducible between the laboratories and consistent with the expected archaeological chronology. We found that differences in pretreatment, conversion to CO₂ and accelerator mass spectrometry (AMS) measurement to have no measurable influence on the majority of obtained results, suggesting that any possible diagenesis was probably restricted to the most soluble ≤5% of each sample, as this proportion of the sample mass was removed under all laboratory protocols.

KEYWORDS: comparing laboratory methods, cremated bone, radiocarbon dating, replicate measurements.

INTRODUCTION

Radiocarbon (¹⁴C) dating hydroxyapatite (or bio-apatite) from archaeological samples of cremated bone (CB) has become a standard procedure since Lanting et al. (2001). Results are frequently published in high-ranking journals, yet there are still unknowns in the carbon pathways during cremation and burial (Van Strydonck et al. 2005, 2010; Zazzo et al. 2009, 2012; Hüls et al. 2010; Snoeck et al. 2014, 2016). The re-crystallization of CB makes it less susceptible to contamination from the burial environment, but perception of what sources of contaminants might still be present, influence the choice of pretreatment protocol (Van Strydonck et al. 2005, 2009; Olsen et al. 2008). Indeed, pretreatment protocols vary significantly between the three ¹⁴C laboratories that contributed to this study, which all have a long history of dating CB. They were among the six laboratories which participated in a cremated bone dating intercomparison (Naysmith et al. 2007), in which the analyzed material came from sites in Holland and Belgium, an area of mainly sandy soil with low carbonate levels (Scheele 2016). In that study, which produced uniform results within measurement errors, one laboratory (Kiel) pretreated the material using either an acetic acid treatment (Lanting et al. 2001; Olsen et al. 2008) or a leaching treatment (De Mulder et al. 2007), but the other laboratories used only variations on the first treatment.

We compare methods of pretreatment, conversion to CO₂ and AMS measurement of CB, employed at the Laboratory for Radiocarbon Dating (RICH) in Brussels (Belgium), the Leibniz Laboratory (KIA) in Kiel (Germany), and the Center for Isotope Research (CIO) in Groningen (The Netherlands). The aim is to test whether any differences in methods have a measurable influence on the obtained ¹⁴C results.

*Corresponding author. Email: helene.rose@zbsa.eu.

Different types of replicate measurements allow comparison of different steps of the laboratory protocols. Given the inter-laboratory differences in pretreatment protocols, we considered both type 1 replicates (independent dating by two laboratories of the same CB fragment (“true replicates”) or of different CB fragments from the same burial context, whose ^{14}C ages are expected to be congruent), and type 2 replicates (conversion and measurement at two laboratories of material pretreated by one of them). Measurements of independent type 1 replicates provide an estimate of the interlab reproducibility, whereas replicating type 2 measurements of pretreated material at more laboratories provide insight into specific steps of the conversion and measuring process. A single grave was measured in duplicate within the same laboratory (KIA), and even though the results were congruent, we do not attempt to assess intra-laboratory reproducibility based on such limited data.

MATERIAL

White and fully calcined bone material was selected by visual inspection, following standards described in Olsen et al. (2008). The material came from two archaeological sites ca. 40 km apart in Southern Jutland, Denmark, both on sandy soil with low carbonate levels (Aarre ca. 8°dH , Aarupgaard ca. 10°dH). Both sites are urnfield cemeteries, spanning several phases of the Pre-Roman Iron Age, ca. 500–150 BC. There are only a few absolute dates available from this period and archaeologists instead rely on typo-chronologies (Jensen 2005). The cremated human remains were interred in ceramic urns and covered by small earthen mounds within a circular ditch. A minority of the graves contained metal artifacts, which can be approximately dated by seriation of typological traits.

Aarre urnfield cemetery is a large and well-documented site, with originally up to 1000 burials. Only three graves are included in this study, as most of the site was excavated in the 1950s, before cremated human remains were routinely stored by archaeological institutions (Becker 1961; Lorange 2015).

Aarupgaard urnfield cemetery is an even larger site, with originally up to 1500 burials. Although there is no direct stratigraphic relationship between any of the burials, typo-chronology shows that the cemetery extended southwards over time. The site was totally excavated in the early 1970s and the cremated remains are today archived at the Laboratory of Forensic Anthropology at University of Copenhagen (Jørgensen 1975; Terkildsen 2015). Seventeen graves are included in this study, spanning the entire typo-chronological sequence (Jensen 2005). Both sites were sampled by a physical anthropologist, ensuring there were not multiple individuals in the selected cremations urns.

METHODS

To confirm that all bone samples were fully calcined, aliquots of powdered untreated CB samples were analyzed by Fourier-transform infrared spectroscopy (FTIR). The crystallinity index (CI) is a measurement of the re-crystallization in a sample, where high CI values indicate high burning temperatures and thus a higher degree of re-crystallization. CI was estimated as the splitting factor between the two absorption band at ca. 603 and ca. 565 cm^{-1} ($\text{CI} = (\text{A}_{603} + \text{A}_{565})/\text{A}_{\text{valley}}$) (Olsen et al. 2008; Person et al. 1995).

Overall, 58 graves were dated as part of the first author’s doctoral project, of which replicates from 16 graves are included in this study. Three rounds of selected samples from 20 graves were sent to the three laboratories involved in this study (Brussels [RICH], Kiel [KIA], and

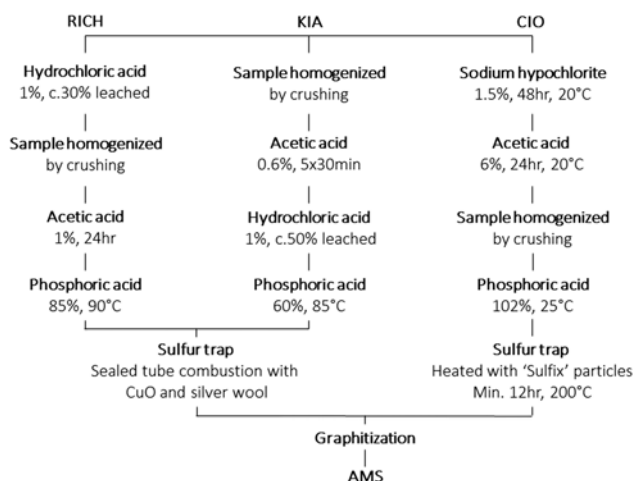


Figure 1 Pretreatment protocols for cremated bone. Laboratory for Radiocarbon Dating (RICH) in Brussels (Belgium), the Leibniz Laboratory (KIA) in Kiel (Germany), and the Center for Isotope Research (CIO) in Groningen (The Netherlands).

Groningen [CIO]), with a few samples replicated between laboratories. CIO uses the traditional acetic acid treatment (Lanting et al. 2001), whereas RICH and KIA use variations of an acid-leaching treatment (Figure 1; De Mulder et al. 2007).

RICH Protocol for Cremated Bone

Initially, ca. 30% by weight of each solid CB sample was leached in 1% hydrochloric acid. The bone was then ground to powder and ca. 1g was treated with 1% acetic acid (24 hr) to remove calcite. CO₂ was extracted from the sample with 85% phosphoric acid (90°C). To remove any sulfur compounds, the CO₂ was heated together with Ag for 30 min at 1000°C. The purified CO₂ was reduced using H₂ and Fe as catalyst and then pressed into targets for AMS measurements (De Mulder et al. 2007; Van Strydonck et al. 2009).

AMS ¹⁴C dating was conducted using a Micadas (195.5 kV) AMS system (Boudin et al. 2015). The resulting ¹⁴C-content was corrected for fractionation using the simultaneously AMS-measured ¹⁴C/¹²C and ¹³C/¹²C isotope ratios (Stuiver and Polach 1977).

KIA Protocol for Cremated Bone

A 1.5g piece of CB was first crushed and washed 5 × 30 min in 0.6% (0.1M) acetic acid at room temperature to remove any calcite. After repeated rinsing in demineralized water, ca. 50% of the solid sample was leached in hydrochloric acid (10 mL 1% HCl 1h + 1.6mL HCl conc. until pH < 1). After washing, drying and weighing, the sample was reacted with 60% phosphoric acid (85°C) to produce CO₂. To remove any sulfur compounds, the CO₂ was sealed in a quartz tube with CuO and silver wool and heated for 4 hr at 900°C. The purified CO₂ was reduced at 600°C using H₂ and iron powder as catalyst and then pressed into targets for AMS measurements (Hüls et al. 2010).

AMS ^{14}C dating was conducted using a HVE 3MV Tandetron 4130 AMS system (Nadeau et al. 1997). The resulting ^{14}C -content was corrected for fractionation using the simultaneously AMS-measured $^{14}\text{C}/^{12}\text{C}$ and $^{13}\text{C}/^{12}\text{C}$ isotope ratios (Stuiver and Polach 1977).

Some samples were pretreated in Groningen following the CIO protocol, but were subsequently converted to CO_2 and dated in Kiel. They followed the KIA protocol from the phosphoric acid step onwards.

CIO Protocol for Cremated Bone

1.5% sodium hypochlorite is used to remove organic material from the entire CB sample (48 hr, 20°C), which was then rinsed with decarbonized water. 6% (1M) acetic acid was added to remove readily soluble calcite, absorbed carbonates and the less crystalline fractions of apatite (24 hr, 20°C) (Lanting et al. 2001). The apatite was rinsed with decarbonized water to neutral pH, dried and crushed ($\sim 2 \times 2$ mm). CO_2 was extracted from ca. 1800 mg apatite with 102% (1.89 kg/m³) phosphoric acid (24 hr, 25°C). To remove any sulfur compounds, the CO_2 was heated with “Sulfix” particles (containing Ag_2O and Co_3O_4 ; WAKO, mesh 8–20; min. 12 hr, 200°C). The purified CO_2 was graphitized with iron as a catalyst and pressed into targets for AMS measurement.

AMS ^{14}C dating was conducted using the previous HVEE 4130 2.5 MV Tandetron AMS system (Wijma et al. 1996) and the present Micadas (180 kV) AMS system, which is in operation since 2017 (Aerts-Bijma et al., in prep.). The resulting ^{14}C -content was corrected for fractionation using the simultaneously AMS-measured $^{14}\text{C}/^{12}\text{C}$ and $^{13}\text{C}/^{12}\text{C}$ isotope ratios (Stuiver and Polach 1977).

RESULTS

Initially, CIO results were often significantly younger than results from RICH and KIA, and inconsistent with the expected chronology of the Aarupgaard cemetery. Results from RICH and KIA were in good agreement with each other, and with the expected chronology, thus an anomaly was suspected in the CIO dating process, leading to offsets of 100–300 years. The anomaly was apparently unrelated to AMS measurement, as it occurred in measurements performed on both the previous HVEE AMS and the present Micadas system. Through laboratory testing at CIO and KIA, the source of the anomaly was identified as a contaminated batch of “Sulfix” in the period April 2017–March 2018 (see supplemental Appendix 1). The CIO laboratory protocol was updated following the test results, and this paper only reports results obtained using the updated protocol.

A total of 43 ^{14}C results on 20 samples are reported in this paper. Summary results on type 1 replicates are given in Table 1 and replicate sets of ^{14}C measurements are shown in Figure 2. Summary results on type 2 replicates are given in Table 2 and replicate pairs of ^{14}C measurements are shown in Figure 3 (see supplemental Appendix 2 for full details).

Replicate measurements have been tested for consistency and weighted means calculated as described by Ward and Wilson (1978) using the R_Combine function in OxCal (Bronk Ramsey 1995). The function can be used where dates arise from the same event (within the resolution of the calibration curve, <5 yr), rather than just from the same sample. This certainly applies to the type 2 replicate measurements on apatite pretreated by CIO and type 1 “true

Table 1 ¹⁴C results, summary statistics and χ^2 test results on type 1 replicates from Aarupgaard.

Sample ID	KIA	RICH	CIO	Absolute difference (yr)	Sigma difference ¹	Weighted mean (BP)	χ^2 test
Grave 3869	2456 ± 25*	2504 ± 26	2540 ± 20*	—	—	2507 ± 14	6.9 ²
Grave 3330	2503 ± 27	—	2535 ± 20 ³	32 ± 34	0.9	2524 ± 17	0.9 ⁴
Grave 51	2448 ± 26*	—	2445 ± 20*	3 ± 33	0.1	2446 ± 16	0.0 ⁴
Grave 1076	—	2198 ± 27	2260 ± 20	62 ± 34	1.8	2246 ± 14	4.0 ⁴
Grave 1847	2228 ± 25*	—	2255 ± 20*	27 ± 32	0.8	2244 ± 16	0.7 ⁴
Grave 1791	2167 ± 25*	—	2230 ± 25*	63 ± 35	1.8	2199 ± 18	3.2 ⁴

*“True replicates.”

¹The absolute difference (yr) divided by its uncertainty.

²T(5%) = 6.0, df = 2.

³Date used as both type 1 and 2 replicate.

⁴T(5%) = 3.8, df = 1.

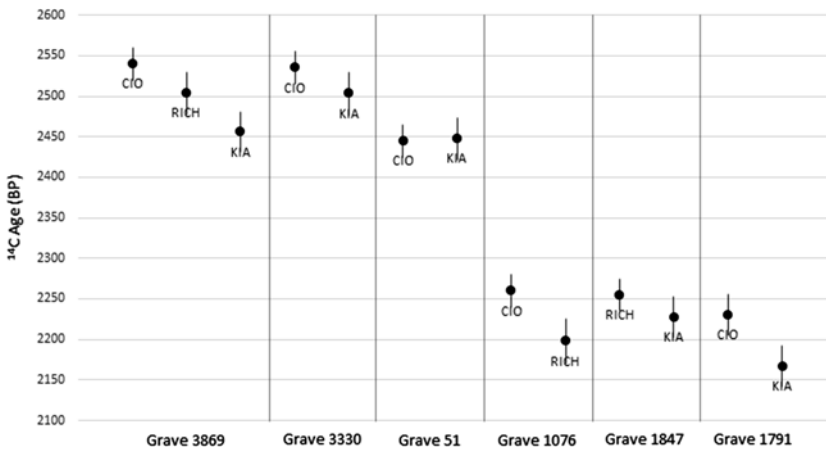


Figure 2 ¹⁴C results (±1σ) on type 1 replicate dates from Aarupgaard.

replicates,” and we argue that it also applies to the remaining type 1 replicate measurements, as we expect different CB fragments from the same burial context to have congruent ¹⁴C ages.

Four out of six pairs of results on type 1 replicates pass the Ward and Wilson (1978) χ^2 test, i.e. are statistically consistent at the 5% significance level. CIO results are on average slightly older than RICH and KIA results, as are RICH results compared to KIA results. Grave 1076 results narrowly fail the χ^2 test (T = 4.0, T(5%)=3.8, $\nu=1$), but would be regarded as consistent based on the traditional formula whereby their difference is less than 2σ (twice the uncertainty in the

Table 2 ^{14}C results, summary statistics and χ^2 test results on type 2 replicates.

Sample ID	CIO	KIA	Absolute difference (yr)	Sigma difference ¹	Weighted mean (BP)	χ^2 test ²
Aarre, grave A394, x785	2465 ± 18	2422 ± 20	46 ± 37	1.2	2446 ± 14	2.6
Aarre, grave A117, x762	2445 ± 20	2416 ± 20	29 ± 28	1.0	2431 ± 15	1.1
Aarre, grave A281, x484	2320 ± 20	2271 ± 20	49 ± 28	1.8	2296 ± 15	3.0
Aarupgaard, grave 3330	2535 ± 20 ²	2471 ± 26	64 ± 33	1.9	2511 ± 16	3.8
Aarupgaard, grave 83	2485 ± 30	2409 ± 27	76 ± 40	1.9	2443 ± 21	3.5
Aarupgaard, grave 1186	2465 ± 20	2408 ± 20	57 ± 28	2.0	2437 ± 15	4.1
Aarupgaard, grave 280	2405 ± 20	2402 ± 22	3 ± 30	0.1	2404 ± 15	0.0
Aarupgaard, grave 81	2425 ± 30	2379 ± 22	46 ± 37	1.2	2395 ± 18	1.5
Aarupgaard, grave 230	2546 ± 19	2362 ± 25	184 ± 31	5.9	2480 ± 16	34.1
Aarupgaard, grave 766	2285 ± 20	2252 ± 23	33 ± 30	1.1	2271 ± 16	1.2
Aarupgaard, grave 681	2310 ± 19	2305 ± 20	5 ± 28	0.2	2308 ± 14	0.0
Aarupgaard, grave 1001	2235 ± 20	2253 ± 21	18 ± 29	0.6	2244 ± 15	0.4
Aarupgaard, grave 382	2280 ± 20	2229 ± 25	51 ± 32	1.6	2260 ± 16	2.5
Aarupgaard, grave 1076	2260 ± 20 ²	2199 ± 29	61 ± 35	1.7	2240 ± 17	3.0
Aarupgaard, grave 1363	2225 ± 20	2195 ± 24	30 ± 31	1.0	2213 ± 16	0.9
Aarupgaard, grave 2262	2255 ± 25	2214 ± 28	41 ± 38	1.1	2237 ± 19	1.2

¹The absolute difference (yr) divided by its uncertainty.

² $T^*(5\%) = 3.8$, $df = 1$.

difference). A slight discrepancy like this might possibly reflect an inhomogeneity of ^{14}C ages in the two dated CB fragments, caused by an uneven influence of “old-wood” from the pyre-fuel (Olsen et al. 2013). Grave 3869 results narrowly fail the χ^2 test ($T = 6.9$, $T^*(5\%) = 6.0$, $\nu = 2$), whereas if the test is limited to results from either KIA and RICH ($T = 1.8$, $T^*(5\%) = 3.8$, $\nu = 1$) or RICH and CIO ($T = 1.8$, $T^*(5\%) = 3.8$, $\nu = 1$) it is acceptable.

Fifteen out of 16 pairs of results on type 2 replicates are also statistically consistent at the 5% significance level. One or both dates on grave 230 must however be an outlier ($T = 34.1$, $T^*(5\%) = 3.8$, $\nu = 1$, difference = 5.9σ), which cannot be explained by differences in wood-age offset, as the sample was homogenized by crushing before being split between laboratories.

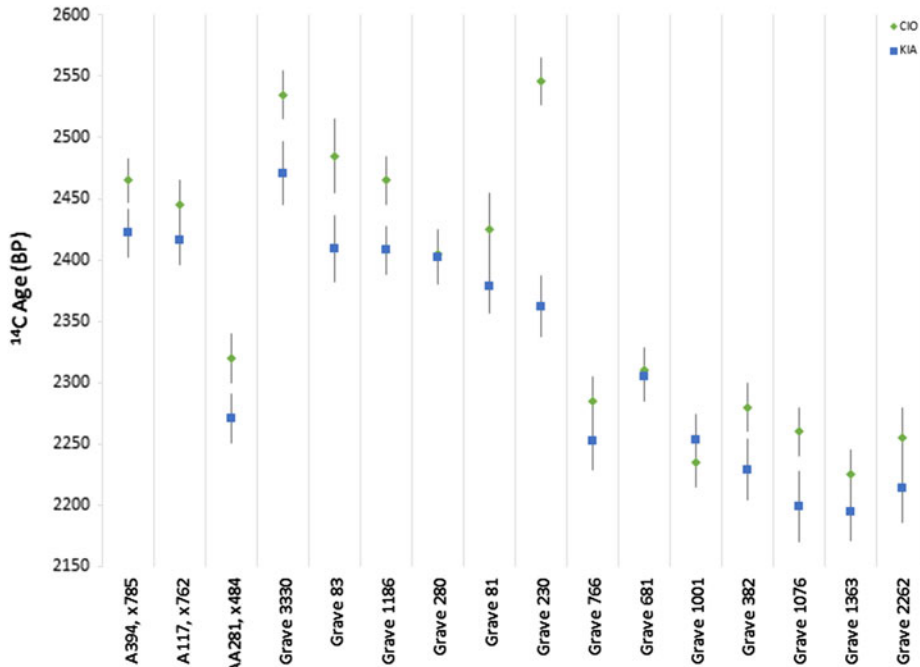


Figure 3 ^{14}C results ($\pm 1\sigma$) on type 2 replicate dates from Aarre and Aarupgaard.

The KIA date fits the expected age range, whereas the CIO date is well back in the Late Bronze Age and can thus be rejected, based on the archaeological information. We do however have no technical explanation for this difference, with $\delta^{13}\text{C}$ and $\%C$ values from both laboratories within the normal ranges.

Stable isotope values on $\delta^{13}\text{C}$ (measured by AMS) are plotted against ^{14}C ages in Figure 4. CIO has a slight tendency towards lower $\delta^{13}\text{C}$ values compared to KIA, which could indicate incomplete conversion, but here probably reflects use of different AMS systems and does not account for the pattern of slightly higher ^{14}C ages at CIO. $\%C$ results are plotted against ^{14}C ages in Figure 5. Overall CIO has lower $\%C$ values (mean= 0.09%) than KIA (mean= 0.23%) and RICH values fall in between (mean= 0.16%, $n= 2$). Differences in $\%C$ do however not appear to be correlated with ^{14}C ages.

DISCUSSION

The reported results from Aarupgaard, with the CIO date for grave 230 as an exception, are consistent with the typo-chronological phasing of the burials, based on an overall Bayesian model of the site chronology (Rose, dissertation in prep.). Results on the three graves from Aarre are consistent with the expected ages of the metal artifacts from these burials. Small wood-age offsets affecting the ^{14}C ages of CB cannot be excluded based on typo-chronology alone.

The independent replicate pretreatment and measurement of the same CB fragment or of different CB fragments from the same burial context by two laboratories (type 1 replicates) should allow us to test whether differences in pretreatment have a measurable influence on

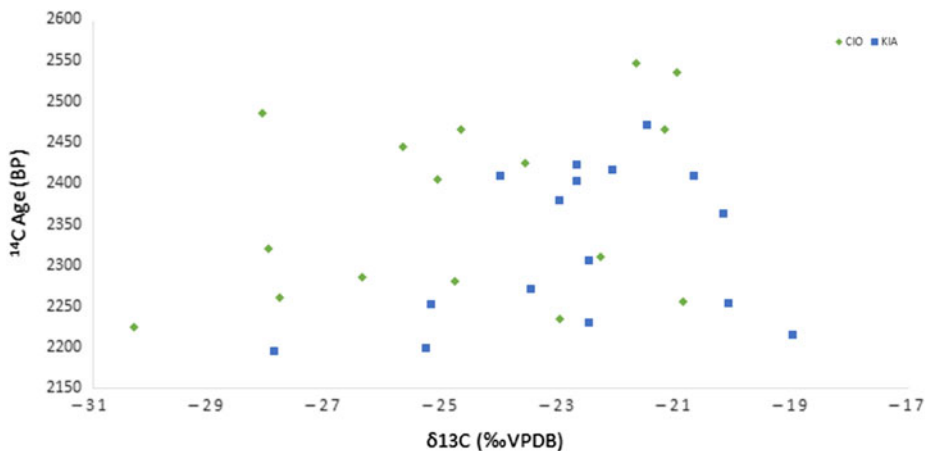


Figure 4 $\delta^{13}\text{C}$ (AMS) values and ^{14}C results on type 2 replicate dates from Aarre and Aarupgaard.

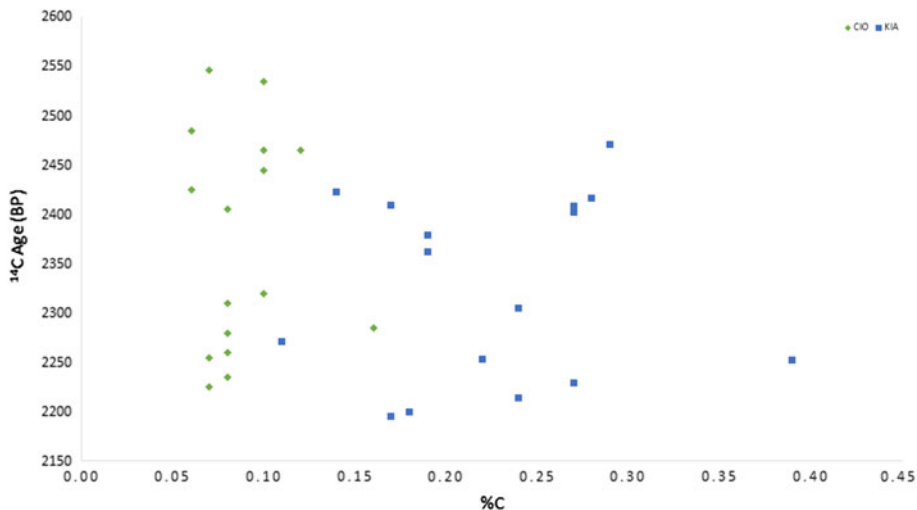


Figure 5 %C values and ^{14}C results on type 2 replicate dates from Aarre and Aarupgaard.

the ^{14}C results. Grave 3869 is the only one to be dated by all three laboratories, but while the three dates are not statistically consistent with a single ^{14}C age, only the KIA and CIO measurements are significantly different to each other. The chi-test statistic is slightly too high for the three results to be considered accurate measurements of the same ^{14}C age, but whether this means that the errors are slightly underestimated or whether there is a real difference between the ^{14}C ages of the extracts (e.g. due to differences in pretreatment) is hard to answer. It is difficult to discern a clear pattern from a single case, but we find it interesting that CIO, which removed only 3% of the sample mass during pretreatment, produced the oldest date, RICH removed 36.5% and produced a younger date, whereas KIA, which removed 41.2%, produced the youngest date, which incidentally also fits the archaeological chronology best (Rose, dissertation in prep.). There is no clear linear relationship between % material removed and ^{14}C ages and we do not know if even younger results would be obtained if

even more material was removed. Applying the logic of mortar dating, the youngest (KIA) date would be the most reliable, but we do not know if this is the true date of the sample as we have too few measurements to observe the necessary plateau of ^{14}C ages (Lindroos et al. 2007). Results on the remaining five type 1 replicates are consistent (differences less than 2σ) and demonstrate ^{14}C results on CB to be reproducible between the laboratories. Yet, we note that ^{14}C ages appear to fit the same order of laboratories as in grave 3869, and we therefore cannot rule out that some post-depositional contamination was not completely removed under all laboratory protocols, but to investigate this further would necessitate a pretreatment protocol with stepwise etching (Van Strydonck et al. 2009).

CIO assumes apatite to be resistant to contamination and uses the least aggressive pretreatment method, removing calcite, absorbed carbonates and the less crystalline fractions of apatite (Van Strydonck et al. 2005, 2009; Olsen et al. 2008). KIA and RICH assume the apatite might also be diagenetically altered and consequently etch the outer 30–50% of the samples. The assumption is that any diagenetic carbon substitution must be greater near the surface of a bone. Our results cannot be used to test whether apatite can indeed be contaminated, but it is possible that any diagenesis was mainly restricted to the most soluble $\leq 5\%$ of the sample, as this proportion of the samples mass was removed under all protocols. If diagenesis went beyond this $\leq 5\%$, we would expect the RICH and KIA dates to fit the archaeological chronology better than CIO dates, which is not the case (Rose, dissertation in prep.). The material comes from low carbonate burial environments, but we expect material from carbonate-rich environments might need different pretreatment (Van Strydonck et al. 2009).

All three laboratories use acetic acid to dissolve calcite, but add it at different points in the process and at different concentrations, temperatures and reaction times. After an initial sodium hypochlorite treatment, CIO treats the solid bone with acetic acid for 24 hr, thus targeting the surface of the sample along with the surface in the voids of the CB. KIA starts the pretreatment with acetic acid, but only washes the crushed bone for 5×30 min. RICH on the other hand uses acetic acid for 24 hr, but only after first leaching and grinding the sample. These differences in method result in varying weight losses: KIA removed less than 0.5% of the starting weights, CIO removed $\leq 5\%$ and RICH removed ca. 15% (see supplemental [Appendix 2](#) for full details). The comparatively high removal percentage by RICH, even though CIO uses a higher concentration of acetic acid, suggests that the increased surface area due to grinding is the decisive factor. These differences also suggest that much of the material dissolved during the 24 hr acetic acid treatments at CIO and RICH was apatite, not calcite.

The overall consistent results on type 1 replicate dates from the three laboratories indicate that CIO's bleaching and acetic acid pretreatment was probably sufficient in most cases. The results do not show whether the weaker acetic acid wash in KIA would also be adequate in this case. Also, the opposite order of the acetic acid and the hydrochloric acid steps between KIA and RICH appears to have no influence on the results. Both outcomes would be expected, of course, if the samples were only contaminated by secondary calcite, without diagenetic alteration of apatite (or if diagenetically altered apatite was soluble in 6% acetic acid).

Type 2 replicate measurements were introduced to the study when anomalously younger results from Groningen were observed. Apatite pretreated by CIO was sent to KIA for CO_2 extraction and AMS dating, allowing us to focus specifically on differences in the conversion and measuring processes between CIO and KIA. The results show that the differences in these processes between the Groningen and Kiel laboratories did not significantly affect the ^{14}C

results. CIO results are on average slightly older than KIA results, but differences in blank correction would account for most of this pattern; the KIA results are calculated using KIA's blank correction, but as these samples were pretreated at CIO, the CIO blank correction is perhaps more appropriate.

There are no agreed indicators to assess sample quality when ^{14}C dating CB, but quality nevertheless needs to be considered when judging if results are reliable. It is already common to test whether CB is fully calcined, but we suggest also reporting type of burial environment along with any other risk of contamination (ex. chalk manuring). Experimental studies have shown values of $\delta^{13}\text{C}$ to be highly influenced, although to variable degrees, by fuel source, cremation temperature and duration (Van Strydonck et al. 2005; Zazzo et al. 2009, 2012; Hüls et al. 2010; Snoeck et al. 2016), but we expect $\delta^{13}\text{C}$ values from a single site, or from sites that used similar cremation techniques, to cluster. A greater scatter may be expected for results measured by AMS rather than IRMS, but clear outliers will need further investigation. Comparing infrared spectroscopy (FTIR) and x-ray diffractometry (XRD) spectra at different stages in pretreatment, and giving more weight to results from samples whose spectra do not change much between pretreatment steps might here prove useful, but it needs to be further investigated. Inter-laboratory replication may be a useful approach to detecting contamination problems, particularly when there are significant differences in laboratory protocols; the consistency of results based on more or less aggressive pretreatments helps to validate the dates obtained.

CONCLUSION

We have replicated ^{14}C dates of CB at three laboratories and shown differences in pretreatment, conversion to CO_2 and AMS measurement to have no measurable influence on the majority of obtained results. The material comes from low carbonate burial environments and except for material from a single context any possible diagenesis was probably restricted to the more soluble $\leq 5\%$ of the samples, as this proportion of the samples mass was removed under all laboratory protocols. The ^{14}C results are reproducible and consistent with the expected archaeological chronology.

SUPPLEMENTARY MATERIAL

To view supplementary material for this article, please visit <https://doi.org/10.1017/RDC.2019.70>

ACKNOWLEDGMENTS

Analyses were funded through the Center for Baltic and Scandinavian Archaeology (ZBSA)'s Man and Environment research theme and by the Deutsche Forschungsgemeinschaft (DFG, German Research Foundation - Projektnummer 2901391021 – SFB 1266) subproject G1: Timescales of Change - Chronology of cultural and environmental transformations of the Collaborative Research Center “Scales of Transformation: Human-environmental Interaction in Prehistoric and Archaic Societies.” The authors would like to thank Museum Sønderjylland and ARKVEST – Arkæologi Vestjylland for access to the material.

REFERENCES

- Becker CJ. 1961. Førrømersk jernalder i Syd- og Midtjylland. Kbh.: Nationalmuseet.
- Boudin M, Van Strydonck M, van den Brande T, Synal H-A, Wacker L. 2015. RICH – A new AMS facility at the Royal Institute for Cultural Heritage, Brussels, Belgium. *Nuclear Instruments and Methods in Physics Research B* 361:120–123.
- Bronk Ramsey C. 1995. Radiocarbon calibration and analysis of stratigraphy: the OxCal Program. *Radiocarbon* 37(2):425–430.
- De Mulder G, Van Strydonck M, Boudin M, Leclercq W, Paridaens N, Warmenbol E. 2007. Re-evaluation of the Late Bronze Age and Early Iron Age chronology of the western Belgian urnfields based on ¹⁴C dating of cremated bones. *Radiocarbon* 49(2):499–514.
- Hüls CM, Erlenkeuser H, Nadeau MJ, Grootes PM, Andersen N. 2010. Experimental study on the origin of cremated bone apatite carbon. *Radiocarbon* 52(2):587–599.
- Jensen CK. 2005. Kontekstuel kronologi: en revision af det kronologiske grundlag for førrømersk jernalder i Sydsjælland. Højbjerg: Kulturlaget.
- Jørgensen E. 1975. Tuernes mysterier. *Skalk* 1975(1):3–10.
- Lanting JN, Aerts-Bijma AT, van der Plicht J. 2001. Dating of cremated bones. *Radiocarbon* 43(2A):249–254.
- Lindroos A, Heinemeier J, Ringbom Å, Braskén M, Sveinbjörnsdóttir Á. 2007. Mortar dating using AMS ¹⁴C and sequential dissolution: examples from medieval, non-hydraulic lime mortars from the Åland Islands, SW Finland. *Radiocarbon* 49(1):47–67.
- Lorange T. 2015. Det sakrale landskab ved Årre. Landskabets hukommelse gennem 4.000 års gravriter. In: Foss P, Møller NA, editors. *De dødes landskab. Grav og gravskik i ældre jernalder i Danmark*. Ribe: SAXO-instituttet, Københavns Universitet. p. 21–36.
- Nadeau MJ, Grootes PM, Schleicher M, Hasselberg P, Rieck A, Bitterling M. 1997. Sample throughput and data quality at the Leibniz-Labor AMS Facility. *Radiocarbon* 40(1): 239–445.
- Naysmith P, Scott EM, Cook GT, Heinemeier J, Van der Plicht J, Van Strydonck M, Bronk Ramsey C, Grootes PM, Freeman SPHT. 2007. A cremated bone intercomparison study. *Radiocarbon* 49(2): 403–408.
- Olsen J, Heinemeier J, Bennike P, Krause C, Margrethe Hornstrup K, Thrane H. 2008. Characterisation and blind testing of radiocarbon dating of cremated bone. *Journal of Archaeological Science* 35(3):791–800.
- Olsen J, Heinemeier J, Hornstrup KM, Bennike P, Thrane H. 2013. “Old wood” effect in radiocarbon dating of prehistoric cremated bones? *Journal of Archaeological Science* 40(1):30–34.
- Person A, Bocherens H, Saliège J-F, Paris F, Zeitoun V, Gérard M. 1995. Early diagenetic evolution of bone phosphate: an x-ray diffractometry analysis. *Journal of Archaeological Science* 22(2):211–221.
- Scheele E. 2016. The Wapse urnfield revisited: the search for groups of urnfield users (prov. Drenthe, The Netherlands). *LUNULA. Archaeologia Protohistorica XXIV*(2016):81–90.
- Snoeck C, Brock F, Schulting RJ. 2014. Carbon exchanges between bone apatite and fuels during cremation: impact on radiocarbon dates. *Radiocarbon* 56(2):591–602.
- Snoeck C, Schulting RJ, Lee-Thorp JA, Lebon M, Zazzo A. 2016. Impact of heating conditions on the carbon and oxygen isotope composition of calcined bone. *Journal of Archaeological Science* 65:32–43.
- Stuiver M, Polach HA. 1977. Discussion: reporting of ¹⁴C data. *Radiocarbon* 19(3):355–363.
- Terkildsen KF. 2015. Gravpladsen Årupgård som kilde til social stratifikation i førrømersk jernalder. In: Foss P, Møller NA, editors. *De dødes landskab. Grav og gravskik i ældre jernalder i Danmark*. Ribe. p. 51–70.
- Van Strydonck M, Boudin M, Hoefkens M, De Mulder G. 2005. ¹⁴C-dating of cremated bones, why does it work? *Lunula. Archaeologia Protohistorica XIII*:3–10.
- Van Strydonck M, Boudin M, De Mulder G. 2009. ¹⁴C dating of cremated bones: the issue of sample contamination. *Radiocarbon* 51(2):553–568.
- Van Strydonck M, Boudin M, Mulder GD. 2010. The carbon origin of structural carbonate in bone apatite of cremated bones. *Radiocarbon* 52(2):578–586.
- Ward GK, Wilson SR. 1978. Procedures for comparing and combining radiocarbon age determinations: a critique. *Archaeometry* 20(1): 19–31.
- Wijma S, Aerts AT, van der Plicht J, Zondervan A. 1996. The Groningen AMS facility. *Nuclear Instruments and Methods in Physics Research B* 113:465–469.
- Zazzo A, Saliège JF, Person A, Boucher H. 2009. Radiocarbon dating of calcined bones: where does the carbon come from? *Radiocarbon* 51(2):601–611.
- Zazzo A, Saliège J-F, Lebon M, Lepetz S, Moreau C. 2012. Radiocarbon dating of calcined bones: insights from combustion experiments under natural conditions. *Radiocarbon* 54(3–4): 855–866.

Appendix 7 Paper 4

Bayesian modeling of wood-age offsets in cremated bone

Authors: Rose, H. A., Meadows, J., & Henriksen, M. B

Published 2020 in *Radiocarbon*: 1-23. doi:10.1017/RDC.2020.3

To view supplementary material for this article, please visit

<https://doi.org/10.1017/RDC.2020.3>

Printed with permission by Cambridge University Press

© 2020 by the Arizona Board of Regents on behalf of the University of Arizona. This is an Open Access article, distributed under the terms of the Creative Commons Attribution licence (<https://creativecommons.org/licenses/by/4.0/>), which permits unrestricted re-use, distribution, and reproduction in any medium, provided the original work is properly cited.

BAYESIAN MODELING OF WOOD-AGE OFFSETS IN CREMATED BONE

Helene Agerskov Rose^{1*}  • John Meadows^{1,2}  • Mogens Bo Henriksen³

¹Foundation of Museums of the State of Schleswig-Holstein – Centre for Baltic and Scandinavian Archaeology, Schleswig, Schleswig-Holstein, Germany

²Christian-Albrechts-Universität zu Kiel – Leibniz-Laboratory for AMS Dating and Stable Isotope Research, Kiel, Schleswig-Holstein, Germany

³Odense City Museums – Archaeology, DK-5000 Odense C, Denmark

ABSTRACT. Experimental studies have shown that significant carbon exchange occurs between bone-apatite and the pyre atmosphere during cremation, which can cause a calendar date offset between the radiocarbon (¹⁴C) event and the date of cremation. There are limited empirical data available to assess the magnitude of such wood-age offsets, but the aim of this paper is to test if they can be modeled statistically. We present new ¹⁴C dates on modern bone cremated in realistic open-air experiments and on archaeological samples of cremated bone and associated organic material. Experimental results demonstrate a wide range of carbon exchange with a mean of $58.6 \pm 14.8\%$. Archaeological results indicate that the wood-age offsets have an approximately exponential distribution. We test whether the default Charcoal Outlier_Model in OxCal v4.3, developed to reduce the impact of wood-age offsets in dates of charcoal, is appropriate for cremated bone, but find that it slightly underestimates apparent offsets. To counter the intrinsic age of both pyre fuel and unburned bio-apatite, we instead propose a bespoke Cremation Outlier_Model, which combines an exponential distribution of calendar age offsets with a minimum offset, and provides better estimates of the actual dates of cremations.

KEYWORDS: Bayesian modeling, cremated bone, experimental archaeology, outlier modeling, wood-age offset.

INTRODUCTION

Experimental studies (Zazzo et al. 2009, 2012; Hüls et al. 2010; Van Strydonck et al. 2010) have shown that only a fraction of original bone apatite carbon remains in the bone after cremation, but that there is a significant carbon uptake from the pyre atmosphere, which is derived mainly from the burning fuel. This was not realized almost two decades ago when a pioneering study on radiocarbon (¹⁴C) dating cremated bone (CB) demonstrated that dates on the bio-apatite of fully calcined bone were comparable to those on associated charcoal (Lanting et al. 2001). As other studies tested the validity of dating CB using charcoal and other contemporaneous organic materials, they obtained similar results, and cases of charcoal dates being older than their associated CB were attributed to the “old-wood effect” (Lanting et al. 2001; De Mulder et al. 2009). Research continue investigating what isotopic changes bone undergoes when cremated (Van Strydonck et al. 2005, 2010; Naysmith et al. 2007; Olsen et al. 2008; Zazzo et al. 2009; Snoeck et al. 2016a). Experimental studies on the origin of CB apatite carbon demonstrated that bone exchanges carbon with the combustion atmosphere during cremation, giving calcined bone a mixed carbon signal. Hüls et al. (2010) cremated modern bone in a sealed furnace filled with ¹⁴C-free CO₂ obtained from fossil fuel, and by dating the CB found that 53–86% of carbon in re-crystallized bio-apatite was derived from the cremation atmosphere. This was confirmed by open-air experiments under natural conditions, where Zazzo et al. (2012) using archaeological bone and recent wood measured a carbon exchange of 48–91%, while Snoeck et al. (2014), using modern bone and old wood of known-age, measured a carbon exchange of 39–95%. Carbon exchange between the bone and the combustion atmosphere will cause a calendar date offset between the calibrated ¹⁴C measurement and the main event of interest (the date of cremation), which we will in the present paper refer to as a wood-age offset.

*Corresponding author. Email: helene.rose@zbsa.eu

Unless a body is cremated with recent, short-lived fuel, the wood-age offset will always make the CB date older than original unburned bio-apatite. From an archaeological perspective, cremation is a separate event occurring after death and before burial, but they are here regarded as the same event, as their total duration is shorter than the resolution of the ^{14}C calibration curve for the Holocene (true in most but not all cultures). However, what is dated is a ^{14}C event, i.e. when atmospheric CO_2 is sequestered as organic carbon in a living organism, and the time over which this occurs (i.e. from formation to death) is here defined as the intrinsic age (IA) of any given material. We note that unburned bio-apatite also has an unknown IA, which may vary between individuals (depending on e.g. their age at death) and between bones of the same individual (due to differences in bio-apatite remodeling rates). Beside a lack of empirical data on bio-apatite remodeling rates, both age-at-death and skeletal element sampled are more difficult to determine in cremations than in inhumation burials. Nevertheless, given expected mortality patterns, we assume that the IA of unburned bio-apatite in prehistoric cremations seldom exceeds 1–2 decades.

The Importance of Fuel

The consequence of carbon exchange taking place between the bone and the pyre atmosphere is that dating CB is equivalent to or at least close to directly dating the fuel used on the pyre. If the pyre wood has a low IA, even a high degree of carbon exchange will lead to limited wood-age offsets, but conversely even low degrees of carbon exchange may cause significant wood-age offsets if the wood has a high IA. Another possible scenario is that the IA of fuel and bone may be close, causing constant CB ^{14}C ages, regardless of the degree of carbon exchange. It has long been recognized that charcoal might have a high IA, making the chronological relationship between the sample and the context from which it is recovered difficult to interpret (Bayliss 1999). There is however little information about the IA of the vast majority of archaeological charcoal samples, which is not only problematic when wood-age offsets are transferred to CB, but also when charcoal is used as known-age reference material.

It is clear that the choice of pyre wood is of concern when ^{14}C dating CB. Modern open-air experiments indicate cremation of a human body takes 5–7 hr and requires 1–2 m³ of firewood, but with large variation dependent on wood type and quality, weather conditions, maintenance of the fire, etc. (Henriksen 2016). Prehistoric cremation graves are abundant worldwide, but actual pyre sites are rarely located, leaving only limited information on processes prior to interment, e.g. fuel procurement strategies and pyrotechnical operations of a cremation pyre. Even when pyre sites are located, they hold limited information, as the cremation process will have destroyed most of the fuel. Moreover, anthracological studies of pyre charcoal often only identify the wood taxa, without discussing wood-age. Hornstrup et al. (2005) analyzed charcoals from 16 cremation graves from Late Bronze Age to Early Iron Age in North and West Jutland showing a predominance of oak (75% *Quercus* sp.), followed by pine (25% *Pinus* sp.), alder (12.5% *Alnus* sp.), birch (12.5% *Betula* sp.), hazel (12.5% *Corylus* sp.) and willow (6% *Salix* sp.). Heather (*C. vulgaris*) was present in low frequencies in the majority of cremation graves at Hellegård in Central Jutland, demonstrating the practice of maintaining heath plains in the area. A similar distribution of wood species was used at contemporaneous settlement sites in the area, probably reflecting the local vegetation, but with a clear preference for oak. Although it requires seasoning for a few years, oak wood can produce long-lasting fires with high temperatures, and was widely used as a funerary fuel (e.g. Hissel et al. 2007; Henriksen 2009; Moskal-del Hoyo 2012; O'Donnell 2016; Martín-Seijo and César Vila 2018; Henriksen 2019). Anthracological studies of charcoal

from prehistoric burial and settlement sites in Denmark show a fuel procurement strategy with a preference for gathering deadwood with limited branch diameters, whereas actual production of fire wood was a later phenomenon associated with the establishment of towns in a time when cremation was no longer practiced (Hornstrup et al. 2005).

In this paper we analyze archaeological material from Aarre urnfield cemetery in West Jutland, Denmark. The archaeobotanical analyses of material from 11 urn graves at Aarre show a dominance of oak charcoal, followed by alder and maple (*Acer* sp.) (Online Supplementary Information 3, Effenberger 2017a, 2017b, 2019), corresponding well to the expected taxonomic availability in the area (Iversen 1974). All elements of the trees are represented, from twig to heartwood, with no apparent differences between graves. There would have been few oak trees in the open landscape around Aarre and wood gathering must have extended beyond the immediate surroundings (Iversen 1974). Alder is surprisingly common, given that it produces little heat and does not burn for long, but this may reflect the local abundance of the species. All elements of the trees were used, possibly reflecting gathering of deadwood or felling of younger trees, creating a combination of low IA for the young wood and IA ranging from ≥ 50 and up to 80 yr for alder and probably up to a few centuries for oak. Small caliber wood might have been used as kindling material, but might also reflect a landscape with few larger trees (Iversen 1974). The strategies for wood procurement at Aarre were probably determined by a combination of different factors, where wood availability both in close proximity and beyond seems to have played a large role.

Approaching the Issue of Wood-Age Offsets

There is limited empirical data available on the scale of wood-age offsets in CB, although multiple studies report ^{14}C dates on paired CB and charcoal (e.g. Lanting et al. 2001; Van Strydonck et al. 2005; Olsen et al. 2008; De Mulder et al. 2009; Chatters et al. 2017). As charcoal can be affected by variable wood-age offsets, it is difficult to infer what offset is transferred from the cremation fuel to the CB. To assess the scale of wood-age offsets in CB, it is desirable to focus on associated material with no IA, e.g. charred twigs or cereal grains, but such samples are often difficult to obtain from an archaeological context. Olsen et al. (2008) reported five pairs of ^{14}C dates on CB and pitch (wood resin with negligible IA) from the Danish Bronze Age, with a mean difference (CB – pitch ^{14}C age) of 26 ± 26 ^{14}C yr (ranging from 8 to 92 yr). In another paper, two combined CB ^{14}C ages were compared to a dendrochronological date, indicating that the CB was 73 ± 26 ^{14}C yr older than the date of cremation (Olsen et al. 2013). In a recent study of a historically attested Buddhist monk from medieval Japan, Minami et al. (2019) ^{14}C dated three samples of fully cremated white bone and a combination of the dates shows them to correspond well with the lifetime of the monk. As wood-age offsets are on the calendar scale (“type t” offsets: Bronk Ramsey 2009b), we calibrate these dates before comparing them using the Difference function in OxCal v4.3 (Bronk Ramsey 2009a). We model all the differences from Olsen et al. (2008; 2013) and Minami et al. (2019) in a bounded phase starting at zero (i.e. requiring the CB to have a wood-age offset) and summarize the now-constrained wood-age offsets using the KDE_Plot function (Bronk Ramsey 2017). Assuming an exponential distribution of wood-age offsets (i.e. applying a Tau_Boundary (Bronk Ramsey 2009a) to the end of the bounded phase), the posterior estimates of the offsets have a 22 yr median and a 1- σ range of 32 yr (Online Supplementary Information 1, Part 1). Based on this limited empirical data set, wood-age offsets in CB appear to be relatively small.

When bone is cremated, isotopic fractionation of carbon takes place as a function of time and temperature (Olsen et al. 2008; Zazzo et al. 2009), which in effect means there are no proxies available (e.g. $\delta^{13}\text{C}$ values) for assessing the scale of wood-age offsets in individual CB samples. Because of this, ^{14}C dates on CB are sometimes used as simple *termini post quem*, but this means discarding information about the dates of cremations and will be close to useless in cases where only CB dates are available. We propose to instead handle CB dates statistically using the Outlier_Model function of OxCal v4.3 (Bronk Ramsey 2009b)(OM), which allows dates to be weighted according to a prior probability for how likely they are to be misleading, and allows the user to specify a distribution for potential offsets. Calendar age offsets in samples susceptible to IA, e.g. charcoal from trunk wood, are assumed to approximately follow an exponential probability density function, i.e. most samples will date close to the event in question, but a diminishing number of dates will be increasingly older (Nicholls and Jones 2001; Dee and Bronk Ramsey 2014). This assumption can be modeled using the default Charcoal OM (Bronk Ramsey 2009b; Dee and Bronk Ramsey 2014), developed to reduce the impact of wood-age offsets in dates of charcoal, and it has been suggested to also apply this with varying scales to ^{14}C dates on CB (Garrow et al. 2014; Fitzpatrick et al. 2017). We will in this study take a step back and empirically investigate the scale of wood-age offsets and their underlying distribution, before finally proposing a suitable OM for ^{14}C dates on CB.

MATERIAL AND METHODS

Archaeological Material

CB and context associated organic samples were selected from an archaeological site in West Jutland, Denmark. Aarre urnfield cemetery (sandy soil with low carbonate levels, ca. 8°dH) is a large and well-documented site, with originally up to ca. 1000 burials. The cremated human remains were interred in funerary urns and covered by small earthen mounds enclosed by a ditch. A minority of the graves contained metal artifacts, which can be approximately dated by seriation of typological traits (Becker 1961; Jensen 1996). No cremation pyres have been located in the area and all graves are secondary deposits (Lorange 2015). Samples from 10 graves were selected for this study, comprising CB, charcoal and other charred plant material. The graves were excavated over the last decade and the contents of the cremation urns were excavated in a controlled indoor environment. Charcoal is interpreted as remains of pyre fuel, whereas cereal grains and seeds might have accompanied the deceased on the pyre. Grass (stems and a bulb of *Arrhenatherum elatius* ssp. *bulbosum*) and stems of heather (*Calluna vulgaris*) probably came from the area underneath or surrounding the pyre, and might have been used as kindling material, but might also have an altogether unintentional relationship to the cremation (Roehrs et al. 2013). All charcoal dates are susceptible to IA, and individual wood-age offsets were therefore estimated based on the typical lifespan of the species and the sampled section of the plant (e.g. trunk wood or twig).

Experimental Material

The third author carried out four separate open-air cremation experiments over the period 2014–2017, cremating modern animal bone using either recent wood or old wood of known age. The experiments took place in the author's garden on Funen in central Denmark. They were designed to mimic a prehistoric cremation pyre, albeit in a scaled down version, and did not allow close control of environmental parameters. Comparable amounts of bone and wood (ca. 6–7 kg wood per pyre) were burned in an iron brazier, which protected the

Table 1 Pyre fuel for experimental pyres with dendro dates and values of F^{14C} and 14C age (Hua et al. 2013; Levin et al. 2013; Reimer et al. 2013; Hammer and Levin 2017).

Pyre	Fuel	Dendro date	F^{14C}	14C age
No. 8	Recent wood (<i>Fraxinus</i> sp.)	AD 1986–2013	1.0954 ± 0.0032	-729 ± 24
No. 9	Old wood (<i>Quercus</i> sp.)	AD 1100–1282	0.8987 ± 0.0013	858 ± 11
No. 11	As pyre no. 8	—	—	—
No. 16	Old wood (<i>Quercus</i> sp.)	AD 34–251	0.7926 ± 0.0017	1867 ± 14

Table 2 Animal bone for experimental pyres with slaughter dates and values of F^{14C} and 14C years. 2017 values are extrapolated from the 14C activity of the previous decade (Hua et al. 2013; Levin et al. 2013; Hammer and Levin 2017).

Pyre	Bone	Slaughter date	F^{14C}	14C age
No. 8	Sheep (<i>Ovis aries</i>), single cut of a hind limb	2013	1.0231 ± 0.0018	-183 ± 14
No. 9	Cattle (<i>Bos taurus</i>), single cut of a large diaphysis	2013	1.0231 ± 0.0018	-183 ± 14
No. 11	Sheep (<i>Ovis aries</i>), single cut of a hind limb	2015	1.0133 ± 0.0019	-106 ± 15
	Cattle (<i>Bos taurus</i>), single cut of a large diaphysis	2013	1.0231 ± 0.0018	-183 ± 14
No. 16	Sheep (<i>Ovis aries</i>), single cut of a hind limb	2017	1.0062 ± 0.0013	-50 ± 10

fire from the wind and ensured the bones were in close contact with the fuel until the fires burned down after 2–2.5 hr. Beyond igniting the fires, no additional wood was added (Henriksen 2016). Snoeck et al. (2014) conducted similar experiments, albeit with fleshed modern bone. The new contribution of our experiment is the dating of multiple bone fragments from the same bone, from the same pyre, thereby documenting variable uptake of exogenous carbon during cremation.

Pyres no. 8 and no. 11 used recent wood and pyres no. 9 and no. 16 used old dendro-dated wood (Table 1) (Daly 2011; Daly 2014). To obtain F^{14C} values and 14C ages for the old wood, the mean was calculated of the raw curve points over the dendro-dated growth periods (pyre no. 9: 850–670 cal BP, pyre no. 16: 1915–1700 cal BP) in the IntCal13 Northern Hemisphere atmospheric 14C data set (Reimer et al. 2013). For the recent wood, data from the Bomb13NH1 (AD1650–2010) calibration curve (Hua et al. 2013) was combined with additional data points from the Hammer and Levin datasets of atmospheric 14C activity from Jungfrauoch in the Swiss Alps (Online Supplementary Information 4) (Levin et al. 2013; Hammer and Levin 2017). Wood will have an inhomogeneous 14C signal, but our approach effectively assumes that it was fully homogenized by combustion, and any differences in CB 14C ages from each pyre are therefore due to differential carbon exchange. Cuts of cattle (*Bos taurus*) and sheep (*Ovis aries*) reared in Denmark were cooked and defleshed prior to cremation (Table 2). Although we assume that prehistoric humans were not defleshed before cremation, skin and flesh will combust at

lower temperatures before bio-apatite recrystallization occurs (Zazzo et al. 2009; Snoeck et al. 2014). Collagen from the bones themselves might however contribute to the carbon composition of the pyre atmosphere, but must be burnt out before recrystallization can begin, and should therefore have little effect on the CB ^{14}C age. The animals were all young specimens, so the slaughter dates are compared with recent measurements of atmospheric ^{14}C activity to obtain values of F^{14}C and ^{14}C age before cremation (Levin et al. 2013; Hammer and Levin 2017). No measurements are yet available for 2017, but because the decline in atmospheric ^{14}C in recent years was relatively steady, we extrapolate a value from the trend over the previous decade. ^{14}C units were converted using Stuiver and Polach (1977), but as we report post-bomb ^{14}C data indicative of ^{14}C activity of the atmosphere rather than radioactive decay, we use the F^{14}C convention rather than pMC (Reimer et al. 2004).

Laboratory Methods

Only samples of white CB were selected. To confirm they were fully calcined, aliquots of powdered untreated CB were analyzed by Fourier-transform infrared spectroscopy (FTIR). The crystallinity index (CI) was estimated as the splitting factor between the two absorption bands at ca. 603 and ca. 565 cm^{-1} ($\text{CI} = (\text{A}_{603} + \text{A}_{565})/\text{A}_{\text{valley}}$) (Person et al. 1995; Olsen et al. 2008). CB samples were sent to the Centre for Isotope Research (CIO) in Groningen, the Leibniz Laboratory (KIA) in Kiel and the Laboratory for Radiocarbon Dating (RICH) in Brussels for ^{14}C dating. As part of a comparison study, two CB samples were replicated between CIO and KIA; they were pretreated in Groningen following the CIO protocol, but were subsequently converted to CO_2 and dated in Kiel (Rose et al. 2019). It has been suggested that it may be unnecessary to bleach CB samples with e.g. sodium hypochlorite to remove any organic material (Snoeck et al. 2016b), but Groningen maintains the procedure as initially introduced by Lanting et al. (2001). Samples of context-associated organic material were sent for archaeobotanical analysis (Effenberger 2017a, 2017b, 2019) and identified single fragments were ^{14}C dated in Brussels or Kiel.

Pretreatment and Combustion

Samples of charred organics were extracted in Kiel and Brussels following standard acid–alkali–acid procedures (Grootes et al. 2004; Boudin et al. 2015). Samples of CB were extracted using different pretreatment procedures at the three laboratories (Rose et al. 2019). Brussels leached ca. 30% by weight of each solid CB sample in 1% hydrochloric acid, before it was powdered and treated with 1% acetic acid (24 hr) to remove calcite (Van Strydonck et al. 2009). Kiel crushed each CB sample before treating it with 0.6% acetic acid (5×30 min) and leaching ca. 50% with 1% hydrochloric acid (Hüls et al. 2010). Groningen treated CB samples with 1.5% sodium hypochlorite (48 hr, 20°C), followed by 6% (1M) acetic acid (24 hr, 20°C) (Dee et al. 2019). Kiel hydrolyzed two aliquots of the extracted apatite for five CB samples to increase measurement precision. All CB extracts were reacted with phosphoric acid to produce CO_2 and combusted to remove sulfur compounds.

Graphitization and AMS Measurement

Purified CO_2 of charred organics and CB was reduced to graphite for AMS measurement. Measurements in Brussels were performed on a Micadas (195.5 kV) AMS system (Boudin et al. 2015). Kiel used a HVEE 3 MV Tandetron 4130 AMS system (Nadeau et al. 1997) and Groningen used a Micadas (180 kV) AMS system (Dee et al. 2019). The laboratories corrected the resulting ^{14}C -contents for fractionation using the simultaneously AMS-measured $^{14}\text{C}/^{12}\text{C}$ and $^{13}\text{C}/^{12}\text{C}$ isotope ratios (Stuiver and Polach 1977).

Calculating Carbon Exchange

^{14}C ages of CB have been shown to plot along or close to a mixing line between the end-members unburned apatite and burning atmosphere ($\text{CO}_2_{\text{AIR}} + \text{CO}_2_{\text{FUEL}}$) (Hüls et al. 2010; Zazzo et al. 2012). Bone organic matter does not contribute to the CB carbon signal, as it degrades at lower temperatures before apatite recrystallization takes place (Zazzo et al. 2009; Snoeck et al. 2014). The percent carbon exchange between unburned apatite and the pyre atmosphere, as indicated by $F^{14}\text{C}$, can be calculated using mass balance Equation (1), assuming the $F^{14}\text{C}$ content to be evenly distributed throughout the wood and animals.

$$\% \text{carbon exchange} = \frac{F^{14}\text{C}_{\text{unburned apatite}} - F^{14}\text{C}_{\text{CB}}}{F^{14}\text{C}_{\text{unburned apatite}} - F^{14}\text{C}_{\text{pyre atmosphere}}} * 100(\%) \quad (1)$$

Where $F^{14}\text{C}_{\text{unburned apatite}}$ is the atmospheric $F^{14}\text{C}$ when the animal was slaughtered, $F^{14}\text{C}_{\text{CB}}$ is the $F^{14}\text{C}$ concentration in cremated bone, and $F^{14}\text{C}_{\text{pyre atmosphere}}$ is the mean $F^{14}\text{C}$ over the period of wood growth, as it will be dominated by CO_2 generated by the wood combustion (Tables 1 and 2) (Zazzo et al. 2012). % carbon exchange uncertainties for individual samples can be calculated using Equation (2), where σ_{bone} is the uncertainty in unburned apatite $F^{14}\text{C}$, σ_{CB} is the uncertainty in cremated bone $F^{14}\text{C}$, σ_{fuel} is the uncertainty in wood (fuel) $F^{14}\text{C}$, and $F^{14}\text{C}_{\text{CB}}$ is the $F^{14}\text{C}$ concentration in cremated bone. The uncertainties are however relatively trivial (ca. $\pm 0.5\%$) compared to the observed range of values.

$$\% \text{uncertainty} = \frac{\sqrt{\sigma_{\text{bone}}^2 + \sigma_{\text{CB}}^2 + \sigma_{\text{bone}}^2 + \sigma_{\text{fuel}}^2}}{F^{14}\text{C}_{\text{CB}}} * 100(\%) \quad (2)$$

RESULTS

Archaeological Dataset

We report a total of 43 AMS dates measured on 36 unique samples from 10 individual urnfield graves (Table 3). These include measurements on CB, charcoal and short-lived charred plant material (cereal grains and fragments of grass). CI values of CB are all acceptable (>5) and CB $\delta^{13}\text{C}$ values (mean = $-23.2 \pm 1.9 \delta^{13}\text{C}$) and %C (mean = $0.19 \pm 0.09 \%$ C) fall within expected ranges. Values of $\delta^{13}\text{C}$ are measured by AMS and the results will be affected by fractionation during acid extraction, graphitization and AMS measurement. Also %C is not strictly comparable between laboratories, as pretreatment methods vary and %C is calculated at different steps in the process (Rose et al. 2019). Archaeobotanical results are provided in Online Supplementary Information 3.

AMS dates are calibrated in OxCal v4.3 using the IntCal13 calibration curve (Bronk Ramsey 2009a; Reimer et al. 2013) and differences between context associated material and CB are calculated (Figure 1, Online Supplementary Information 1, Part 2). As expected, differences cluster around zero (indicated by the vertical line), but are strongly skewed towards positive values, i.e. associated samples often date older than the CB. The large majority of charcoal samples are much older than the CB dates, however, and might be derived from residual material relating to documented extensive Bronze Age activities in the area (Lorange 2015), notwithstanding the excavation of these urns under laboratory conditions. The pyre site or sites have not been located and there is no information on whether a new area was used for each pyre, or whether the same area was used repeatedly. It is possible that some pyres have been constructed on top of older cooking pits from the Bronze Age.

Table 3 Radiocarbon results on the archaeological data set from Aarre urnfield cemetery (West Jutland, Denmark). Replicate measurements have been tested for consistency and combined following Ward and Wilson (1978).

Context	Lab code	Sample ID	Material	CI	%C of extract	Corrected pMC	AMS $\delta^{13}\text{C}$ (‰ VPDB) ¹	¹⁴ C age (BP)
Grave A86, urn	KIA-53941	x339	<i>Acer</i> sp. trunk wood charcoal ($\text{\O} > 10$ cm)	—	63.96	73.60 ± 0.23	-25.3	2463 ± 25
	KIA-53942	x340	Cremated bone (human)	5.4	0.35	74.37 ± 0.24	-19.7	2379 ± 26
	KIA-53942	X340	Cremated bone (human), replicate	—	—	74.31 ± 0.23	-22.8	2385 ± 25
Weighted mean: sample x340, T' = 0.0, T' (5%) = 3.8, v = 1, 2382 ± 19 BP								
Grave A95, pit	KIA-53984	x368 no.1	<i>Quercus</i> sp. twig charcoal ($\text{\O} < 0.3$ cm)	—	70.68	74.45 ± 0.23	-28.4	2370 ± 25
	KIA-53985	x368 no.3	<i>Acer</i> sp. twig charcoal ($\text{\O} < 0.5$ cm)	—	70.49	73.90 ± 0.23	-27.7	2430 ± 26
Grave A95, urn	RICH-25342	x369	Cremated bone (human)	7.8	0.11	73.90 ± 0.25	-24.3	2428 ± 27
Grave A99, pit	RICH-25071	x65 no.2	<i>Alnus</i> sp. trunk wood charcoal ($\text{\O} 8\text{-}10$ cm)	—	60.00	75.39 ± 0.28	-33.3	2269 ± 29
	RICH-25067	x65 no.3	<i>Quercus</i> sp. trunk wood charcoal ($\text{\O} < 10$ cm)	—	61.00	67.85 ± 0.26	-31.6	3115 ± 31
Grave A99, urn	GrM-16774	x345	Cremated bone (human)	6.5	0.06	75.50 ± 0.17	-26.5	2255 ± 20
	RICH-25069	x346 no.1	<i>Alnus</i> sp. twig charcoal ($\text{\O} < 0.3$ cm)	—	53.50	77.14 ± 0.28	-31.8	2085 ± 29
	RICH-25066	x346 no.27	<i>Alnus</i> sp. trunk wood charcoal ($\text{\O} > 10$ cm)	—	61.60	75.56 ± 0.28	-35.3	2251 ± 30
Grave A117, urn	GrM-14604 ²	x762	Cremated bone (human)	6.0	0.10	73.75 ± 0.13	-25.7	2445 ± 20
	KIA-53098 ²	x762	Replicate of GrM-14604	—	0.28	74.03 ± 0.19	-22.1	2416 ± 20
Weighted mean: sample x762, T' = 1.1, T' (5%) = 3.8, v = 1, 2431 ± 15 BP								
Grave A130, urn	KIA-53943	x769	<i>Quercus</i> sp. charcoal ($\text{\O} > 10$ cm) 1 annual ring sampled	—	31.21	73.72 ± 0.23	-23.6	2449 ± 25
	KIA-53944	x774	<i>Quercus</i> sp. charcoal ($\text{\O} > 10$ cm)	—	60.58	73.30 ± 0.22	-25.0	2495 ± 24
	KIA-53945	x82 no.1	Charred grass stem	—	68.30	72.49 ± 0.23	-25.1	2585 ± 25
	KIA-53946	x82 no.2	<i>Triticum</i> cf. <i>aestivum</i> , charred cereal	—	64.19	76.46 ± 0.23	-28.5	2156 ± 24
	KIA-53947	x217	Cremated bone (human)	5.8	0.24	75.57 ± 0.23	-20.9	2250 ± 25
Weighted mean: sample x217, T' = 0.0, T' (5%) = 3.8, v = 1, 2253 ± 18 BP								
Grave 155, urn	KIA-53948	x127 no.1	cf. <i>Triticum</i> sp., charred cereal	—	50.00	73.31 ± 0.22	-26.4	2494 ± 24
	KIA-53949	x127 no.2	<i>Arrhenatherum elatius</i> ssp. <i>Bulbosum</i> , charred grass bulb	—	65.52	73.56 ± 0.22	-28.2	2466 ± 24
Grave A130, urn	KIA-53950	x281	Cremated bone (human)	6.1	0.26	74.55 ± 0.23	-23.6	2359 ± 25
	KIA-53950	x281	Cremated bone (human), replicate	—	—	74.41 ± 0.23	-24.1	2374 ± 25

Weighted mean: sample x281, T' = 0.2, T' (5%) = 3.8, v = 1, 2367 ± 18 BP									
Grave A198, urn	KIA-53951	x338	<i>Alnus</i> sp. trunk wood charcoal (Ø > 10 cm)	—	57.02	69.12 ± 0.21	-24.9	2967 ± 24	
	KIA-53952	x338 CB	Cremated bone (human)	5.9	0.28	74.89 ± 0.24	-24.9	2323 ± 26	
	KIA-53952	x338 CB	Cremated bone (human), replicate	—	—	74.82 ± 0.29	-25.9	2330 ± 35	
Weighted mean: sample x338 CB, T' = 0.0, T' (5%) = 3.8, v = 1, 2325 ± 21 BP									
Grave A278, urn	KIA-53953	x782 no.1	Charred grass stem	—	74.57	74.17 ± 0.23	-27.5	2400 ± 25	
	KIA-53954	x782 no.2	Charred grass, stem and root fragment	—	67.11	73.76 ± 0.23	-26.2	2445 ± 25	
	KIA-53955	x783	Cremated bone (human)	5.5	0.2	73.47 ± 0.24	-22.7	2477 ± 26	
	KIA-53955	x783	Cremated bone (human), replicate	—	—	73.71 ± 0.23	-22.9	2450 ± 25	
Weighted mean: sample x783, T' = 0.6, T' (5%) = 3.8, v = 1, 2463 ± 19 BP									
Grave A393, pit	RICH-25068	x568 no.1	<i>Triticum dicoccum</i> , charred cereal	—	61.10	69.69 ± 0.28	-29.9	2901 ± 32	
	RICH-25070	x568 no.2	<i>Hordeum vulgare nudum</i> , charred cereal	—	44.30	69.58 ± 0.28	-27.2	2914 ± 32	
Grave A393, urn	RICH-25341	x561 CB	Cremated bone (human)	6.4	0.16	73.90 ± 0.25	-25.3	2480 ± 27	
	KIA-52411	x561 no.1	<i>Hordeum vulgare nudum</i> , charred cereal	—	54.67	67.70 ± 0.21	-24.0	3134 ± 25	
	KIA-52412	x561 no.3	<i>Hordeum vulgare nudum</i> , charred cereal	—	32.35	67.57 ± 0.22	-21.9	3150 ± 27	
	KIA-52413	x561	<i>Quercus</i> sp. trunk wood charcoal (Ø > 10 cm)	—	24.78	72.25 ± 0.24	-25.7	2611 ± 27	
Grave A394, urn	KIA-52414	x556 no.1	<i>Quercus</i> sp. charcoal from branch sapwood (Ø 3-5 cm)	—	26.74	70.77 ± 0.23	-24.9	2778 ± 27	
	KIA-53983	X781 no.9	<i>Acer</i> sp. trunk wood charcoal (Ø > 10 cm)	—	66.85	68.58 ± 0.21	-27.0	3029 ± 24	
	GrM-14708 ²	x785 CB	Cremated bone (human)	6.3	0.10	73.57 ± 0.11	-21.2	2465 ± 18	
	KIA-53099 ²	x785 CB	Replicate of GrM-14708	—	0.14	73.97 ± 0.19	-22.7	2422 ± 20	
Weighted mean: sample x785 CB, T' = 2.6, T' (5%) = 3.8, v = 1, 2446 ± 14 BP									
	KIA-52415	X785 no.1	<i>Triticum aestivum</i> , charred cereal	—	37.76	70.19 ± 0.23	-23.0	2843 ± 26	
	KIA-52416	X785 no.4	<i>Alnus</i> sp. heartwood charcoal (Ø 2-3 cm)	—	28.07	70.82 ± 0.23	-27.9	2772 ± 26	
	KIA-52417	X786 no.1	<i>Quercus</i> sp. trunk wood charcoal (Ø > 10 cm)	—	51.01	71.29 ± 0.24	-25.2	2719 ± 27	

²Two CB samples were replicated between CIO and KIA; they were pretreated in Groningen following the CIO protocol, but were subsequently converted to CO₂ and dated in Kiel (Rose et al. 2019).

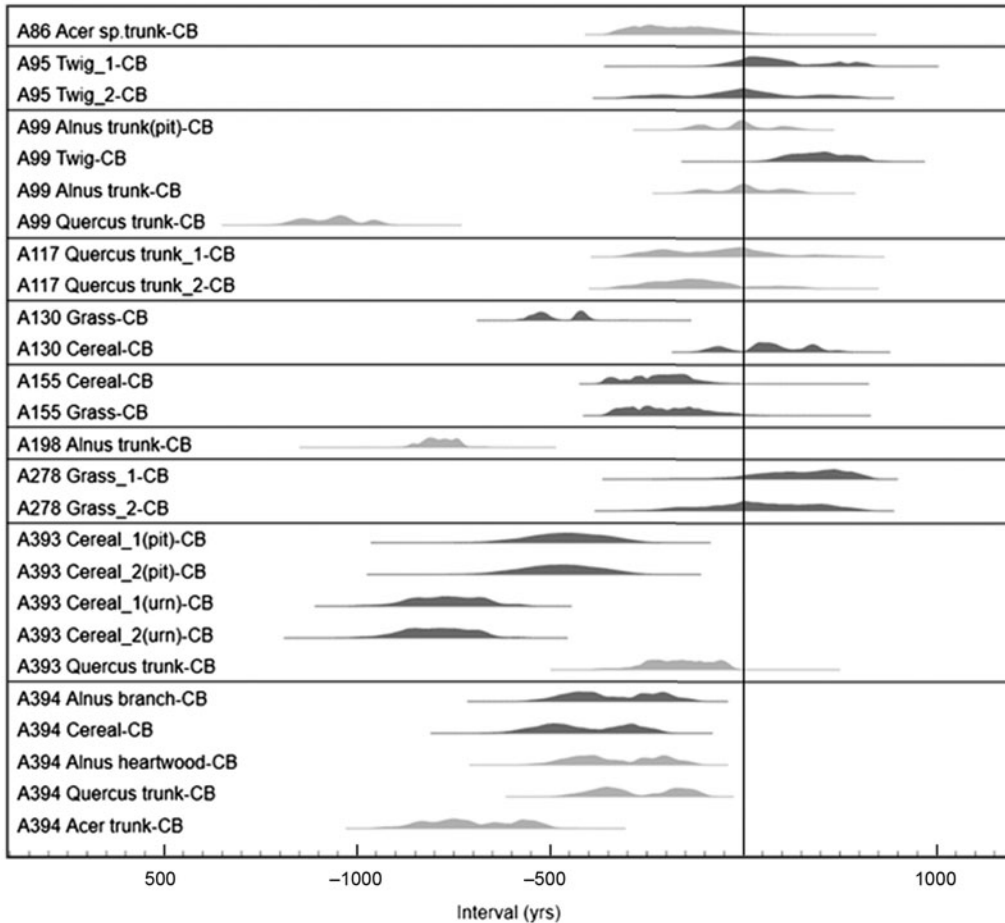


Figure 1 Differences (yr) between calibrated ^{14}C results on context-associated material and CB. Archaeological data set from Aarre urnfield cemetery, grouped by grave. Distributions in black are differences relative to short-lived samples and gray distributions are differences relative to medium- to long-lived samples. Differences that plot on or to the right of the vertical zero line imply that a sample is contemporaneous with or more recent than the CB calibrated date.

All kinds of re-use of an area will severely increase the risk of residual material being re-deposited in a younger context, which appears to have occurred frequently in Aarre. This also underlines the risk of testing the validity of CB dates using associated charcoal dates as “known-age reference material.”

Four single cereal grains from the pit and within the urn of grave A393 are considerably older than the associated CB date. Only a single cereal date (KIA-53946, grave A130) is close to its associated CB date. Out of four samples of charred grass, only two (KIA-53953-54) are similar to the associated CB dates or possibly even slightly younger, while the remainder are older. Three dates on charred twigs (KIA-53984-85; RICH-25069) are similar to or younger than their associated CB dates, whereas a date on alder branch sapwood (KIA-52414) is 138–521 yr older (95.4% probability) than the CB. Single entity, short-lived samples from secure, in situ deposits are in general preferred for ^{14}C dating, but as illustrated here the taphonomic processes might be more complicated than otherwise indicated by the archaeological interpretation, and

samples with negligible IA do not necessarily offer the best estimate of the date of the cremation event.

Experimental Dataset

We report 20 new AMS dates from four separate experimental pyres (Table 4). CI values are generally acceptable (>5), except for pyre no. 16, with three out of four samples having CI values <5 , indicating they are not fully calcined. Experiments using archaeological wood proved challenging, as it was difficult to ignite. Pyre no. 9 burned with unusual low, bluish flames omitting an unpleasant sulfurous odor. Even though pyre no. 16 was conducted in the same way as the others, it failed to fully cremate the bone and results from this pyre are not included in the discussion. We suspect the old wood was altered by diagenetic contamination from the burial environment, influencing the pyrotechnical process and complicating the interpretation of ^{14}C measurements. Nevertheless, CB $\delta^{13}\text{C}$ (mean = $-24.3 \pm 2.1 \delta^{13}\text{C}$) and $\%C$ (mean = $0.15 \pm 0.09 \%$) from pyre no. 16 fall within expected ranges and correspond to results observed in archaeological CB (e.g. Olsen et al. 2008). Again, values of $\delta^{13}\text{C}$ (measured by AMS) and $\%C$ are not directly comparable between laboratories (Rose et al. 2019).

CB ^{14}C ages from individual pyres are statistically inconsistent¹ (Figure 2) (Ward and Wilson 1978). Pyre no. 11 includes both sheep and cattle bone, however, and the combined results on sheep bones are consistent (weighted mean = -442 ± 14 BP), whereas results on cattle bones remain inconsistent, albeit approaching acceptable test values². The maximum difference between ^{14}C ages from individual pyres are highly significant, ranging from 120 ± 28 yr ($> 4 \sigma$) to 169 ± 39 yr ($> 4 \sigma$). This is an example of how the shape of the ^{14}C calibration curve has an impact on the magnitude of offsets measured in ^{14}C ages. The post-bomb curve is especially steep, thus a small difference in calendar-age offsets between samples will have a large effect on the ^{14}C determinations. The maximum differences between results among sheep or cattle bone samples from pyre no. 11 are smaller but are still significantly different ($> 2 \sigma$). These samples come from the same animals, but it is not possible to reconcile the ^{14}C dates from individual experiments without accounting for wood-age offsets in the CB.

Samples from pyres no. 8 and no. 11, using recent wood, have $F^{14}\text{C}$ values >1 , indicating the presence of bomb ^{14}C (Figure 3a–c), and thus negative ^{14}C ages, whereas samples from pyre no. 9, using medieval wood, have $F^{14}\text{C}$ values <1 and positive ^{14}C ages, as a result of mixing carbon reservoirs with different ^{14}C activities (Figure 3d). ^{14}C ages are calibrated in OxCal v4.3 using multiple calibration curves (Bronk Ramsey 2009a). Negative ^{14}C ages are calibrated using the Bomb13NH1 (AD 1650–2010) calibration curve with a 0.5-yr resolution (Hua et al. 2013), with additional data points from the Hammer and Levin datasets (Online Supplementary Information 4) (Levin et al. 2013; Hammer and Levin 2017). Positive ^{14}C ages are calibrated using the IntCal13 Northern Hemisphere atmospheric ^{14}C calibration curve (Reimer et al. 2013).

Carbon exchange results range from $29.3 \pm 0.5\%$ to $83.5 \pm 0.4\%$ and have an overall mean of $58.6 \pm 14.8\%$. Samples cremated using recent wood have a mean exchange of $52.2 \pm 10.9\%$, ranging from $29.3 \pm 0.5\%$ to $67.5 \pm 0.5\%$, whereas experimental pyre no. 9 has a mean exchange of $77.5 \pm 5.0\%$, with a narrower range from $72.3 \pm 0.4\%$ to $83.5 \pm 0.4\%$. There appears to be no correlation between $\%$ carbon exchange and CI values (Figure 4a), but

¹Pyre no. 8: $T' = 18.4$, $T'(5\%) = 7.8$, $v = 3$. Pyre no. 9: $T' = 21.9$, $T'(5\%) = 7.8$, $v = 3$. Pyre no. 11: $T' = 30.4$, $T'(5\%) = 14.1$, $v = 7$. Pyre no. 16: $T' = 880.5$, $T'(5\%) = 7.8$, $v = 3$.

²Pyre no. 11 cattle: $T' = 9.0$, $T'(5\%) = 7.8$, $v = 3$, sheep: $T' = 7.6$, $T'(5\%) = 7.8$, $v = 3$.

Table 4 Radiocarbon results on the experimental data set.

Context	Cremation duration (hr)	Lab code	Sample ID	Material	CI	%C	F ¹⁴ C	Corrected pMC	AMS δ ¹³ C (‰VPDB) ¹	Conventional ¹⁴ C age (BP)	% C exchange with old CO ₂ F ¹⁴ C indicated
Pyre no. 8	2	RICH-25820	x231_1	Cremated bone (<i>Ovis aries</i>)	6.6	0.39	1.0443 ± 0.0018	104.43 ± 0.31	-21.4	-348 ± 24	29.3 ± 0.5
		RICH-25821	x231_2	Cremated bone (<i>Ovis aries</i>)	6.2	0.16	1.0632 ± 0.0031	106.32 ± 0.31	-26.0	-492 ± 24	55.5 ± 0.5
		RICH-25822	x231_3	Cremated bone (<i>Ovis aries</i>)	5.6	0.20	1.0559 ± 0.0033	105.59 ± 0.33	-24.8	-437 ± 25	45.4 ± 0.5
		RICH-25823	x231_4	Cremated bone (<i>Ovis aries</i>)	5.9	0.12	1.0543 ± 0.0038	105.43 ± 0.38	-21.2	-425 ± 29	43.2 ± 0.5
Pyre no. 9	2.5	GrM-14698	x238_1	Cremated bone (<i>Bos taurus</i>)	5.7	0.12	0.9332 ± 0.0023	93.32 ± 0.23	-22.1	555 ± 20	72.3 ± 0.4
		GrM-14700	x238_2	Cremated bone (<i>Bos taurus</i>)	7.0	0.10	0.9242 ± 0.0023	92.42 ± 0.23	-22.6	635 ± 20	79.5 ± 0.4
		GrM-14701	x238_3	Cremated bone (<i>Bos taurus</i>)	5.5	0.08	0.9303 ± 0.0024	93.03 ± 0.24	-22.9	580 ± 20	74.6 ± 0.4
		GrM-14702	x238_4	Cremated bone (<i>Bos taurus</i>)	5.6	0.10	0.9192 ± 0.0023	91.92 ± 0.23	-25.3	675 ± 20	83.5 ± 0.4
Pyre no. 11	2	RICH-25737	x246_1	Cremated bone (<i>Bos taurus</i>)	6.0	0.07	1.0719 ± 0.0039	107.19 ± 0.39	-25.4	-558 ± 29	67.5 ± 0.5
		RICH-25738	x246_2	Cremated bone (<i>Bos taurus</i>)	6.7	0.06	1.0714 ± 0.0039	107.14 ± 0.39	-27.1	-554 ± 29	66.8 ± 0.5
		RICH-25739	x246_3	Cremated bone (<i>Bos taurus</i>)	6.8	0.34	1.0587 ± 0.0034	105.87 ± 0.34	-22.9	-458 ± 26	49.2 ± 0.5
		RICH-25740	x246_4	Cremated bone (<i>Bos taurus</i>)	6.6	0.21	1.0648 ± 0.0034	106.48 ± 0.34	-23.9	-504 ± 26	57.7 ± 0.5
Pyre no. 16	2	RICH-25744	x246_5	Cremated bone (<i>Ovis aries</i>)	6.2	0.12	1.0629 ± 0.0038	106.29 ± 0.38	-27.1	-490 ± 29	60.4 ± 0.5
		RICH-25745	x246_6	Cremated bone (<i>Ovis aries</i>)	6.1	0.14	1.0496 ± 0.0033	104.96 ± 0.33	-23.6	-389 ± 26	44.2 ± 0.5
		RICH-25753	x246_7	Cremated bone (<i>Ovis aries</i>)	8.5	0.16	1.0594 ± 0.0035	105.94 ± 0.35	-28.5	-464 ± 27	56.2 ± 0.5
		RICH-25754	x246_8	Cremated bone (<i>Ovis aries</i>)	6.8	0.10	1.0556 ± 0.0039	105.56 ± 0.39	-24.0	-434 ± 30	51.5 ± 0.5
Pyre no. 16	2	GrM-14692	x251_1	Cremated bone (<i>Ovis aries</i>)	4.3	0.24	0.9467 ± 0.0024	94.67 ± 0.24	-26.8	440 ± 20	—
		GrM-14693	x251_2	Cremated bone (<i>Ovis aries</i>)	5.5	0.23	0.9366 ± 0.0023	93.66 ± 0.23	-31.3	525 ± 20	—
		GrM-14695	x251_3	Cremated bone (<i>Ovis aries</i>)	4.6	0.11	0.8791 ± 0.0022	87.91 ± 0.22	-30.5	1035 ± 20	—
		GrM-14697	x251_4	Cremated bone (<i>Ovis aries</i>)	4.1	0.14	0.9703 ± 0.0024	97.03 ± 0.24	-22.3	240 ± 20	—

¹Measured by AMS. Values are not the true ¹³C values of the investigated materials, as they are affected by isotope fractionation during acid extraction, graphitization and AMS measurement.

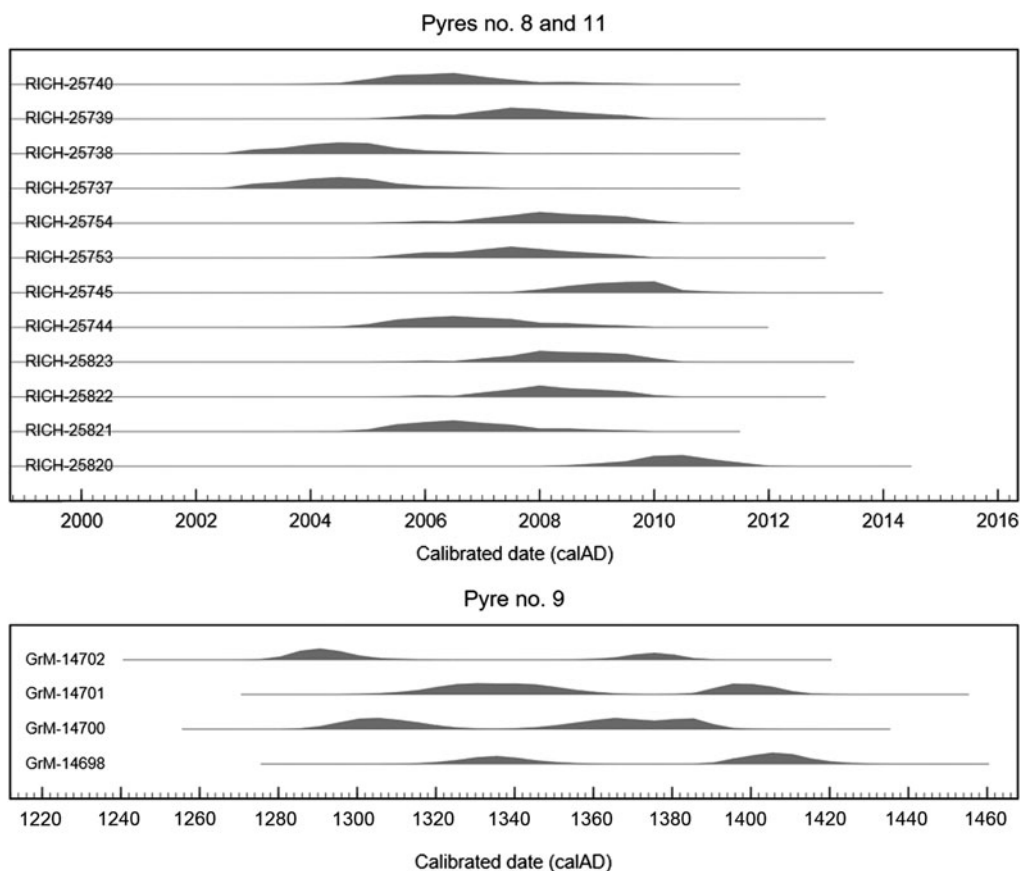


Figure 2 Calibrated ^{14}C results on the experimental data set. Results from pyre no. 9 are calibrated using the IntCal13 Northern Hemisphere atmospheric ^{14}C data set (Reimer et al. 2013). Results from pyres no. 8 and 11 are calibrated using the Bomb13NH1 (AD1650–2010) calibration curve (Hua et al. 2013) with additional data points from the Hammer and Levin datasets of atmospheric ^{14}C activity from Jungfrauoch in the Swiss Alps (Levin et al. 2013; Hammer and Levin 2017).

there is a clear relationship between % carbon exchange and duration of the cremations (hr) (Figure 4b). Pyre no. 9 was burning for ca. 30 min longer than the others and produced higher carbon exchange percentages, but it is difficult to ascertain whether this apparent difference in range is caused by the longer cremation duration itself or by possible differences in temperatures (not measured) and type of fuel wood. The bone apatite, bone collagen and wood from pyres no. 8 and no. 11 have similar ages, and we cannot rule out collagen might have contributed to the carbon composition of the pyre atmosphere. This could possibly explain the smaller % carbon exchange, as compared to pyre no. 9. Values of % carbon exchange and $\delta^{13}\text{C}$ appear to be related, but do not suggest a clear linear mixing model between unburned apatite and wood (Figure 4c).

DISCUSSION

We have presented results from 10 archaeological graves with a combination of ^{14}C dated CB and associated material. Charcoal samples from oak trunk wood can have considerable IA, and even trunk wood samples of shorter-lived alder and maple have an average ^{14}C signal

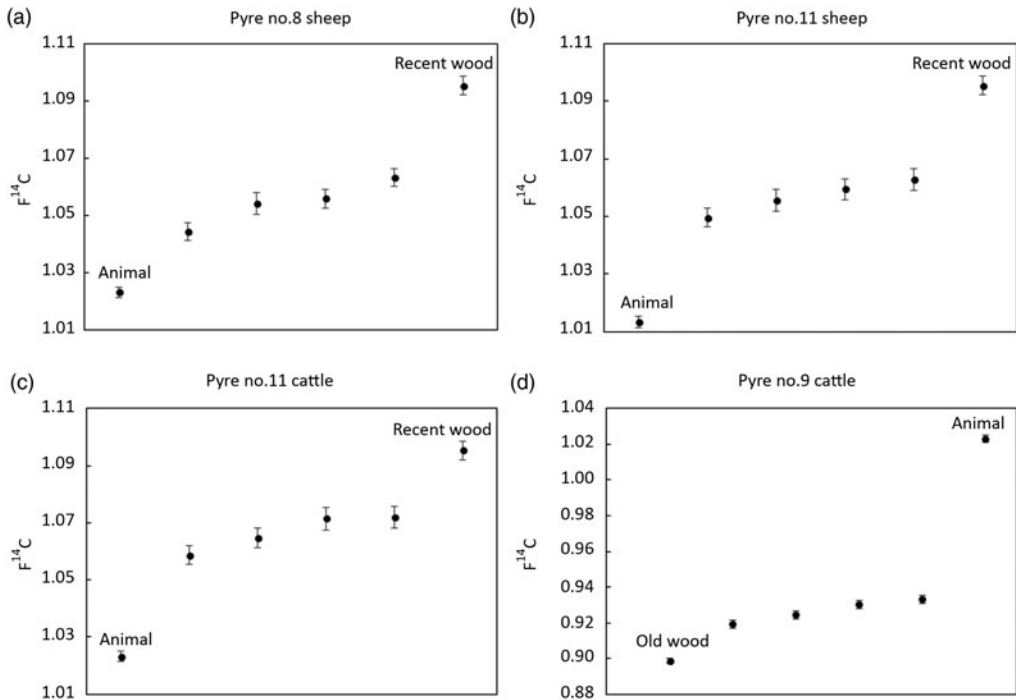


Figure 3 Experimental $F^{14}C$ results with 1σ uncertainties: (a) pyre no. 8 sheep, (b) pyre no. 11 sheep, (c) pyre no. 11 cattle and (d) pyre no. 9 cattle. Endmember values of animal and wood indicated directly in the figures.

predating the cremation event and can, with a high % carbon exchange, cause a significant wood-age offset in the CB. Two charcoal samples of alder trunk wood from grave A99 have calibrated dates agreeing with the CB date, whereas a charred twig dates younger. A charcoal sample of oak trunk wood from the same grave predating the other samples by approximately a millennium is probably residual and unrelated to the grave. In this scenario the twig with negligible IA will best reflect the date of the cremation event. In the following, we will focus on graves containing short-lived samples (i.e. with negligible IA). Furthermore, because wood-age offsets can only make the CB older (unless old bone is cremated with young wood, which is an unlikely archaeological scenario), we ignore short-lived samples dating older than the CB, and only discuss samples whose dates are similar to or later than the date of the associated CB (i.e. differences plot on or to the right of the zero line in Figure 1). We regard the calibrated dates of these short-lived samples as dating the cremation event, and thus indicating possible wood-age offsets in the CB samples.

Graves A95, A99, A130 and A278 contain material meeting these criteria. Graves A95 and A278 each provided two such short-lived samples with statistically consistent ^{14}C ages, whose weighted means (A95: 2399 ± 19 BP, $df = 1$, $T' = 2.8$ ($5\% = 3.8$); A278: 2423 ± 18 BP, $df = 1$, $T' = 1.6$ ($5\% = 3.8$)) provide better estimates of the dates of the respective cremations. The calibrated date differences between CB and short-lived samples are assumed to be exponentially distributed and modeled in a bounded phase starting at zero and ending with a $\text{Tau}_{\text{Boundary}}$ (Bronk Ramsey 2009a). Results are summarized in a KDE_Plot in Figure 5 (Bronk Ramsey 2017). The posterior distribution estimate differences to have a median of 62 yr and a $1-\sigma$ range of 173 yr (Online Supplementary Information 1, Part 2). The median offset is larger than we

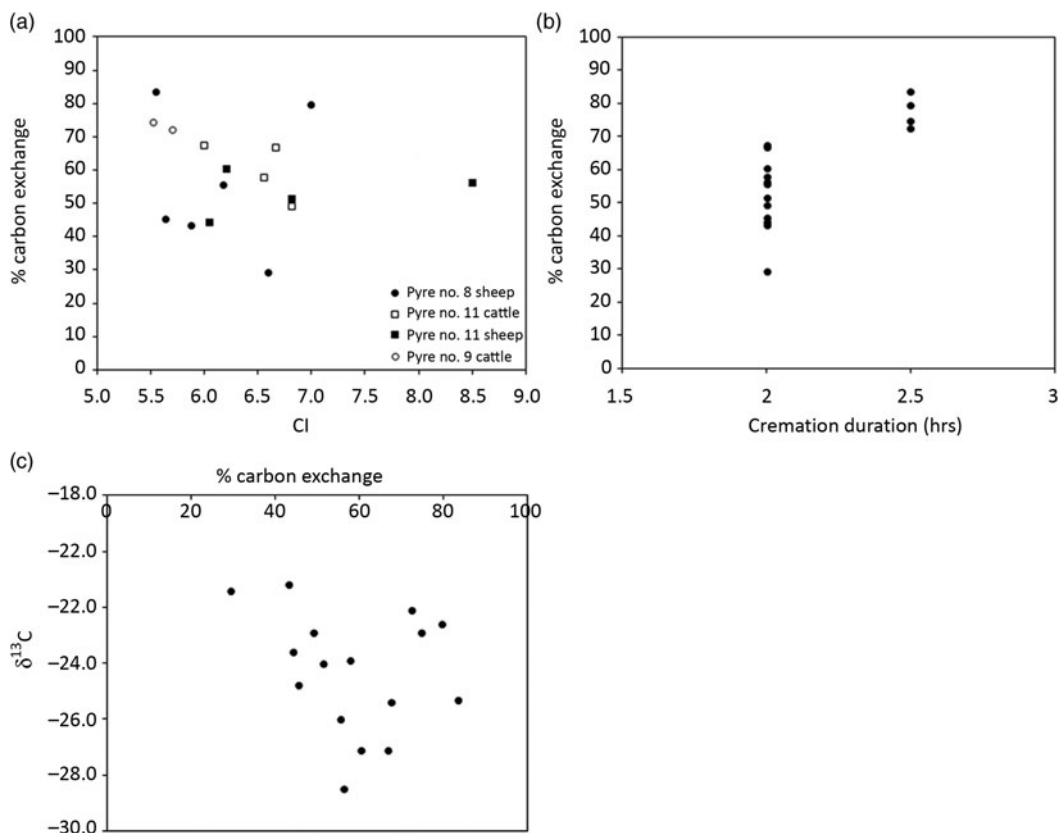


Figure 4 Results of % carbon exchange plotted against different measurement parameters of the experimental data set: (a) % carbon exchange plotted against CI, (b) % carbon exchange plotted against cremation duration (hr) and (c) % carbon exchange plotted against $\delta^{13}\text{C}$ values.

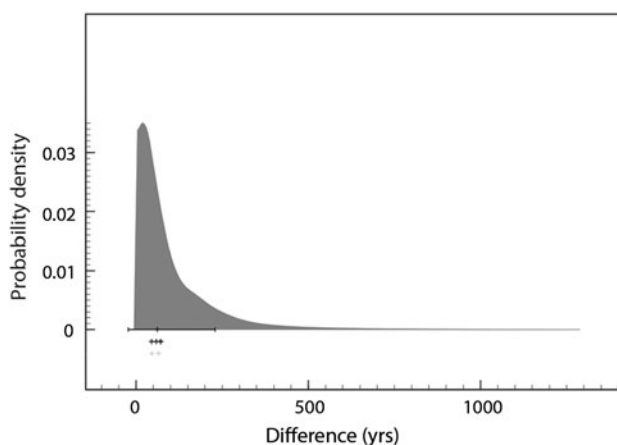


Figure 5 Constrained differences between selected short-lived samples and CB (see text) summarized in a KDE_Plot. Differences calculated using weighted means of short-lived samples from grave A95 (2399 ± 19 ^{14}C yr, $df=1$, $T^* = 2.8$ (5% = 3.8)) and grave A278 (2423 ± 18 ^{14}C yr, $df=1$, $T^* = 1.6$ (5% = 3.8)). Median offset of 62 yr and a 1- σ range of 173 yr. Black bar indicates the 1- σ range and crosses the median values of individual differences.

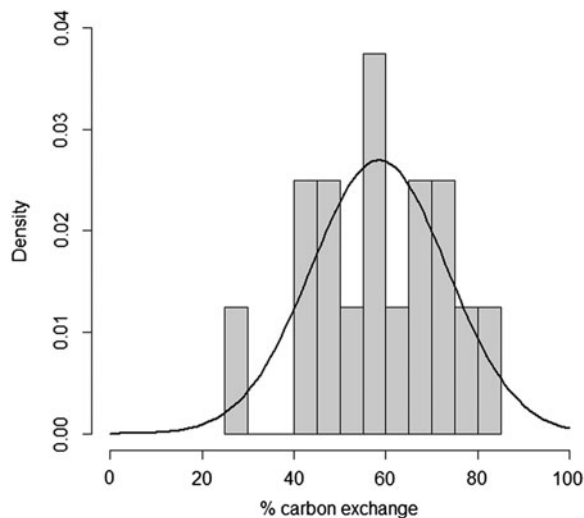


Figure 6 Density plot of % carbon exchange from the experimental data set (gray bars). The added curve depicts 1000 random numbers drawn from a normal distribution with mean and standard deviation derived from the experimental data set.

have just modeled for combined legacy dates from Bronze Age Denmark and medieval Japan (median = 22 yr, $1\text{-}\sigma$ range = 32 yr), although they do overlap within $1\text{-}\sigma$ ranges (Olsen et al. 2008; Olsen et al. 2013; Minami et al. 2019). The median of the archaeological differences falls within the 50–100 yr offset that has been suggested in the literature, although this now looks to underestimate the total range (Hüls et al. 2010; Van Strydonck et al. 2010; Zazzo and Saliège 2011; Snoeck et al. 2014).

Experimental cremation studies have documented a high degree of carbon substitution both in laboratory and open-air experimental setups (Hüls et al. 2010; Van Strydonck et al. 2010; Zazzo et al. 2012; Snoeck et al. 2014). Our open-air experimental results show similarly wide substitution ranges in samples from the same individual (animal cut) when the pyre is fueled by recent wood (pyre no. 8 and no. 11: from $29.3 \pm 0.5\%$ to $67.5 \pm 0.5\%$ with mean exchange $52.2 \pm 10.9\%$), whereas using old wood (pyre no. 9: from $72.3 \pm 0.4\%$ to $83.5 \pm 0.4\%$ with mean exchange $77.5 \pm 5.0\%$) produce slightly more consistent results. The variability in CB $F^{14}\text{C}$ within each pyre is exaggerated due to large differences in ^{14}C content of the old wood and modern bone amplifying the effect of % carbon exchange differences between bone fragments, and perhaps due to the ^{14}C inhomogeneity of the recent wood affected by the ^{14}C bomb spike. We would therefore expect less variation in CB ^{14}C ages from real prehistoric cremations. Figure 3b indicates a possible correlation of % carbon exchange and cremation duration, which requires further investigation. However, a density plot of % carbon exchange (Figure 6) closely resembles a normal distribution, suggesting that the expected wood-age offsets in CB within individual pyres will be normally distributed.

The only source of carbon in bio-apatite is carbonate ions formed through energy production in cells, which can substitute with hydroxyl (OH, A-type carbonates) or phosphate (PO_4 , B-type

carbonates) in the bone-matrix (Lee-Thorp 2008; Hüls et al. 2010). This results in an IA of the bio-apatite equal to the turn-over rate of the bone-matrix, probably comparable to turn-over rates in bone-collagen (Hedges et al. 2007). This leads us to expect IA of the carbon in the original bio-apatite to be unevenly distributed throughout a human skeleton, but given the short lifespan of the animals used in our experiments, their ^{14}C contents must be fairly homogenous. Thus, the large dispersion of % carbon exchange results in CB from a single pyre must here reflect a differential uptake of exogenous carbon, but also variations in temperature and CO_2 concentration within a small pyre might play a role. Our % carbon exchange results underline a certain degree of dispersion is to be expected when ^{14}C dating CB, which again points to the need of handling these offsets statistically.

Outlier Modeling

We consider the calibrated offsets between CB and selected short-lived samples from the archaeological data set, and find the distribution in Figure 5 to visually resemble the exponentially distribution otherwise expected for charcoal dates, i.e. most samples dating close to the event in question, but a diminishing number of samples dating increasingly older (Nicholls and Jones 2001; Dee and Bronk Ramsey 2014). OxCal's default Charcoal OM may therefore be a reasonable model for dealing with wood-age offsets in CB, as proposed by Garrow et al. (2014) and Fitzpatrick et al. (2017). All modeling is conducted in OxCal v4.3 (Bronk Ramsey 2009a, 2009b).

To test this idea, we model the archaeological results from Aarre urnfield cemetery as a bounded phase of activity. Individual graves are modeled as phases including dates on CB and selected short-lived samples, except graves A95, A99, A130 and A278 where CB dates are combined with dates on contemporaneous, short-lived samples. Dates of charcoal samples with potentially significant IA are modeled as *terminus post quem* (TPQ) dates. In *Model 1* (Online Supplementary Information 1, Part 3, Model 1), we apply the Charcoal OM to all CB dates, with a prior probability of 1 (i.e. all CB dates are assumed to be affected by wood-age offsets). The Charcoal OM posterior estimates the CB dates to date 2–91 yr or 0–252 yr older than their cremation events (68.2% and 95.4% probabilities), with a median of 55 yr. The offsets agree within the 68.2% probability range with the offsets otherwise indicated by the calibrated differences between selected short-lived material and CB (median 62 yr and 1- σ range 173 yr), although the Charcoal OM might underestimate the offsets slightly.

Based on our experimental results, the CB dates should always fall between the short-lived sample dates and the average age of charcoal, although individual fragments of charcoal can be younger than the CB. The pyre wood will have an IA some years older than the cremation event, as will carbon in the unburned bio-apatite. Both are type-t offsets (on the calendar scale, as opposed to “type-r” offsets in ^{14}C space, such as dietary reservoir effects). In *Model 2* (Figure 7a) we apply a minimum offset to all CB dates, by creating a “Cremation OM” (Online Supplementary Information 1, Part 3, Model 2). This uses the same exponential distribution as the default Charcoal OM, but with an exponential constant of 0.9 and running from -10 to -0.1 to ensure the peak of the OM posterior distribution is shifted away from zero. The scale parameter is set to $U(1,3)$, rather than $U(0,3)$, i.e. offsets can vary between 10^1 and 10^3 rather than 10^0 – 10^3 yr, reducing the chances of sub-decadal offsets. We apply the Cremation OM to all CB dates, with a prior probability of 1, and otherwise construct *Model 2* as *Model 1*. The Cremation OM

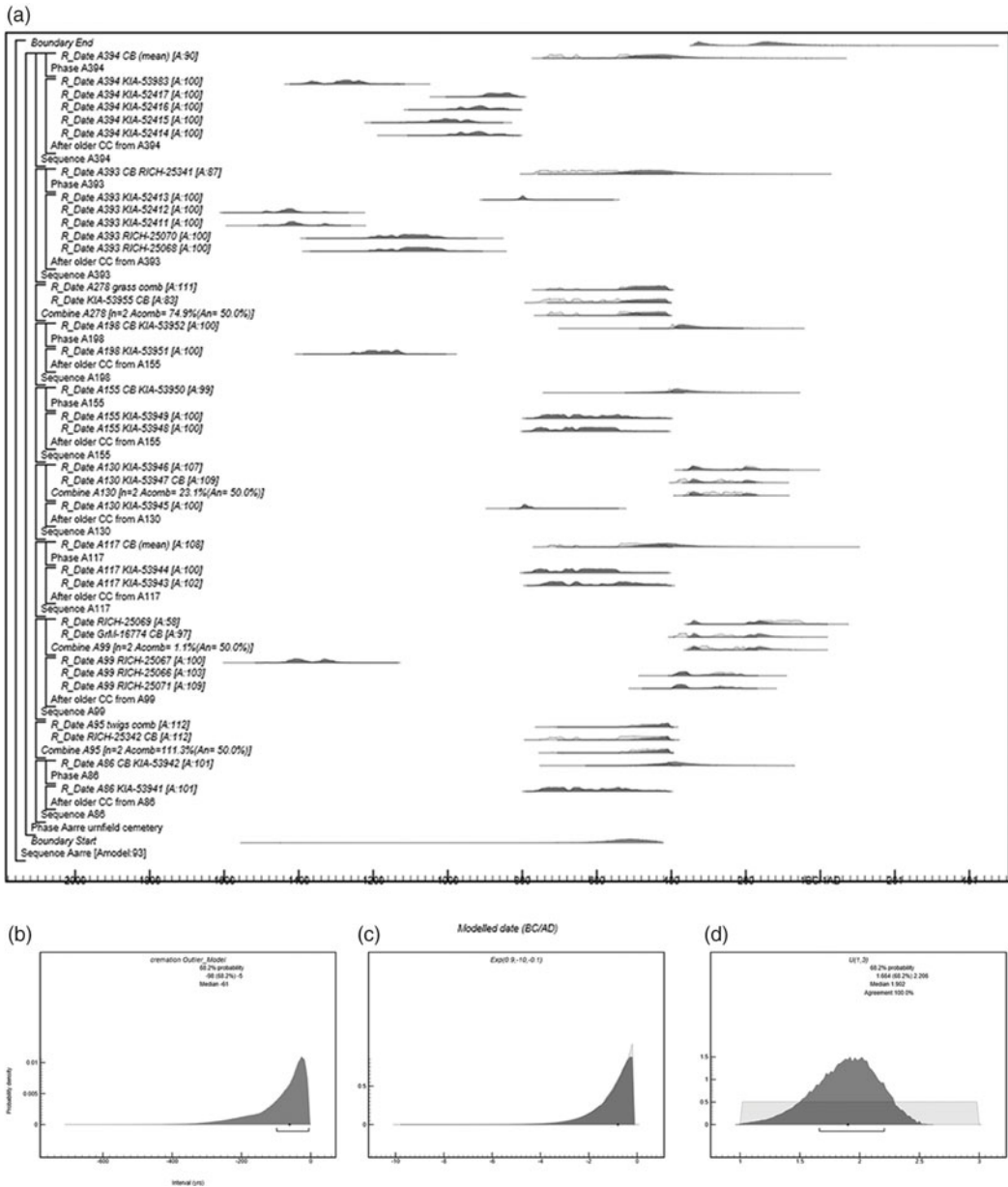


Figure 7 Chronological *Model 2* of all ^{14}C results from Aarre urnfield cemetery (a) with a bespoke cremation outlier model applied to CB dates. In the middle left plot (b) is the posterior distribution of the outlier offsets (5–98 yr with 68% probability). In the middle right plot (c) is the effective prior and in the lower plot (d) the estimated timescale for wood-age offset in CB (posterior distribution in gray and uniform prior shown in outline).

estimates the CB dates to date 5–98 yr or 2–252 yr older than their cremation events (68.2% and 95.4% probabilities), with a median of 61 yr (Figure 7b–d). The Cremation OM estimates larger offsets than the Charcoal OM does, and the offset median is very close to the median suggested by our archaeological material.

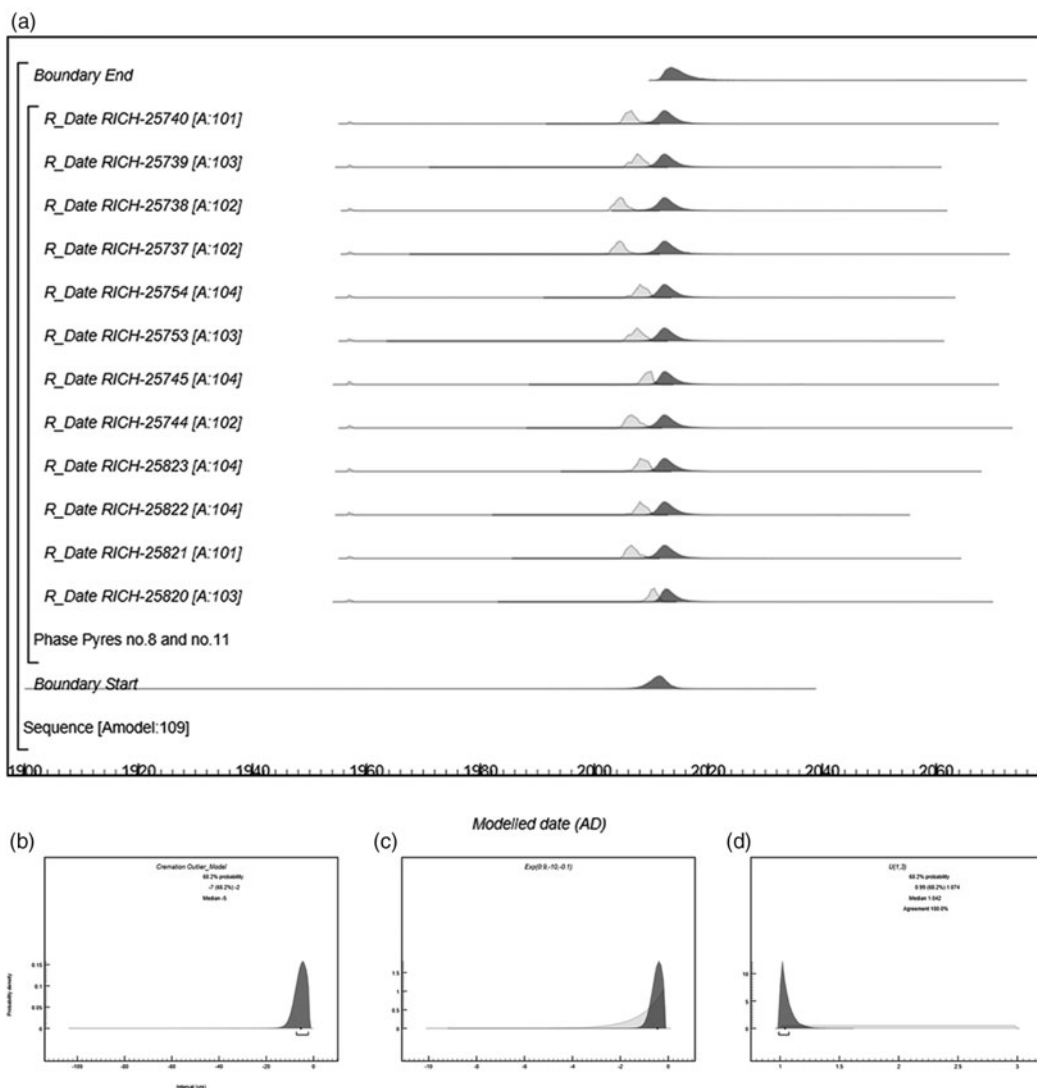


Figure 8 Chronological *Model 4* applying a Cremation OM to experimentally CB (a). In the middle left plot (b) is the posterior distribution of the outlier offsets (2–7 yr with 68.2% probability). In the middle right plot (c) is the effective prior and in the lower plot (d) the estimated timescale for wood-age offset in CB (posterior distribution in gray and uniform prior shown in outline).

Next we test the suitability of both Charcoal and Cremation OM for estimating wood-age offsets in our experimental data set using recent wood (pyres no. 8 and no. 11). In *Model 3* (Online Supplementary [Information 1](#), Part 4, *Model 3*), we treat the CB dates as representing a bounded phase of activity and apply a Charcoal OM to the CB dates with a probability of 1. The model estimates activity to start AD 2004–2010 and end AD 2008–2012 (95.4% probability, $A_{\text{model}}=96$) and the posterior distribution of the OM estimate the CB dates to date 0–2 yr or 0–5 yr older than their cremation events (68.2% and 95.4% probabilities). *Model 3* estimates the cremation events to have occurred before the actual event (AD 2013 and 2015), meaning that the Charcoal OM underestimate the wood-age offsets.

Given the short lifespans of the experimental material it will have a shorter residence time of the unburned bio-apatite, compared to the human CB from the archaeological material. The IA of the pyre wood will however still cause a minimum wood-age offset, why we create *Model 4* with the same chronological construction as described above. We apply the bespoke Cremation OM to the CB dates, with a prior probability of 1 (Figure 8a, Online Supplementary Information 1, Part 4, Model 4). The OM takes all adjusted parameters as described for *Model 2*. *Model 4* ($A_{\text{model}} = 109$) estimates activity to start AD 2006–2014 and end AD 2011–2021 (95.4% probability). The posterior distribution of the Cremation OM estimates the CB dates to date 2–7 yr or 1–11 yr older than their cremation events (68.2% and 95.4% probabilities, Figure 8b–d). These offsets are larger than calculated by the Charcoal OM and enable *Model 4* to estimate start and end boundaries encompassing the true dates of the cremation events.

It is difficult to assess which OM model is best suited for the archaeological data set, as we do not know the true cremation dates. But we find it to be a convincing argument, that the Cremation OM yields a median offset similar to that suggested by differences between the calibrated dates of short-lived material and associated CB. For the experimental data set, the Charcoal OM underestimates the observed offsets, whereas the Cremation OM enables the chronological model to accurately date the cremation events. Earlier studies (Garrow et al. 2014; Fitzpatrick et al. 2017) have used outlier modeling to handle wood-age offsets in CB, but with new empirical data on the scale and distribution of these offsets we can suggest a bespoke Cremation OM with a minimum offset to be better suited to our purposes than the default Charcoal OM.

CONCLUSION AND IMPLICATIONS FOR ARCHAEOLOGY

We have demonstrated significant variation in carbon exchange in experimentally CB, with % carbon exchange among samples from single pyres ranging from $29.3 \pm 0.5\%$ to $83.5 \pm 0.4\%$ (mean $58.6 \pm 14.8\%$). We have confirmed that wood-age offsets in archaeological CB are significant, with a 62 yr median calibrated date offset between short-lived, context associated material and CB (1- σ range of 173 yr). The distribution of wood-age offsets appears to follow an exponential distribution and we test if the default Charcoal OM is applicable for estimating such offsets in archaeological and experimental CB but find that it slightly underestimates apparent offsets. To counter the intrinsic age of both pyre fuel and unburned bio-apatite we instead propose a bespoke Cremation OM, which combines an exponential distribution of calendar age offsets with a minimum offset, and provides better estimates of the actual dates of cremations.

It is important to stress that carbon exchange can vary even within a single cremated bone, and that the shape of the ^{14}C calibration curve can have great impact on the magnitude of these offsets measured in ^{14}C age. Instead of trying to quantify and correct for the offset individually, we urge that they be treated statistically using formal outlier modeling.

ACKNOWLEDGMENTS

Analyses were funded through the Center for Baltic and Scandinavian Archaeology (ZBSA)'s Man and Environment research theme and by the Deutsche Forschungsgemeinschaft (DFG, German Research Foundation – Project number 2901391021 – SFB 1266) subproject G1: Timescales of Change – Chronology of cultural and environmental transformations of the Collaborative Research Center “Scales of Transformation: Human-environmental

Interaction in Prehistoric and Archaic Societies”. The authors would like to thank Odense City Museums and ARKVEST – Arkæologi Vestjylland for access to material. We are thankful to Ingeborg Levin and Samuel Hammer from the Institute of Environmental Physics at Heidelberg University for letting us work with their recent measurements of atmospheric ^{14}C activity from Jungfrauoch in the Swiss Alps. Without this it would not have been possible to analyze our post-bomb data.

SUPPLEMENTARY MATERIAL

To view supplementary material for this article, please visit <https://doi.org/10.1017/RDC.2020.3>

REFERENCES

- Bayliss A. 1999. On the taphonomy of charcoal samples for radiocarbon dating. In: Evin J, editor. Actes du 3ème Congrès International 14 C et Archéologie: Lyon 6-10 avril 1998. Paris: Soc. Préhist. Française. p 51–6.
- Becker CJ. 1961. Førromersk jernalder i Syd- og Midtjylland. Kbh.: Nationalmuseet.
- Boudin M, Van Strydonck M, van den Brande T, Synal H-A, Wacker L. 2015. RICH – A new AMS facility at the Royal Institute for Cultural Heritage, Brussels, Belgium. Nuclear Instruments and Methods in Physics Research Section B: Beam Interactions with Materials and Atoms 361:120–3.
- Bronk Ramsey C. 2009a. Bayesian analysis of radiocarbon dates. Radiocarbon 51(1):337–60.
- Bronk Ramsey C. 2009b. Dealing with outliers and offsets in radiocarbon dating. Radiocarbon 51(3):1023–45.
- Bronk Ramsey C. 2017. Methods for summarizing radiocarbon datasets. Radiocarbon:1–25.
- Chatters JC, Brown JW, Hackenberger S, McCutcheon P, Adler J. 2017. Calcined bone as a reliable medium for radiocarbon dating: A test using paired North American samples. American Antiquity 82(3):593–608.
- Daly A. 2011. Dendrochronological analysis of timbers from a well at Odense Adelige Jomfrukloster, Fyn. OBM137 Dendro.dk.
- Daly A. 2014. Dendrochronological analysis of timbers from a well at Skovgård, Sdr. Nørå, Fyn. OBM 1613. Dendro.dk.
- De Mulder G, Van Strydonck M, Boudin M. 2009. The impact of cremated bone dating on the archaeological chronology of the Low Countries. Radiocarbon 51(2):579–600.
- Dee MW, Bronk Ramsey C. 2014. High-precision Bayesian modeling of samples susceptible to inbuilt age. Radiocarbon 56(1):83–94.
- Dee MW, Palstra SWL, Aerts-Bijma AT, Bleeker MO, de Bruijn S, Ghebru F, Jansen HG, Kuitens M, Paul D, Richie RR, Spriensma JJ, Scifo A, van Zonneveld D, Verstappen-Dumoulin BMAA, Wietzes-Land P, Meijer HAJ. 2019. Radiocarbon dating at Groningen: New and updated chemical pretreatment procedures. Radiocarbon:1–12.
- Effenberger H. 2017a. Report about the results of the charcoal analysis and selection of datable material for the sites HOM and VAM1600. Effenberger Archäobotanik.
- Effenberger H. 2017b. Report about the results of the charcoal analysis and selection of datable material for the sites ARV113 and VAM1600. Effenberger Archäobotanik.
- Effenberger H. 2019. Report about the results of the charcoal analysis and selection of datable material for the site VAM1600. Effenberger Archäobotanik.
- Fitzpatrick AP, Hamilton WD, Haselgrove CC. 2017. Radiocarbon dating and Bayesian modelling of the Late Iron Age cremation burial cemetery at Westhampnett, West Sussex, GB. Archaeologisches Korrespondenzblatt 47:359–81.
- Garrow D, Meadows J, Evans C, Tabor J. 2014. Dating the dead: A high-resolution radiocarbon chronology of burial within an Early Bronze age barrow cemetery at Over, Cambridgeshire. Proceedings of the Prehistoric Society 80:207–36.
- Grootes PM, Nadeau M-J, Rieck A. 2004. ^{14}C -AMS at the Leibniz-Labor: Radiometric dating and isotope research. Nuclear Instruments and Methods in Physics Research Section B: Beam Interactions with Materials and Atoms 223–224:55–61.
- Hammer S, Levin I. 2017. Monthly mean atmospheric D^{14}CO_2 at Jungfrauoch and Schauinsland from 1986 to 2016. heiDATA Dataverse.
- Hedges REM, Clement JG, Thomas CDL, O’Connell TC. 2007. Collagen turnover in the adult femoral mid-shaft: Modeled from anthropogenic radiocarbon tracer measurements. American Journal of Physical Anthropology 133(2):808–16.
- Henriksen MB. 2009. Brudager Mark – en romertidsgravplads nær Gudme på Sydøst Fyn.
- Henriksen MB. 2016. Bålets betydning [Doctoral dissertation]: Copenhagen University.

- Henriksen MB. 2019. Experimental cremations – can they help us to understand prehistoric cremation graves? In: Ciesliński A, Kontny B, editors. *Interacting barbarians contacts, exchange and migrations in the first millennium AD*. Warsaw: Neue Studien zur Sachsenforschung Band 9. p 289–96.
- Hissel M, Parlevliet M, Verspay J. 2007. Begraven, bewonen, beakkeren. Archeologisch onderzoek bij de uitbreiding van de woonwijk Genoenhuis, gemeente Geldrop-Mierlo (Noord-Brabant). Amsterdam.
- Hornstrup KM, Glintborg Overgaard K, Andersen S, Bennike P, Hambro Mikkelsen P, Malmros C. 2005. Hellegård – en gravplads fra omkring år 500 f. Kr. Aarbøger for Nordisk Oldkyndighed og Historie 2002:83–162.
- Hua Q, Barbetti M, Rakowski AZ. 2013. Atmospheric Radiocarbon for the Period 1950–2010. Radiocarbon 55(04):2059–72.
- Hüls CM, Erlenkeuser H, Nadeau MJ, Grootes PM, Andersen N. 2010. Experimental study on the origin of cremated bone apatite carbon. Radiocarbon 52(2):587–99.
- Iversen J. 1974. The development of Denmark's nature since the Last Glacial.
- Jensen CK. 1996. Chronologische Probleme der Vorrömische Eisenzeit Dänemarks. Prähistorische Zeitschrift 1996(2):194–216.
- Lanting JN, Aerts-Bijma AT, van der Plicht J. 2001. Dating of cremated bones. Radiocarbon 43(2A):249–54.
- Lee-Thorp JA. 2008. On isotopes and old bones. Archaeometry 50(6):925–50.
- Levin I, Kromer B, Hammer S. 2013. Atmospheric $\Delta^{14}\text{CO}_2$ trend in Western European background air from 2000 to 2012. Tellus B: Chemical and Physical Meteorology 65(1):20092.
- Lorange T. 2015. Det sakrale landskab ved Årre. Landskabets hukommelse gennem 4.000 års gravriter. In: Foss P, Møller NA, editors. *De dødes landskab. Grav og gravskik i ældre jernalder i Danmark*. Ribe: SAXO-instituttet, Københavns Universitet. p 21–36.
- Martín-Seijo M, César Vila M. 2018. Oak, ash and pine: The role of firewood in funerary rituals at the Roman site of Reza Vella (Ourense, Spain). Archaeological and Anthropological Sciences.
- Minami M, Mukumoto H, Wakaki S, Nakamura T. 2019. Effect of crystallinity of apatite in cremated bone on carbon exchanges during burial and reliability of radiocarbon dating. Radiocarbon:1–12.
- Moskal-del Hoyo M. 2012. The use of wood in funerary pyres: Random gathering or special selection of species? Case study of three necropolises from Poland. Journal of Archaeological Science 39(11): 3386–95.
- Nadeau MJ, Grootes PM, Schleicher M, Hasselberg P, Rieck A, Bitterling M. 1997. Sample throughput and data quality at the Leibniz-Labor AMS Facility. Radiocarbon 40(1):239–45.
- Naysmith P, Scott EM, Cook GT, Heinemeier J, Van der Plicht J, Van Strydonck M, Bronk Ramsey C, Grootes PM, Freeman SPHT. 2007. A cremated bone intercomparison study. Radiocarbon 49(2):403–8.
- Nicholls G, Jones M. 2001. Radiocarbon dating with temporal order constraints. Journal of the Royal Statistical Society. Series C (Applied Statistics) 50(4):503–21.
- O'Donnell L. 2016. The power of the pyre – A holistic study of cremation focusing on charcoal remains. Journal of Archaeological Science 65:161–71.
- Olsen J, Heinemeier J, Bennike P, Krause C, Margrethe Hornstrup K, Thrane H. 2008. Characterisation and blind testing of radiocarbon dating of cremated bone. Journal of Archaeological Science 35(3):791–800.
- Olsen J, Heinemeier J, Hornstrup KM, Bennike P, Thrane H. 2013. 'Old wood' effect in radiocarbon dating of prehistoric cremated bones? Journal of Archaeological Science 40(1):30–4.
- Person A, Bocherens H, Saliège J-F, Paris F, Zeitoun V, Gérard M. 1995. Early diagenetic evolution of bone phosphate: An x-ray diffractometry analysis. Journal of Archaeological Science 22(2):211–21.
- Reimer PJ, Brown TA, Reimer RW. 2004. Discussion: Reporting and calibration of post-bomb ^{14}C data. Radiocarbon 46(3):1299–304.
- Reimer PJ, Bard E, Bayliss A, Beck JW, Blackwell PG, Ramsey CB, Buck CE, Cheng H, Edwards RL, Friedrich M, Grootes PM, Guilderson TP, Haflidason H, Hajdas I, Hatté C, Heaton TJ, Hoffmann DL, Hogg AG, Hughen KA, Kaiser KF, Kromer B, Manning SW, Niu M, Reimer RW, Richards DA, Scott EM, Southon JR, Staff RA, Turney CSM, van der Plicht J. 2013. IntCal13 and Marine13 radiocarbon age calibration curves 0–50,000 years cal BP. Radiocarbon 55(04):1869–87.
- Roehrs H, Klooss S, Kirleis W. 2013. Evaluating prehistoric finds of *Arrhenatherum elatius* var. *bulbosum* in north-western and central Europe with an emphasis on the first Neolithic finds in Northern Germany. Archaeological and Anthropological Sciences 5(1):1–15.
- Rose HA, Meadows J, Palstra S, Hamann C, Boudin M, Hüls CM. 2019. Radiocarbon dating cremated bone: A case study comparing laboratory methods. Radiocarbon. doi:10.1017/RDC.2019.70.
- Snoeck C, Brock F, Schulting RJ. 2014. Carbon Exchanges between bone apatite and fuels during cremation: Impact on radiocarbon dates. Radiocarbon 56(2):591–602.
- Snoeck C, Schulting RJ, Lee-Thorp JA, Lebon M, Zazzo A. 2016a. Impact of heating conditions on the carbon and oxygen isotope composition of calcined bone. Journal of Archaeological Science 65:32–43.

- Snoeck C, Staff RA, Brock F. 2016b. A reassessment of the routine pretreatment protocol for radiocarbon dating cremated bones. *Radiocarbon* 58(1):1–8.
- Stuiver M, Polach HA. 1977. Discussion: Reporting of ^{14}C data. *Radiocarbon* 19(3):355–63.
- Van Strydonck M, Boudin M, Hoefkens M, De Mulder G. 2005. ^{14}C -dating of cremated bones, why does it work? *Lunula. Archaeologia protohistorica* XIII:3–10.
- Van Strydonck M, Boudin M, De Mulder G. 2009. ^{14}C dating of cremated bones: The issue of sample contamination. *Radiocarbon* 51(2): 553–68.
- Van Strydonck M, Boudin M, Mulder GD. 2010. The carbon origin of structural carbonate in bone apatite of cremated bones. *Radiocarbon* 52(2):578–86.
- Ward GK, Wilson SR. 1978. Procedures for comparing and combining radiocarbon age determinations: A critique. *Archaeometry* 20(1):19–31.
- Zazzo A, Saliège JF, Person A, Boucher H. 2009. Radiocarbon dating of calcined bones: Where does the carbon come from? *Radiocarbon* 51(2):601–11.
- Zazzo A, Saliège JF. 2011. Radiocarbon dating of biological apatites: A review. *Palaeogeography, Palaeoclimatology, Palaeoecology* 310(1):52–61.
- Zazzo A, Saliège J-F, Lebon M, Lepetz S, Moreau C. 2012. Radiocarbon dating of calcined bones: Insights from combustion experiments under natural conditions. *Radiocarbon* 54(3-4):855–66.